WESTINGHOUSE CLASS 3 (Non-Prorietary)

WCAP-13935

Analysis of the 137° Capsule from the Arizona Public Service Company Palo Verde Unit No. 2 Reactor Vessel Radiation Surveillance Program

E. Terek
E. P. Lippincott
A. Madeyski

February 1994

Work Performed Under Shop Order MFYP-106

Prepared by Westinghouse Electric Corporation
for the Arizona Public Service Company

Approved by: _____ for
T. A. Meyer, Manager
Structural Reliability and
Plant Life Optimization

WESTINGHOUSE ELECTRIC CORPORATION
Nuclear and Advanced Technology Division
P.O. Box 355
Pittsburgh, Pennsylvania 15230-0355

PREFACE

This report has been technically reviewed and verified.

	Reviewer:	
Sections 1 through 5, 7, 8, and Appendix A	J. M. Chicots	J.M. Chicots PAP
Section 6	G. N. Wrights	G.N. Wrights

TABLE OF CONTENTS

LIST OF TABLES

LIST OF TABLES (continued)

LIST OF TABLES (continued)

LIST OF TABLES (continued)

LIST OF ILLUSTRATIONS

LIST OF ILLUSTRATIONS

LIST OF ILLUSTRATIONS

SECTION 1.0
SUMMARY OF RESULTS

The analysis of the reactor vessel materials contained in the surveillance capsule removed from the 137° location, the first capsule to be removed from the Palo Verde Unit 2 reactor pressure vessel, led to the following conclusions:

- The capsule received an average fast neutron fluence (E > 1.0 MeV) of 4.071×10^{18} n/cm^2 after 4.54 effective full power years (EFPY) of plant operation.

- Irradiation of the reactor vessel lower shell plate F-773-1 Charpy specimens, oriented with the longitudinal axis of the specimen parallel to the major rolling direction of the plate (longitudinal orientation), to 4.071×10^{18} n/cm^2 (E > 1.0 MeV) resulted in a 30 ft-lb transition temperature increase of 10°F and a 50 ft-lb transition temperature increase of 25°F. This results in an irradiated 30 ft-lb transition temperature of 10°F and an irradiated 50 ft-lb transition temperature of 60°F for the longitudinally oriented specimens.

- Irradiation of the reactor vessel lower shell plate F-773-1 Charpy specimens, oriented with the longitudinal axis of the specimen normal to the major rolling direction of the plate (transverse orientation), to 4.071×10^{18} n/cm^2 (E > 1.0 MeV) resulted in a 30 ft-lb transition temperature increase of 19°F and a 50 ft-lb transition temperature increase of 25°F. This results in an irradiated 30 ft-lb transition temperature of 15°F and an irradiated 50 ft-lb transition temperature of 55°F for transversely oriented specimens.

- Irradiation of the weld metal Charpy specimens to 4.071×10^{18} n/cm^2 (E > 1.0 MeV) resulted in a 30 and 50 ft-lb transition temperature increase of 15°F. This results in an irradiated 30 ft-lb transition temperature of -28°F and an irradiated 50 ft-lb transition temperature of 4°F.

- Irradiation of the weld Heat-Affected-Zone (HAZ) metal Charpy specimens to 4.071×10^{18} n/cm^2 (E > 1.0 MeV) resulted in a 30 ft-lb transition temperature increase of 57°F and a 50 ft-lb transition temperature increase of 18°F. This results in an irradiated 30 ft-lb transition temperature of 45°F and an irradiated 50 ft-lb transition temperature of 75°F.

- The average upper shelf energy of the lower shell plate F-773-1 Charpy specimens (longitudinal orientation) resulted in an average energy increase of 6 ft-lbs after irradiation to 4.071 x 10^{18} n/cm^2 (E > 1.0 MeV). This results in an irradiated average upper shelf energy of 118 ft-lbs for the longitudinally oriented specimens.

- The average upper shelf energy of the lower shell plate F-773-1 Charpy specimens (transverse orientation) resulted in an average energy decrease of 21.5 ft-lbs after irradiation to 4.071 x 10^{18} n/cm^2 (E > 1.0 MeV). This results in an irradiated average upper shelf energy of 115 ft-lbs for the transversely oriented specimens.

- The average upper shelf energy of the weld metal Charpy specimens resulted in an average energy decrease of 1 ft-lb after irradiation to 4.071 x 10^{18} n/cm^2 (E > 1.0 MeV). This results in an irradiated average upper shelf energy of 108 ft-lbs for the weld metal specimens.

- The average upper shelf energy of the weld HAZ metal Charpy specimens increased 29 ft-lbs after irradiation to 4.071 x 10^{18} n/cm^2 (E > 1.0 MeV). This results in an irradiated average upper shelf energy of 113 ft-lbs for the weld HAZ metal.

- A comparison of the Palo Verde Unit 2 surveillance material 30 ft-lb transition temperature shifts and upper shelf energy decreases with Regulatory Guide 1.99, Revision 2[1], lead to the following conclusions:

  - The 30 ft-lb transition temperature increases of the surveillance weld metal and the longitudinally oriented lower shell plate F-773-1 Charpy test results are less than the Regulatory Guide 1.99, Revision 2[1], predictions.

  - The 30 ft-lb transition temperature increase and average upper shelf energy decrease of transversely oriented lower shell plate F-773-1 Charpy test results are in good agreement with Regulatory Guide 1.99, Revision 2[1], predictions.

  - The measured average upper shelf energy decrease of the weld metal and lower shell plate F-773-1 longitudinally oriented Charpy test results are less than the Regulatory Guide 1.99, Revision 2[1], predictions.

- The precracked Charpy specimen test results are in good agreement with the unirradiated test results[2]. The data are bounded by the K_{IR} curve, which provides a lower bound estimate for the fracture toughness.

- The calculated end-of-life (EOL) 32 effective full power years (EFPY) maximum neutron fluence (E > 1.0 MeV) for the Palo Verde Unit 2 reactor vessel is as follows:

Vessel inner radius*	$= 2.047 \times 10^{19}$ n/cm^2
Vessel 1/4 thickness	$= 1.087 \times 10^{19}$ n/cm^2
Vessel 3/4 thickness	$= 2.157 \times 10^{18}$ n/cm^2

* Clad/base metal interface

SECTION 2.0
INTRODUCTION

This report presents the results of the examination of the Palo Verde Unit 2 surveillance capsule removed from the 137° location. This is the first capsule to be removed from the reactor in the continuing surveillance program which monitors the effects of neutron irradiation on the Arizona Public Service Company Palo Verde Unit 2 reactor pressure vessel materials under actual operating conditions.

The surveillance program for the Arizona Public Service Company Palo Verde Unit 2 reactor pressure vessel materials was designed and recommended by ABB Combustion Engineering. A description of the preirradiation mechanical properties of the reactor vessel materials is presented in TR-V-MCM-013, "Arizona Public Service Company Palo Verde Unit 2 Evaluation for Baseline Specimens Reactor Vessel Materials Irradiation Surveillance Program"[2]. The surveillance program was planned to cover the 40-year design life of the reactor pressure vessel and was based on ASTM E185-82, "Standard Practice for Conducting Surveillance Tests for Light-Water Cooled Nuclear Power Reactor Vessels". The 137° capsule was removed from the reactor after less than 5 EFPY of exposure and shipped to the Westinghouse Science and Technology Center Hot Cell Facility, where the postirradiation mechanical testing of the Charpy V-notch impact, tensile and precracked Charpy V-notch surveillance specimens was performed.

This report summarizes the testing of and the post irradiation data obtained from the surveillance capsule removed from the 137° location of the Arizona Public Service Company Palo Verde Unit 2 reactor vessel and discusses the analysis of the data.

SECTION 3.0
BACKGROUND

The ability of the large steel pressure vessel containing the reactor core and its primary coolant to resist fracture constitutes an important factor in ensuring safety in the nuclear industry. The beltline region of the reactor pressure vessel is the most critical region of the vessel because it is subjected to significant fast neutron bombardment. The overall effects of fast neutron irradiation on the mechanical properties of low alloy, ferritic pressure vessel steels such as SA533 Grade B Class 1 (base material of the Palo Verde Unit 2 reactor pressure vessel) are well documented in the literature. Generally, low alloy ferritic materials show an increase in hardness and tensile properties and a decrease in ductility and toughness during high-energy irradiation.

A method for performing analyses to guard against fast fracture in reactor pressure vessels has been presented in "Protection Against Nonductile Failure," Appendix G to Section III of the ASME Boiler and Pressure Vessel Code[3]. The method uses fracture mechanics concepts and is based on the reference nil-ductility transition temperature (RT_{NDT}).

RT_{NDT} is defined as the greater of either the drop weight nil-ductility transition temperature (NDTT per ASTM E-208[4]) or the temperature 60°F less than the 50 ft-lb (and 35-mil lateral expansion) temperature as determined from Charpy specimens oriented normal (transverse) to the major working direction of the plate. The RT_{NDT} of a given material is used to index that material to a reference stress intensity factor curve (K_{IR} curve) which appears in Appendix G to the ASME Code[3]. The K_{IR} curve is a lower bound of dynamic, crack arrest, and static fracture toughness results obtained from several heats of pressure vessel steel. When a given material is indexed to the K_{IR} curve, allowable stress intensity factors can be obtained for this material as a function of temperature. Allowable operating limits can then be determined using these allowable stress intensity factors.

RT_{NDT} and, in turn, the operating limits of nuclear power plants can be adjusted to account for the effects of radiation on the reactor vessel material properties. The changes in mechanical properties of a given reactor pressure vessel steel, due to irradiation, can be monitored by a reactor vessel surveillance program, such as the Palo Verde Unit 2 reactor vessel materials irradiation surveillance program[2], in which a surveillance capsule is periodically removed from the operating nuclear reactor and the encapsulated specimens tested.

The increase in the average Charpy V-notch 30 ft-lb temperature (ΔRT_{NDT}) due to irradiation is added to the initial RT_{NDT} to adjust the RT_{NDT} (ART) for radiation embrittlement. The ART (RT_{NDT} initial + ΔRT_{NDT}) is used to index the material to the K_{IR} curve and, in turn, to set operating limits for the nuclear power plant that take into account the effects of irradiation on the reactor vessel materials.

SECTION 4.0
DESCRIPTION OF PROGRAM

Six surveillance capsules for monitoring the effects of neutron exposure on the Palo Verde Unit 2 reactor pressure vessel core region materials were inserted in the reactor vessel prior to initial plant start-up. The six capsules were positioned in the reactor vessel between the core support barrel and the vessel wall as shown in Figure 4-1. The vertical center of the capsules is opposite the vertical center of the core. The capsule, removed from the 137° location, consisted of three compartments (Figure 4-2). Each compartment consisted of two sections attached by a connecting spacer. The top and bottom compartments of the capsule (Figure 4-3) contained Charpy V-notch and precracked Charpy V-notch specimens along with flux monitors. The middle compartment of the capsule (Figure 4-4) contained tension and Charpy V-notch specimens along with flux and temperature monitors. The test specimens contained in the capsule were made from lower shell plate F-773-1 and submerged arc weld metal fabricated with Mil B-4 weld filler wire and are representative of the reactor vessel beltline region materials. The capsule was removed after 4.54 EFPY of plant operation. This capsule contained Charpy V-notch, tensile, and precracked Charpy V-notch specimens made from lower shell plate F-773-1 and submerged arc weld metal representative of the reactor vessel beltline welds. In addition, this capsule contained Charpy V-notch specimens from the Heavy Section Steel Technology (HSST) plate 01MY and the weld HAZ metal from lower shell plate F-773-1.

The Palo Verde Unit 2 reactor vessel lower shell plate F-773-1 was fabricated from steel plate produced according to ASME Specification SA-533 Grade B Class 1 mechanical properties. The Palo Verde Unit 2 surveillance plate material was taken from sections of lower shell plate F-773-1. Weld metal material was fabricated by welding together lower shell plates F-773-2 and F-773-3. Weld HAZ test material was fabricated by welding together lower shell plates F-773-1 and F-773-2. Test specimens were machined from approximately the 1/4 thickness (1/4T) location. Specimens from the weld metal were machined from a weldment joining lower shell plate F-773-2 and adjacent lower shell plate F-773-3. All heat-affected-zone specimens were obtained from the weld heat-affected-zone of lower shell plate F-773-1. The Palo Verde Unit 2 surveillance capsule also contained Charpy V-notch specimens from a standard heat of ASTM A 533 Grade B Class 1 manganese-molybdenum-nickel steel made available by the NRC sponsored HSST Program. This reference material has been fully processed and characterized and was used for Charpy impact specimen correlation monitors.

Charpy V-notch impact and tension specimens were machined from lower shell plate F-773-1 in both the longitudinal orientation (longitudinal axis of the specimen parallel to the major rolling direction of the plate) and transverse orientation (longitudinal axis of the specimen normal to the major rolling direction of the plate). Charpy V-notch and tensile specimens from the weld metal were oriented such that the long dimension of the specimen was normal to the welding direction. The notch of the weld metal Charpy specimens was machined such that the direction of crack propagation in the specimen is in the welding direction. Precracked Charpy V-notch test specimens from lower shell plate F-773-1 were machined in both the longitudinal and transverse orientations and precracked Charpy V-notch specimens from the weld metal were machined such that the simulated crack in the specimen would propagate in the direction of welding.

The chemical composition and heat treatment of the surveillance material is presented in Tables 4-1 and 4-2. The chemical analysis reported in Table 4-1 was obtained from unirradiated material used in the surveillance program[2].

The capsule contained flux monitors made of sulfur, titanium, iron, nickel (cadmium shielded), copper (cadmium shielded), cobalt (cadmium shielded and unshielded) and uranium (cadmium shielded and unshielded).

The capsule contained thermal monitors made from four low-melting-point eutectic alloys sealed in glass tubes. These thermal monitors were used to define the maximum temperature attained by the test specimens during irradiation. The composition of the four eutectic alloys and their melting points are as follows:

80% Au, 20% Sn	Melting Point: 536°F (280°C)
90% Pb, 5% Sn, 5% Ag	Melting Point: 558°F (292°C)
2.5% Ag, 97.5% Pb	Melting Point: 580°F (304°C)
1.75% Ag, 0.75% Sn, 97.5% Pb	Melting Point: 590°F (310°C)

TABLE 4-1		
Chemical Composition (wt%) of the Palo Verde Unit 2 Reactor Vessel Surveillance Materials[2]		
Element	Plate F-773-1	Weld Metal F-773-2/F-773-3
Si	0.21	0.47
S	0.009	0.011
P	0.006	0.010
Mn	1.54	1.46
C	0.24	0.12
Cr	0.03	0.10
Ni	0.68	0.09
Mo	0.52	0.51
V	0.003	0.005
Cb	<0.01	<0.01
B	<0.001	<0.001
Co	0.016	0.010
Cu	0.04	0.07
Al	0.015	0.005
W	0.010	0.010
Ti	<0.01	<0.01
As	0.021	0.010
Sn	0.003	0.004
Zr	<0.001	<0.001
N	0.014	0.011
Sb	0.0018	0.0114

TABLE 4-2

Heat Treatment of the Palo Verde Unit 2 Reactor Vessel Surveillance Materials[2]

Material	Temperature (°F)	Time (hr)	Coolant
Surveillance Program Test Plate F-773-1	Austenitizing: 1600 ± 25	4	Water quenched
	Tempered: 1225 ± 25	4	Air cooled
	Stress Relief: 1150 ± 50	40	Furnace cooled to 600°F
Weldment	Stress Relief: 1125 ± 25	44 hr. & 48 min.	Furnace cooled to 600°F

TABLE 4-3

Summary of Unirradiated Surveillance Material Data[2]

Material and Code	C_v Upper Shelf (ft-lb)	30 ft-lb Index (°F)	50 ft-lb Index (°F)	35 Mils Lat. Exp. Index (°F)	NDTT (°F)	RT_{NDT} (°F)	RT Yield Strength (ksi)	
							Static	Dynamic
Base Metal Plate F-773-1 (WR) (Transverse)	136.5	-4	30	5	-40	-10	61.7	107.7
Base Metal Plate F-773-1 (RW) (Longitudinal)	112	0	35	12	-40	10	64.1	91.4
Weld Metal F-773-2/F-773-3	109	-43	-11	-41	-70	-50	63.3/62.2	85.0
HAZ Metal F-773-1/F-773-2	84	-12	57	2	-30	50	-	-
SRM HSST Plate 01MY (RW) (Longitudinal)	136	3	34	14	0	-	-	-

TABLE 4-4		
Arrangement of Encapsulated Test Specimens by Code Number within the Palo Verde Unit 2 137° Capsule[5]		
Compartment Position	Compartment Number	Specimen Numbers
1	1B312	1B23L 1B23P 1B243 1B26D 1B22E 1B2AE 1B24J 1B23M 1B267 1B22M 1B224 1B2AM 1B255 1B22U 1B21U
2	1B322-1	1B27B 1B213 1B23T 1B226 1B26C 1B245 1B275 1B25Y 1B22T 1B14J 1B11K 1B116 1B141 1B13M 1B14B 1B151 1B113 1B12L
3	1B332-4	1B2K1 1B2J3 1B2J2 1B44D 1B43B 1B43K 1B444 1B432 1B43Y 1B41B 1B44L 1B43T 1B411 1B456 1B43M
4	1B34D-3	1BD43 1BD35 1BD52 1BD4P 1BD2D 1BD3E 1BD2M 1BD3Y 1BD2B 1B3J5 1B3JY 1B3J7
5	1B353	1B35E 1B34U 1B3AL 1B34E 1B35P 1B35M 1B3A3 1B33E 1B3AD 1B31B 1B316 1B32A 1B342 1B326 1B312
6	1B363-1	1B33Y 1B36M 1B33J 1B37A 1B31U 1B3AT 1B31A 1B31K 1B323 1B11M 1B11E 1B124 1B14Y 1B145 1B15D 1B14D 1B12B 1B136

CODE:

Specimen ID.	Material
1B1XX	Lower Shell Plate F-773-1 (Longitudinal Orientation)
1B2XX	Lower Shell Plate F-773-1 (Transverse Orientation)
1B3XX	Weld Metal
1B4XX	Heat-Affected-Zone Material
1BDXX	SRM HSST 01MY Material (Longitudinal Orientation)

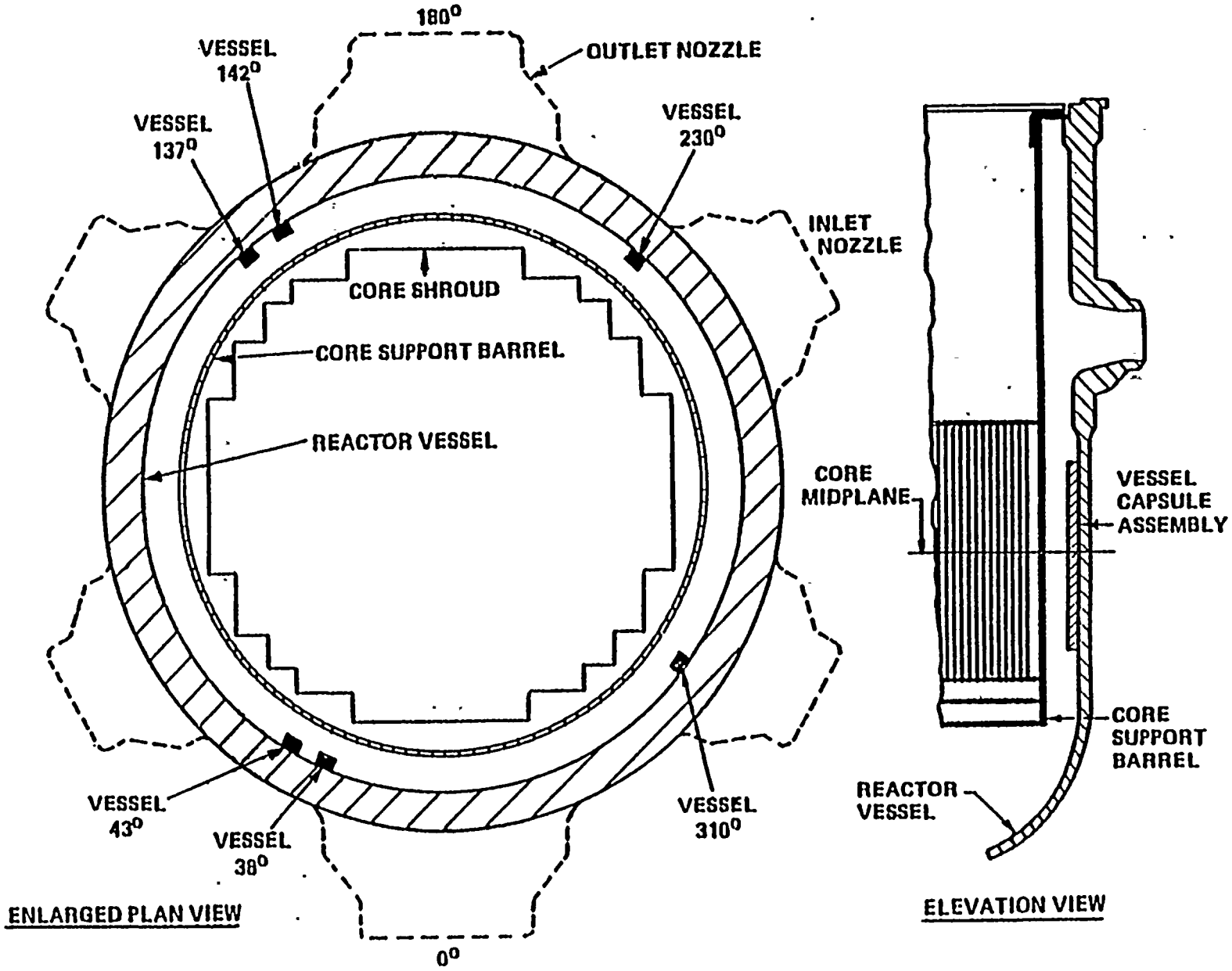

Figure 4-1. Arrangement of Surveillance Capsules in the Palo Verde Unit 2 Reactor Vessel

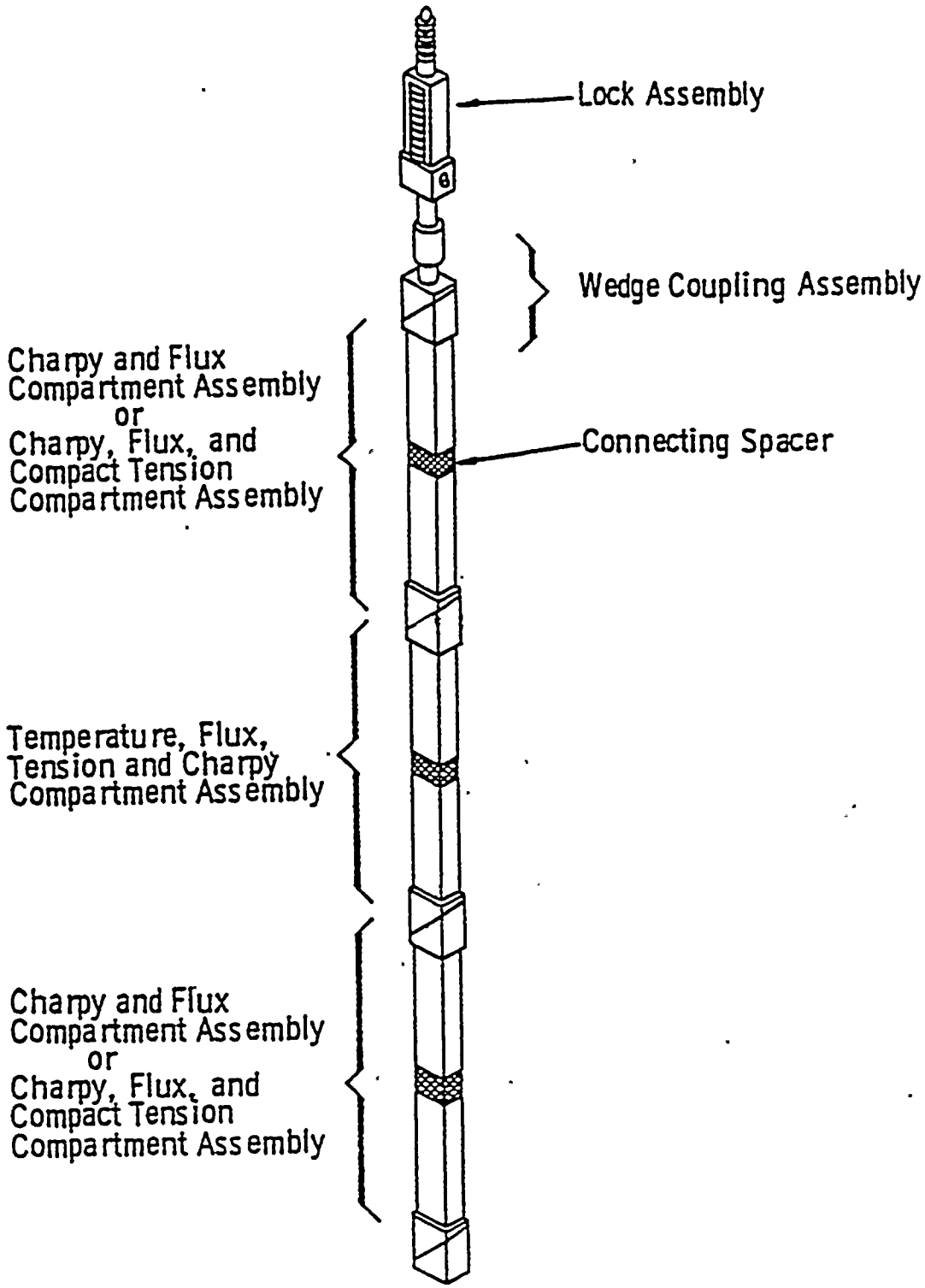

Figure 4-2. Typical Palo Verde Unit 2 Surveillance Capsule Assembly

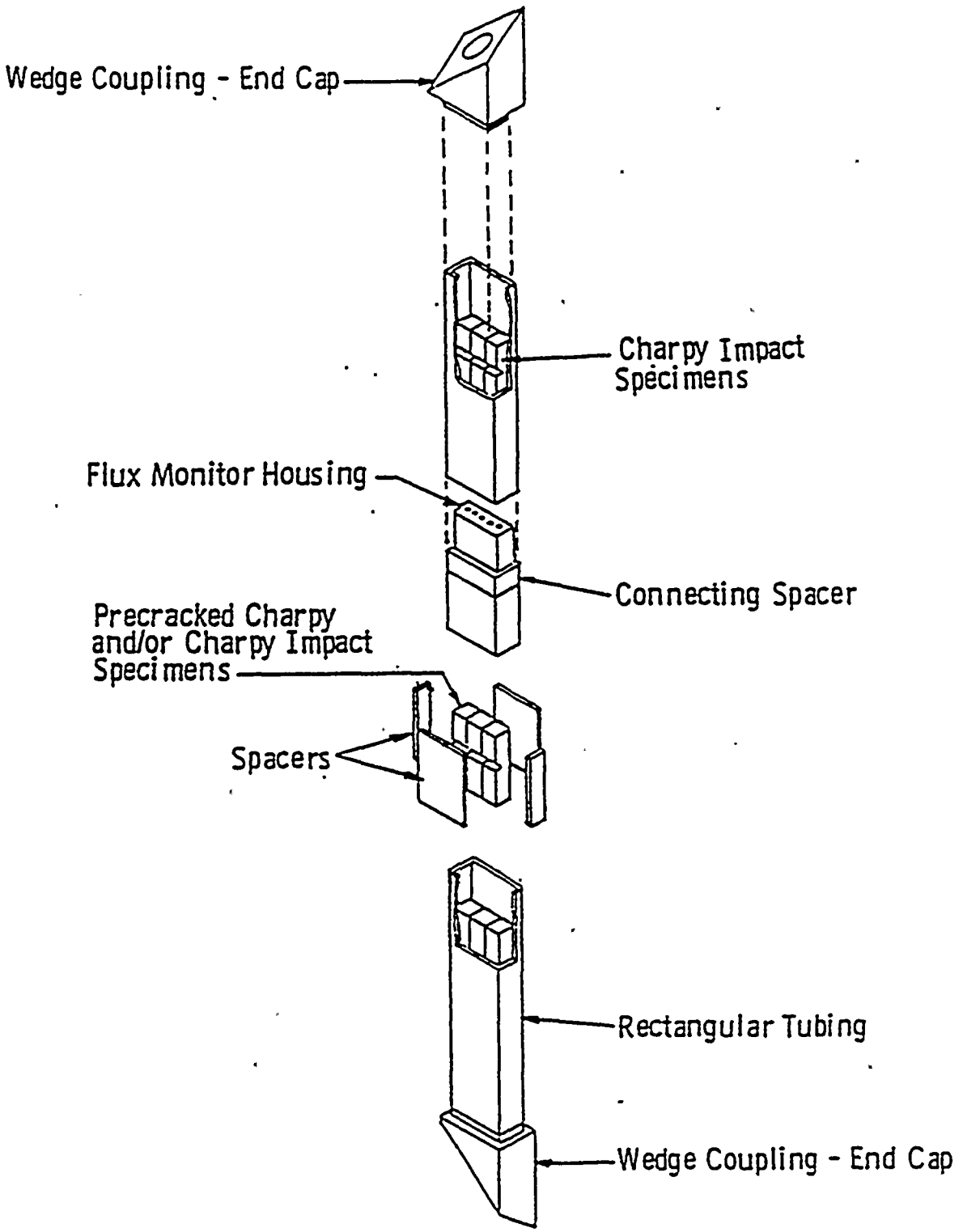

Figure 4-3. Typical Palo Verde Unit 2 Surveillance Capsule Charpy Impact Compartment Assembly

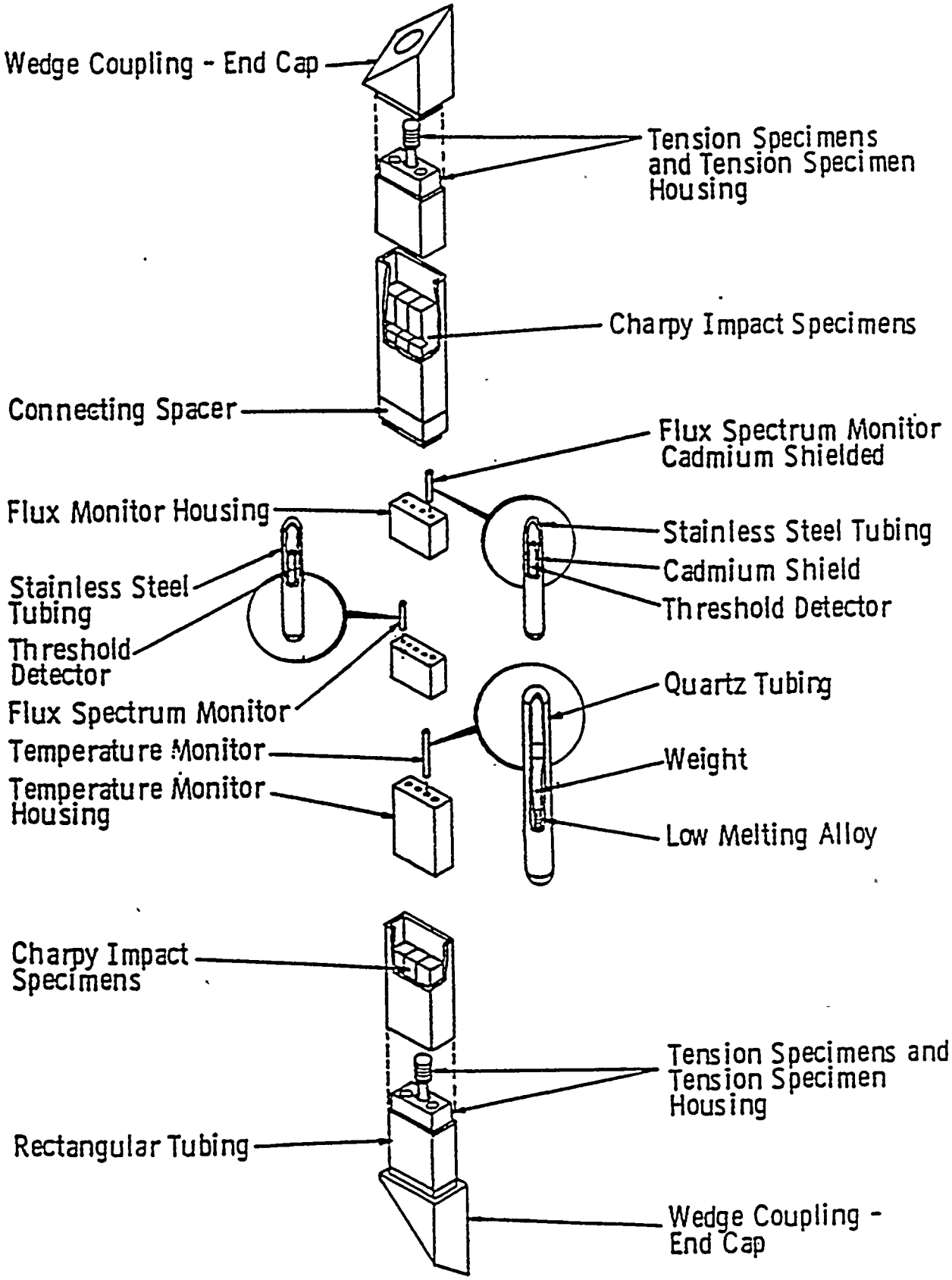

Figure 4-4. Typical Palo Verde Unit 2 Surveillance Capsule Tensile-Monitor Compartment Assembly

SECTION 5.0
TESTING OF SPECIMENS FROM CAPSULE W137

5.1 Overview

The post-irradiation mechanical testing of the Charpy V-notch impact, precracked Charpy and tensile specimens was performed in the Remote Metalograhpic Facility (RMF) at the Westinghouse Science and Technology Center. Testing was performed in accordance with 10CFR50, Appendices G and H[6] and ASTM Specification E185-82[7] and Westinghouse Procedure RMF 8402, Revision 2 as modified by Westinghouse RMF Procedure 8102, Revision 1, and 8103, Revision 1.

Upon receipt of the capsule at the hot cell laboratory, the specimens and spacer blocks were carefully removed, inspected for identification number, and checked against the master list in Reference 5. No discrepancies were found.

Examination of the four low-melting point 536°F (280°C), 558°F (292°C), 580°F (304°C) and 590°F (310°C) eutectic alloys indicated that the two thermal monitors with melting points of 536°F (280°C) and 558°F (292°C) melted (Figure 5-1). Based on this examination, the maximum temperature to which the test specimens were exposed was less than 580°F (304°C).

The Charpy impact tests were performed per ASTM Specification E23-92[8] and RMF Procedure 8103, Revision 1, and NSMT Procedure 9306, on a Tinius-Olsen Model 74, 358J machine. The tup (striker) of the Charpy impact test machine is instrumented with a GRC 830-I instrumentation system, feeding information into an IBM XT Computer. With this system, load-time and energy-time signals can be recorded in addition to the standard measurement of Charpy energy (E_D). From the load-time curve, the load of general yielding (P_{GY}), the time to general yielding (t_{GY}), the maximum load (P_M), and the time to maximum load (t_M) can be determined. Under some test conditions, a sharp drop in load indicative of fast fracture was observed. The load at which fast fracture was initiated is identified as the fast fracture load (P_F), and the load at which fast fracture terminated is identified as the arrest load (P_A). The energy at maximum load (E_M) was determined by comparing the energy-time record and the load-time record. The energy at maximum load is approximately equivalent to the energy required to initiate a crack in the specimen. Therefore, the propagation energy for the crack (E_p) is the difference between the total energy to fracture (E_D) and the energy at maximum load (E_M).

The yield stress (σ_Y) was calculated from the three-point bend formula having the following expression:

$$\sigma_Y = [P_{GY} * L] / [B * (W - a)^2 * C] \quad (1)$$

where: L = distance between the specimen supports in the impact machine
B = the width of the specimen measured parallel to the notch
W = height of the specimen, measured perpendicularly to the notch
a = notch depth

The constant C is dependent on the notch flank angle (ϕ), notch root radius (ρ) and the type of loading (ie. pure bending or three-point bending). In three-point bending, for a Charpy specimen in which $\phi = 45°$ and $\rho = 0.010"$, Equation 1 is valid with C = 1.21. Therefore, (for L = 4W),

$$\sigma_Y = [P_{GY} * L] / [B * (W - a)^2 * 1.21] = [3.3 * P_{GY} * W] / [B * (W - a)^2] \quad (2)$$

For the Charpy specimen, B = 0.394", W = 0.394" and a = 0.079" Equation 2 then reduces to:

$$\sigma_Y = 33.3 * P_{GY} \quad (3)$$

where σ_Y is in units of psi and P_{GY} is in units of lbs. The flow stress was calculated from the average of the yield and maximum loads, also using the three-point bend formula.

Percent shear was determined from post-fracture photographs using the ratio-of-areas methods in compliance with ASTM Specification A370-92[9]. The lateral expansion was measured using a dial gage rig similar to that shown in the same specification.

In addition to the standard Charpy test specimens, the capsule also contained precracked Charpy specimens. Testing of the precracked Charpy specimens provides estimates of the dynamic fracture toughness of the irradiated materials contained in the capsule using small specimens, rather than much larger ones used in Fracture Mechanics.

Although the Charpy specimens are too small to allow valid determinations of the fracture toughness, the testing of sub-sized specimens, makes it feasible to test multiple irradiated specimens.

The precracked Charpy test offers the further advantage of being simple to perform. The test requires an instrumented Charpy impact machine and the ability to adjust the drop height of the impact hammer. The load-time data for each test is recorded using high speed data acquisition equipment. The tests in this program were conducted using the same system as for standard Charpy specimens, ie., a Tinius-Olsen Model 74 Charpy impact machine equipped with a Dynatup Products Model 830-I data acquisition system. The adjustable drop height capability is required to allow proper analysis of the test records. The early portion of the test record is dominated by oscillations in the load signal caused by the inertial loading that occurs when the hammer impacts the specimen. The Charpy hammer must be lowered to reduce the inertial effects and to increase the length of the test. In general, the primary points of analysis (general yielding, etc.) should occur at least 100 msec after the initial impact.

The load time records must be analyzed to determine fracture toughness values. The initial velocity of the Charpy hammer was determined using the Dynatup instrumentation system. The velocity measurement was then used to interpret the load-time record in terms of load and displacement. This data was then analyzed to provide an energy versus time curve. The analysis of the instrumented data was performed using the standard Dynatup system software. At low temperatures, the specimens fail in a brittle manner, with no evidence of yielding in the test record. Specimens that failed in a brittle manner were analyzed using standard linear-elastic techniques to determine a dynamic fracture toughness, K_{Id}. The determination of K_{Id} requires only a knowledge of the precrack length, which was determined from post test photos, and the maximum load, which was determined from the test record. At higher temperatures, the test records indicate that general yielding of the specimens occurs prior to failure. Elastic-plastic analysis was required to estimate a dynamic fracture toughness value, K_{Jd}, in the higher temperature specimens. In small specimens, maximum load generally occurs at the onset of crack growth. The determination of K_{Jd} requires a knowledge of the energy absorbed in the specimen at maximum load, and the crack length. The energy calculated by the instrumentation system includes both the energy absorbed in the specimen and the energy absorbed by the elastic deformation of the Charpy system. The total system compliance was determined and the Charpy specimen compliance was calculated to allow correction of the measured energy values. The corrected value of energy absorbed at maximum load, E_I, was then used to calculate K_{Jd} according to the formula:

$$K_{Jd} = [(2*E_I*E)/(b*B)]^{1/2} \quad (4)$$

where,

E = Young's Modulus

b = Remaining ligament (specimen depth less crack length)

B = Specimen thickness

The test records were also analyzed to determine the dynamic yield strength, s_{yd}. The general formula for the determination of general yielding for a member in three point bending is (in analogy to equation 2):

$$s_{yd} = [(3.3 * P_{gy} * W)/(b * B)^2] \quad (5)$$

where,

W = Specimen depth

P_{gy} = Load at general yielding

Three sets of precracked Charpy specimens were contained in the surveillance capsule. These sets included specimens from plate F-773-1 (both transverse and longitudinal orientations) and from the surveillance weld metal.

Tensile tests were performed on a 20,000-pound Instron, split-console test machine (Model 1115) per ASTM Specification E8-91[10] and E21-79(1988)[11], and RMF Procedure 8102, Revision 1. All pull rods, grips, and pins were made of Inconel 718. The upper pull rod was connected through a universal joint to improve axiality of loading. The tests were conducted at a constant crosshead speed of 0.05 inches per minute throughout the test.

Extension measurements were made with a linear variable displacement transducer extensometer. The extensometer knife edges were spring-loaded to the specimen and operated through specimen failure. The extensometer gage length was 1.00 inch. The extensometer is rated as Class B-2 per ASTM E83-92[12].

Elevated test temperatures were obtained with a three-zone electric resistance split-tube furnace with a 9-inch hot zone. All tests were conducted in air. Because of the difficulty in remotely attaching a thermocouple directly to the specimen, the following procedure was used to monitor specimen temperatures. Chromel-alumel thermocouples were positioned at center and each end of

the gage section of a dummy specimen and in each grip. In the test configuration, with a slight load on the specimen, a plot of specimen temperature versus upper and lower grip and controller temperatures was developed over the range from room temperature to 550°F (288°C). During the actual testing, the grip temperatures were used to obtain desired specimen temperatures. Experiments indicated that this method is accurate to $\pm$2°F.

The yield load, ultimate load, fracture load, total elongation, and uniform elongation were determined directly from the load-extension curve. The yield strength, ultimate strength, and fracture strength were calculated using the original cross-sectional area. The final diameter and final gage length were determined from post-fracture photographs. The fracture area used to calculate the fracture stress (true stress at fracture) and percent reduction in area was computed using the final diameter measurement.

5.2 Charpy V-Notch Impact Test Results

The results of the Charpy V-notch impact tests performed on the various materials contained in the capsule, which was irradiated to 4.071 x 10^{18} n/cm^2 (E > 1.0 MeV), are presented in Tables 5-1 through 5-10 and are compared with unirradiated results[2] as shown in Figures 5-2 through 5-6. The transition temperature increases and upper shelf energy changes for the surveillance materials are summarized in Table 5-11.

Irradiation of the reactor vessel lower shell plate F-773-1 Charpy specimens oriented with the longitudinal axis of the specimen parallel to the major rolling direction of the plate (longitudinal orientation) to 4.071 x 10^{18} n/cm^2 (E > 1.0 MeV) at 550°F (Figure 5-2) resulted in a 30 ft-lb transition temperature increase of 10°F and a 50 ft-lb transition temperature increase of 25°F. This resulted in an irradiated 30 ft-lb transition temperature of 10°F and an irradiated 50 ft-lb transition temperature of 60°F (longitudinal orientation).

The average upper shelf energy (USE) of the lower shell plate F-773-1 Charpy specimens (longitudinal orientation) resulted in an energy increase of 6 ft-lb after irradiation to 4.071 x 10^{18} n/cm^2 (E > 1.0 MeV) at 550°F. This results in an irradiated average USE of 118 ft-lb (Figure 5-2).

Irradiation of the reactor vessel lower shell plate F-773-1 Charpy specimens oriented with the longitudinal axis of the specimen normal to the major rolling direction of the plate (transverse

orientation) to 4.071 x 10^{18} n/cm^2 (E > 1.0 MeV) at 550°F (Figure 5-3) resulted in a 30 ft-lb transition temperature increase of 19°F and a 50 ft-lb transition temperature increase of 25°F. This results in an irradiated 30 ft-lb transition temperature of 15°F and an irradiated 50 ft-lb transition temperature of 55°F (transverse orientation).

The average USE of the lower shell plate F-773-1 Charpy specimens (transverse orientation) resulted in an average energy decrease of 21.5 ft-lbs after irradiation to 4.071 x 10^{18} n/cm^2 (E > 1.0 MeV) at 550°F. This results in an irradiated average USE of 115 ft-lb (Figure 5-3).

Irradiation of the surveillance weld metal Charpy specimens to 4.071 x 10^{18} n/cm^2 (E > 1.0 MeV) at 550°F (Figure 5-4) resulted in a 30 and 50 ft-lb transition temperature increase of 15°F. This results in an irradiated 30 ft-lb transition temperature of -28°F and an irradiated 50 ft-lb transition temperature of 4°F.

The average USE of the surveillance weld metal resulted in an energy decrease of 1 ft-lb after irradiation to 4.071 x 10^{18} n/cm^2 (E > 1.0 MeV) at 550°F. This resulted in an irradiated average USE of 108 ft-lb (Figure 5-4).

Irradiation of the reactor vessel weld HAZ metal Charpy specimens to 4.071 x 10^{18} n/cm^2 (E > 1.0 MeV) at 550°F (Figure 5-5) resulted in a 30 ft-lb transition temperature increase of 57°F and a 50 ft-lb transition temperature increase of 18°F. This results in an irradiated 30 ft-lb transition temperature of 45°F and an irradiated 50 ft-lb transition temperature of 75°F.

The average USE of the weld HAZ metal resulted in an energy increase of 29 ft-lbs after irradiation to 4.071 x 10^{18} n/cm^2 (E > 1.0 MeV) at 550°F. This resulted in an irradiated average USE of 113 ft-lb (Figure 5-5).

Irradiation of the HSST plate 01MY Charpy specimens to 4.071 x 10^{18} n/cm^2 (E > 1.0 MeV) at 550°F (Figure 5-6) resulted in a 30 ft-lb transition temperature increase of 117°F and a 50 ft-lb transition temperature increase of 151°F. This results in an irradiated 30 ft-lb transition temperature of 120°F and an irradiated 50 ft-lb transition temperature of 185°F.

The average USE of the HSST plate 01MY Charpy specimens resulted in an energy decrease of 31 ft-lbs after irradiation to 4.071 x 10^{18} n/cm^2 (E > 1.0 MeV) at 550°F. This resulted in an irradiated average USE of 105 ft-lb (Figure 5-6)

The fracture appearance of each irradiated Charpy specimen from the various materials is shown in Figures 5-7 through 5-11 and show an increasingly ductile or tougher appearance with increasing test temperature.

A comparison of the 30 ft-lb transition temperature increases and upper shelf energy decreases for the various Palo Verde Unit 2 surveillance materials with predicted values using the methods of NRC Regulatory Guide 1.99, Revision 2[1] is presented in Table 5-12 and led to the following conclusions:

- The 30 ft-lb transition temperature increases for the surveillance weld metal and the longitudinally oriented lower shell plate F-773-1 Charpy test results are less than the Regulatory Guide 1.99, Revision 2, predictions.

- The 30 ft-lb transition temperature increase and average upper shelf energy decrease of transversely oriented lower shell plate F-773-1 Charpy test results are in good agreement with Regulatory Guide 1.99, Revision 2, predictions.

- The measured average USE decrease of the weld metal and lower shell plate F-773-1 longitudinally oriented Charpy test results are less than the Regulatory Guide 1.99, Revision 2, predictions.

The load-time records for the Charpy impact tests are provided in Figures A-2 through A-31 in Appendix A.

5.3 Precracked Charpy Specimen Test Results

The results of the precracked Charpy specimen tests are reported in Tables 5-13 through 5-15 and in Figures 5-12 through 5-14. Data for the unirradiated materials was reported in the original ABB-Combustion Engineering report[2]. The unirradiated and irradiated precrack Charpy data are both included in Figures 5-12 through 5-14. The data is plotted on the basis of the RT_{NDT} value to eliminate the effects of the relatively small shifts in the ductile-to-brittle temperature. These figures indicate good agreement between the irradiated and unirradiated test results. The K_I reference (K_{IR}) curve is also shown in Figures 5-12 through 5-14. The data is bounded by the K_{IR} curve, which should provide a lower bound estimate for the fracture toughness. The low temperature

unirradiated and irradiated data, which was determined using linear-elastic procedures (K_{Id}), approaches the bounding curve. The low fracture toughness values may be attributed to the sub-sized specimens, which do not meet standard validity requirements.

The load-time records and comparisons of data for the unirradiated and irradiated precracked Charpy specimen tests are provided in Figures A-32 through A-56 in Appendix A.

5.4 Tension Test Results

The results of the tension tests performed on the various materials contained in the capsule irradiated to 4.071 x 10^{18} n/cm^2 (E > 1.0 MeV) are presented in Table 5-16 and are compared with unirradiated results[2] as shown in Figures 5-18 and 5-19.

The results of the tension tests performed on the lower shell plate F-773-1 (transverse orientation) indicated that irradiation to 4.071 x 10^{18} n/cm^2 (E > 1.0 MeV) at 550°F caused a 0 to 4 ksi increase in the 0.2 percent offset yield strength and a 0 to 3 ksi increase in the ultimate tensile strength when compared to unirradiated data[2] (Figure 5-18).

The results of the tension tests performed on the surveillance weld metal indicated that irradiation to 4.071 x 10^{18} n/cm^2 (E > 1.0 MeV) at 550°F caused a 5 to 8 ksi increase in the 0.2 percent offset yield strength and a 4 to 5 ksi increase in the ultimate tensile strength when compared to unirradiated data[2] (Figure 5-19).

The fractured tension specimens for the lower shell plate F-773-1 material are shown in Figure 5-20, while the fractured specimens for the surveillance weld metal are shown in Figure 5-21.

The engineering Stress-strain curves for the tension tests are shown in Figures 5-22 through 5-25.

TABLE 5-1

Charpy V-notch Data for the Palo Verde Unit 2 Lower Shell Plate F-773-1
Irradiated at 550°F to a Fluence of 4.071 X 10^{18} n/cm^2 (E > 1.0 MeV)
(Longitudinal Orientation)

Sample Number	Temperature		Impact Energy		Lateral Expansion		Shear
	(°F)	(°C)	(ft-lb)	(J)	(mils)	(mm)	(%)
1B11E	-5	-21	28	38	30	0.76	10
1B124	10	-12	27	37	26	0.66	20
1B11M	25	-4	47	64	43	1.09	25
1B15D	50	10	33	45	33	0.84	30
1B14Y	75	24	58	79	54	1.37	50
1B136	115	46	82	111	70	1.78	70
1B145	150	66	92	125	77	1.96	85
1B14D	200	93	108	146	79	2.01	100
1B12B	250	121	127	172	94	2.39	100

TABLE 5-2

Charpy V-notch Data for the Palo Verde Unit 2 Lower Shell Plate F-773-1
Irradiated at 550°F to a Fluence of 4.071 X 10^{18} n/cm^2 (E > 1.0 MeV)
(Transverse Orientation)

Sample	Temperature		Impact Energy		Lateral Expansion		Shear
Number	(°F)	(°C)	(ft-lb)	(J)	(mils)	(mm)	(%)
1B255	-25	-32	16	22	15	0.38	5
1B23L	0	-18	24	33	24	0.61	10
1B2AE	15	-9	30	41	29	0.74	20
1B224	25	-4	62	84	54	1.37	25
1B267	35	2	42	57	38	0.97	30
1B23P	50	10	43	58	45	1.14	40
1B2AM	65	18	58	79	50	1.27	40
1B26D	75	24	43	58	41	1.04	45
1B21U	85	29	63	85	55	1.40	50
1B22U	100	38	67	91	57	1.45	60
1B22E	125	52	73	99	67	1.70	70
1B24J	150	66	105	142	89	2.26	95
1B243	200	93	116	157	83	2.11	95
1B22M	250	121	115	156	90	2.29	100
1B23M	300	149	115	156	92	2.34	100

TABLE 5-3

Charpy V-notch Data for the Palo Verde Unit 2 Surveillance Weld Metal Irradiated at 550°F to a Fluence of 4.071 X 10^{18} n/cm^2 (E > 1.0 MeV)

Sample Number	Temperature		Impact Energy		Lateral Expansion		Shear
	(°F)	(°C)	(ft-lb)	(J)	(mils)	(mm)	(%)
1B3AD	-90	-68	13	18	16	0.41	10
1B316	-80	-62	38	52	38	0.97	15
1B35E	-50	-46	12	16	15	0.38	15
1B342	-30	-34	28	38	36	0.91	25
1B34U	-20	-29	33	45	33	0.84	30
1B312	-10	-23	53	72	51	1.30	35
1B34E	0	-18	50	68	46	1.17	35
1B35P	25	-4	57	77	56	1.42	50
1B326	50	10	88	119	78	1.98	70
1B3A3	75	24	75	102	70	1.78	80
1B3AL	100	38	93	125	81	2.06	90
1B35M	125	52	92	126	85	2.16	95
1B33E	150	66	106	144	95	2.41	100
1B31B	200	93	107	145	86	2.18	100
1B32A	250	121	112	152	95	2.41	100

TABLE 5-4

Charpy V-notch Data for the Palo Verde Unit 2 Heat-Affected-Zone (HAZ) Metal Irradiated at 550°F to a Fluence of 4.071 X 10^{18} n/cm^2 (E > 1.0 MeV)

Sample Number	Temperature		Impact Energy		Lateral Expansion		Shear
	(°F)	(°C)	(ft-lb)	(J)	(mils)	(mm)	(%)
1B411	-35	-37	16	22	16	0.41	5
1B44D	0	-18	20	27	24	0.61	10
1B43B	25	-4	20	27	15	0.38	15
1B43Y	35	2	28	38	29	0.74	20
1B432	50	10	18	24	24	0.61	30
1B43T	60	16	49	66	47	1.19	40
1B444	75	24	71	96	59	1.50	50
1B43M	100	38	86	117	71	1.80	65
1B43K	120	49	108	146	82	2.08	80
1B44L	155	68	77	104	70	1.78	95
1B456	200	93	133	180	87	2.21	100
1B41B	250	121	92	125	79	2.01	100

TABLE 5-5

Charpy V-notch Data for the Palo Verde Unit 2 Correlation Monitor Standard Reference Material HSST 01MY Irradiated at 550°F to a Fluence of 4.071 X 10^{18} n/cm^2 (E > 1.0 MeV) (Longitudinal Orientation)

Sample	Temperature		Impact Energy		Lateral Expansion		Shear
Number	(°F)	(°C)	(ft-lb)	(J)	(mils)	(mm)	(%)
1BD3Y	0	-18	7	9	8	0.20	5
1BD43	50	10	17	23	20	0.51	15
1BD4P	100	38	32	43	30	0.76	20
1BD35	150	66	45	61	46	1.17	40
1BD2D	200	93	35	47	32	0.81	35
1BD52	200	93	57	77	53	1.35	60
1BD3E	225	107	88	119	75	1.91	85
1BD2M	275	135	104	141	84	2.13	100
1BD2B	350	177	106	144	87	2.21	100

TABLE 5-6

Instrumented Charpy Impact Test Results for the Palo Verde Unit 2 Lower Shell Plate F-773-1
Irradiated at 550°F to a Fluence of 4.071 X 10^{18} n/cm^2 (E > 1.0 MeV) (Longitudinal Orientation)

Sample No.	Test Temp. (°F)	Charpy Energy E_D (ft-lb)	Normalized Energies (ft-lb/in^2)			Yield Load P_{GY} (lbs)	Time to Yield t_{GY} (μsec)	Max. Load P_M (lbs)	Time to Max. t_M (μsec)	Fast Fract. Load P_F (lbs)	Arrest Load P_A (lbs)	Yield Stress σ_Y (ksi)	Flow Stress (ksi)
			Charpy E_D/A	Max. E_M/A	Prop. E_P/A								
1B11E	-5	28	225	182	43	3189	0.17	3845	0.48	3839	397	106	117
1B124	10	27	217	155	62	3096	0.16	3719	0.43	3700	630	103	113
1B11M	25	47	378	278	101	3080	0.17	3959	0.68	3936	902	102	117
1B15D	50	33	266	154	112	3019	0.16	3750	0.42	3740	1276	100	112
1B14Y	75	58	467	280	187	2931	0.14	3969	0.68	3931	1707	97	115
1B136	115	82	660	343	317	2828	0.15	3936	0.82	3643	2115	94	112
1B145	150	92	741	272	469	2743	0.19	3724	0.72	2897	1628	91	107
1B14D	200	108	870	245	624	2427	0.14	3569	0.68	*	*	81	100
1B12B	250	127	1023	322	700	2499	0.14	3731	0.82	*	*	83	103

* Fully ductile fracture.

TABLE 5-7

Instrumented Charpy Impact Test Results for the Palo Verde Unit 2 Lower Shell Plate F-773-1
Irradiated at 550°F to a Fluence of 4.071 X 10^{18} n/cm^2 (E > 1.0 MeV) (Transverse Orientation)

Sample No.	Test Temp. (°F)	Charpy Energy E_D (ft-lb)	Normalized Energies (ft-lb/in^2)			Yield Load P_{GY} (lbs)	Time to Yield t_{GY} (μsec)	Max. Load P_M (lbs)	Time to Max. t_M (μsec)	Fast Fract. Load P_F (lbs)	Arrest Load P_A (lbs)	Yield Stress σ_Y (ksi)	Flow Stress (ksi)
			Charpy E_D/A	Max. E_M/A	Prop. E_P/A								
1B255	-25	16	129	89	40	3350	0.17	3648	0.28	3632	141	111	116
1B23L	0	24	193	147	46	3342	0.17	3869	0.40	3865	241	111	120
1B2AE	15	30	242	165	77	3136	0.16	3877	0.44	3864	904	104	116
1B224	25	62	499	359	104	3083	0.16	4094	0.82	3988	1116	102	119
1B267	35	42	338	252	86	2987	0.16	3881	0.63	3872	1022	99	114
1B23P	50	43	346	217	130	2931	0.17	3805	0.57	3792	1538	97	112
1B2AM	65	58	467	351	116	2948	0.16	4036	0.82	4023	1511	98	116
1B26D	75	43	346	197	149	2951	0.16	3873	0.52	3867	1900	98	113
1B21U	85	63	507	357	151	2922	0.14	4062	0.82	4053	2286	97	116
1B22U	100	67	540	279	261	2914	0.16	3986	0.69	3893	2155	97	115
1B22E	125	73	588	261	327	2639	0.14	3704	0.69	3663	2285	88	105
1B24J	150	105	845	260	586	2615	0.15	3693	0.69	2660	1858	87	105
1B243	200	116	934	313	621	2606	0.16	3774	0.80	*	*	87	106
1B22M	250	115	926	247	679	2371	0.14	3572	0.69	*	*	79	99
1B23M	300	115	926	279	647	2242	0.15	3393	0.80	*	*	74	94

* Fully ductile fracture.

TABLE 5-8

Instrumented Charpy Impact Test Results for the Palo Verde Unit 2 Surveillance Weld Metal
Irradiated at 550°F to a Fluence of 4.071 X 10^{18} n/cm^2 (E > 1.0 MeV)

Sample No.	Test Temp. (°F)	Charpy Energy E_D (ft-lb)	Normalized Energies (ft-lb/in^2)			Yield Load P_{GY} (lbs)	Time to Yield t_{GY} (μsec)	Max. Load P_M (lbs)	Time to Max. t_M (μsec)	Fast Fract. Load P_F (lbs)	Arrest Load P_A (lbs)	Yield Stress σ_Y (ksi)	Flow Stress (ksi)
			Charpy E_D/A	Max. E_M/A	Prop. E_P/A								
1B3AD	-90	13	105	63	42	3630	0.17	3681	0.21	3668	561	121	121
1B316	-80	38	306	210	96	3237	0.17	3810	0.54	3804	1644	108	117
1B35E	-50	12	97	43	54	3142	0.14	3463	0.18	3457	415	104	110
1B342	-30	28	225	149	76	3268	0.16	3767	0.41	3748	1384	109	117
1B34U	-20	33	266	172	94	3301	0.18	3862	0.46	3846	1556	110	119
1B312	-10	53	427	268	159	2961	0.15	3734	0.67	3673	1915	98	111
1B34E	0	50	403	269	134	3169	0.16	3878	0.65	3843	2864	105	117
1B35P	25	57	459	261	198	3042	0.16	3759	0.65	3746	2622	101	113
1B326	50	88	709	258	451	2758	0.14	3620	0.68	3277	2550	92	106
1B3A3	75	75	604	274	330	2974	0.16	3847	0.67	3443	2246	99	113
1B3AL	100	92	741	275	466	2922	0.15	3816	0.69	*	*	97	112
1B35M	125	93	749	269	480	2820	0.15	3751	0.69	*	*	94	109
1B33E	150	106	854	312	541	2586	0.14	3535	0.82	*	*	86	102
1B31B	200	107	862	301	561	2400	0.16	3451	0.82	*	*	80	97
1B32A	250	112	902	293	609	2318	0.16	3353	0.83	*	*	77	94

* Fully ductile fracture.

TABLE 5-9

Instrumented Charpy Impact Test Results for the Palo Vede Unit 2 Surveillance Heat-Affected-Zone (HAZ) Metal Irradiated at 550°F to a Fluence of 4.071 X 10^{18} n/cm^2 (E > 1.0 MeV)

Sample No.	Test Temp. (°F)	Charpy Energy E_D (ft-lb)	Normalized Energies (ft-lb/in^2)			Yield Load P_{GY} (lbs)	Time to Yield t_{GY} (μsec)	Max. Load P_M (lbs)	Time to Max. t_M (μsec)	Fast Fract. Load P_F (lbs)	Arrest Load P_A (lbs)	Yield Stress σ_Y (ksi)	Flow Stress (ksi)
			Charpy E_D/A	Max. E_M/A	Prop. E_P/A								
1B411	-35	16	129	89	40	3356	0.17	3645	0.28	3641	170	111	116
1B44D	0	20	161	105	56	3331	0.16	3732	0.31	3729	536	111	117
1B43B	25	20	161	105	56	3136	0.16	3491	0.32	3487	928	104	110
1B43Y	35	28	225	155	70	3248	0.17	3797	0.42	3768	1136	108	117
1B432	50	18	145	69	76	3057	0.16	3250	0.25	3244	1287	102	105
1B43T	60	49	395	270	125	3122	0.16	3919	0.65	3909	1724	104	117
1B444	75	71	572	284	288	3041	0.14	4024	0.67	3905	2022	101	117
1B43M	100	86	692	284	409	3057	0.16	4014	0.69	3189	1540	102	117
1B43K	120	108	870	377	492	2997	0.25	4086	0.94	3006	1940	100	118
1B44L	155	77	620	255	365	2807	0.15	3720	0.65	2775	1772	93	108
1B456	200	133	1071	345	726	2836	0.16	3833	0.86	*	*	94	111
1B41B	250	92	741	249	492	2650	0.17	3554	0.68	*	*	88	103

* Fully ductile fracture

TABLE 5-10

Instrumented Charpy Impact Test Results for the Palo Verde Unit 2 Surveillance Standard Reference Material HSST 01MY Irradiated at 550°F to a Fluence of 4.071 X 10^{18} n/cm^2 (E > 1.0 MeV) (Longitudinal Orientation)

Sample No.	Test Temp. (°F)	Charpy Energy E_D (ft-lb)	Normalized Energies (ft-lb/in^2)			Yield Load P_{GY} (lbs)	Time to Yield t_{GY} (μsec)	Max. Load P_M (lbs)	Time to Max. t_M (μsec)	Fast Fract. Load P_F (lbs)	Arrest Load P_A (lbs)	Yield Stress σ_Y (ksi)	Flow Stress (ksi)
			Charpy E_D/A	Max. E_M/A	Prop. E_P/A								
1BD3Y	0	7	56	29	27	3186	0.14	3289	0.15	3282	-	106	108
1BD43	50	17	137	96	41	3405	0.17	3783	0.29	3777	176	113	119
1BD4P	100	32	258	195	62	3263	0.17	4115	0.49	4096	521	108	123
1BD35	150	45	362	281	81	3096	0.16	4172	0.65	4156	1112	103	121
1BD2D	200	35	282	208	74	3090	0.16	4095	0.52	4085	845	103	119
1BD52	200	57	459	278	181	2965	0.15	4115	0.66	3994	1804	98	118
1BD3E	225	88	709	289	419	2966	0.16	4145	0.68	3485	2521	99	118
1BD2M	275	104	837	278	559	2900	0.17	4050	0.68	*	*	96	115
1BD2B	350	106	854	267	587	2724	0.16	3898	0.67	*	*	90	110

* Fully ductile fracture.

TABLE 5-11

Effect of 550°F Irradiation to 4.071 X 10^{18} n/cm^2 (E > 1.0 MeV) on the Notch Toughness Properties of the Palo Verde Unit 2 Reactor Vessel Surveillance Materials

Material	Average 30 (ft-lb) [a] Transition Temperature (°F)			Average 35 mil Lateral [a] Expansion Temperature (°F)			Average 50 ft-lb [a] Transition Temperature (°F)			Average Energy Absorption [a] at Full Shear (ft-lb)		
	Unirradiated	Irradiated	ΔT	Unirradiated	Irradiated	ΔT	Unirradiated	Irradiated	ΔT	Unirradiated	Irradiated	Δ
Plate F-773-1 (longitudinal)	0	10	10	12	25	13	35	60	25	112	118	+ 6
Plate F-773-1 (transverse)	- 4	15	19	5	25	20	30	55	25	136.5	115	- 21.5
Weld Metal	- 43	- 28	15	- 41	- 33	8	- 11	4	15	109	108	- 1
HAZ Metal	- 12	45	57	2	45	43	57	75	18	84	113	+ 29
SRM 01MY	3	120	117	14	155	141	34	185	151	136	105	- 31

(a) "Average" is defined as the value read from the curve fit through the data points of the Charpy tests (see Figures 5-1 through 5-5)

TABLE 5-12

Comparison of the Palo Verde Unit 2 Surveillance Material 30 ft-lb Transition Temperature Shifts and Upper Shelf Energy Decreases with Regulatory Guide 1.99 Revision 2 Predictions

Material	Fluence (E > 1.0 MeV) (X 10^{18} n/cm^2)	30 ft-lb Transition Temperature Shift		Upper Shelf Energy Decrease	
		Predicted [a] (°F)	Measured (°F)	Predicted [a] (%)	Measured (%)
Lower Shell Plate F-773-1 (longitudinal)	4.071	19.5	10	15.5	0
Lower Shell Plate F-773-1 (transverse)	4.071	19.5	19	15.5	16
Weld Metal	4.071	31.5	15	17	1
HAZ Metal	4.071	-	57	-	0
SRM HSST Plate 01MY (longitudinal)	4.071	-	117	-	23

(a) Based on Regulatory Guide 1.99, Revision 2 methodology using wt. % values of Cu and Ni from Reference 2.

TABLE 5-13

Precracked Instrumented Charpy Impact Test Results for the Palo Verde Unit 2 Lower Shell Plate F-773-1
Irradiated at 550°F to a Fluence of 4.071 X 10^{18} n/cm^2 (E > 1.0 MeV)
(Longitudinal Orientation)

Sample No.	Test Temp. (°F)	Specimem Comp.	Initial Velocity (in/sec)	Time to Yield (μsec)	Yield Load (lbs)	Time to Max. (μsec)	Max. Load (lbs)	Energy at Initiation (in-lbs)	Available Energy (in-lbs)	Crack Length (in.)	a/W	K_{Id} (ksi√in)	K_{Jd} (ksi√in)	Yield Stress (ksi)
1B151	0	45.6	57.4	-	-	170	1047	-	256	0.176	0.447	38.2	-	72.2
1B14B	25	47.3	57.5	-	-	180	1172	-	256	0.180	0.457	44.0	-	83.9
1B116	50	45.6	71.7	-	-	170	1235	-	399	0.176	0.447	45.0	-	83.3
1B14J	71	66.4	71.6	157	1040	300	1066	15.5	398	0.213	0.541	-	102.9	104.8
1B113	76	51.6	71.6	150	1120	860	1285	64.4	398	0.189	0.480	-	210.9	87.9
1B11K	100	50.1	90.6	135	1200	560	1381	54.2	637	0.186	0.472	-	187.4	91.5
1B13M	150	51.6	90.9	140	1100	1035	1341	101.6	642	0.189	0.480	-	263.6	86.4
1B12L	200	49.6	90.8	145	1170	1135	1499	122.1	640	0.185	0.470	-	285.0	88.4
1B141	250	47.8	90.8	105	940	1105	1375	108.0	640	0.181	0.459	-	266.0	68.4

TABLE 5-14

Precracked Instrumented Charpy Impact Test Results for the Palo Verde Unit 2 Lower Shell Plate F-773-1
Irradiated at 550°F to a Fluence of 4.071 X 10^{18} n/cm^2 (E > 1.0 MeV)
(Transverse Orientation)

Sample No.	Test Temp. (°F)	Specimem Comp.	Initial Velocity (in/sec)	Time to Yield (μsec)	Yield Load (lbs)	Time to Max. (μsec)	Max. Load (lbs)	Energy at Initiation (in-lbs)	Available Energy (in-lbs)	Crack Length (in.)	a/W	K_{Id} (ksi√in)	K_{Jd} (ksi√in)	Yield Stress (ksi)
1B213	25	45.2	57.4	-	-	225	1395	-	256	0.175	0.444	50.4	-	95.0
1B26C	50	50.6	71.9	-	-	185	1306	-	401	0.187	0.475	51.8	-	94.7
1B23T	76	44.4	71.5	155	1200	455	1354	32.1	397	0.173	0.439	-	137.1	81.1
1B27B	100	51.6	90.7	110	1060	295	1186	22.6	639	0.189	0.480	-	118.1	83.2
1B22T	150	50.1	90.6	150	1260	560	1434	54.4	638	0.186	0.472	-	185.7	96.1
1B245	200	54.2	90.5	112	1080	950	1365	92.1	636	0.194	0.492	-	254.2	89.1
1B226	250	49.2	90.6	113	880	1145	1398	112.4	637	0.184	0.467	-	271.6	65.9

TABLE 5-15

Precracked Instrumented Charpy Impact Test Results for the Palo Verde Unit 2 Surveillance Weld Metal Irradiated at 550°F to a Fluence of 4.071 X 10^{18} n/cm^2 (E > 1.0 MeV)

Sample No.	Test Temp. (°F)	Specimem Comp.	Initial Velocity (in/sec)	Time to Yield (μsec)	Yield Load (lbs)	Time to Max. (μsec)	Max. Load (lbs)	Energy at Initiation (in-lbs)	Available Energy (in-lbs)	Crack Length (in.)	a/W	K_{Id} (ksi√in)	K_{Jd} (ksi√in)	Yield Stress (ksi)
1B3AT	-50	52.6	90.9	-	-	115	995	-	642	0.191	0.485	40.7	-	79.3
1B31U	-25	48.2	57.5	-	-	175	1085	-	257	0.182	0.462	41.4	-	75.6
1B323	0	50.1	71.5	-	-	155	1215	-	397	0.186	0.472	47.8	-	92.3
1B33J	50	47.3	71.5	150	1240	550	1390	42.0	397	0.180	0.457	-	163.5	89.4
1B31A	71	44.8	71.8	150	1240	1035	1456	86.2	400	0.174	0.442	-	236.4	85.4
1B33Y	100	49.2	90.5	140	1200	720	1286	70.0	636	0.184	0.467	-	215.5	89.8
1B36M	125	51.6	203.0	60	950	300	1223	56.4	3201	0.189	0.480	-	191.7	74.6
1B31K	150	50.6	90.9	110	1000	860	1267	80.0	642	0.187	0.475	-	233.8	77.0
1B37A	200	50.1	90.6	110	1000	715	1319	67.6	637	0.186	0.472	-	211.8	76.3

TABLE 5-16

Tensile Properties of the Palo Verde Unit 2 Reactor Vessel Surveillance Materials Irradiated at 550°F to 4.071 X 10^{18} n/cm^2 (E > 1.0 MeV)

Material	Sample Number	Test Temp. (°F)	0.2% Yield Strength (ksi)	Ultimate Strength (ksi)	Fracture Load (kip)	Fracture Stress (ksi)	Fracture Strength (ksi)	Uniform Elongation (%)	Total Elongation (%)	Reduction in Area (%)
Plate F-773-1 (transverse)	1B2J2	75	63.9	84.5	3.65	206.5	74.4	13.5	29.1	64
Plate F-773-1 (transverse)	1B2K1	200	63.2	80.5	2.55	126.8	51.9	11.4	25.4	59
Plate F-773-1 (transverse)	1B2J3	550	54.0	81.5	2.80	130.9	57.0	12.3	24.8	56
Weld Metal	1B3J7	5	73.3	90.7	2.89	194.6	58.9	13.5	27.9	70
Weld Metal	1B3JY	125	70.3	83.5	2.75	141.2	56.0	10.8	23.4	60
Weld Metal	1B3J5	550	62.6	82.5	2.75	160.9	56.0	9.9	21.0	65

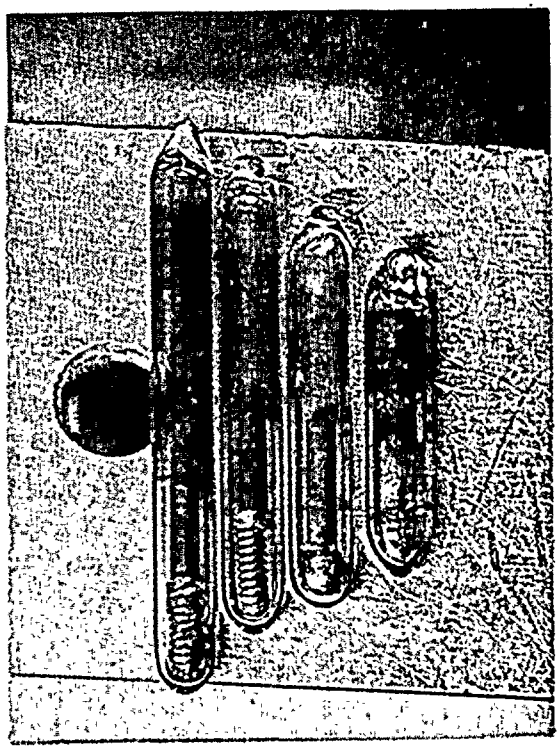

Figure 5-1 Palo Verde Unit 2 Capsule W-137 Thermal Monitors

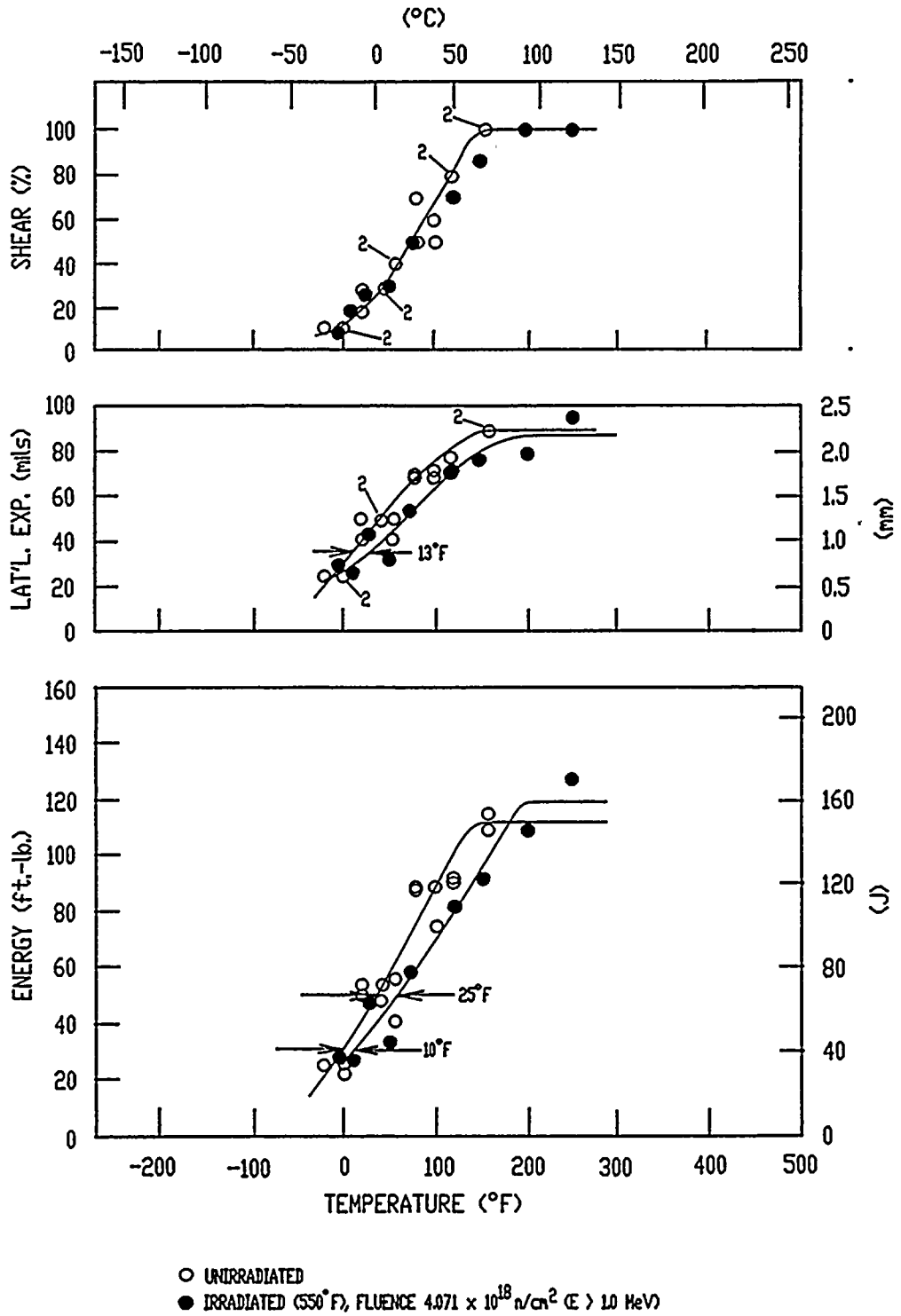

Figure 5-2 Charpy V-Notch Impact Properties for Palo Vedre Unit 2 Reactor Vessel Lower Shell Plate F-773-1 (Longitudinal Orientation)

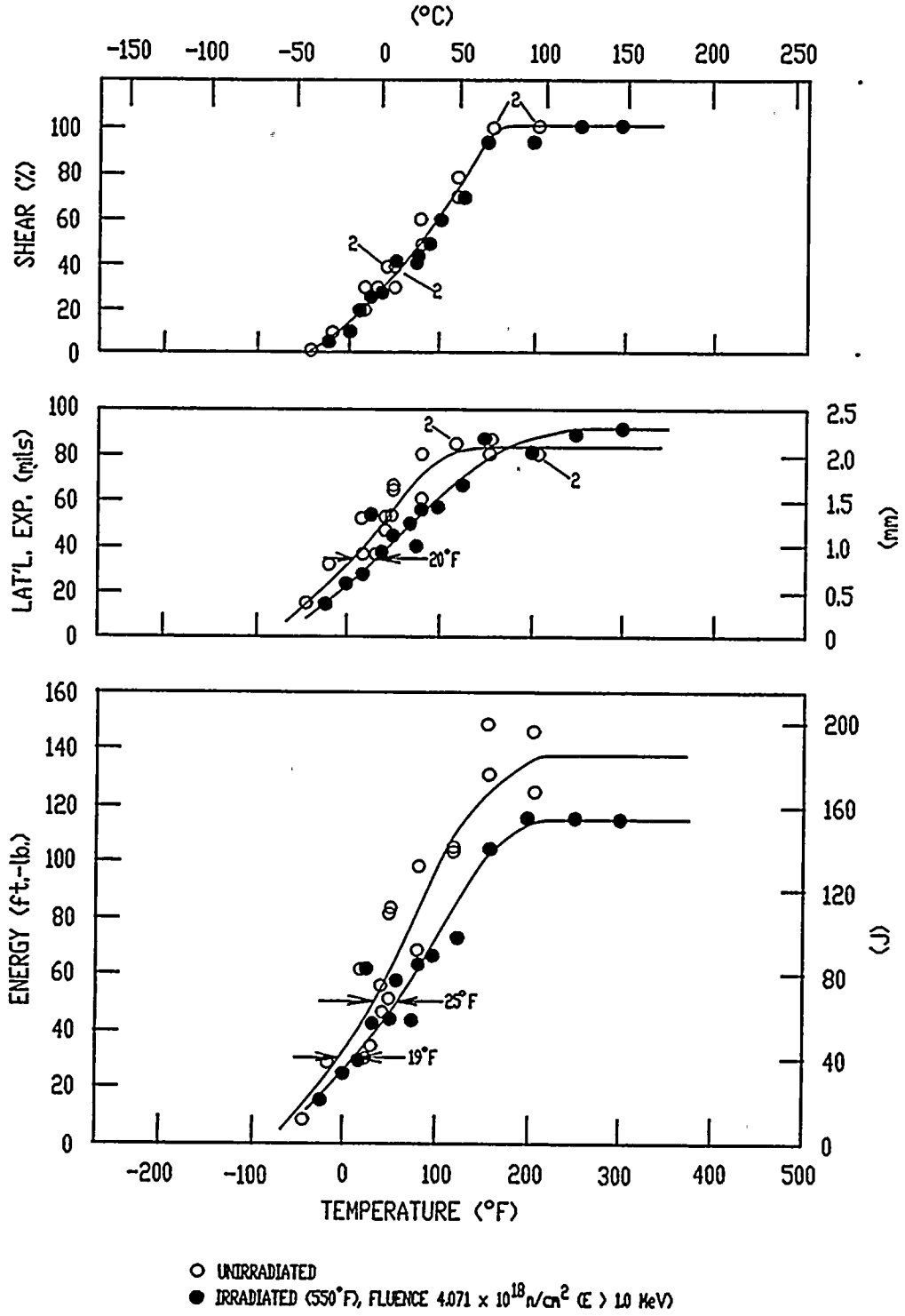

Figure 5-3 Charpy V-Notch Impact Properties for Palo Verde Unit 2 Reactor Vessel Lower Shell Plate F-773-1 (Transverse Orientation)

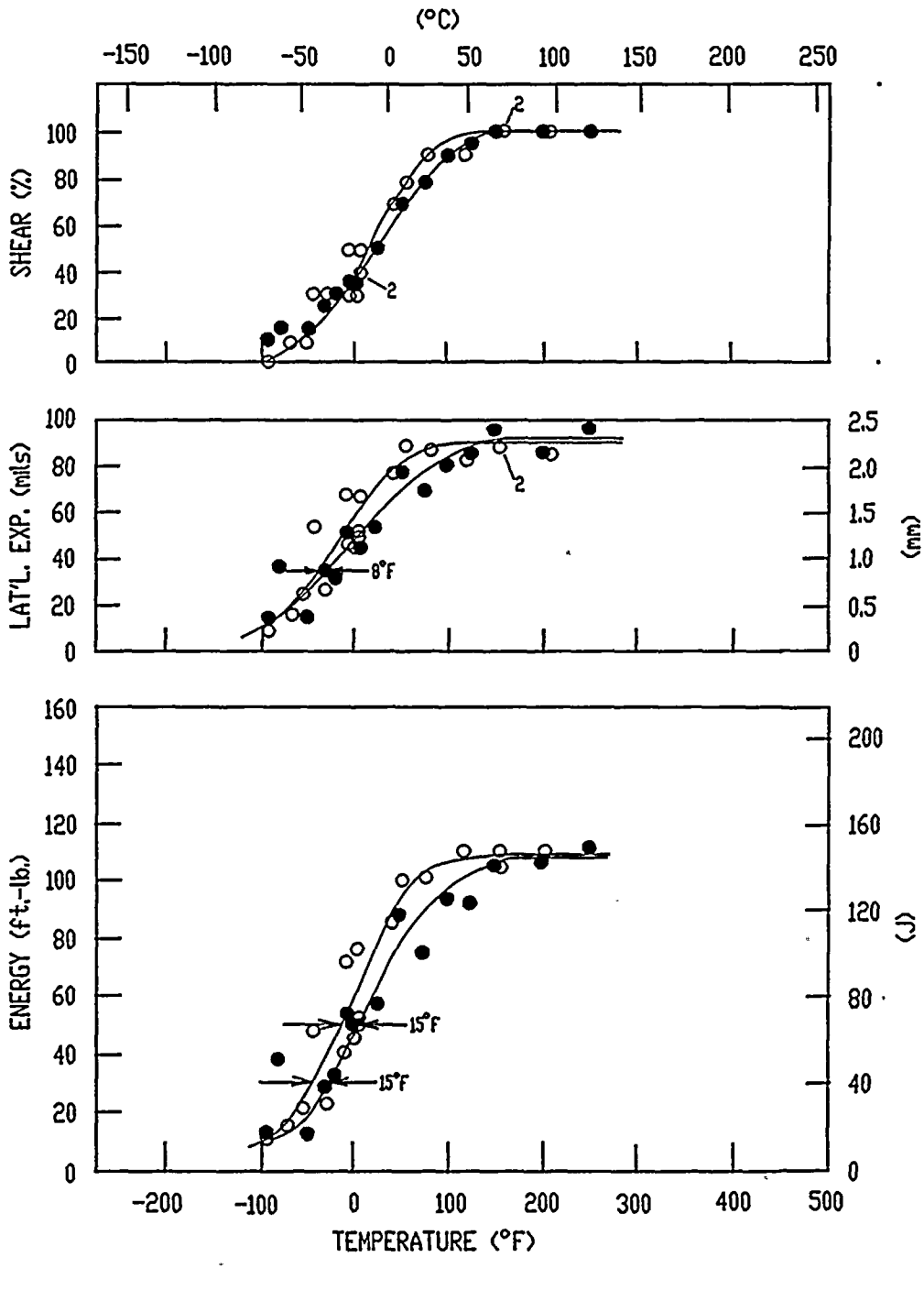

Figure 5-4 Charpy V-Notch Impact Properties for Palo Verde Unit 2 Reactor Vessel Surveillance Weld Metal (F-773-2/F-773-3)

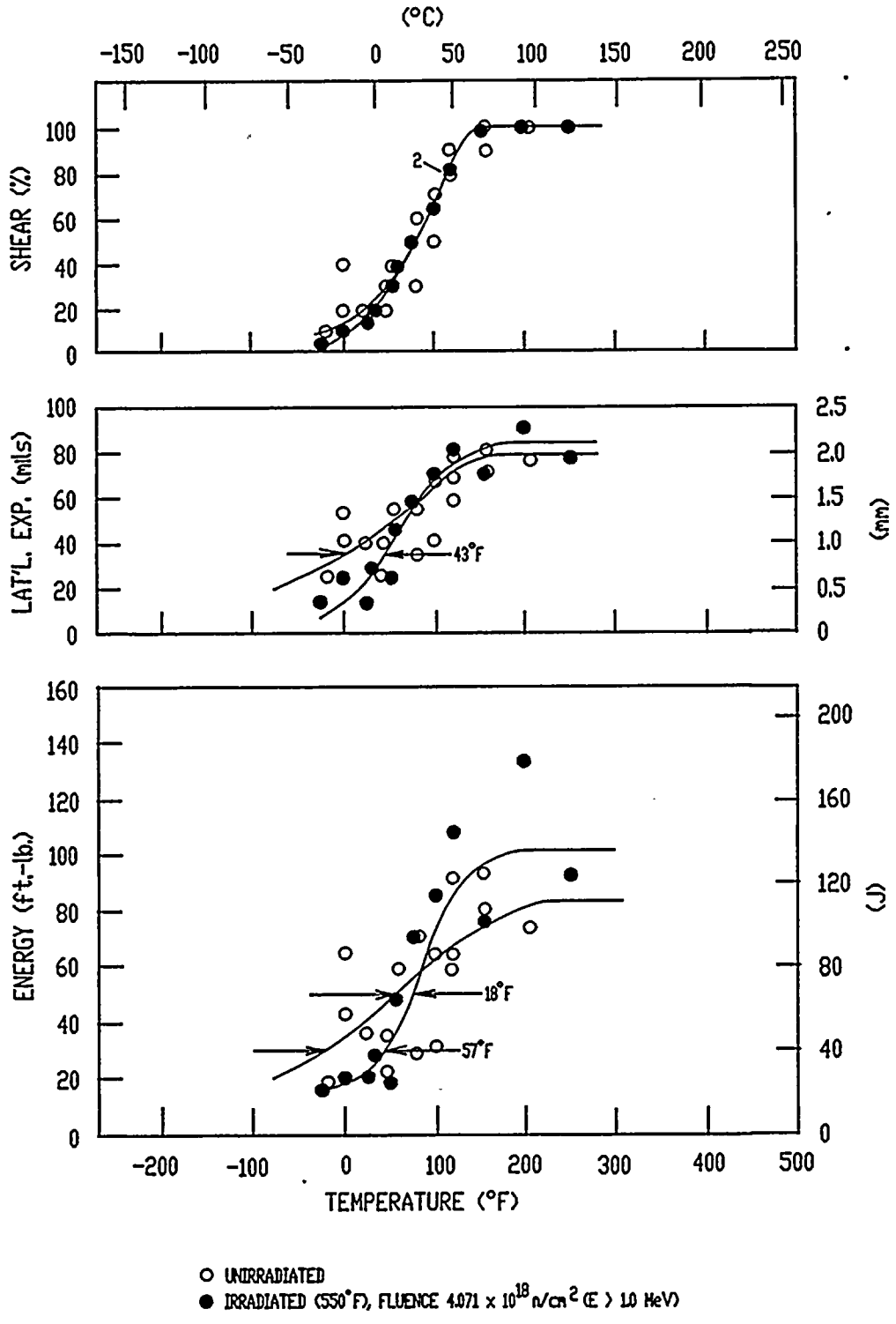

Figure 5-5 Charpy V-Notch Impact Properties for Palo Verde Unit 2 Reactor Vessel Weld Heat-Affected-Zone Metal

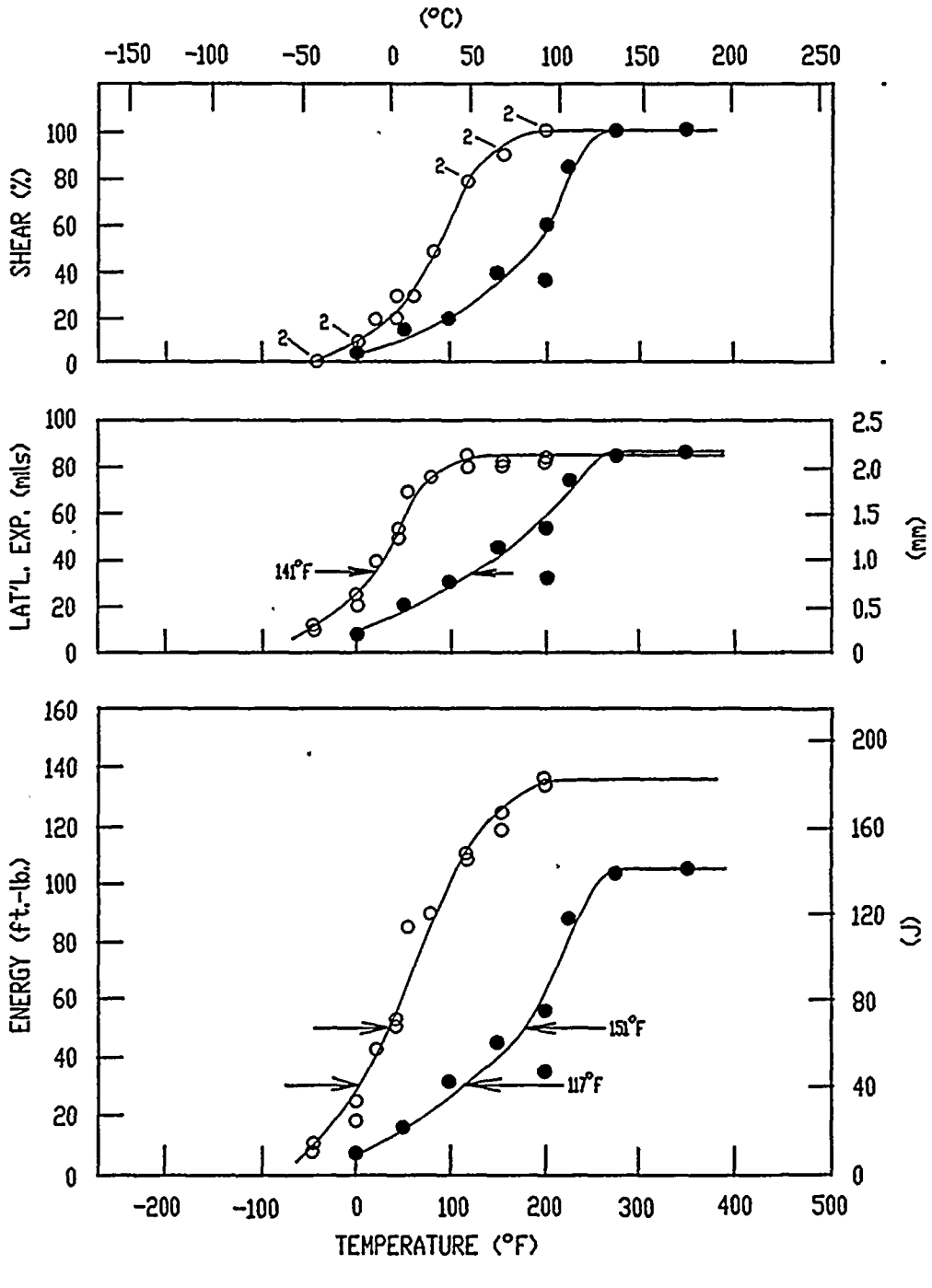

Figure 5-6 Charpy V-Notch Impact Properties for Palo Verde Unit 2 SRM HSST 01MY (Longitudinal Orientation)

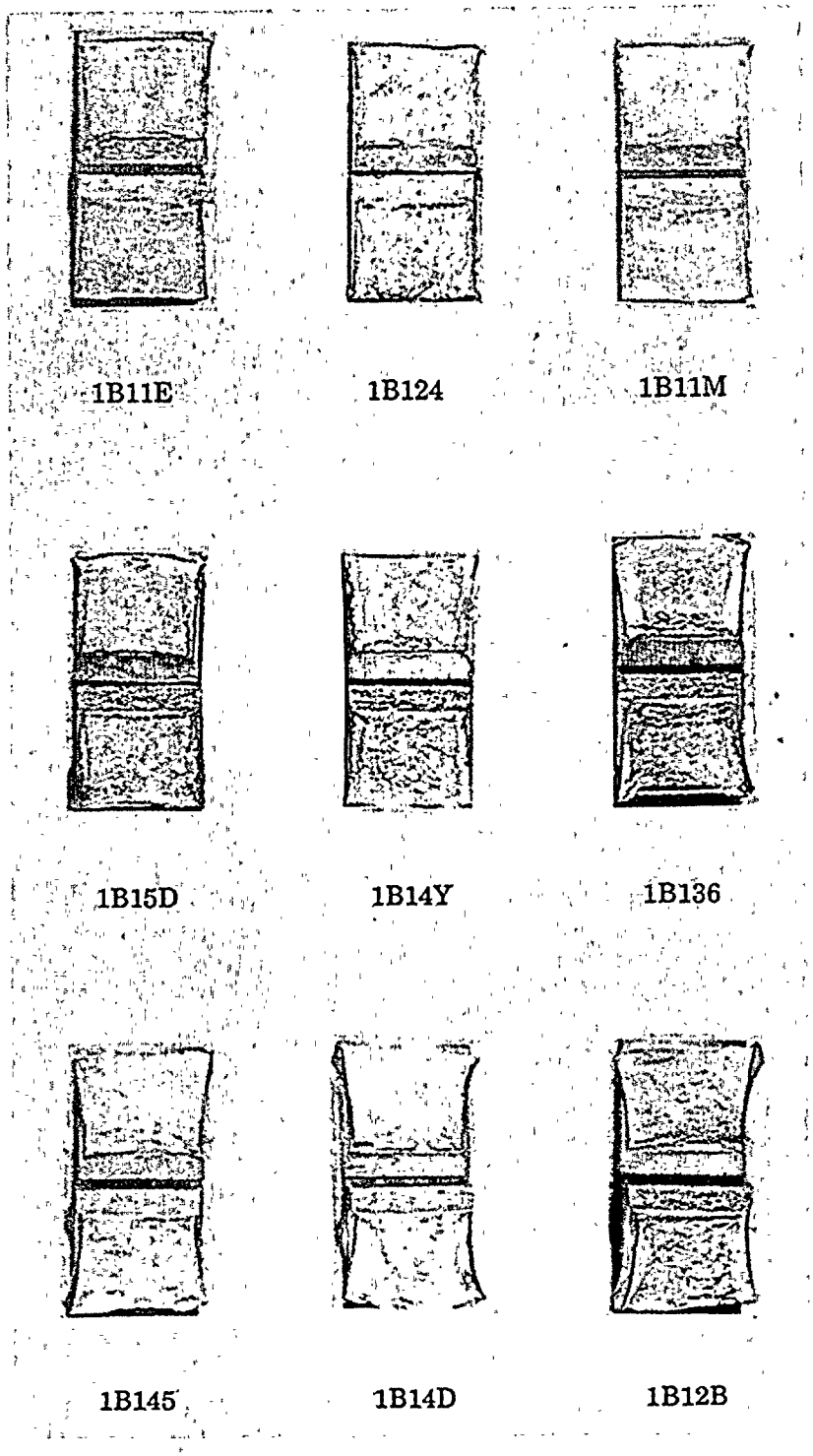

Figure 5-7 Charpy Impact Specimen Fracture Surfaces for Palo Verde Unit 2 Reactor Vessel Lower Shell Plate F-773-1 (Longitudinal Orientation)

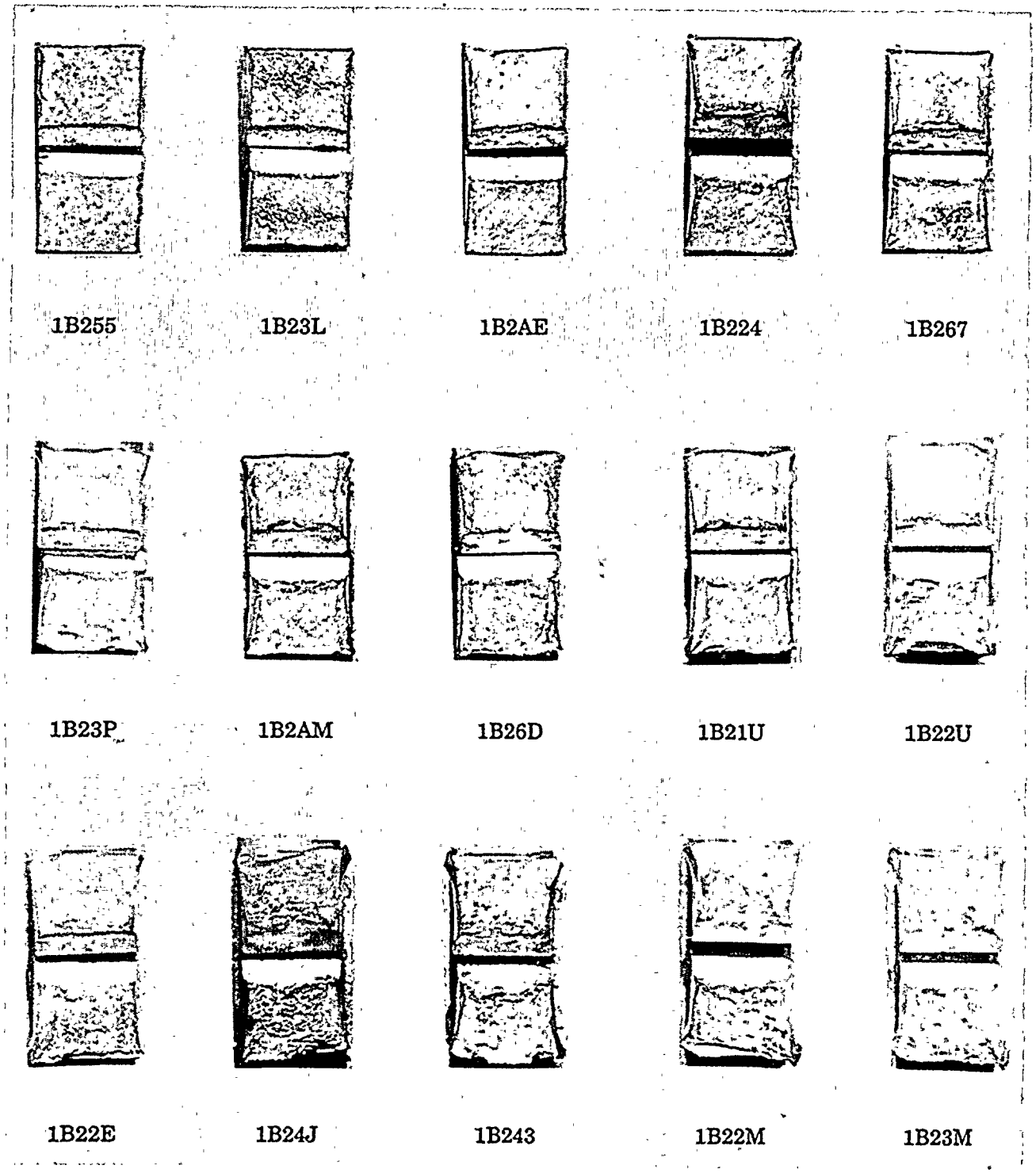

Figure 5-8 Charpy Impact Specimen Fracture Surfaces for Palo Verde Unit 2 Reactor Vessel Lower Shell Plate F-773-1 (Transverse Orientation)

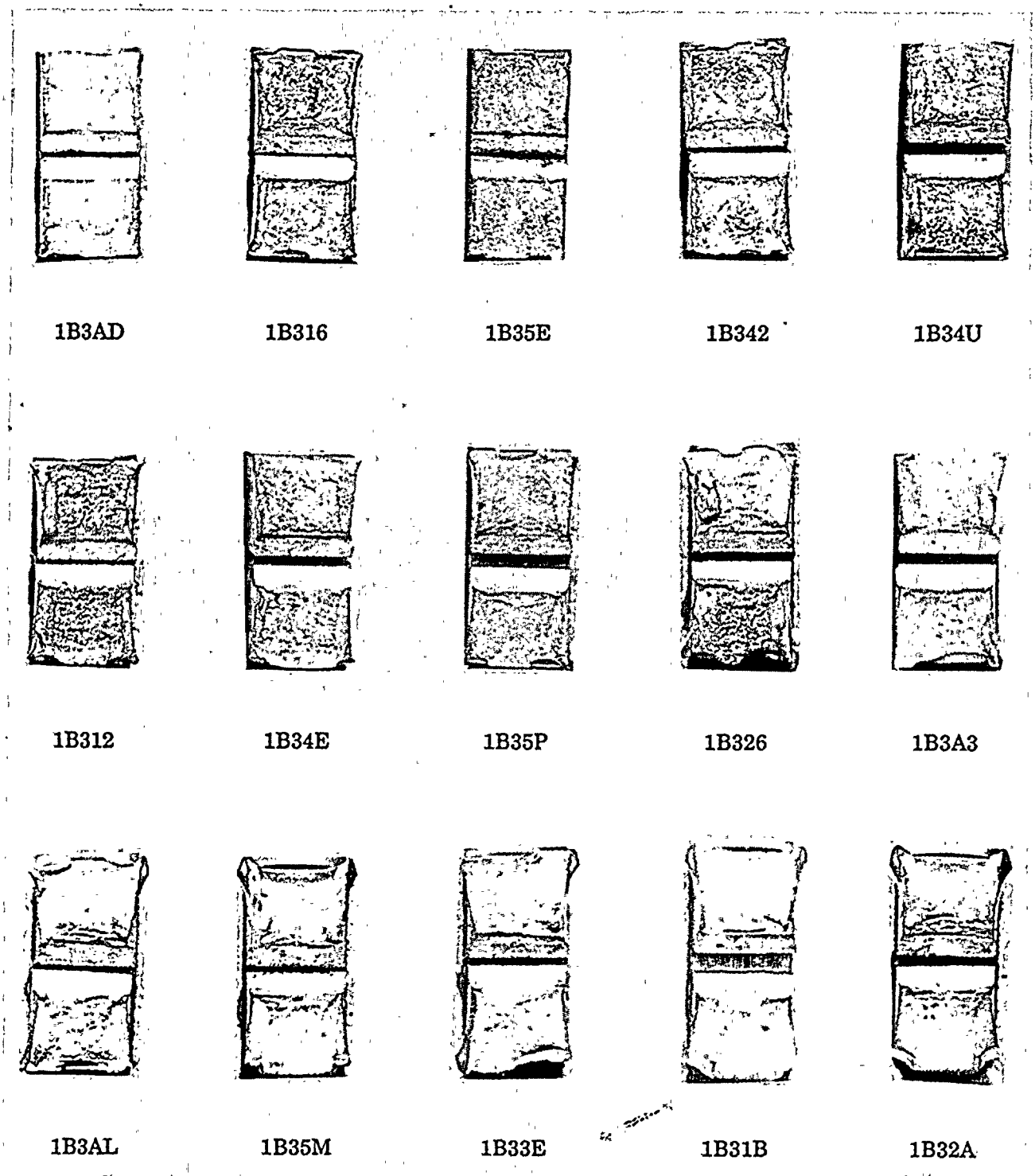

Figure 5-9 Charpy Impact Specimen Fracture Surfaces for Palo Verde Unit 2 Reactor Vessel Surveillance Weld Metal

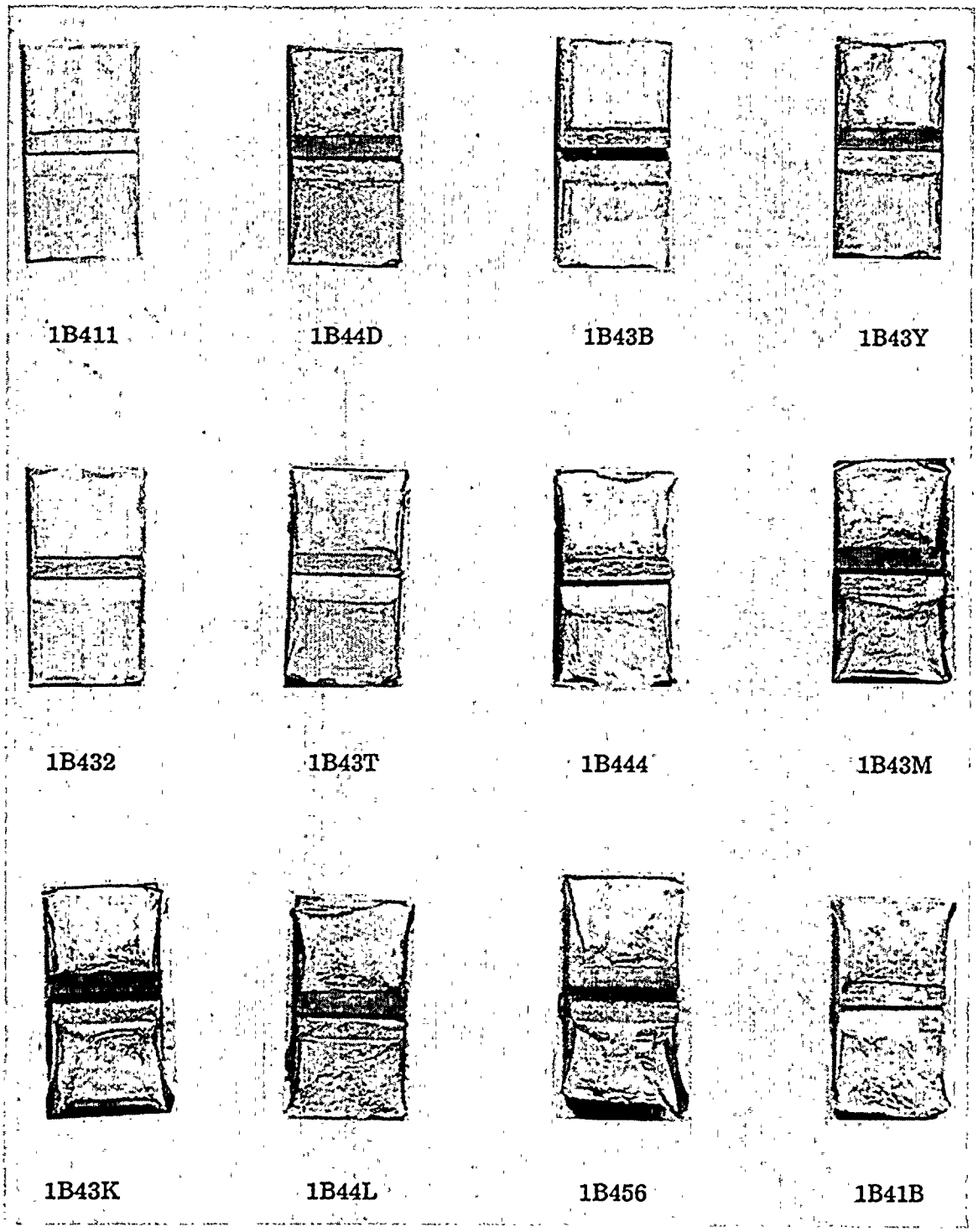

Figure 5-10 Charpy Impact Specimen Fracture Surfaces for Palo Verde Unit 2 Reactor Vessel Heat-Affected-Zone Metal

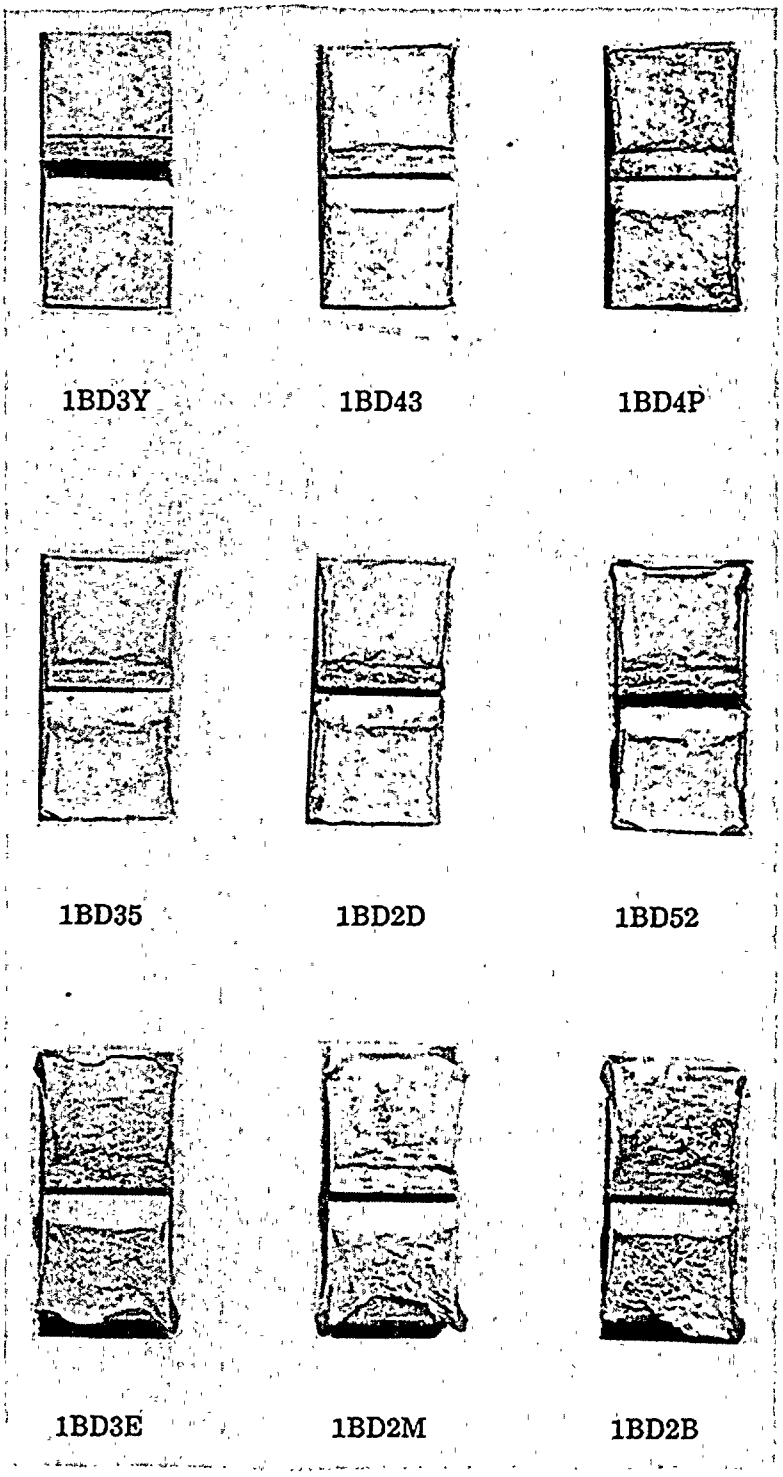

Figure 5-11 Charpy Impact Specimen Fracture Surfaces for Palo Verde Unit 2 SRM HSST 01MY (Longitudinal Orientation)

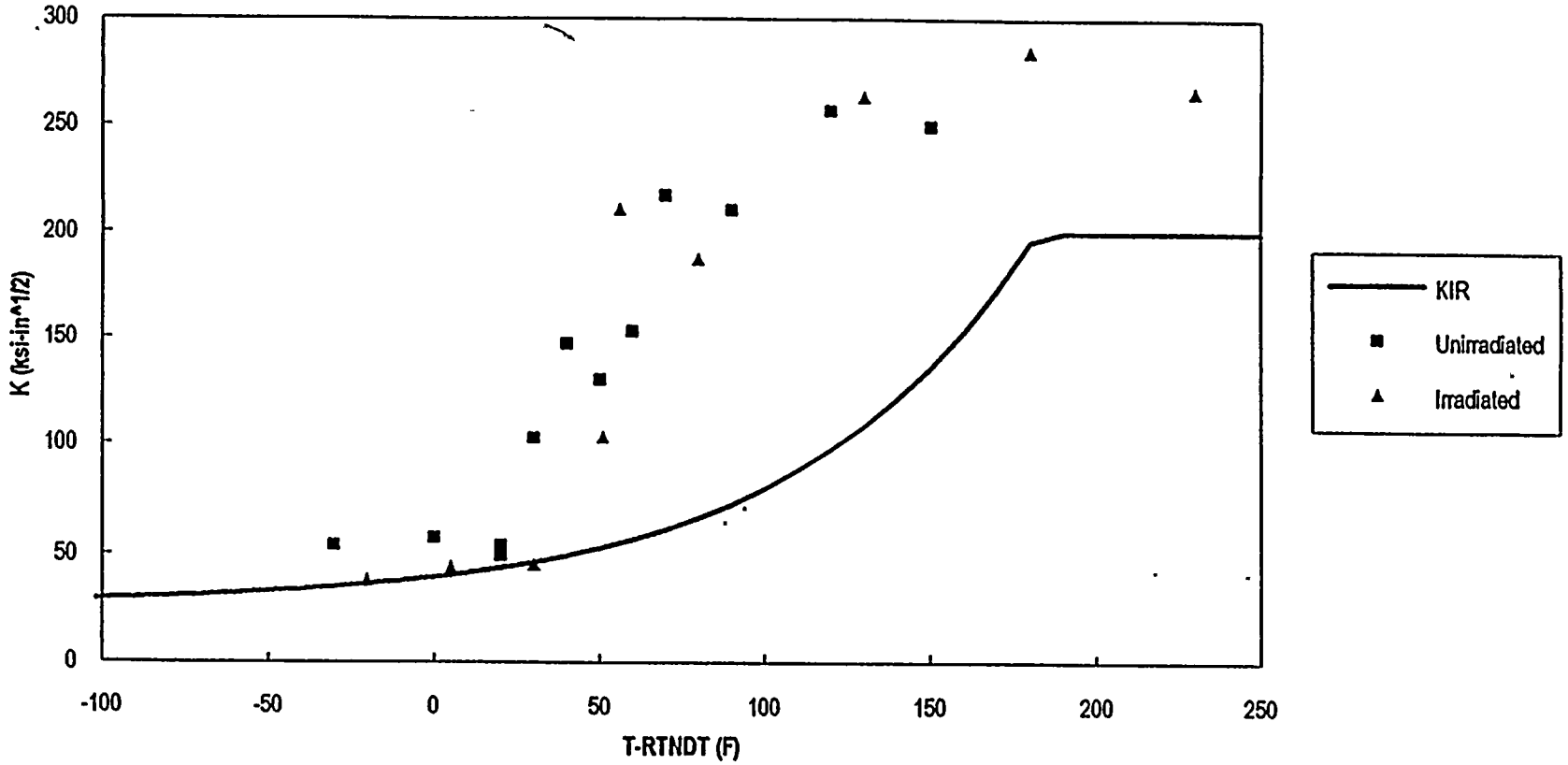

Figure 5-12 Comparison of Unirradiated and Irradiated Dynamic Fracture Toughness Values Determined by Testing of Precracked Charpy Specimens from Lower Shell Plate F-773-1 (Longitudinal Orientation)

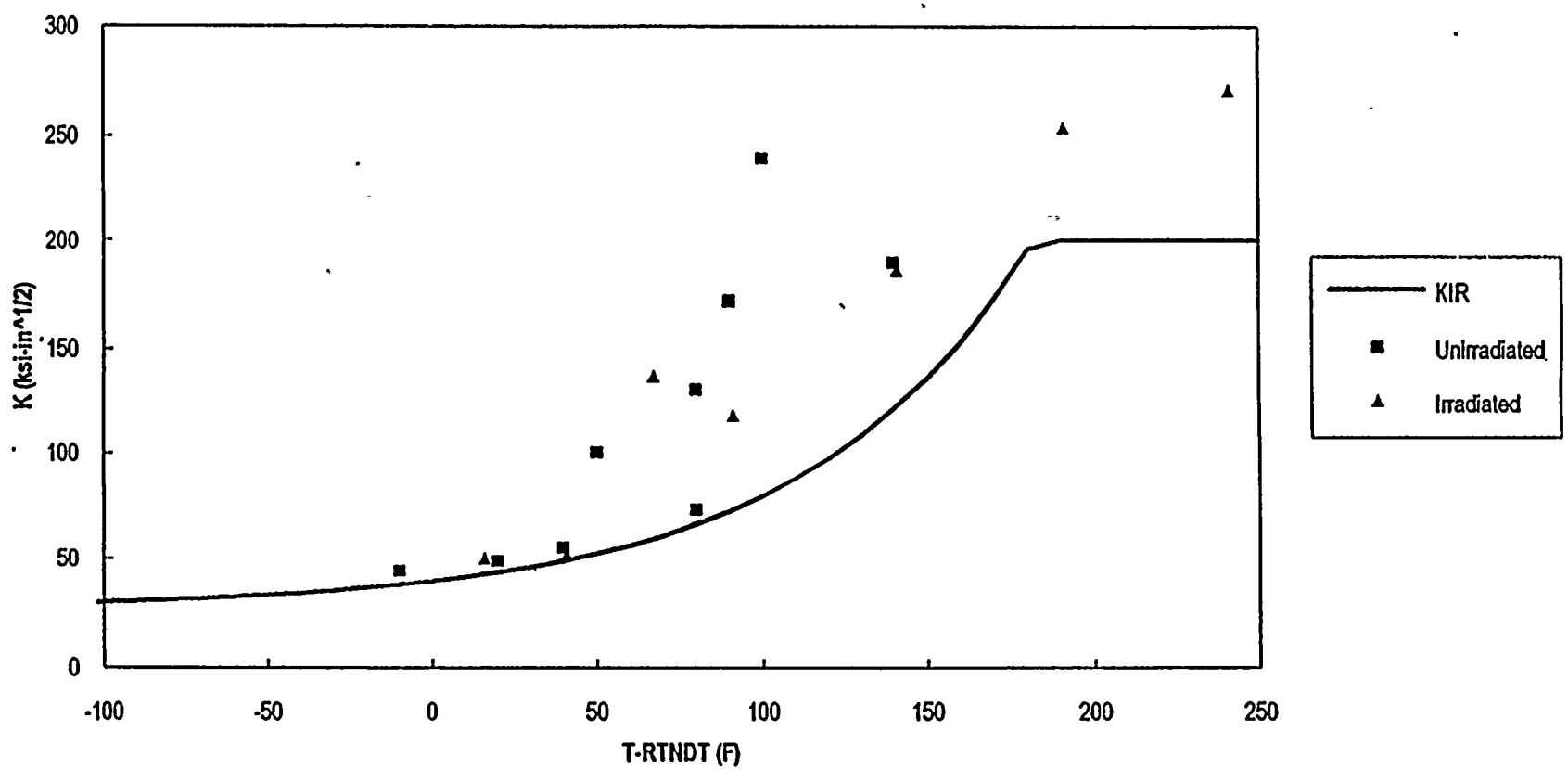

Figure 5-13 Comparison of Unirradiated and Irradiated Dynamic Fracture Toughness Values Determined by Testing of Precracked Charpy Specimens from Lower Shell Plate F-773-1 (Transverse Orientation)

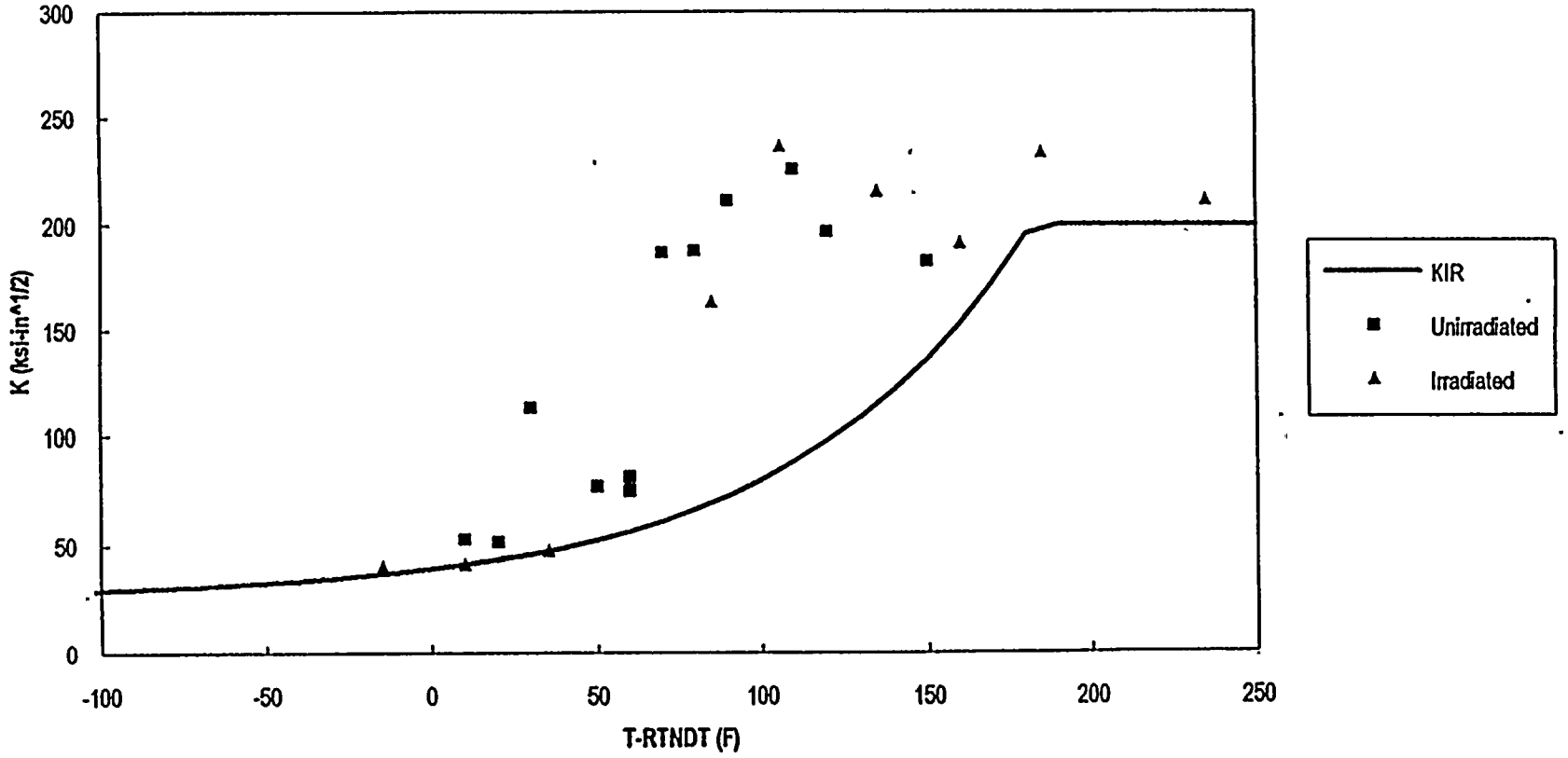

Figure 5-14 Comparison of Unirradiated and Irradiated Dynamic Fracture Toughness Values Determined by Testing of Precracked Charpy Specimens from the Palo Verde Unit 2 Surveillance Weld Metal

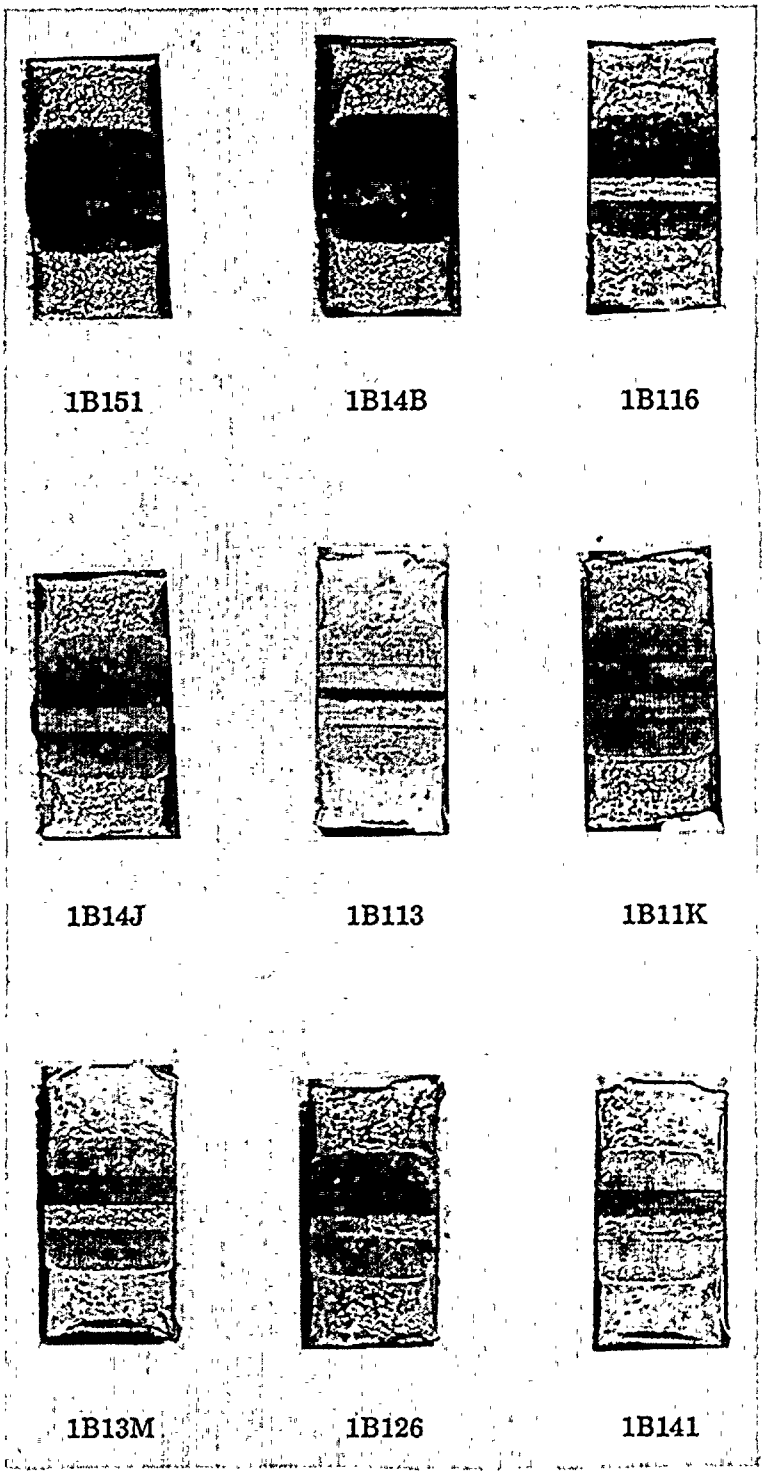

Figure 5-15 Precracked Charpy Impact Specimen Fracture Surfaces for Palo Verde Unit 2 Lower Shell Plate F-773-1 (Longitudinal Orientation)

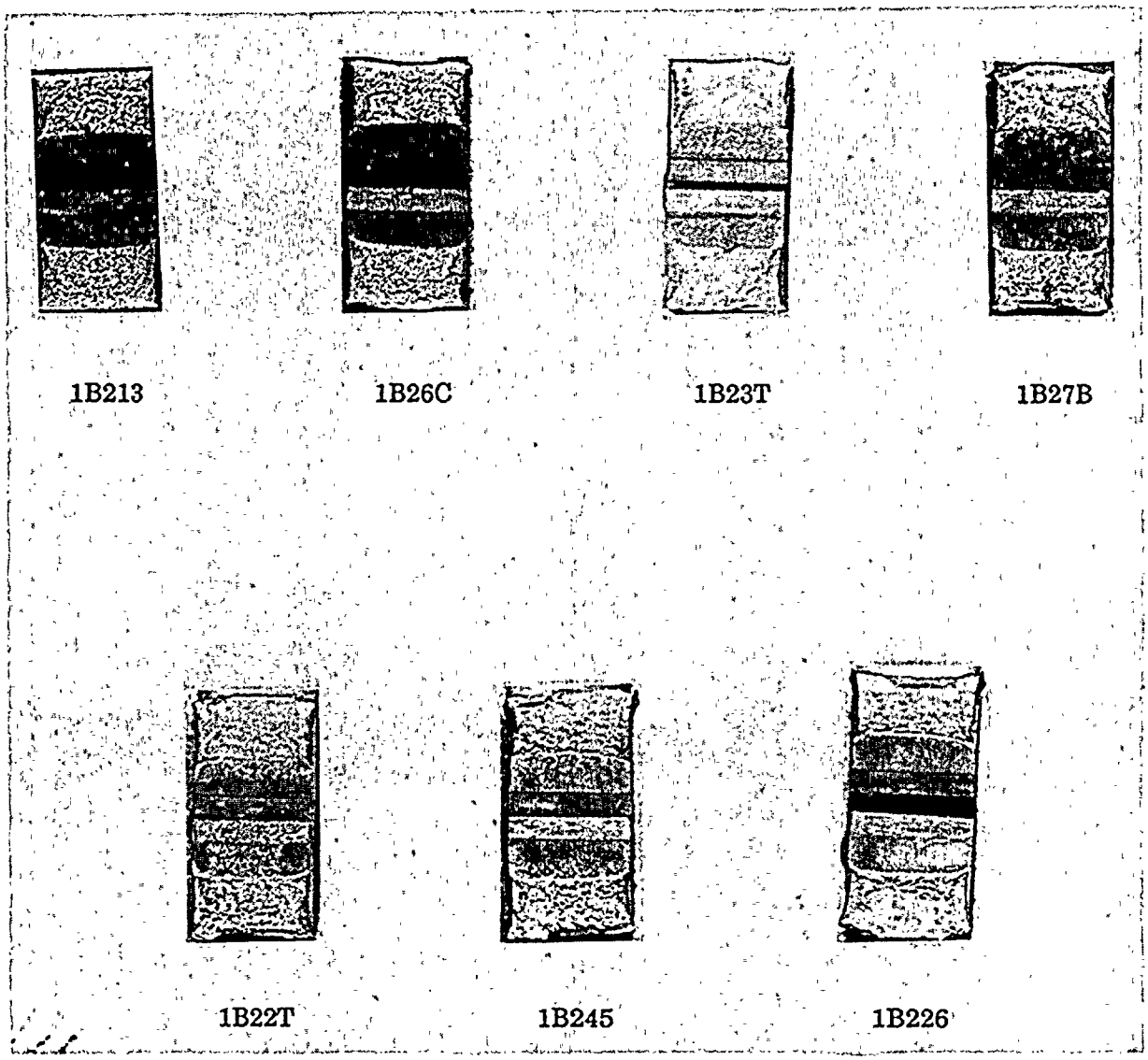

Figure 5-16 Precracked Charpy Impact Specimen Fracture Surfaces for Palo Verde Unit 2 Lower Shell Plate F-773-1 (Transverse Orientation)

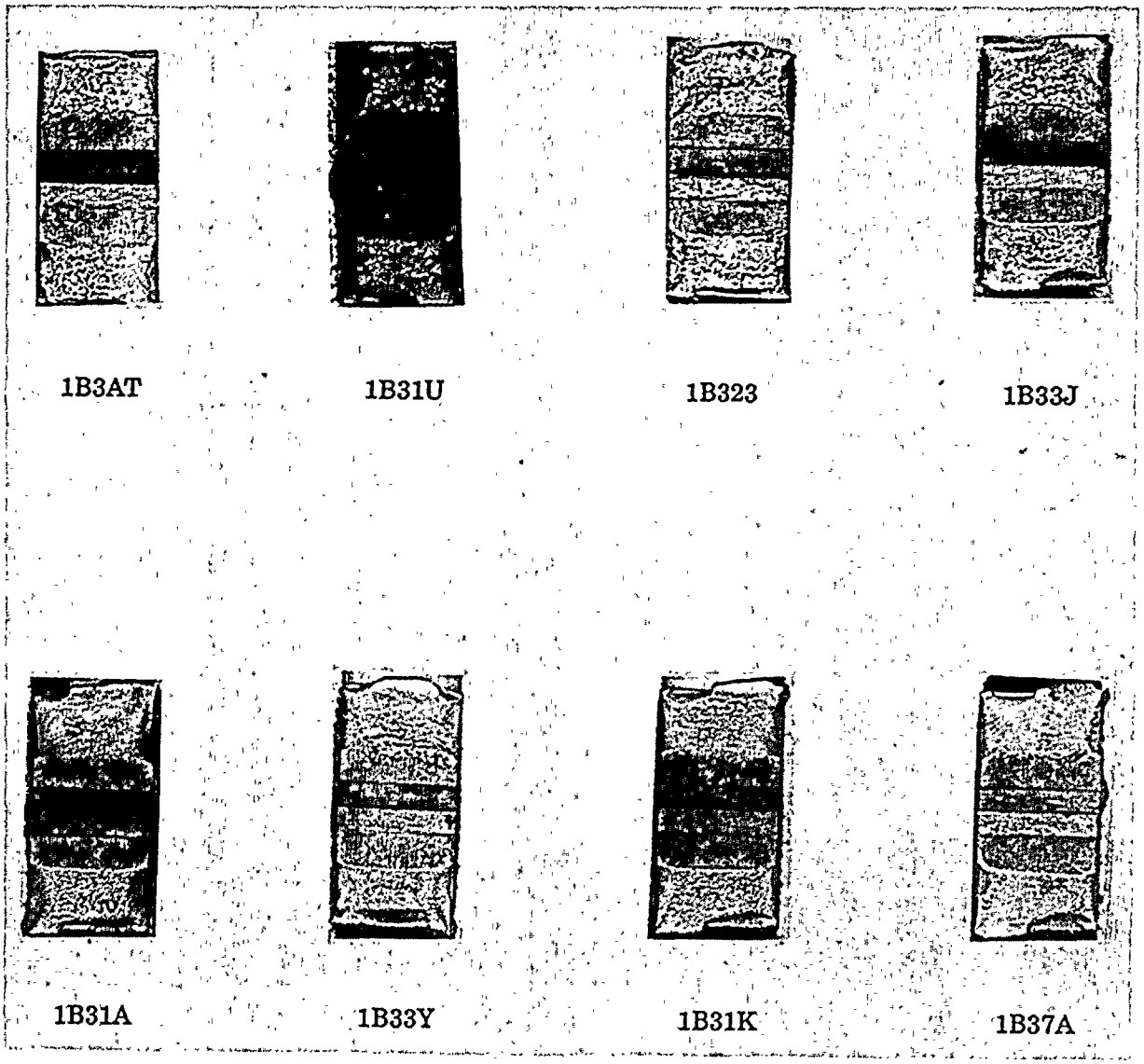

Figure 5-17 Precracked Charpy Impact Specimen Fracture Surfaces for Palo Verde Unit 2 Reactor Vessel Surveillance Weld Metal

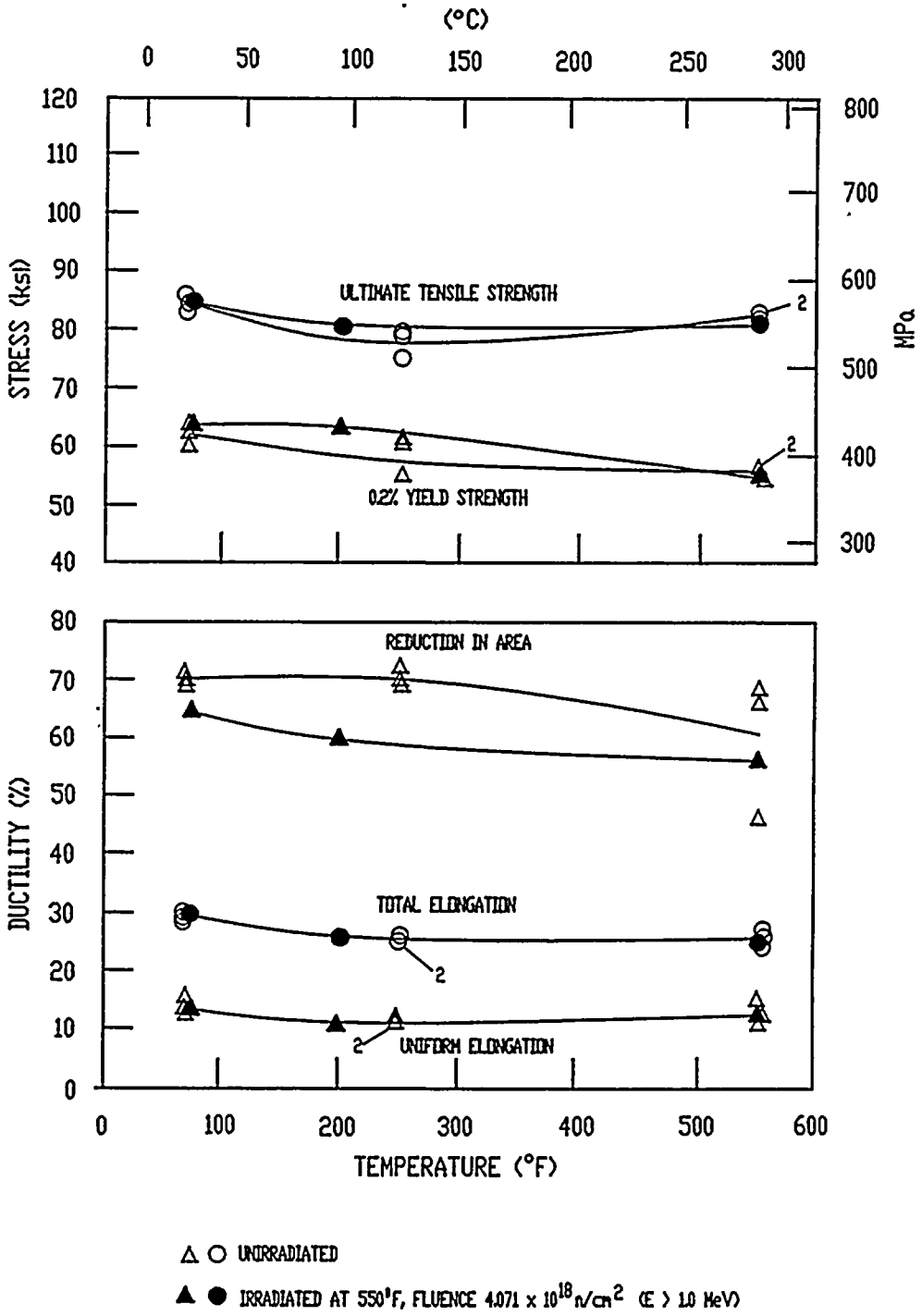

Figure 5-18 Tensile Properties for Palo Verde Unit 2 Reactor Vessel Lower Shell Plate F-773-1 (Transverse Orientation)

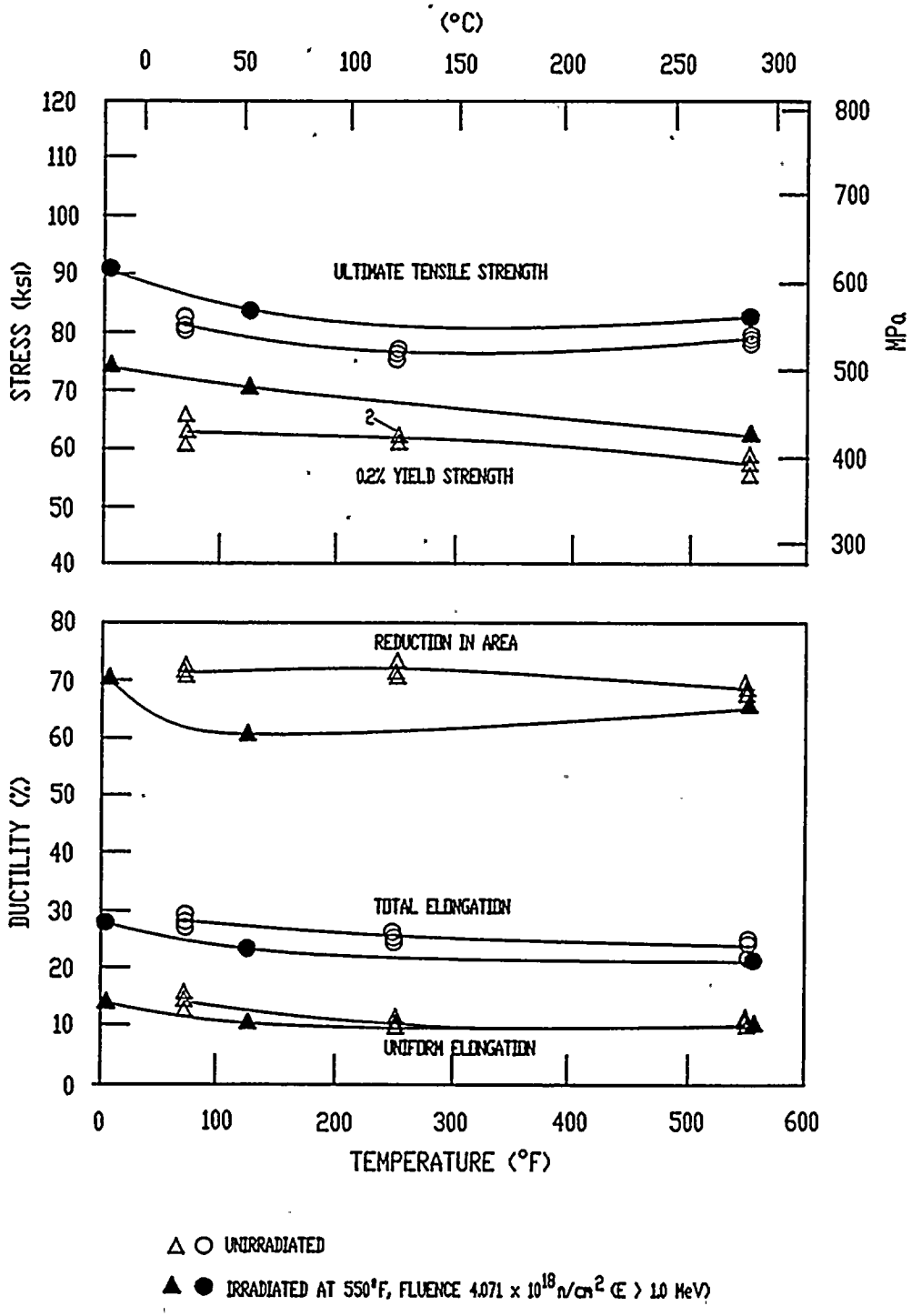

Figure 5-19 Tensile Properties for Palo Verde Unit 2 Reactor Vessel Surveillance Weld Metal

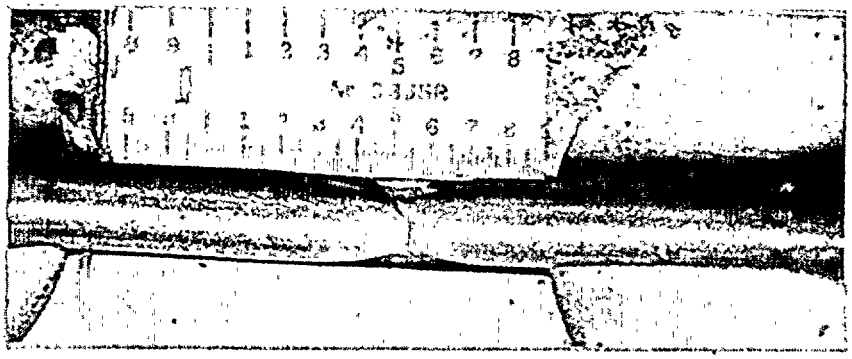

Specimen 1B2J2 75°F

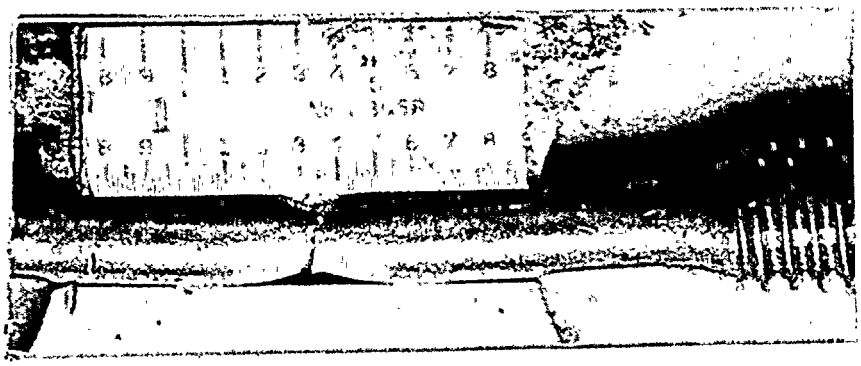

Specimen 1B2K1 200°F

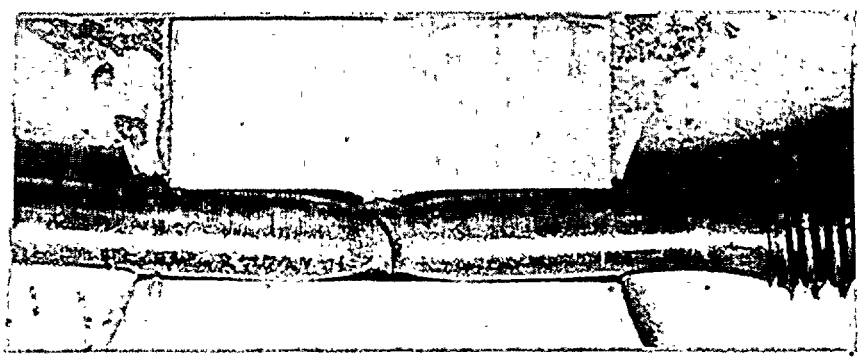

Specimen 1B2J3 550°F

Figure 5-20 Fractured Tensile Specimens from Palo Verde Unit 2 Reactor Vessel Lower Shell Plate F-773-1 (Transverse Orientation)

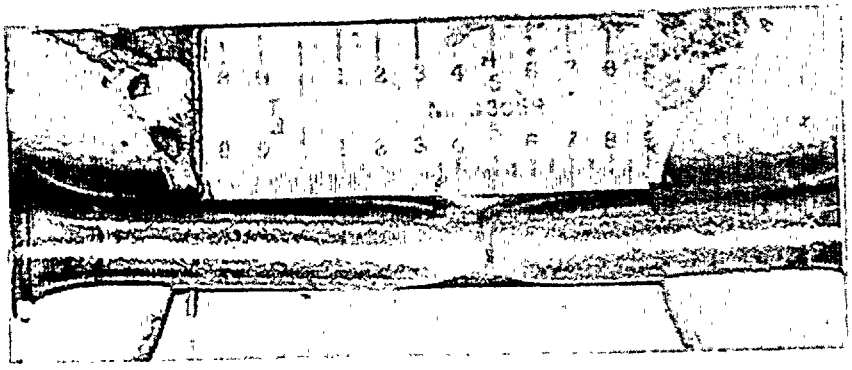

Specimen 1B3J7 5°F

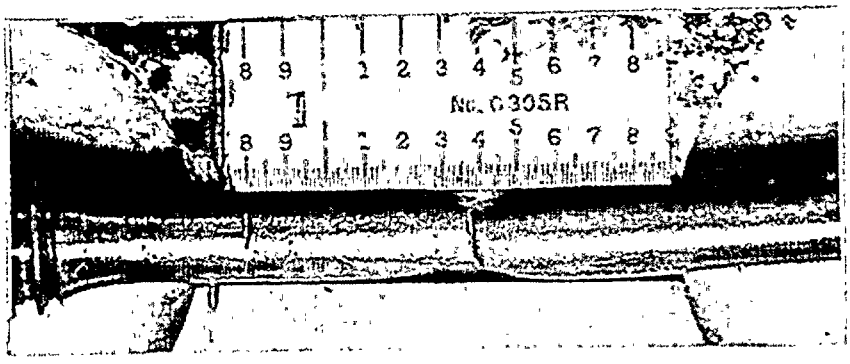

Specimen 1B3JY 125°F

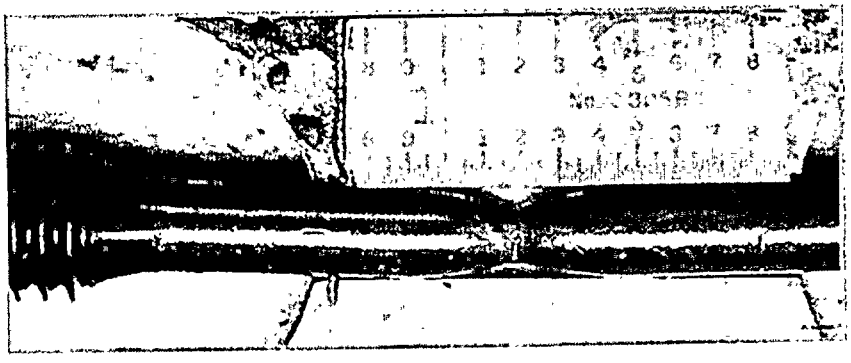

Specimen 1B3J5 550°F

Figure 5-21 Fractured Tensile Specimens from Palo Verde Unit 2 Reactor Vessel Surveillance Weld Metal

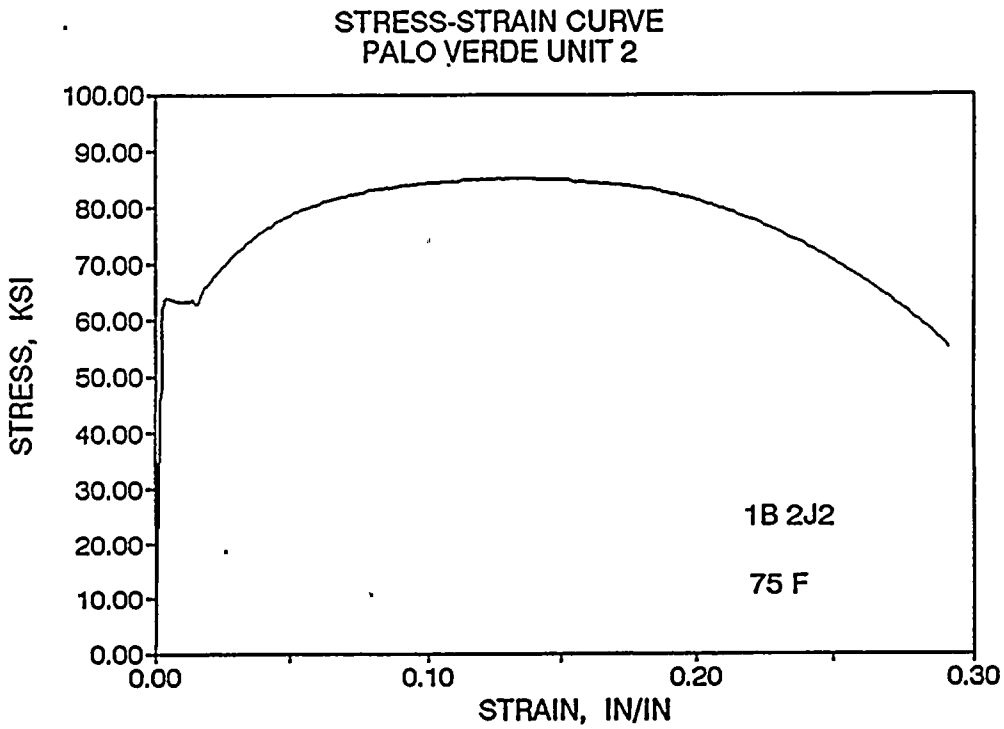

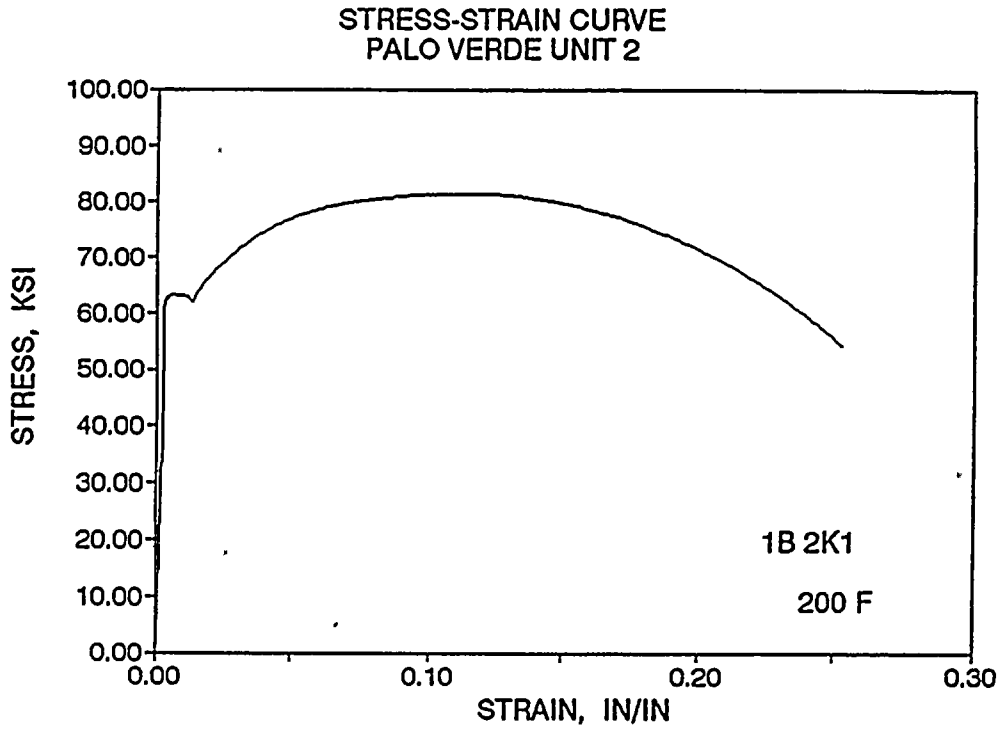

Figure 5-22 Engineering Stress-Strain Curves for Lower Shell Plate F-773-1 Tensile Specimens 1B2J2 and 1B2K1 (Transverse Orientation)

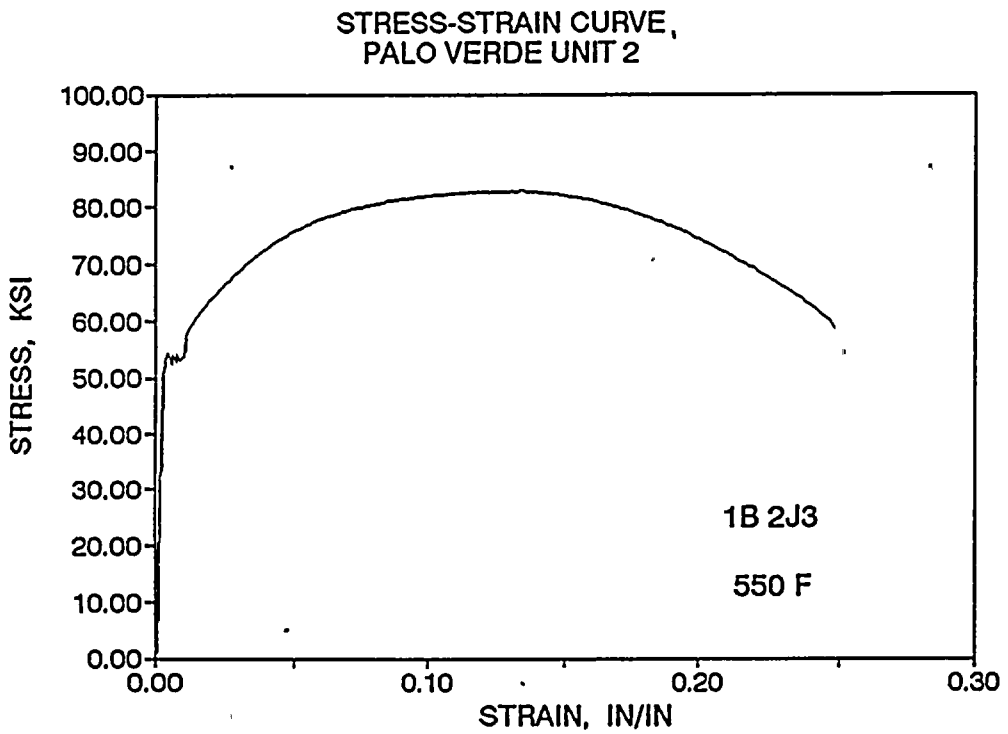

Figure 5-23 Engineering Stress-Strain Curve for Lower Shell Plate F-773-1 Tensile Specimen 1B2J3 (Transverse Orientation)

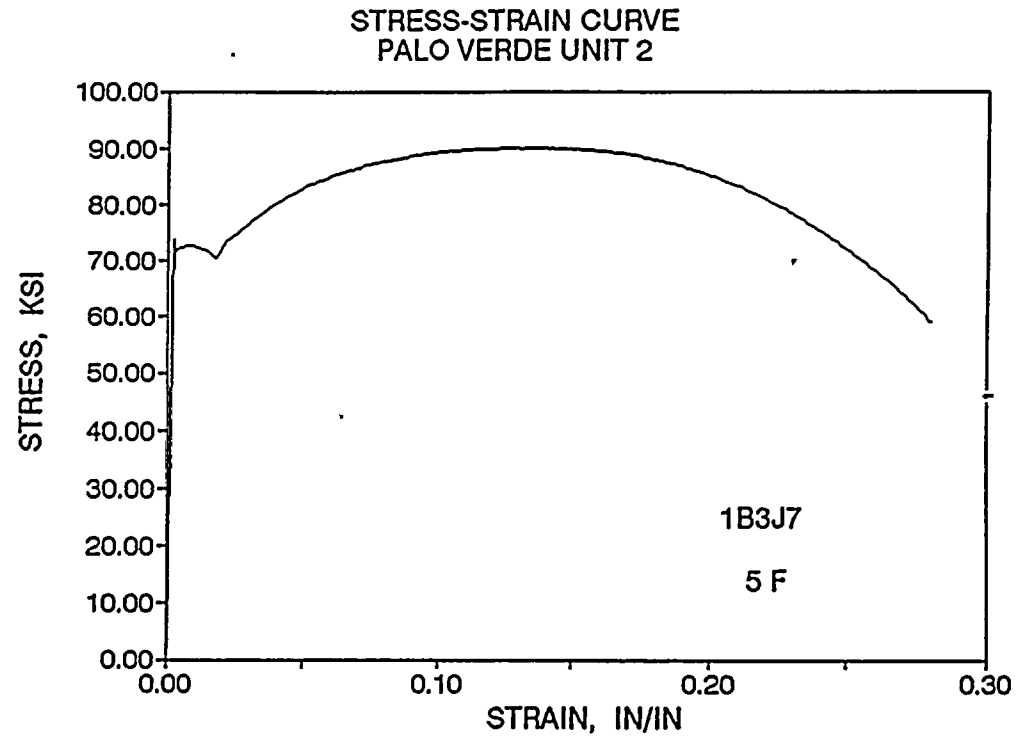

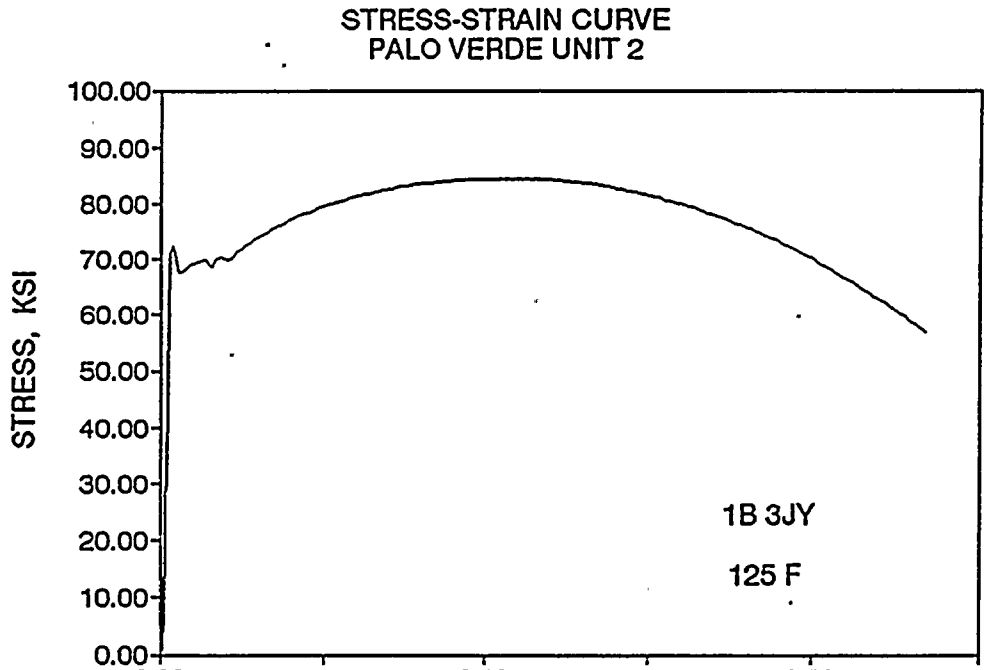

Figure 5-24 Engineering Stress-Strain Curves for Weld Metal Tensile Specimens 1B3J7 and 1B3JY

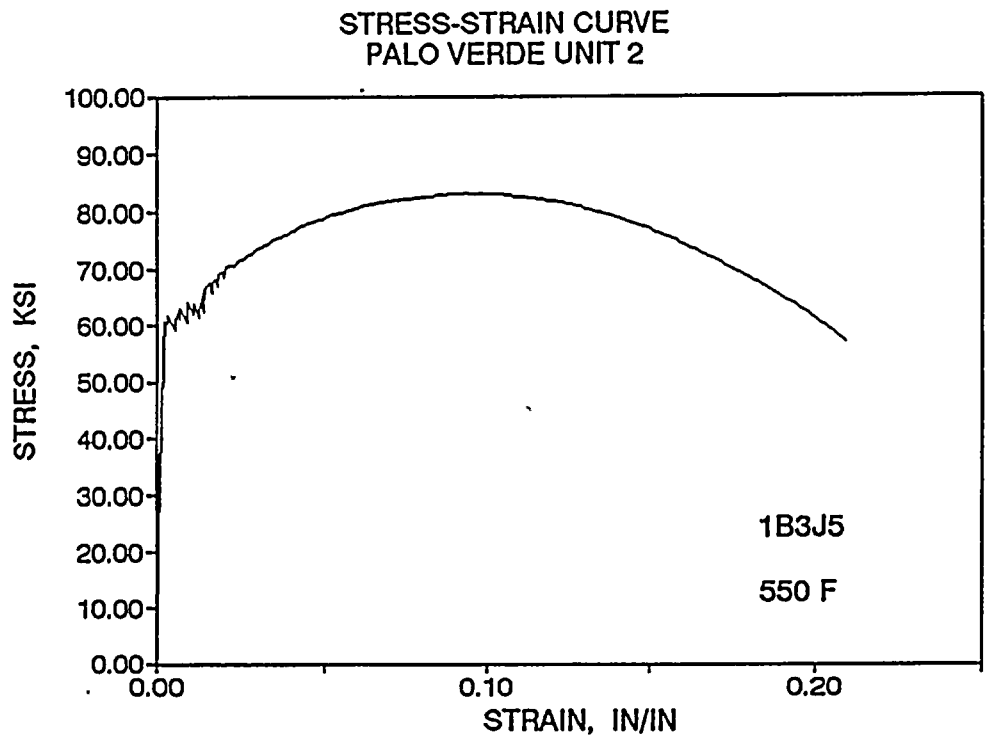

Figure 5-25 Engineering Stress-Strain Curve for Weld Metal Tensile Specimen 1B3J5

SECTION 6.0
RADIATION ANALYSIS AND NEUTRON DOSIMETRY

6.1 Introduction

Knowledge of the neutron environment within the reactor pressure vessel and surveillance capsule geometry is required as an integral part of LWR reactor pressure vessel surveillance programs for two reasons. First, in order to interpret the neutron radiation induced material property changes observed in the test specimens, the neutron environment (energy spectrum, flux, fluence) to which the test specimens were exposed must be known. Second, in order to relate the changes observed in the test specimens to the present and future condition of the reactor vessel, a relationship must be established between the neutron environment at various positions within the pressure vessel and that experienced by the test specimens. The former requirement is normally met by employing a combination of rigorous analytical techniques and measurements obtained with passive neutron flux monitors contained in each of the surveillance capsules. The latter information is generally derived solely from analysis.

The use of fast neutron fluence (E > 1.0 MeV) to correlate measured material property changes to the neutron exposure of the material has traditionally been accepted for development of damage trend curves as well as for the implementation of trend curve data to assess vessel condition. In recent years, however, it has been suggested that an exposure model that accounts for differences in neutron energy spectra between surveillance capsule locations and positions within the vessel wall could lead to an improvement in the uncertainties associated with damage trend curves as well as to a more accurate evaluation of damage gradients through the pressure vessel wall.

Because of this potential shift away from a threshold fluence toward an energy dependent damage function for data correlation, ASTM Standard Practice E853, "Analysis and Interpretation of Light Water Reactor Surveillance Results,"[13] recommends reporting displacements per iron atom (dpa) along with fluence (E > 1.0 MeV) to provide a data base for future reference. The energy dependent dpa function to be used for this evaluation is specified in ASTM Standard Practice E693, "Characterizing Neutron Exposures in Ferritic Steels in Terms of Displacements per Atom."[14] The application of the dpa parameter to the assessment of embrittlement gradients through the thickness of the pressure vessel wall has already been promulgated in Revision 2 to Regulatory Guide 1.99, "Radiation Damage to Reactor Vessel Materials."

This section provides the results of the neutron dosimetry evaluations performed in conjunction with the analysis of test specimens contained in surveillance capsule W137, withdrawn at the end of the fourth fuel cycle. This analysis is based on current state-of-the-art methodology and nuclear data, and is carried out in accordance with applicable ASTM standards[13 through 19]. The results provide a consistent fluence evaluation for use in determining the material properties of the Palo Verde Unit 2 reactor vessel.

In the dosimetry evaluation, fast neutron exposure parameters in terms of neutron fluence ($E > 1.0$ MeV), neutron fluence ($E > 0.1$ MeV), and iron atom displacements (dpa) are established for the capsule irradiation history. The analytical formalism relating the measured capsule exposure to the exposure of the vessel wall is described and used to project the integrated exposure of the vessel wall. Also, uncertainties associated with the derived exposure parameters at the surveillance capsules and with the projected exposure of the pressure vessel are provided.

6.2 Discrete Ordinates Analysis

A plan view of the reactor geometry at the core midplane is shown in Figure 4-1. Six irradiation capsules attached to the reactor vessel wall are included in the reactor design to constitute the reactor vessel surveillance program. The capsules are located at azimuthal angles of 38°, 43°, 137°, 142°, 230°, and 310° relative to the core cardinal axis as shown in Figure 4-1. A view of a surveillance capsule shown in Figure 4-2. The stainless steel specimen containers are 1.5 by 0.75-inch and approximately 96 inches in height. The containers are positioned axially such that the test specimens are centered on the core midplane, thus spanning the central 8 feet of the 12.5 foot high reactor core.

From a neutronic standpoint, the surveillance capsules and associated support structures are significant. The presence of these materials has a marked effect on both the spatial distribution of neutron flux and the neutron energy spectrum in the region near the location of each capsule. In order to determine the neutron environment at the test specimen location, the capsules themselves must therefore be included in the analytical model. A plan view of the 1/8 core model is shown in Figure 6-1.

In performing the fast neutron exposure evaluations for the surveillance capsules and reactor vessel, two distinct sets of transport calculations were carried out. The first set, a computation in the conventional forward mode, was used primarily to obtain relative neutron energy distributions

throughout the reactor geometry as well as to establish relative radial distributions of exposure parameters {ϕ(E > 1.0 MeV), ϕ(E > 0.1 MeV), and dpa/sec} through the vessel wall. The neutron spectral information was required for the interpretation of neutron dosimetry withdrawn from the surveillance capsules as well as for the determination of exposure parameter ratios; i.e., [dpa/sec]/[ϕ(E > 1.0 MeV)], within the pressure vessel geometry. The relative radial gradient information was required to permit the projection of measured exposure parameters to locations interior to the pressure vessel wall; i.e., the 1/4T, 1/2T, and 3/4T locations.

As shown in Figure 4-1, Palo Verde has four 45 degree octants with no surveillance capsules, two with one surveillance capsule at 40°, and two with two surveillance capsules at 38° and 43°. The forward calculational model is for the octant geometry with two surveillance capsules. Since the capsules are located adjacent to the vessel wall near the azimuthal maximum flux points, it was necessary to calculate the maximum vessel exposure using a second model with no surveillance capsules present. A comparison of the flux level at the reactor vessel inner radius with and without the surveillance capsules present at 38 and 43 degrees is shown in Figure 6-2. The calculation indicates that the maximum vessel fluence occurs near an angle of 40 degrees.

The second set of calculations consisted of a series of adjoint analyses relating the fast neutron flux, ϕ(E > 1.0 MeV), at surveillance capsule positions and at several azimuthal locations on the pressure vessel inner radius to neutron source distributions within the reactor core. These calculations used separate models for each of the three octant types as appropriate to determine the fluence in each surveillance capsule position and at vessel positions without capsules. The source importance functions generated from these adjoint analyses provided the basis for all absolute exposure calculations and comparison with measurement. These importance functions, when combined with fuel cycle specific neutron source distributions, yielded absolute predictions of neutron exposure at the locations of interest for each cycle of irradiation. They also established the means to perform similar predictions and dosimetry evaluations for all subsequent fuel cycles. It is important to note that the cycle specific neutron source distributions utilized in these analyses included not only spatial variations of fission rates within the reactor core but also accounted for the effects of varying neutron yield per fission and fission spectrum introduced by the build-up of plutonium as the burnup of individual fuel assemblies increased.

The absolute cycle specific data from the adjoint evaluations together with the relative neutron energy spectra and radial distribution information from the reference forward calculation provided the means to:

1 - Evaluate neutron dosimetry obtained from surveillance capsules.
2 - Extrapolate dosimetry results to key locations at the inner radius and through the thickness of the pressure vessel wall.
3 - Enable a direct comparison of analytical prediction with measurement.
4 - Establish a mechanism for projection of pressure vessel exposure as the design of each new fuel cycle evolves.

The forward transport calculation for the reactor model summarized in Figure 6-1 was carried out in R,θ geometry using the DOT two-dimensional discrete ordinates code[20] and the SAILOR cross-section library[21]. The SAILOR library is a 47 energy group ENDF/B-IV based data set produced specifically for light water reactor applications. In these analyses anisotropic scattering was treated with a P_3 expansion of the scattering cross-sections and the angular discretization was modeled with an S_8 order of angular quadrature.

The core power distribution utilized in the forward transport calculations was taken as an average of the first four cycles of operation for Palo Verde Unit 2. The neutron spectrum used was based on the burnup of the outer assemblies and utilized ENDF/B-V fission spectra for the contributing uranium and plutonium isotopes. The fuel power distributions were supplied by the Palo Verde staff in the form of beginning-of-cycle and end-of-cycle fuel pin and assembly burnups, and axial power shapes.

All adjoint calculations were also carried out using an S_8 order of angular quadrature and the P_3 cross-section approximation from the SAILOR library. Adjoint source locations were chosen at four azimuthal locations along the pressure vessel inner radius (0, 15, 30, 40, and 45 degrees) as well as at the geometric center of each surveillance capsule. Again, these calculations were run in R,θ geometry to provide neutron source distribution importance functions for the exposure parameter of interest, in this case $\phi(E > 1.0 \text{ MeV})$.

Having the importance functions and appropriate core source distributions, the response of interest is calculated as:

$$R(r,\theta) = \int_{r'} \int_{\theta'} \int_{E} I(r',\theta',E)\, S(r',\theta',E)\, r'\, dr'\, d\theta'\, dE$$

where:

$R(r,\theta)$ = $\phi(E > 1.0$ MeV) at radius r and azimuthal angle θ.

$I(r',\theta',E)$ = Adjoint source importance function at radius r', azimuthal angle θ', and neutron source energy E for the flux (E > 1 MeV) at location r, θ.

$S(r',\theta',E)$ = Neutron source strength at core location r',θ' and energy E.

Although the adjoint importance functions used in this analysis were based on a response function defined by the threshold neutron flux $\phi(E > 1.0$ MeV), prior calculations[22] have shown that, while the variation in fuel loading patterns significantly impacts both the magnitude and spatial distribution of the neutron field, changes in the relative neutron energy spectrum are of second order. Thus, for a given location the ratio of [dpa/sec]/[$\phi(E > 1.0$ MeV)] is insensitive to changing core source distributions. In the application of these adjoint importance functions to the Palo Verde Unit 2 reactor, therefore, the iron atom displacement rates (dpa/sec) and the neutron flux $\phi(E > 0.1$ MeV) were computed on a cycle specific basis by using [dpa/sec]/[$\phi(E > 1.0$ MeV)] and [$\phi(E > 0.1$ MeV)]/[$\phi(E > 1.0$ MeV)] ratios from the forward analysis in conjunction with the cycle specific $\phi(E > 1.0$ MeV) solutions from the individual adjoint evaluations.

The reactor core power distributions used in the plant specific adjoint calculations were taken from the fuel cycle design data supplied for the first four operating cycles of Palo Verde Unit 2 .

Selected results from the neutron transport analyses are provided in Tables 6-1 through 6-5. The data listed in these tables establish the means for absolute comparisons of analysis and measurement for the capsule irradiation periods and provide the means to correlate dosimetry results with the corresponding exposure of the pressure vessel wall.

In Table 6-1, the calculated exposure parameters [$\phi(E > 1.0$ MeV), $\phi(E > 0.1$ MeV), and dpa/sec] are given at the geometric center of the three surveillance capsule positions for the plant specific core power distributions. The plant specific data, based on the adjoint transport analysis, are meant to establish the absolute comparison of measurement with analysis. Similar data are given in Table 6-2 for the pressure vessel inner radius. Again, the three pertinent exposure parameters are listed for the cycle one through four plant specific power distributions. It is important to note that the data for the

vessel inner radius were taken at the clad/base metal interface; and, thus, represent the maximum predicted exposure levels of the vessel wall itself at the axial midplane.

Radial gradient information applicable to $\phi(E > 1.0\ MeV)$, $\phi(E > 0.1\ MeV)$, and dpa/sec is given in Tables 6-3, 6-4, and 6-5, respectively. The data, obtained from the forward neutron transport calculation, are presented on a relative basis for each exposure parameter at several azimuthal locations. Exposure distributions through the vessel wall may be obtained by normalizing the calculated or projected exposure at the vessel inner radius to the gradient data listed in Tables 6-3 through 6-5. Note that these distributions are developed for the case with no surveillance capsules present. The effect of the capsules is to slightly reduce the relative flux at the inside of the vessel at angles within about $\pm$ 2 degrees of the capsule location.

An example of the derivation of the neutron flux $\phi(E > 1.0\ MeV)$ at the 1/4T depth in the pressure vessel wall along the 45° azimuth is given by: .

$$\phi_{1/4T}(45°) = \phi(233.756, 45°)\ F(239.511, 45°)$$

where: $\phi_{1/4T}(45°)$ = Projected neutron flux at the 1/4T position on the 45° azimuth.

$\phi(233.756,45°)$ = Projected or calculated neutron flux at the vessel inner radius on the 45° azimuth.

$F(239.511,45°)$ = Ratio of the neutron flux at the 1/4T position to the flux at the vessel inner radius for the 45° azimuth. This ratio is obtained by interpolation from Table 6-3.

Similar expressions apply for exposure parameters expressed in terms of $\phi(E > 0.1\ MeV)$ and dpa/sec where the attenuation function F is obtained from Tables 6-4 and 6-5, respectively.

6.3 Neutron Dosimetry

The passive neutron sensors included in the Palo Verde Unit 2 surveillance program are listed in Table 6-6. Also given in Table 6-6 are the primary nuclear reactions and associated nuclear constants that were used in the evaluation of the neutron energy spectrum within the surveillance capsules and in the subsequent determination of the various exposure parameters of interest [$\phi(E > 1.0\ MeV)$, $\phi(E > 0.1\ MeV)$, dpa/sec]. The relative locations of the neutron sensors within the capsules are shown in Figure 4-2. Since the dosimeters are all located very close to the same distance from the core at the radial

center of the capsule, no gradient corrections were necessary. The iron, copper, titanium, and uranium (bare and covered) were each placed at three axial locations in the capsule near the top, middle, and bottom, respectively. The cobalt-aluminum monitors (bare and covered), as well as the nickel and sulfur, were only placed in the middle location in space provided by an extra dosimetry holder.

The use of passive monitors such as those listed in Table 6-6 does not yield a direct measure of the energy dependent neutron flux at the point of interest. Rather, the activation or fission process is a measure of the integrated effect that the time and energy dependent neutron flux has on the target material over the course of the irradiation period. An accurate assessment of the average neutron flux level incident on the various monitors may be derived from the activation measurements only if the irradiation parameters are well known. In particular, the following variables are of interest:

- The measured specific activity of each monitor.
- The physical characteristics of each monitor.
- The operating history of the reactor.
- The energy response of each monitor.
- The neutron energy spectrum at the monitor location.

The specific activity of each of the neutron monitors was determined using established ASTM procedures[23 through 29]. Following sample preparation and weighing, the activity of each monitor was determined by means of a lithium-drifted germanium, Ge(Li), gamma spectrometer. The irradiation history of the Palo Verde Unit 2 reactor during cycles one through four was supplied by NUREG-0020, "Licensed Operating Reactors Status Summary Report," for the applicable period. The irradiation history applicable to capsule W137 is given in Table 6-7.

Having the measured specific activities, the physical characteristics of the sensors, and the operating history of the reactor, reaction rates referenced to full power operation were determined from the following equation:

$$R = \frac{A}{N_0 F Y \sum \frac{P_j}{P_{ref}} C_j [1-e^{-\lambda t_j}] [e^{-\lambda t_d}]}$$

where:

R = Reaction rate averaged over the irradiation period and referenced to operation at a core power level of P_{ref} (rps/nucleus).

A = Measured specific activity (dps/gm).

N_0 = Number of target element atoms per gram of sensor.

F = Weight fraction of the target isotope in the sensor material.

Y = Number of product atoms produced per reaction.

P_j = Average core power level during irradiation period j (MW).

P_{ref} = Maximum or reference power level of the reactor (MW).

C_j = Calculated ratio of $\phi(E > 1.0\ MeV)$ during irradiation period j to the time weighted average $\phi(E > 1.0\ MeV)$ over the entire irradiation period.

λ = Decay constant of the product isotope (1/sec).

t_j = Length of irradiation period j (sec).

t_d = Decay time following irradiation period j (sec).

and the summation is carried out over the total number of monthly intervals comprising the irradiation period.

In the equation describing the reaction rate calculation, the ratio $[P_j]/[P_{ref}]$ accounts for month by month variation of reactor core power level within any given fuel cycle as well as over multiple fuel cycles. The ratio C_j, which was calculated for each fuel cycle using the adjoint transport technology discussed in Section 6.2, accounts for the change in sensor reaction rates caused by variations in flux level induced by changes in core spatial power distributions from fuel cycle to fuel cycle. For a single cycle irradiation C_j is normally taken to be 1.0. However, for multiple cycle irradiations, particularly those employing low leakage fuel management, the additional C_j term can be a significant correction.

For the irradiation history of capsule W137, the flux level term in the reaction rate calculations was developed from the plant specific analysis provided in Table 6-1. Measured and saturated reaction product specific activities as well as the derived full power reaction rates are listed in Table 6-8 for capsule W137. Reactions that are cadmium shielded are denoted in this table by an asterisk (*). Measured activities are given as corrected to 8/8/93. The table contains averages for each dosimeter that were used in the flux derivation except for U-238 which was corrected for U-235 fissions to give a corrected value of 1.53E-14 reactions per atom per second. The average value was used to derive a average value of flux for the capsule since the variation with axial position was found to be small and showed no correlation with the calculated axial shape (Figure 6-3).

Values of key fast neutron exposure parameters were derived from the measured reaction rates using the FERRET least squares adjustment code[30]. The FERRET approach used the measured reaction rate data, sensor reaction cross-sections, and a calculated trial spectrum as input and proceeded to adjust the group fluxes from the trial spectrum to produce a best fit (in a least squares sense) to the measured reaction rate data. The "measured" exposure parameters along with the associated uncertainties were then obtained from the adjusted spectrum.

In the FERRET evaluations, a log-normal least squares algorithm weights both the a priori values and the measured data in accordance with the assigned uncertainties and correlations. In general, the measured values f are linearly related to the flux ϕ by some response matrix A:

$$f_i^{(s,\alpha)} = \sum_g A_{ig}^{(s)} \phi_g^{(\alpha)}$$

where i indexes the measured values belonging to a single data set s, g designates the energy group, and α delineates spectra that may be simultaneously adjusted. For example,

$$R_i = \sum_g \sigma_{ig} \phi_g$$

relates a set of measured reaction rates R_i to a single spectrum ϕ_g by the multigroup reaction cross-section σ_{ig}. The log-normal approach automatically accounts for the physical constraint of positive fluxes, even with large assigned uncertainties.

In the least squares adjustment, the continuous quantities (i.e., neutron spectra and cross-sections) were approximated in a multi-group format consisting of 53 energy groups. The trial input spectrum was converted to the FERRET 53 group structure using the SAND-II code[31]. This procedure was carried out by first expanding the 47 group calculated spectrum into the SAND-II 620 group structure using a SPLINE interpolation procedure in regions where group boundaries do not coincide. The 620 point spectrum was then re-collapsed into the group structure used in FERRET.

The sensor set reaction cross-sections, obtained from the ENDF/B-V dosimetry file, were also collapsed into the 53 energy group structure using the SAND-II code. In this instance, the trial spectrum, as expanded to 620 groups, was employed as a weighting function in the cross-section collapsing procedure. Reaction cross-section uncertainties in the form of a 53 x 53 covariance matrix for each sensor reaction were also constructed from the information contained on the ENDF/B-V data files. These matrices included energy group to energy group uncertainty correlations for each of the individual reactions. However, correlations between cross-sections for different sensor reactions were

not included. The omission of this additional uncertainty information does not significantly impact the results of the adjustment.

Due to the importance of providing a trial spectrum that exhibits a relative energy distribution close to the actual spectrum at the sensor set locations, the neutron spectrum input to the FERRET evaluation was taken from the center of the surveillance capsule modeled in the forward transport calculation with a source distribution averaged over the first four cycles. While the 53 x 53 group covariance matrices applicable to the sensor reaction cross-sections were developed from the ENDF/B-V data files, the covariance matrix for the input trial spectrum was constructed from the following relation:

$$M_{gg'} = R_n^2 + R_g \, R_{g'} \, P_{gg'}$$

where R_n specifies an overall fractional normalization uncertainty (i.e., complete correlation) for the set of values. The fractional uncertainties R_g specify additional random uncertainties for group g that are correlated with a correlation matrix given by:

$$P_{gg'} = [1-\theta] \, \delta_{gg'} + \theta \, e^{-H}$$

where:

$$H = \frac{(g-g')^2}{2 \, \gamma^2}$$

The first term in the correlation matrix equation specifies purely random uncertainties, while the second term describes short range correlations over a group range γ (θ specifies the strength of the latter term). The value of δ is 1 when $g = g'$ and 0 otherwise. For the trial spectrum used in the current evaluations, a short range correlation of $\gamma = 6$ groups was used. This choice implies that neighboring groups are strongly correlated when θ is close to 1. Strong long range correlations (or anti-correlations) were justified based on information presented by R. E. Maerker[32]. Maerker's results are closely duplicated when $\gamma = 6$.

The uncertainties associated with the measured reaction rates included both statistical (counting) and systematic components. The systematic component of the overall uncertainty accounts for counter efficiency, counter calibrations, irradiation history corrections, and corrections for competing reactions in the individual sensors. Uncertainty estimates for the non-fission dosimeter results were taken to be 5% based on consistency studies of capsule dosimetry[33].

The U-238 sensors in the Palo Verde Unit 2 capsules are inserted both bare and cadmium covered. The bare sensors contain a significant contribution from U-235 impurity in the U-238 and also a contribution from plutonium production in the dosimeter. The difference between the bare and covered dosimeters can thus provide an estimated correction for determining the U-238 reaction rate in the covered dosimeters. This correction was found to be quite small. However, comparison of the bare U-238 dosimeter result with the cobalt results indicates that these results are probably inconsistent. In addition, the analysis of the cadmium covered U-238 dosimeters was hampered by incomplete recovery of the U-238 and mixing of the U-238 and cadmium. This necessitated a larger uncertainty assignment for the U-238 result. The inconsistency of the cobalt results also indicated that a larger uncertainty should be assigned to the low energy flux.

Results of the FERRET evaluations of the capsule W137 dosimetry are given in Tables 6-9 through 6-12. The data summarized in Table 6-9 include fast neutron exposure evaluations in terms of $\Phi(E > 1.0$ MeV), $\Phi(E > 0.1$ MeV), and dpa. In general good results were achieved in the fits of the adjusted spectra to the individual measured reaction rates (except for the U-238 which was assigned a large uncertainty as discussed above) as shown in Table 6-10. The adjusted spectra from the least squares evaluations are given in Table 6-11 in the FERRET 53 energy group structure. Table 6-12 compares the flux and fluence results derived from the dosimeter measurements (Table 6-9) with the calculated values (Table 6-1). The results for capsule W137 are the first results for a capsule from Palo Verde and thus cannot be compared with other similar capsules to check for consistency. However, the good agreement between calculated and measured values supports the adequacy of the analysis.

6.4 Projections of Pressure Vessel Exposure

Neutron exposure projections at key locations on the pressure vessel inner radius are given in Table 6-13. Along with the current (4.54 EFPY) exposure, projections are also provided for exposure periods of 15 EFPY and 32 EFPY. In computing these vessel exposures, the calculated values from Table 6-2 were scaled by the average measurement/calculation ratios (M/C) observed from the evaluations of dosimetry from capsule W137 for each fast neutron exposure parameter. This procedure resulted in bias factors of 1.07, 1.16, and 1.14 being applied to the calculated values of $\Phi(E > 1.0$ MeV), $\Phi(E > 0.1$ MeV), and dpa, respectively. Projections for future operation were based on the assumption that the average exposure rates characteristic of the cycle one through four irradiation would continue to be applicable throughout plant life. This is expected to be conservative since the fuel loading patterns employed since the first cycle have led to lower fluence than this average.

The overall uncertainty associated with the best estimate exposure projections at the pressure vessel wall depends on the individual uncertainties in the measurement process, the uncertainty in the dosimetry location, and on the uncertainty in the extrapolation of results from the measurement point to the point(s) of interest in the vessel wall. For Palo Verde Unit 2, the estimated extrapolation uncertainty is 5% and the uncertainty in the plant specific measurement/calculation bias factor derived from the surveillance capsule measurement is 11% as derived by the least squares process. These uncertainties are independent and so the total uncertainty is 12% as calculated by the square root of the sum of the squares of the individual uncertainty contributors. This 12% uncertainty in the projected exposure of the pressure vessel wall is a 1σ estimate for $\Phi(E > 1.0 \text{ MeV})$.

Exposure projections through the vessel at 15 EFPY and 32 EFPY are provided in Table 6-14 for use in the development of heatup and cooldown curves for Palo Verde Unit 2. Data are calculated based on both a $\Phi(E > 1.0 \text{ MeV})$ slope and a plant specific dpa slope through the vessel wall. The dpa equivalent fast neutron fluence levels for the 1/4T and 3/4T positions are defined by the relations:

$$\phi(1/4T) = \phi(0T) \frac{dpa(1/4T)}{dpa(0T)}$$

and

$$\phi(3/4T) = \phi(0T) \frac{dpa(3/4T)}{dpa(0T)} .$$

In Table 6-15 updated lead factors are listed for each of the Palo Verde Unit 2 surveillance capsules. Lead factor data based on the accumulated fluence through cycle four are provided for each capsule.

TABLE 6-1

CALCULATED FAST NEUTRON EXPOSURE RATES AT THE SURVEILLANCE CAPSULE CENTER

	Capsule Location		
	38°	40°	43°
	ϕ(E >1.0 MeV) [n/cm^2-sec]		
Cycle 1	3.376E+10	3.428E+10	3.355E+10
Cycle 2	2.361E+10	2.374E+10	2.328E+10
Cycle 3	2.470E+10	2.520E+10	2.506E+10
Cycle 4	2.461E+10	2.460E+10	2.401E+10
Average	2.672E+10	2.701E+10	2.653E+10
	ϕ(E > 0.1 MeV) [n/cm^2-sec]		
Cycle 1	6.117E+10	6.201E+10	6.060E+10
Cycle 2	4.277E+10	4.294E+10	4.206E+10
Cycle 3	4.475E+10	4.559E+10	4.526E+10
Cycle 4	4.458E+10	4.450E+10	4.338E+10
Average	4.840E+10	4.886E+10	4.792E+10
	Iron Atom Displacement Rate [dpa/sec]		
Cycle 1	4.908E-11	4.985E-11	4.879E-11
Cycle 2	3.432E-11	3.452E-11	3.386E-11
Cycle 3	3.591E-11	3.665E-11	3.644E-11
Cycle 4	3.578E-11	3.577E-11	3.493E-11
Average	3.884E-11	3.927E-11	3.859E-11

TABLE 6-2

CALCULATED AZIMUTHAL VARIATION OF FAST NEUTRON EXPOSURE RATES AT THE PRESSURE VESSEL CLAD/BASE METAL INTERFACE

	0°	15°	30°	40°	45°
			ϕ(E >1.0 MeV) [n/cm^2-sec]		
Cycle 1	1.418E+10	2.010E+10	2.026E+10	2.370E+10	2.299E+10
Cycle 2	1.021E+10	1.422E+10	1.525E+10	1.662E+10	1.613E+10
Cycle 3	1.147E+10	1.538E+10	1.538E+10	1.786E+10	1.733E+10
Cycle 4	1.272E+10	1.606E+10	1.641E+10	1.715E+10	1.664E+10
Average	1.217E+10	1.647E+10	1.684E+10	1.887E+10	1.831E+10
			ϕ(E > 0.1 MeV) [n/cm^2-sec]		
Cycle 1	2.930E+10	4.208E+10	4.244E+10	4.966E+10	4.849E+10
Cycle 2	2.111E+10	2.978E+10	3.195E+10	3.484E+10	3.402E+10
Cycle 3	2.370E+10	3.220E+10	3.222E+10	3.743E+10	3.655E+10
Cycle 4	2.628E+10	3.363E+10	3.438E+10	3.595E+10	3.510E+10
Average	2.515E+10	3.449E+10	3.528E+10	3.955E+10	3.980E+10
			Iron Atom Displacement Rate [dpa/sec]		
Cycle 1	2.194E-11	3.099E-11	3.112E-11	3.626E-11	3.525E-11
Cycle 2	1.580E-11	2.193E-11	2.343E-11	2.544E-11	2.473E-11
Cycle 3	1.775E-11	2.371E-11	2.363E-11	2.733E-11	2.657E-11
Cycle 4	1.968E-11	2.477E-11	2.521E-11	2.625E-11	2.552E-11
Average	1.883E-11	2.540E-11	2.587E-11	2.888E-11	2.893E-11

TABLE 6-3

RELATIVE RADIAL DISTRIBUTION OF $\phi(E > 1.0\ MeV)$
WITHIN THE PRESSURE VESSEL WALL

Radius (cm)	0°	15°	30°	40°	45°
233.756[1]	1.0000	1.0000	1.0000	1.0000	1.0000
234.006	0.9854	0.9851	0.9853	0.9856	0.9854
234.631	0.9368	0.9365	0.9369	0.9366	0.9370
235.506	0.8595	0.8580	0.8587	0.8572	0.8591
236.631	0.7571	0.7549	0.7560	0.7529	0.7554
237.923	0.6460	0.6430	0.6445	0.6405	0.6434
239.409	0.5335	0.5292	0.5310	0.5273	0.5303
241.196	0.4203	0.4159	0.4178	0.4143	0.4171
243.204	0.3194	0.3154	0.3173	0.3143	0.3164
245.062	0.2460	0.2431	0.2450	0.2425	0.2433
246.477	0.2003	0.1974	0.1992	0.1976	0.1981
247.78	0.1656	0.1619	0.1635	0.1631	0.1640
249.191	0.1346	0.1311	0.1326	0.1322	0.1333
250.715	0.1076	0.1041	0.1054	0.1049	0.1062
252.055	0.0877	0.0848	0.0860	0.0854	0.0861
253.098	0.0744	0.0713	0.0723	0.0720	0.0727
254.181	0.0625	0.0592	0.0601	0.0599	0.0604
255.181	0.0527	0.0494	0.0501	0.0497	0.0502
255.994	0.0452	0.0416	0.0422	0.0416	0.0421
256.775[2]	0.0391	0.0353	0.0358	0.0351	0.0356

NOTES: 1) Base Metal Inner Radius
2) Base Metal Outer Radius

TABLE 6-4

RELATIVE RADIAL DISTRIBUTION OF $\phi(E > 0.1$ MeV)
WITHIN THE PRESSURE VESSEL WALL

Radius (cm)	0°	15°	30°	40°	45°
233.756[1]	1.000	1.000	1.000	1.000	1.000
234.006	1.009	1.008	1.009	1.008	1.009
234.631	1.014	1.011	1.013	1.011	1.012
235.506	1.004	0.997	1.000	0.996	1.000
236.631	0.974	0.962	0.967	0.961	0.966
237.923	0.927	0.912	0.918	0.910	0.917
239.409	0.867	0.848	0.856	0.846	0.854
241.196	0.792	0.769	0.778	0.768	0.776
243.204	0.708	0.683	0.693	0.682	0.690
245.062	0.632	0.606	0.616	0.605	0.612
246.477	0.575	0.547	0.557	0.547	0.554
247.780	0.523	0.495	0.504	0.495	0.502
249.191	0.470	0.441	0.450	0.441	0.447
250.715	0.414	0.385	0.393	0.384	0.390
252.055	0.367	0.338	0.345	0.336	0.341
253.098	0.330	0.300	0.307	0.299	0.303
254.181	0.293	0.262	0.268	0.260	0.264
255.181	0.258	0.227	0.232	0.223	0.227
255.994	0.228	0.196	0.199	0.191	0.194
256.775[2]	0.203	0.171	0.173	0.164	0.167

NOTES:
1) Base Metal Inner Radius
2) Base Metal Outer Radius

TABLE 6-5

RELATIVE RADIAL DISTRIBUTION OF dpa/sec
WITHIN THE PRESSURE VESSEL WALL

Radius (cm)	0°	15°	30°	40°	45°
233.756[1]	1.0000	1.0000	1.0000	1.0000	1.0000
234.006	0.9868	0.9865	0.9869	0.9867	0.9870
234.631	0.9455	0.9449	0.9459	0.9450	0.9461
235.506	0.8816	0.8797	0.8816	0.8796	0.8822
236.631	0.7981	0.7951	0.7978	0.7944	0.7980
237.923	0.7073	0.7030	0.7066	0.7024	0.7065
239.409	0.6141	0.6080	0.6124	0.6080	0.6127
241.196	0.5179	0.5106	0.5156	0.5109	0.5159
243.204	0.4283	0.4203	0.4257	0.4209	0.4255
245.062	0.3592	0.3513	0.3567	0.3520	0.3557
246.477	0.3134	0.3047	0.3100	0.3062	0.3095
247.780	0.2761	0.2662	0.2712	0.2682	0.2718
249.191	0.2403	0.2301	0.2348	0.2317	0.2354
250.715	0.2061	0.1955	0.1998	0.1967	0.2000
252.055	0.1788	0.1684	0.1721	0.1689	0.1716
253.098	0.1588	0.1478	0.1511	0.1482	0.1507
254.181	0.1394	0.1278	0.1307	0.1278	0.1299
255.181	0.1223	0.1103	0.1125	0.1094	0.1112
255.994	0.1087	0.0956	0.0973	0.0939	0.0955
256.775[2]	0.0971	0.0834	0.0847	0.0812	0.0826

NOTES:
1) Base Metal Inner Radius
2) Base Metal Outer Radius

TABLE 6-6

NUCLEAR PARAMETERS USED IN THE EVALUATION OF NEUTRON SENSORS

Monitor Material	Reaction of Interest	Target Weight Fraction	Response Range	Product Half-Life	Fission Yield (%)
Copper*	$Cu^{63}(n,\alpha)Co^{60}$	0.6917	E > 5 MeV	5.271 yrs	
Iron	$Fe^{54}(n,p)Mn^{54}$	0.0580	E > 2 MeV	312.5 days	
Nickel*	$Ni^{58}(n,p)Co^{58}$	0.6827	E > 2 MeV	70.78 days	
Titanium	$Ti^{46}(n,p)Sc^{46}$	0.0810	E > 2 MeV	83.83 days	
Uranium-238*	$U^{238}(n,f)Cs^{137}$	1.0	E > 1 MeV	30.17 yrs	6.00
Cobalt-Aluminum*	$Co^{59}(n,\gamma)Co^{60}$	0.0017	0.4ev>E> 0.015 MeV	5.271 yrs	
Cobalt-Aluminum	$Co^{59}(n,\gamma)Co^{60}$	0.0017	E < 0.015 MeV	5.271 yrs	

*Denotes that monitor is cadmium shielded. Both bare and cadmium shielded U-238 monitors were included.

Note: The capsule also contained a sulfur dosimeter but this could not be analyzed due to decay of the P-32 which has a 14.28 day half-life.

TABLE 6-7

MONTHLY THERMAL GENERATION DURING THE FIRST FOUR FUEL CYCLES OF THE PALO VERDE UNIT 2 REACTOR

Year	Month	Thermal Generation (MW-hr)
1986	5	178458
	6	748794
	7	179055
	8	789746
	9	441921
	10	1785522
	11	2573938
	12	2217984
1987	1	816605
	2	0
	3	843281
	4	2523504
	5	2217619
	6	2370470
	7	2667944
	8	2807364
	9	2670655
	10	2794687
	11	2400712
	12	2799320
1988	1	2796621
	2	1711979
	3	0
	4	0
	5	0
	6	510519
	7	2794833
	8	2713036
	9	2702001
	10	2814560
	11	1909336
	12	2766725
1989	1	2800843
	2	1383148
	3	1303549
	4	0
	5	0
	6	20794
	7	1657660
	8	2576391
	9	1206913
	10	1205545
	11	0
	12	2546733
1990	1	2806069
	2	2064631
	3	0
	4	0
	5	0
	6	0
	7	558801
	8	2659419
	9	2724764
	10	2746944
	11	2722657
	12	2809763
1991	1	2810976
	2	2550144
	3	2797277
	4	2733538
	5	2826434
	6	2734422
	7	2825239
	8	1760151
	9	2731841
	10	1454795
	11	0
	12	0
1992	1	1548257
	2	2642730
	3	2150742
	4	2730948
	5	2824993
	6	2735197
	7	2826315
	8	2823534
	9	2701162
	10	2797104
	11	2490116
	12	2819640
1993	1	2825987
	2	2549505
	3	1182454

(Shutdown 3/14/93)

TABLE 6-8

MEASURED SENSOR ACTIVITIES AND REACTION RATES
SURVEILLANCE CAPSULE W137

MONITOR AND AXIAL LOCATION	MEASURED ACTIVITY (dis/sec-gm)	SATURATED ACTIVITY (dis/sec-gm)	REACTION RATE (rps/nucleus)
Cu-63 (n,α) Co-60*			
93-3144 TOP	1.22E+05	3.204E+05	
93-3153 MID	1.19E+05	3.125E+05	
93-3158 BOT	1.19E+05	3.125E+05	
Averages	1.20E+05	3.152E+05	4.808E-17
Fe-54 (n,p) Mn-54			
93-3142 TOP	1.29E+06	2.334E+06	
93-3147 MID	1.28E+06	2.316E+06	
93-3156 BOT	1.24E+06	2.243E+06	
Averages	1.27E+06	2.298E+06	3.674E-15
Ni-58 (n,p) Co-58*			
93-3152 MID	6.81E+06	3.278E+07	4.680E-15
Ti-46 (n,p) Sc-46			
93-3141 TOP	2.01E+05	7.786E+05	
93-3146 MID	1.95E+05	7.553E+05	
93-3155 BOT	1.90E+05	7.360E+05	
Averages	1.95E+05	7.566E+05	7.128E-16
U-238 (n,f) Cs-137*			
93-3143 TOP	2.50E+05	2.607E+06	
93-3151 MID	2.08E+05	2.169E+06	
93-3157 BOT	2.16E+05	2.252E+06	
Averages	2.25E+05	2.343E+06	1.544E-14
U-238 (n,f) Cs-137			
93-3140 TOP	3.25E+06	3.389E+06	
93-3157 BOT	2.79E+05	2.909E+06	
Averages	3.02E+05	3.149E+06	2.075E-14
Co-59 (n,γ) Co-60			
93-3148 MID	6.67E+07	1.752E+08	1.143E-11
Co-59 (n,γ) Co-60*			
93-3150 MID	7.98E+06	2.096E+07	1.367E-12

TABLE 6-9

SUMMARY OF NEUTRON DOSIMETRY RESULTS
SURVEILLANCE CAPSULE W137

Calculation of Measured Fluence	Flux	Time	Fluence	Uncertainty
Meas Fluence < 0.414 ev	3.177E+11	1.433E+08	4.551E+19	±22%
Meas Fluence > 0.1 Mev	5.575E+11	1.433E+08	7.987E+18	±18%
Meas Fluence > 1.0 Mev	2.842E+10	1.433E+08	4.071E+18	±11%
dpa	4.379E-11	1.433E+08	6.273E-03	±11%

TABLE 6-10

COMPARISON OF MEASURED AND FERRET CALCULATED
REACTION RATES AT THE SURVEILLANCE CAPSULE CENTER
SURVEILLANCE CAPSULE W137

REACTION	MEASURED	ADJUSTED CALCULATION	C/M
Cu-63 (n,α) Co-60	4.81E-17	4.85E-17	1.01
Fe-54 (n,p) Mn-54	3.67E-15	3.68E-15	1.00
Ni-58 (n,p) Co-58	4.68E-15	4.71E-15	1.01
Ti-46 (n,p) Sc-46	7.13E-16	7.11E-16	1.00
U-238 (n,f) Cs-137 (Cd)	1.53E-14	1.26E-14	0.83
Co-59 (n,γ) Co-60	1.01E-11	1.00E-11	0.99
Co-59 (n,γ) Co-60 (Cd)	1.21E-12	1.19E-12	0.99

TABLE 6-11

ADJUSTED NEUTRON ENERGY SPECTRUM AT THE CENTER OF SURVEILLANCE CAPSULE W137

GROUP	ENERGY (MeV)	ADJUSTED FLUX (n/cm²-sec)	GROUP	ENERGY (MeV)	ADJUSTED FLUX (n/cm²-sec)
1	17.33	5.60E+06	28	9.119E-03	2.45E+09
2	14.92	1.30E+07	29	5.531E-03	2.77E+09
3	13.50	5.48E+07	30	3.355E-03	9.33E+08
4	11.62	1.28E+08	31	2.839E-03	9.57E+08
5	10.00	2.94E+08	32	2.404E-03	1.01E+09
6	8.607	5.06E+08	33	2.035E-03	3.27E+09
7	7.408	1.23E+09	34	1.234E-03	3.61E+09
8	6.065	1.70E+09	35	7.485E-04	4.08E+09
9	4.966	2.94E+09	36	4.540E-04	4.60E+09
10	3.679	2.82E+09	37	2.754E-04	5.28E+09
11	2.865	4.67E+09	38	1.670E-04	9.97E+09
12	2.231	4.43E+09	39	1.013E-04	5.60E+09
13	1.738	4.51E+09	40	6.144E-05	5.15E+09
14	1.353	3.47E+09	41	3.727E-05	4.59E+09
15	1.108	4.83E+09	42	2.260E-05	4.06E+09
16	8.208E-01	4.42E+09	43	1.371E-05	3.63E+09
17	6.393E-01	3.95E+09	44	8.315E-06	3.33E+09
18	4.979E-01	2.87E+09	45	5.043E-06	3.12E+09
19	3.877E-01	3.24E+09	46	3.059E-06	2.97E+09
20	3.020E-01	4.84E+09	47	1.855E-06	2.82E+09
21	1.832E-01	4.12E+09	48	1.125E-06	2.63E+09
22	1.111E-01	3.39E+09	49	6.826E-07	3.14E+09
23	6.738E-02	2.85E+09	50	4.140E-07	4.11E+09
24	4.087E-02	2.14E+09	51	2.511E-07	1.61E+10
25	2.554E-02	1.49E+09	52	1.523E-07	3.90E+10
26	1.989E-02	1.24E+09	53	9.237E-08	2.59E+11
27	1.503E-02	2.27E+09			

Note: Tabulated energy levels represent the upper energy in each group.

TABLE 6-12

COMPARISON OF CALCULATED AND MEASURED NEUTRON EXPOSURE LEVELS FOR PALO VERDE UNIT 2 SURVEILLANCE CAPSULE W137

Comparison of Calculated and Measured INTEGRATED Neutron EXPOSURE for Capsule W137

	Calculated	Measured	C / M
Fluence (E > 1.0 Mev) [n/cm2-sec]	3.801E+18	4.071E+18	0.934
Fluence (E > 0.1 Mev) [n/cm2-sec]	6.865E+18	7.987E+18	0.860
dpa	5.528E-03	6.273E-03	0.881

Comparison of Calculated and Measured Neutron EXPOSURE RATE for Capsule W137

	Calculated	Measured	C / M
Flux (E > 1.0 Mev) [n/cm2-sec]	2.653E+10	2.842E+10	0.934
Flux (E > 0.1 Mev) [n/cm2-sec]	4.792E+10	5.575E+10	0.860
dpa/s	3.859E-11	4.379E-11	0.881

TABLE 6-13

NEUTRON EXPOSURE PROJECTIONS AT KEY LOCATIONS
ON THE PRESSURE VESSEL CLAD/BASE METAL INTERFACE

BEST ESTIMATE EXPOSURE (4.540 EFPY) AT THE PRESSURE VESSEL INNER RADIUS

	0 DEG[a]	15 DEG	30 DEG[b]	40 DEG[c]	45 DEG
E > 1.0	1.873E+18	2.535E+18	2.592E+18	2.904E+18	2.818E+18
E > 0.1	4.203E+18	5.764E+18	5.897E+18	6.610E+18	6.453E+18
dpa	3.070E-03	4.141E-03	4.219E-03	4.708E-03	4.577E-03

BEST ESTIMATE FLUENCE RATE AT THE PRESSURE VESSEL INNER RADIUS

	0 DEG[a]	15 DEG	30 DEG[b]	40 DEG[c]	45 DEG
E > 1.0	1.307E+10	1.770E+10	1.809E+10	2.027E+10	1.967E+10
E > 0.1	2.934E+10	4.023E+10	4.116E+10	4.614E+10	4.505E+10
dpa	2.143E-11	2.891E-11	2.945E-11	3.287E-11	3.195E-11

BEST ESTIMATE EXPOSURE (15.0 EFPY) AT THE PRESSURE VESSEL INNER RADIUS

	0 DEG[a]	15 DEG	30 DEG[b]	40 DEG[c]	45 DEG
E > 1.0	6.187E+18	8.376E+18	8.565E+18	9.595E+18	9.310E+18
E > 0.1	1.389E+19	1.905E+19	1.949E+19	2.184E+19	2.132E+19
dpa	1.014E-02	1.368E-02	1.394E-02	1.556E-02	1.512E-02

BEST ESTIMATE EXPOSURE (32.0 EFPY) AT THE PRESSURE VESSEL INNER RADIUS

	0 DEG[a]	15 DEG	30 DEG[b]	40 DEG[c]	45 DEG
E > 1.0	1.320E+19	1.787E+19	1.827E+19	2.047E+19	1.986E+19
E > 0.1	2.963E+19	4.063E+19	4.157E+19	4.659E+19	4.549E+19
dpa	2.164E-02	2.919E-02	2.974E-02	3.319E-02	3.226E-02

(a) Applies to axial weld at 90° location.
(b) Applies to axial weld at 210° and 330° locations.
(c) Maximum fluence point.

TABLE 6-14

NEUTRON EXPOSURE VALUES FOR USE IN THE GENERATION OF HEATUP/COOLDOWN CURVES

FLUENCE BASED ON E > 1.0 MeV SLOPE

	0 DEG[a]	15 DEG	30 DEG[b]	40 DEG[c]	45 DEG
			15 EFPY FLUENCE		
SURFACE	6.187E+18	8.376E+18	8.565E+18	9.595E+18	9.301E+18
1/4T	3.256E+18	4.373E+18	4.486E+18	5.025E+18	4.842E+18
3/4T	6.352E+17	8.324E+17	8.621E+17	9.658E+17	9.323E+17
			32 EFPY FLUENCE		
SURFACE	1.320E+19	1.787E+19	1.827E+19	2.047E+19	1.986E+19
1/4T	6.946E+18	9.328E+18	9.570E+18	1.072E+19	1.033E+19
3/4T	1.355E+18	1.776E+18	1.839E+18	2.060E+18	1.989E+18

FLUENCE BASED ON dpa SLOPE

	0 DEG[a]	15 DEG	30 DEG[b]	40 DEG[c]	45 DEG
			15 EFPY FLUENCE		
SURFACE	6.187E+18	8.376E+18	8.565E+18	9.595E+18	9.301E+18
1/4T	3.763E+18	5.042E+18	5.194E+18	5.776E+18	5.604E+18
3/4T	1.235E+18	1.583E+18	1.654E+18	1.823E+18	1.769E+18
			32 EFPY FLUENCE		
SURFACE	1.320E+19	1.787E+19	1.827E+19	2.047E+19	1.986E+19
1/4T	8.028E+18	1.076E+19	1.108E+19	1.232E+19	1.195E+19
3/4T	2.634E+18	3.377E+18	3.528E+18	3.889E+18	3.773E+18

(a) Applies to axial weld at 90° location.

(b) Applies to axial weld at 210° and 330° locations.

(c) Maximum fluence point.

TABLE 6-15

UPDATED LEAD FACTORS FOR PALO VERDE UNIT 2
SURVEILLANCE CAPSULES

CAPSULE	LEAD FACTOR
W38	1.41
W43	1.40
W137	1.40*
W142	1.41
W230	1.43
W310	1.43

* WITHDRAWN EOC 4, BASIS FOR THIS ANALYSIS

FIGURE 6-1

PALO VERDE REACTOR MODEL SHOWING A 45 DEGREE (R,Θ) SECTOR

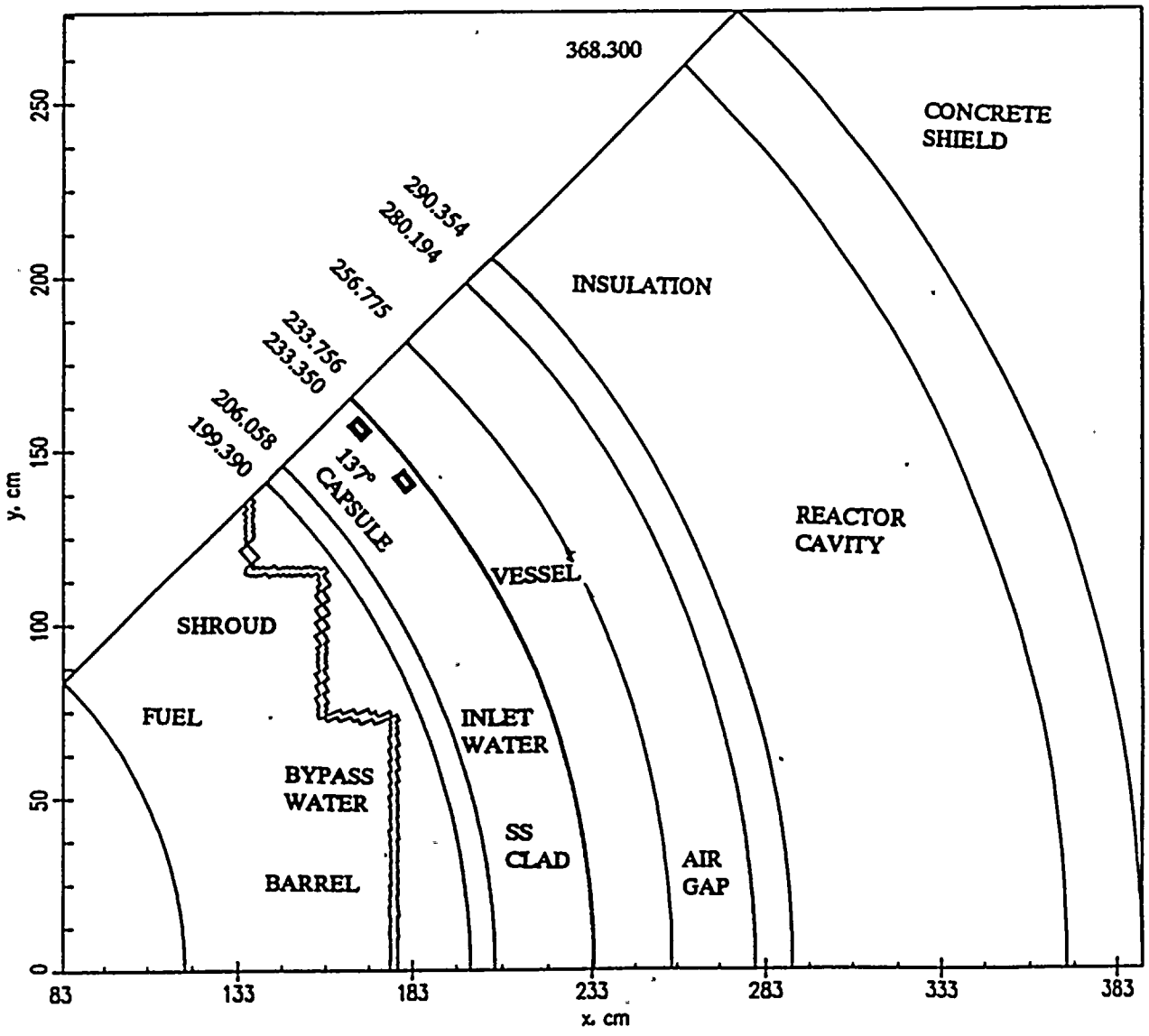

FIGURE 6-2

AZIMUTHAL VARIATION OF NEUTRON FLUX (E > 1.0 MEV)
AT THE REACTOR VESSEL INNER RADIUS

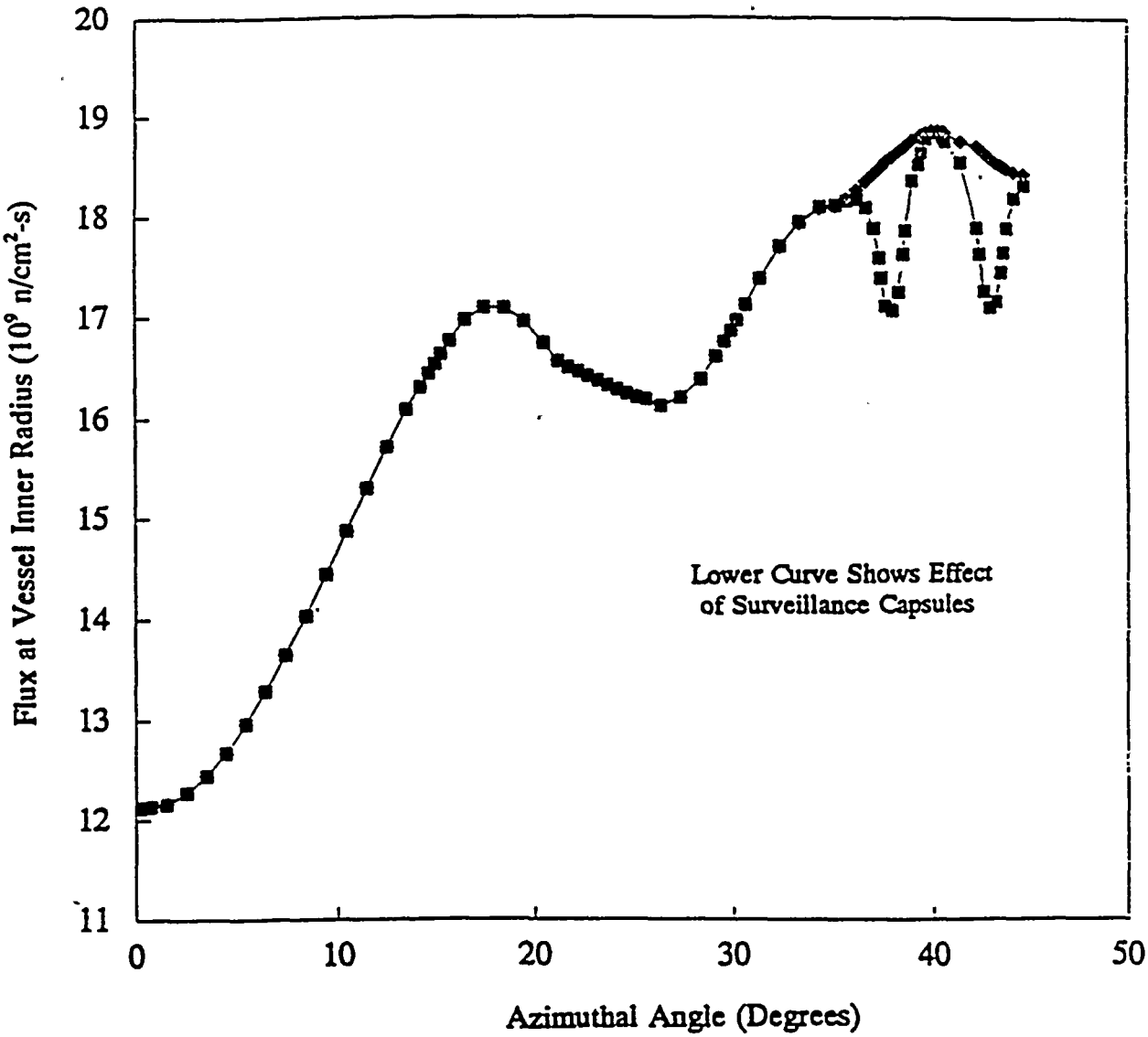

FIGURE 6-3

AXIAL DISTRIBUTION OF REACTOR POWER

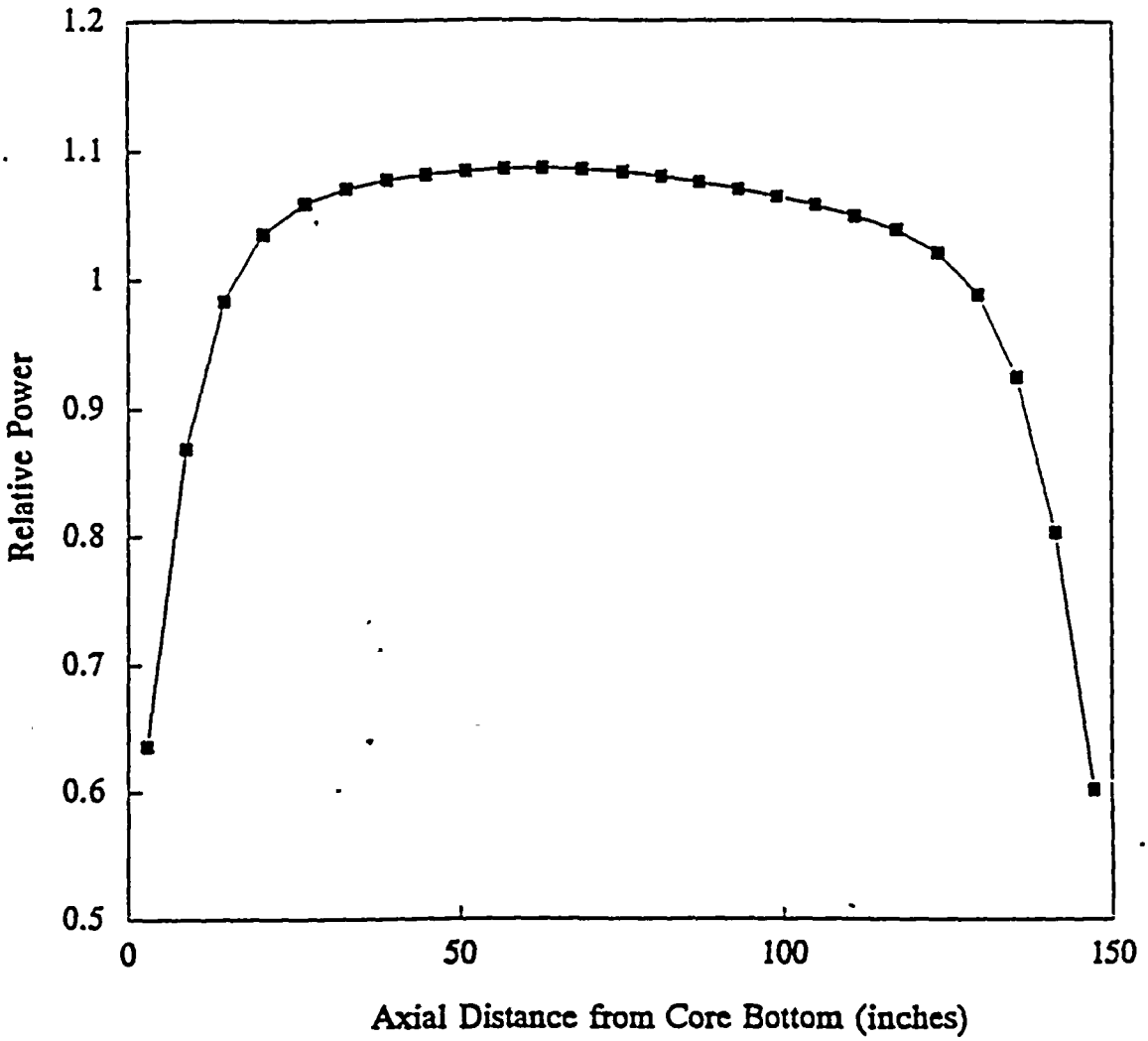

SECTION 7.0

SURVEILLANCE CAPSULE REMOVAL SCHEDULE

The following surveillance capsule removal schedule meets the requirements of ASTM E185-82 and is recommended for future capsules to be removed from the Palo Verde Unit 2 reactor vessel:

Table 7-1

Palo Verde Unit 2 Reactor Vessel Surveillance Capsule Withdraw Schedule

Location	Lead Factor	Removal Time (EFPY)[a]	Fluence (n/cm^2)
137°	1.40	4.540	4.071×10^{18} [b]
230°	1.43	15	1.37×10^{19}
310°	1.43	EOL	2.93×10^{19}
38°	1.41	Stand-by	- -
43°	1.40	Stand-by	- -
142°	1.41	Stand-By	- -

(a) Effective Full Power Years (EFPY) from plant startup.

(b) Actual measured neutron fluence

SECTION 8.0
REFERENCES

1. Regulatory Guide 1.99, Revision 2, *Radiation Embrittlement of Reactor Vessel Materials*, U.S. Nuclear Regulatory Commission, May, 1988.

2. Chang, B.C., *Arizona Public Service Company Palo Verde Unit 2 Evaluation for Baseline Specimens Reactor Vessel Materials Irradiation Surveillance Program*, ABB Combustion Engineering Report TR-V-MCM-013, November 5, 1992.

3. Section III of the ASME Boiler and Pressure Vessel Code, Appendix G, *Protection Against Nonductile Failure.*

4. ASTM E208, *Standard Test Method for Conducting Drop-Weight Test to Determine Nil-Ductility Transition Temperature of Ferritic Steels*, in ASTM Standards, Section 3, American Society for Testing and Materials, Philadelphia, PA.

5. Data package supplied to Westinghouse by the Arizona Public Service Company (File APT-106/13 Capsule W137)).

6. Code of Federal Regulations, 10CFR50, Appendix G, *Fracture Toughness Requirements*, and Appendix H, *Reactor Vessel Material Surveillance Program Requirements*, U.S. Nuclear Regulatory Commission, Washington, D.C.

7. ASTM E185-82, *Standard Practice for Conducting Surveillance Tests for Light-Water Cooled Nuclear Power Reactor Vessels, E706 (IF)*, in ASTM Standards, Section 3, American Society for Testing and Materials, Philadelphia, PA, 1993.

8. ASTM E23-92, *Standard Test Methods for Notched Bar Impact Testing of Metallic Materials*, in ASTM Standards, Section 3, American Society for Testing and Materials, Philadelphia, PA, 1992.

9. ASTM A370-92, *Standard Test Methods and Definitions for Mechanical Testing of Steel Products*, in ASTM Standards, Section 3, American Society for Testing and Materials, Philadelphia, PA, 1993.

10. ASTM E8-91, *Standard Test Methods of Tension Testing of Metallic Materials*, in ASTM Standards, Section 3, American Society for Testing and Materials, Philadelphia, PA, 1991.

11. ASTM E21-79(1988), *Standard Practice for Elevated Temperature Tension Tests of Metallic Materials*, in ASTM Standards, Section 3, American Society for Testing and Materials, Philadelphia, PA, 1989.

12. ASTM E83-92, *Standard Practice for Verification and Classification of Extensometers*, in ASTM Standards, Section 3, American Society for Testing and Materials, Philadelphia, PA, 1992.

13. ASTM Designation E853-87, *Standard Practice for Analysis and Interpretation of Light-Water Reactor Surveillance Results*, in ASTM Standards, Section 12, American Society for Testing and Materials, Philadelphia, PA, 1993.

14. ASTM Designation E693-79, *Standard Practice for Characterizing Neutron Exposures in Ferritic Steels in Terms of Displacements per Atom (dpa)*, in ASTM Standards, Section 12, American Society for Testing and Materials, Philadelphia, PA, 1993.

15. ASTM Designation E706-87, *Standard Master Matrix for Light-Water Reactor Pressure Vessel Surveillance Standard*, in ASTM Standards, Section 12, American Society for Testing and Materials, Philadelphia, PA, 1993.

16. ASTM Designation E482-89, *Standard Guide for Application of Neutron Transport Methods for Reactor Vessel Surveillance*, in ASTM Standards, Section 12, American Society for Testing and Materials, Philadelphia, PA, 1993.

17. ASTM Designation E560-84, *Standard Recommended Practice for Extrapolating Reactor Vessel Surveillance Dosimetry Results*, in ASTM Standards, Section 12, American Society for Testing and Materials, Philadelphia, PA, 1993.

18. ASTM Designation E261-90, *Standard Method for Determining Neutron Flux, Fluence, and Spectra by Radioactivation Techniques*, in ASTM Standards, Section 12, American Society for Testing and Materials, Philadelphia, PA, 1993.

19. ASTM Designation E262-86, *Standard Method for Measuring Thermal Neutron Flux by Radioactivation Techniques*, in ASTM Standards, Section 12, American Society for Testing and Materials, Philadelphia, PA, 1993.

20. R. G. Soltesz, R. K. Disney, J. Jedruch, and S. L. Ziegler, *Nuclear Rocket Shielding Methods, Modification, Updating and Input Data Preparation. Vol. 5--Two-Dimensional Discrete Ordinates Transport Technique*, WANL-PR(LL)-034, Vol. 5, August 1970.

21. *ORNL RSCI Data Library Collection DLC-76 SAILOR Coupled Self-Shielded, 47 Neutron, 20 Gamma-Ray, P3, Cross Section Library for Light Water Reactors.*

22. R. E. Maerker, et al, *Accounting for Changing Source Distributions in Light Water Reactor Surveillance Dosimetry Analysis*, Nuclear Science and Engineering, Volume 94, Pages 291-308, 1986.

23. ASTM Designation E1005-84, *Standard Method for Application and Analysis of Radiometric Monitors for Reactor Vessel Surveillance*, in ASTM Standards, Section 12, American Society for Testing and Materials, Philadelphia, PA, 1993.

24. ASTM Designation E263-88, *Standard Method for Determining Fast-Neutron Reaction Rates by Radioactivation of Iron*, in ASTM Standards, Section 12, American Society for Testing and Materials, Philadelphia, PA, 1993.

25. ASTM Designation E264-92, *Standard Method for Determining Fast-Neutron Reaction Rates by Radioactivation of Nickel*, in ASTM Standards, Section 12, American Society for Testing and Materials, Philadelphia, PA, 1993.

26. ASTM Designation E481-86, *Standard Method for Measuring Neutron Fluence Rate by Radioactivation of Cobalt and Silver*, in ASTM Standards, Section 12, American Society for Testing and Materials, Philadelphia, PA, 1993.

27. ASTM Designation E523-92, *Standard Method for Determining Fast-Neutron Reaction Rates by Radioactivation of Copper*, in ASTM Standards, Section 12, American Society for Testing and Materials, Philadelphia, PA, 1993.

28. ASTM Designation E526-92, *Standard Method for Determining Fast-Neutron Reaction Rates by Radioactivation of Titanium*, in ASTM Standards, Section 12, American Society for Testing and Materials, Philadelphia, PA, 1993.

29. ASTM Designation E704-90, *Standard Method for Measuring Reaction Rates by Radioactivation of Uranium-238*, in ASTM Standards, Section 12, American Society for Testing and Materials, Philadelphia, PA, 1993.

30. F. A. Schmittroth, *FERRET Data Analysis Core*, HEDL-TME 79-40, Hanford Engineering Development Laboratory, Richland, WA, September 1979.

31. W. N. McElroy, S. Berg and T. Crocket, *A Computer-Automated Iterative Method of Neutron Flux Spectra Determined by Foil Activation*, AFWL-TR-7-41, Vol. I-IV, Air Force Weapons Laboratory, Kirkland AFB, NM, July 1967.

32. EPRI-NP-2188, *Development and Demonstration of an Advanced Methodology for LWR Dosimetry Applications*, R. E. Maerker, et al., 1981.

33. WCAP-13390, *Westinghouse Fast Neutron Exposure Methodology for Pressure Vessel Fluence Determination and Dosimetry Evaluation*, S. L. Anderson, May 1992.

APPENDIX A

Load-Time Records for Charpy Specimen Tests and Comparisons of Data for Unirradiated and Irradiated Precarcked Charpy Specimens

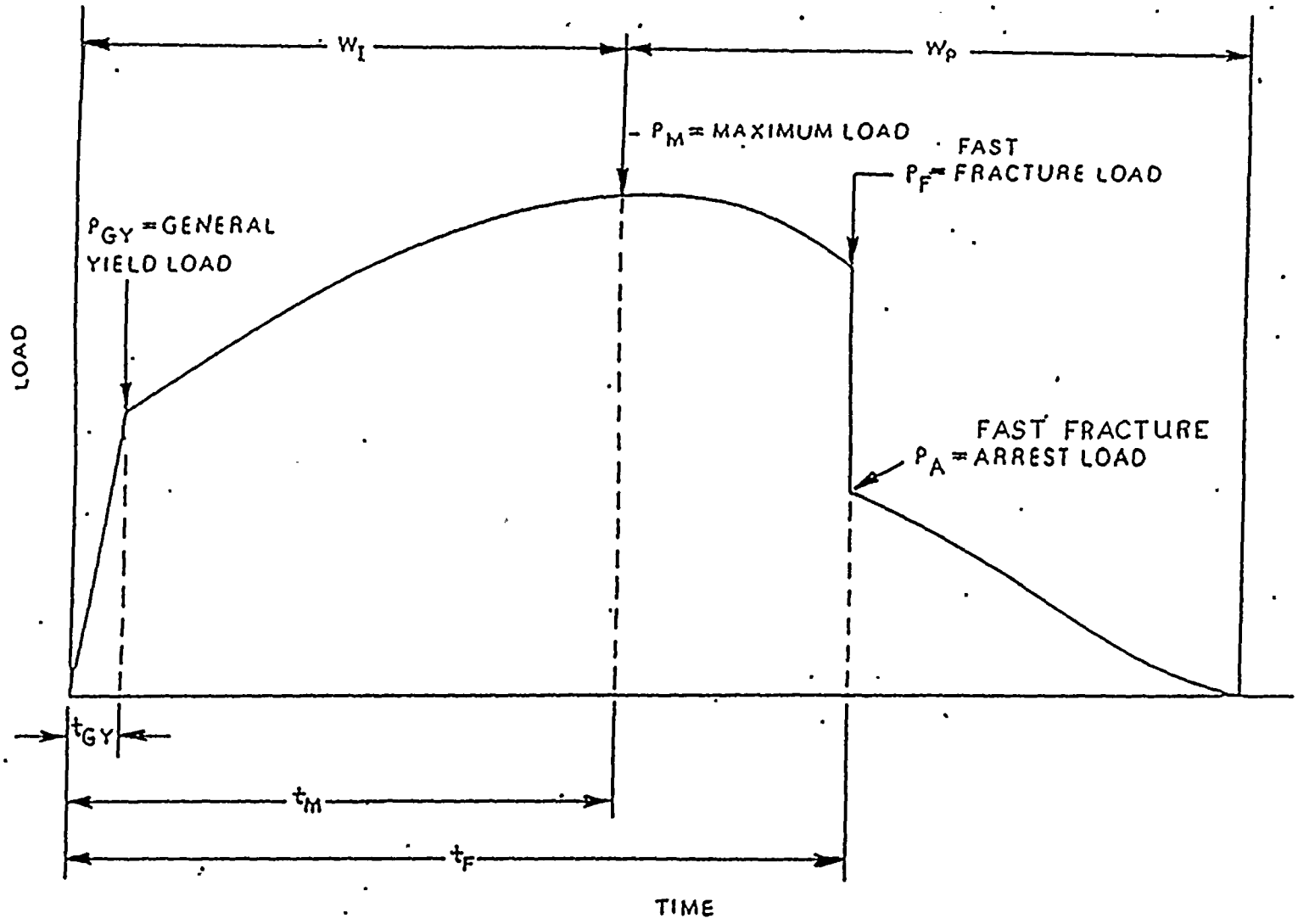

W_I = Fracture initiation region

W_P = Fracture propagation region

t_{GY} = Time to general yielding

t_M = Time to maximum load

t_F = Time to fast (brittle) fracture start

Figure A-1. Idealized load-time record

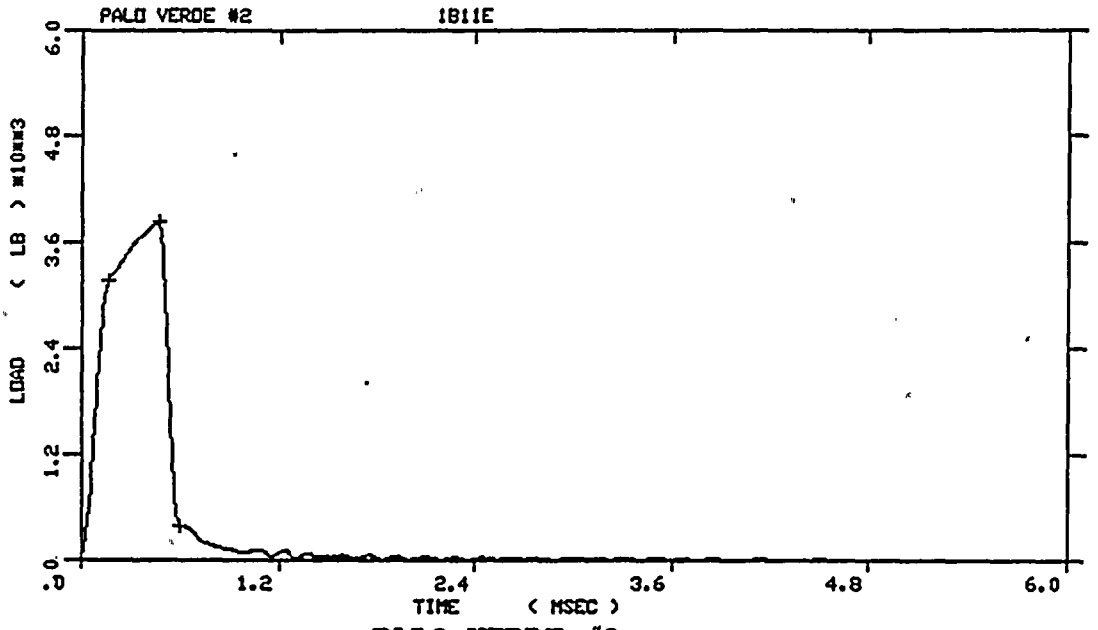

PALO VERDE #2

1B11E :

:

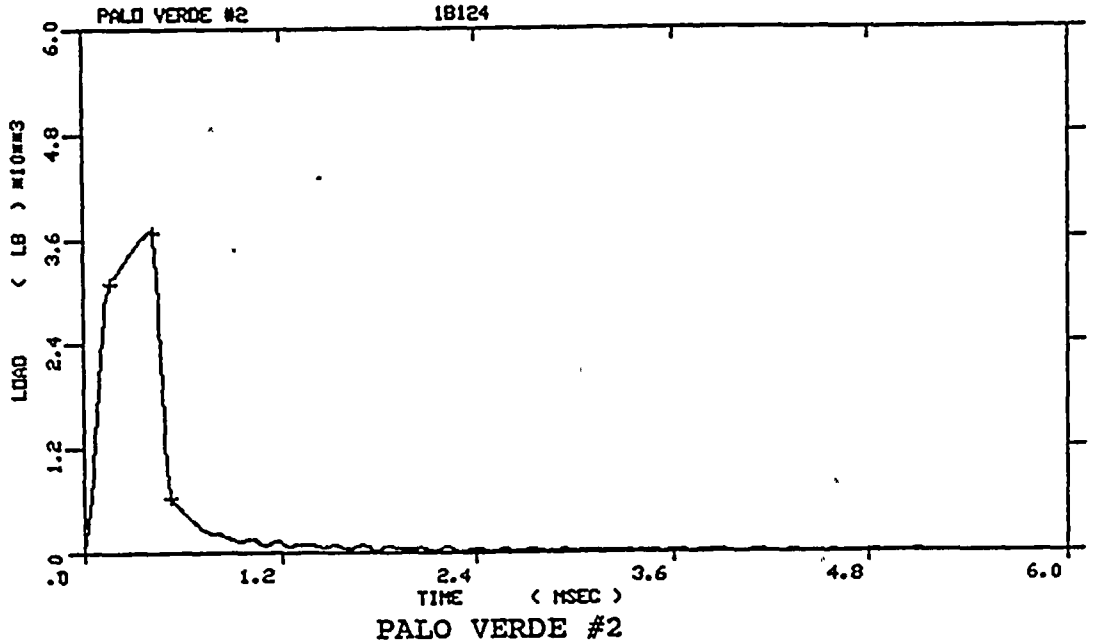

PALO VERDE #2

1B124 :

:

Figure A-2. Load-time records for Specimens 1B11E and 1B124

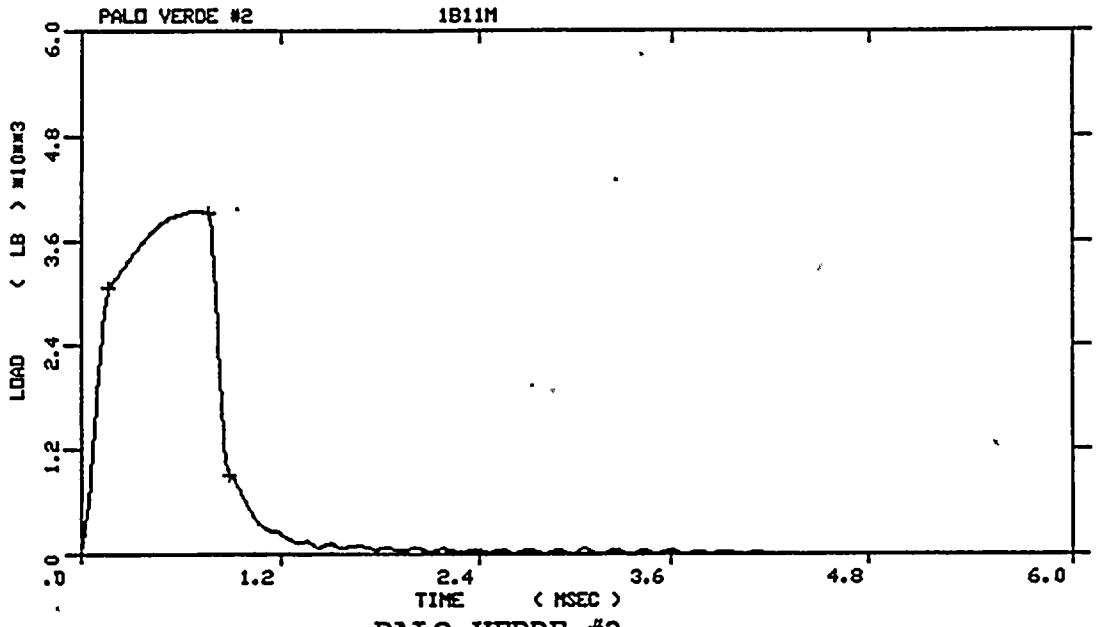

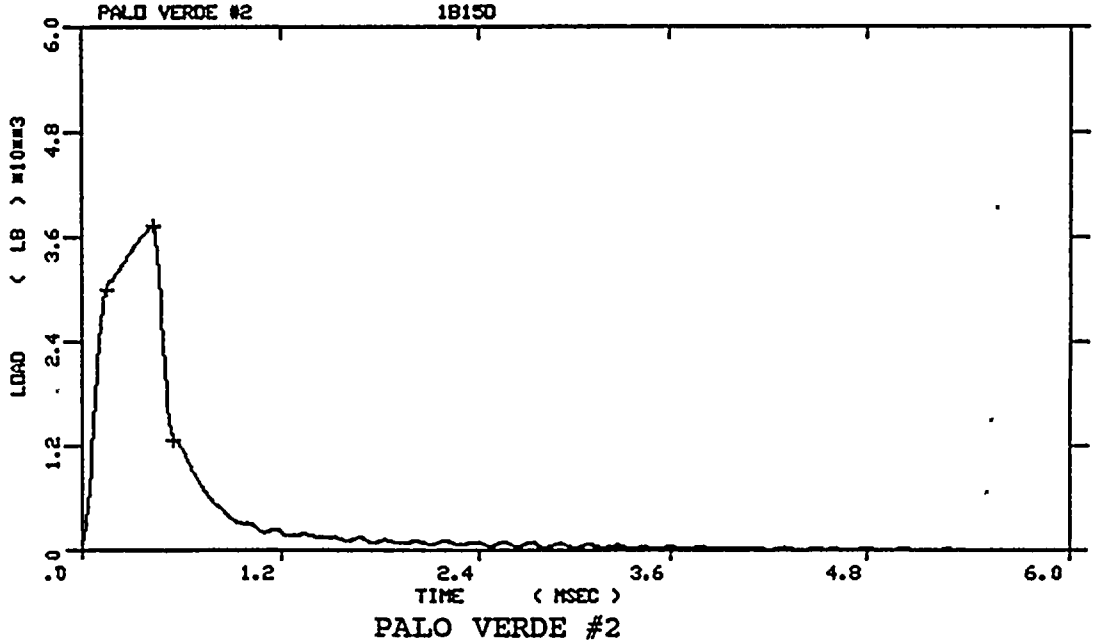

Figure A-3. Load-time records for Specimens 1B11M and 1B15D

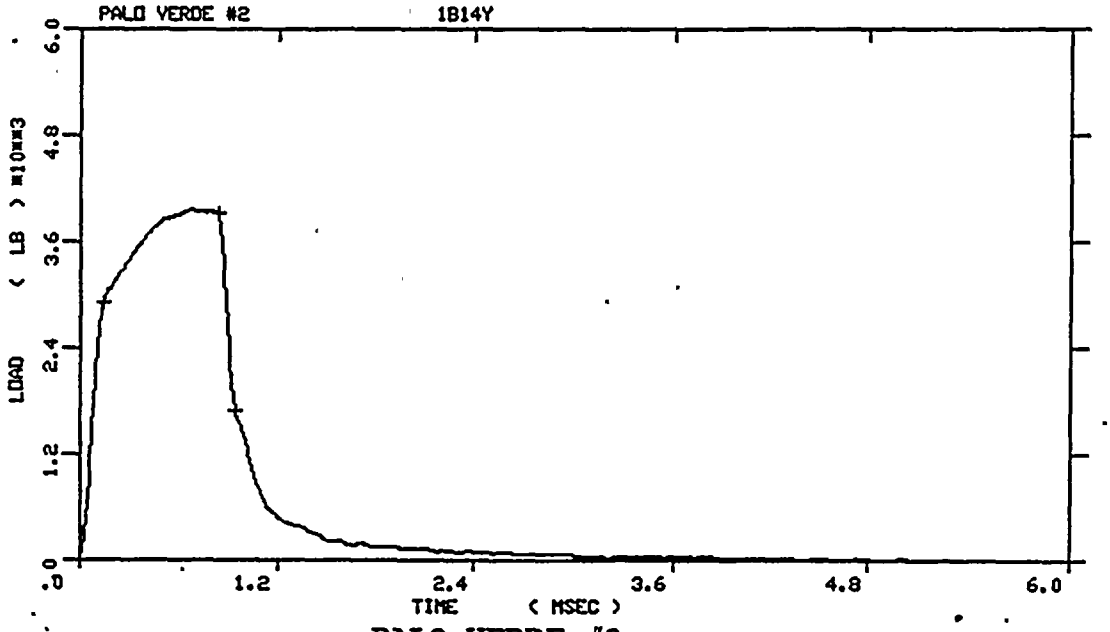

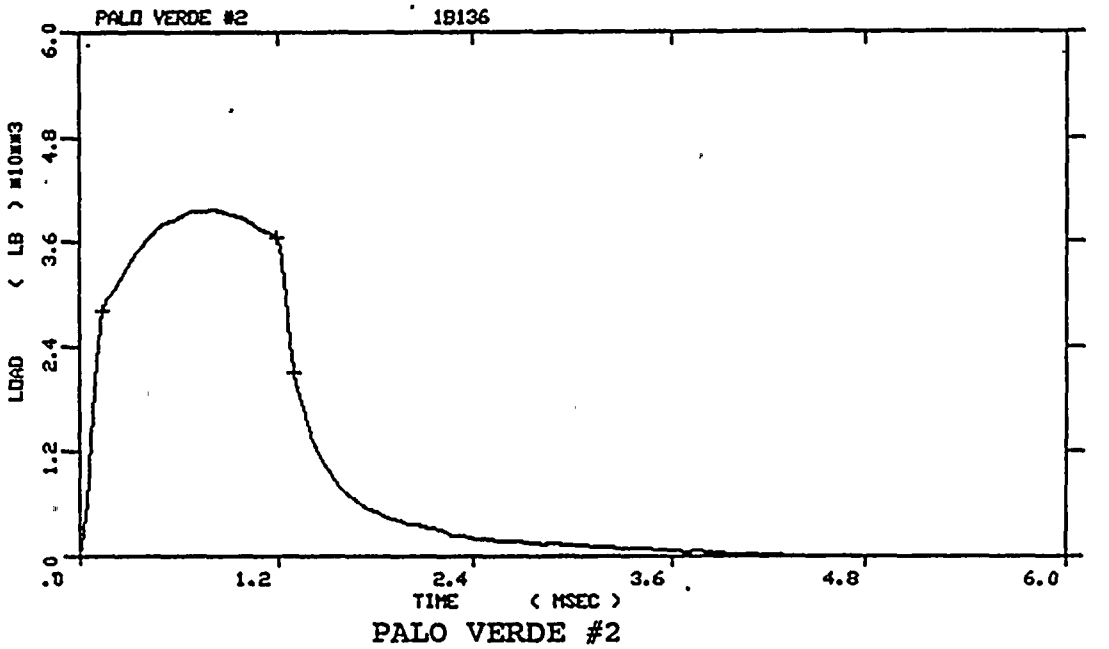

Figure A-4. Load-time records for Specimens 1B14Y and 1B136

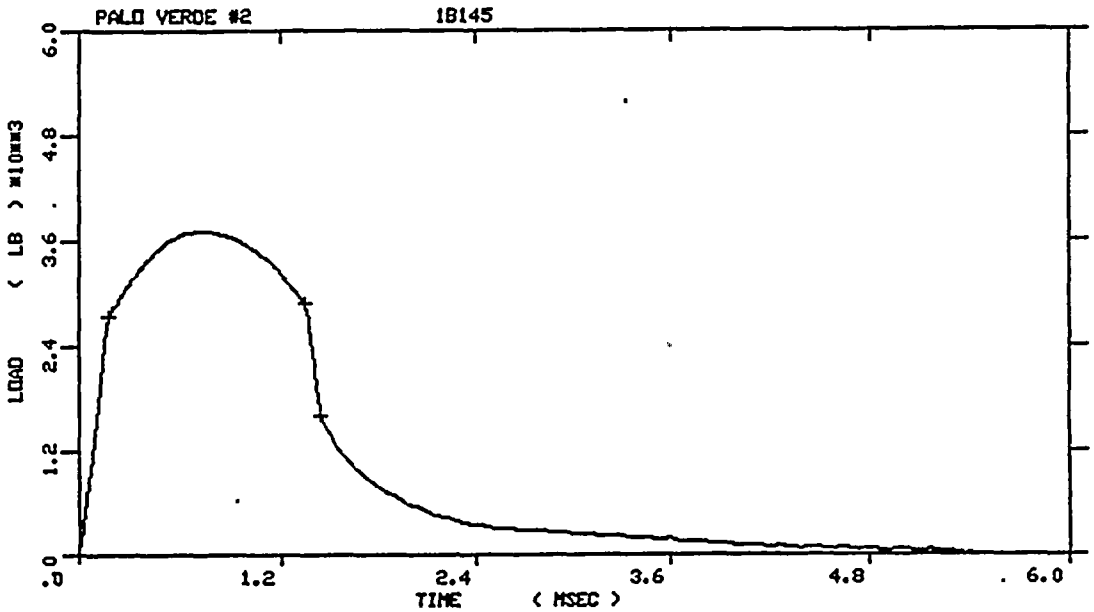

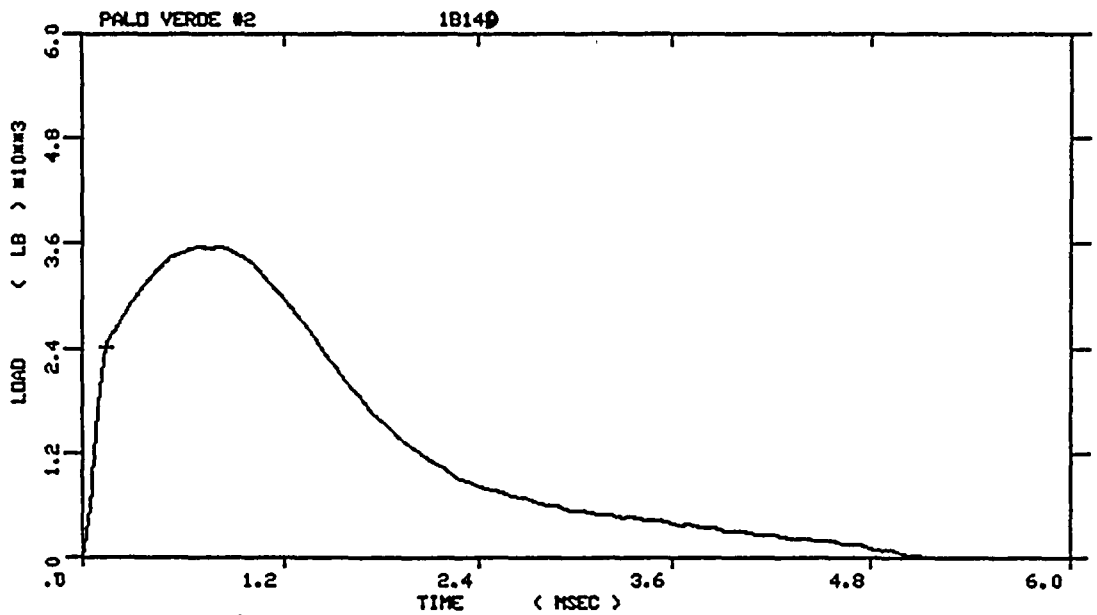

Figure A-5. Load-time records for Specimens 1B145 and 1B14D

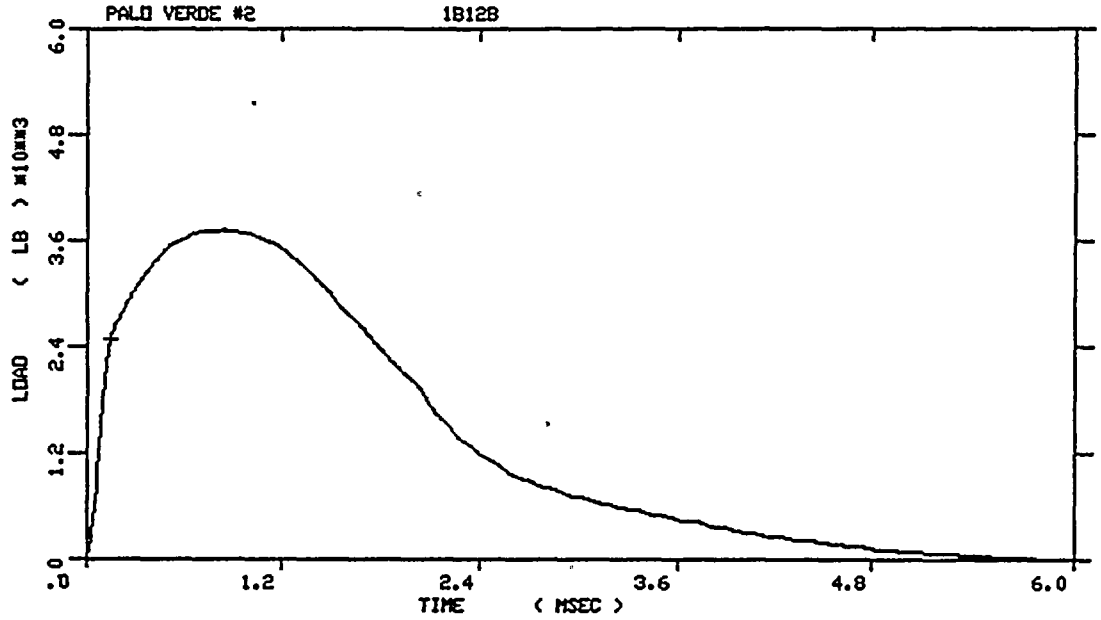

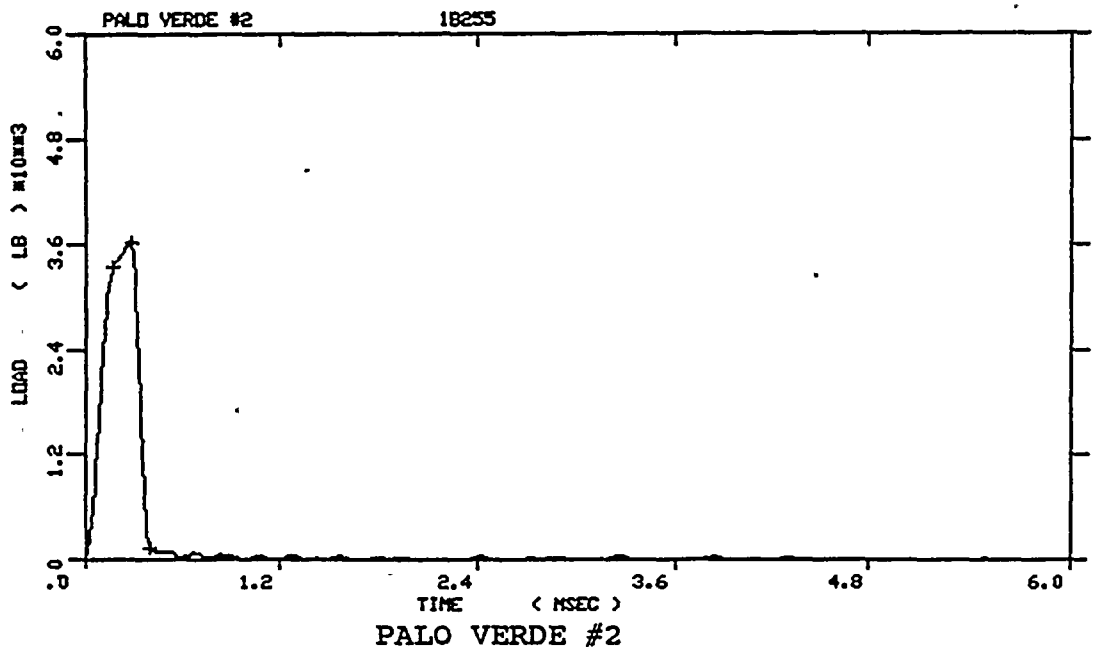

Figure A-6. Load-time records for Specimens 1B12B and 1B255

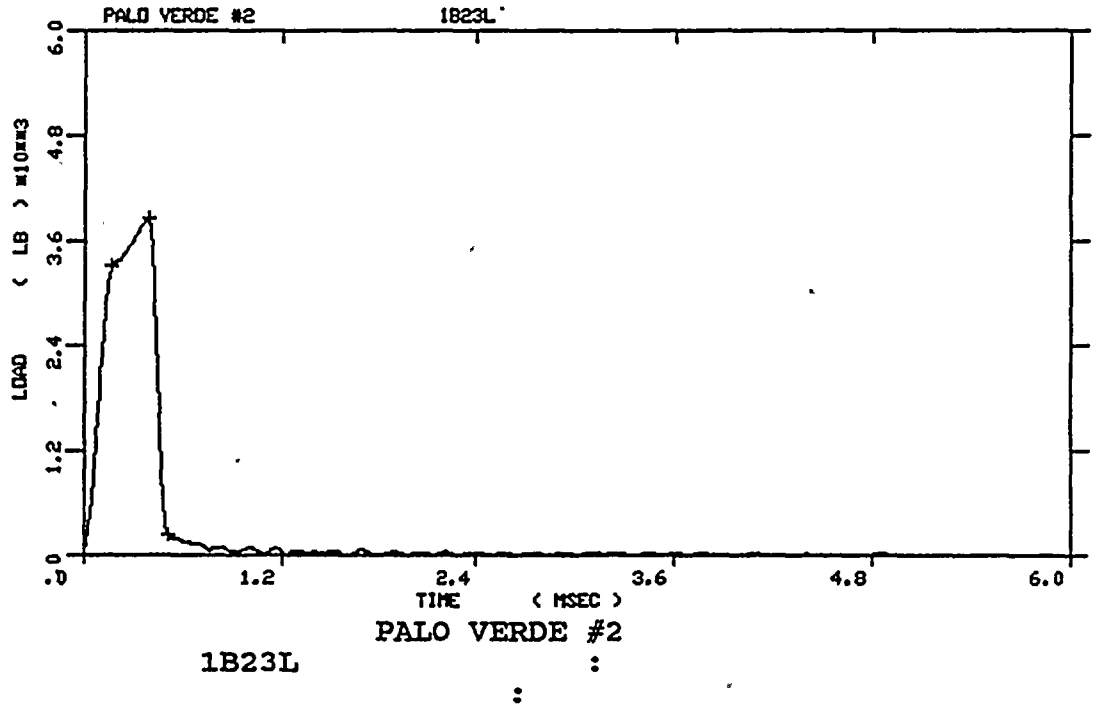

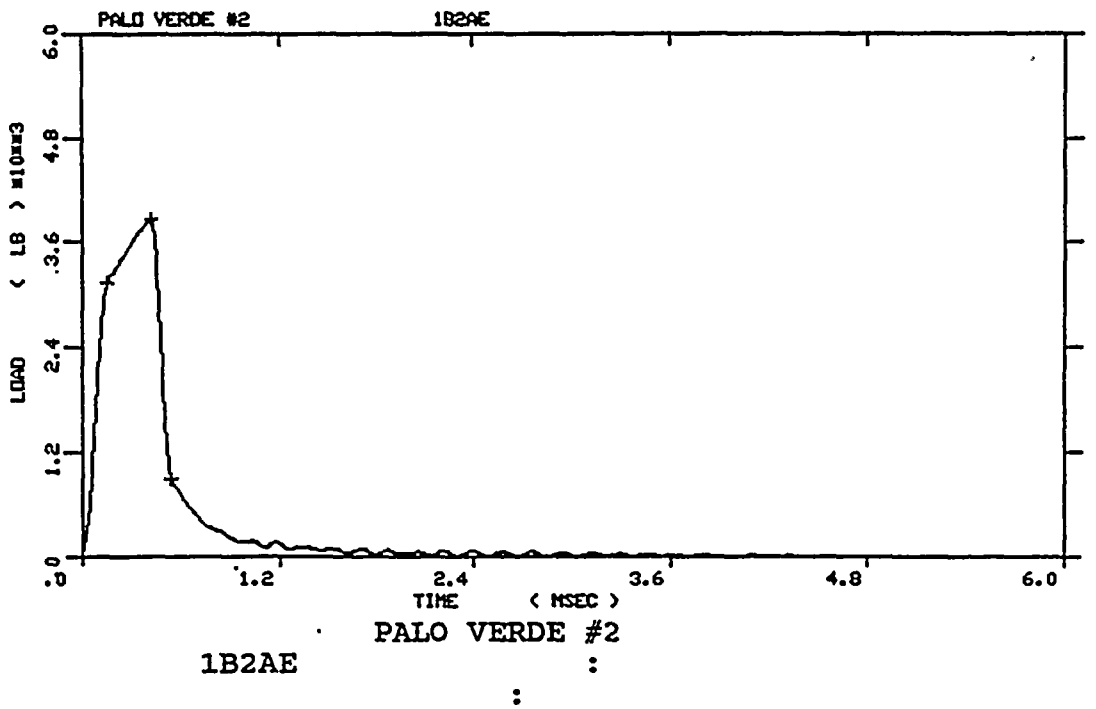

Figure A-7. Load-time records for Specimens 1B23L and 1B2AE

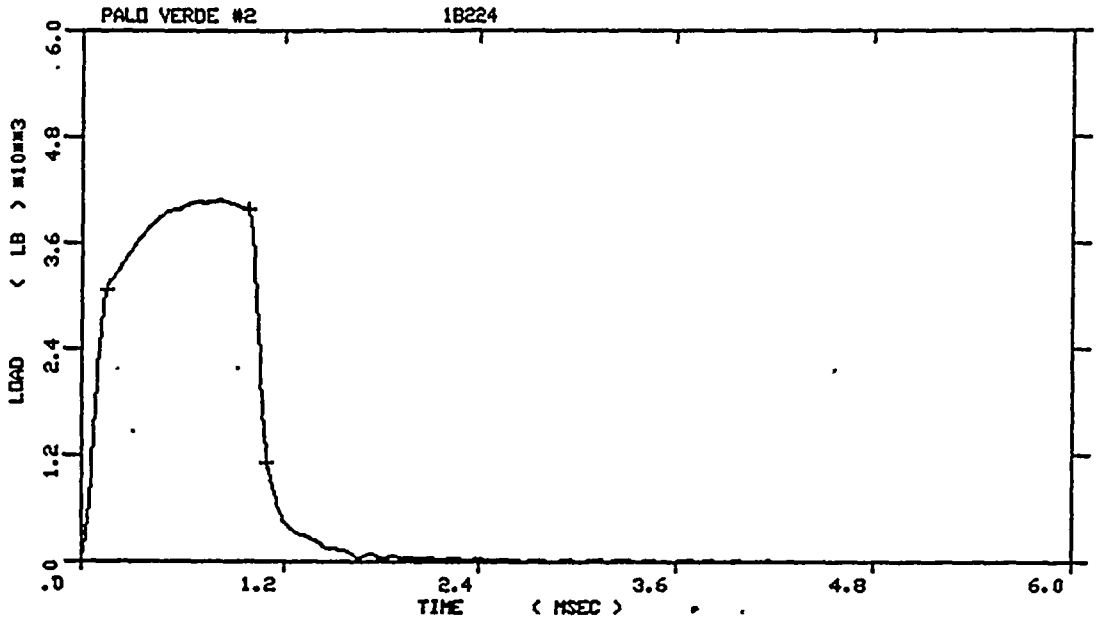

PALO VERDE #2

1B224

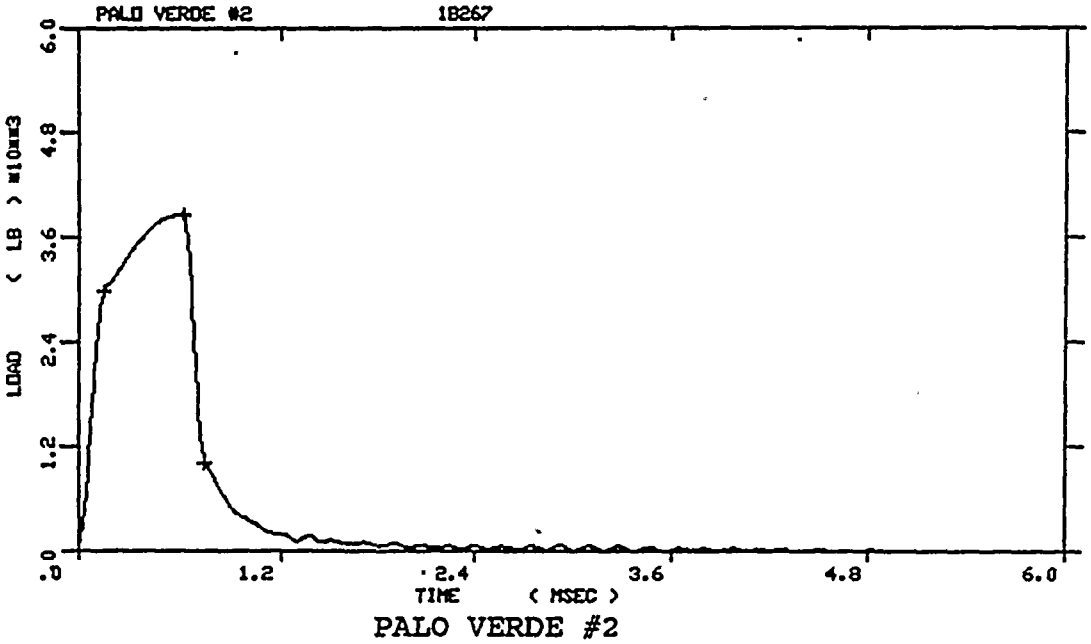

PALO VERDE #2

1B267

Figure A-8. Load-time records for Specimens 1B224 and 1B267

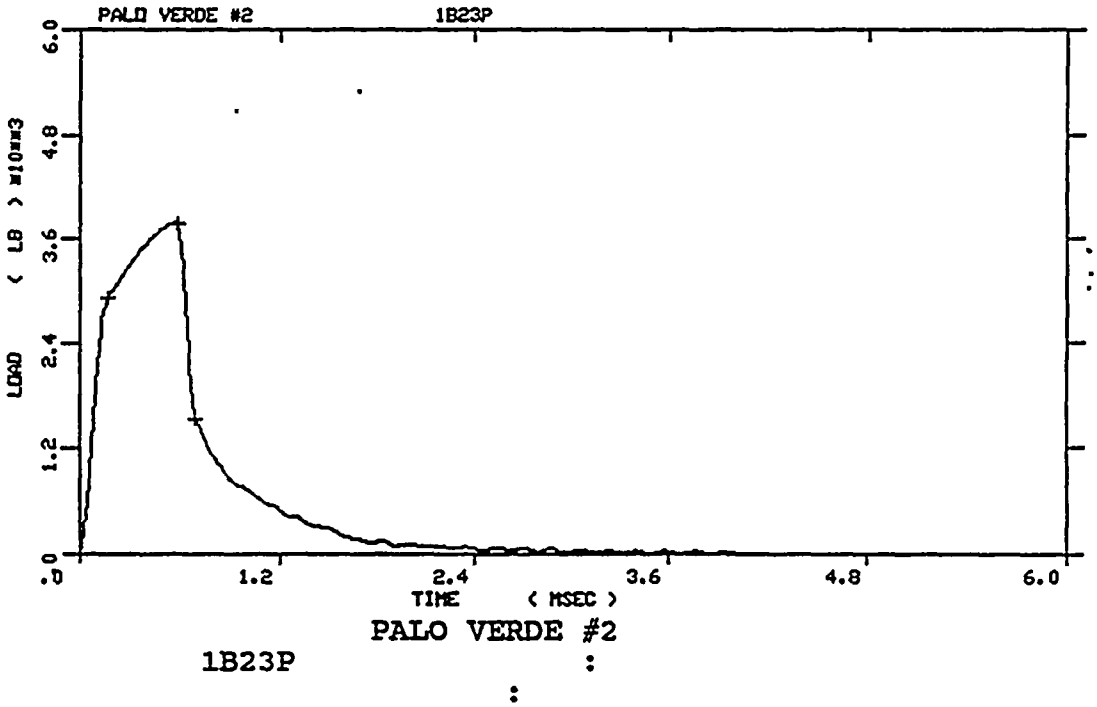

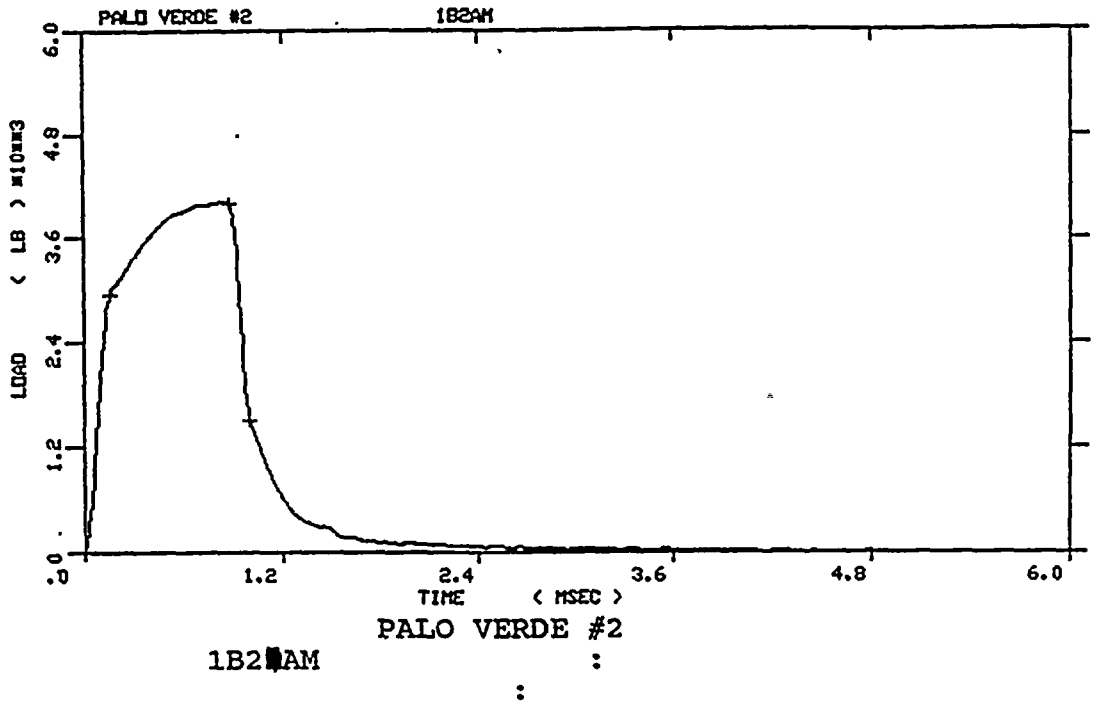

Figure A-9. Load-time records for Specimens 1B23P and 1B2AM

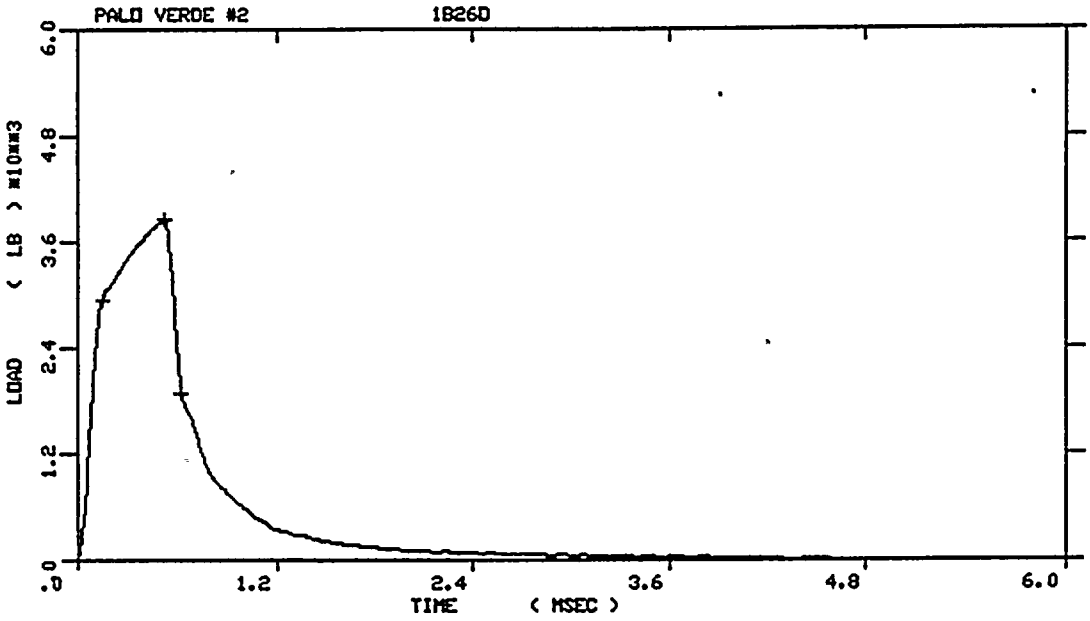

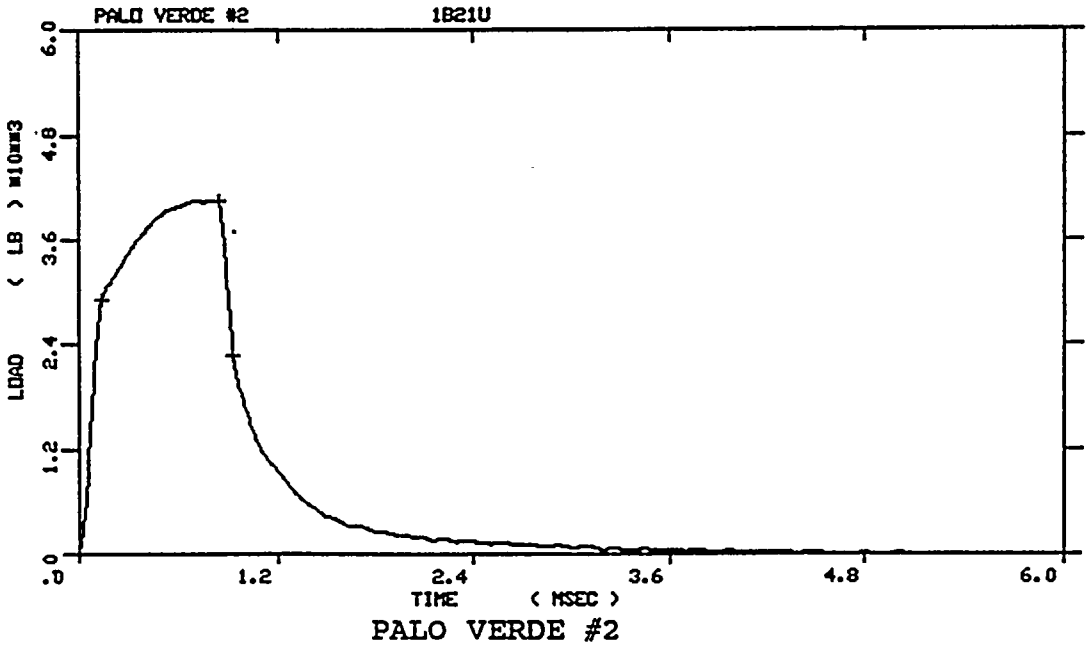

Figure A-10. Load-time records for Specimens 1B26D and 1B21U

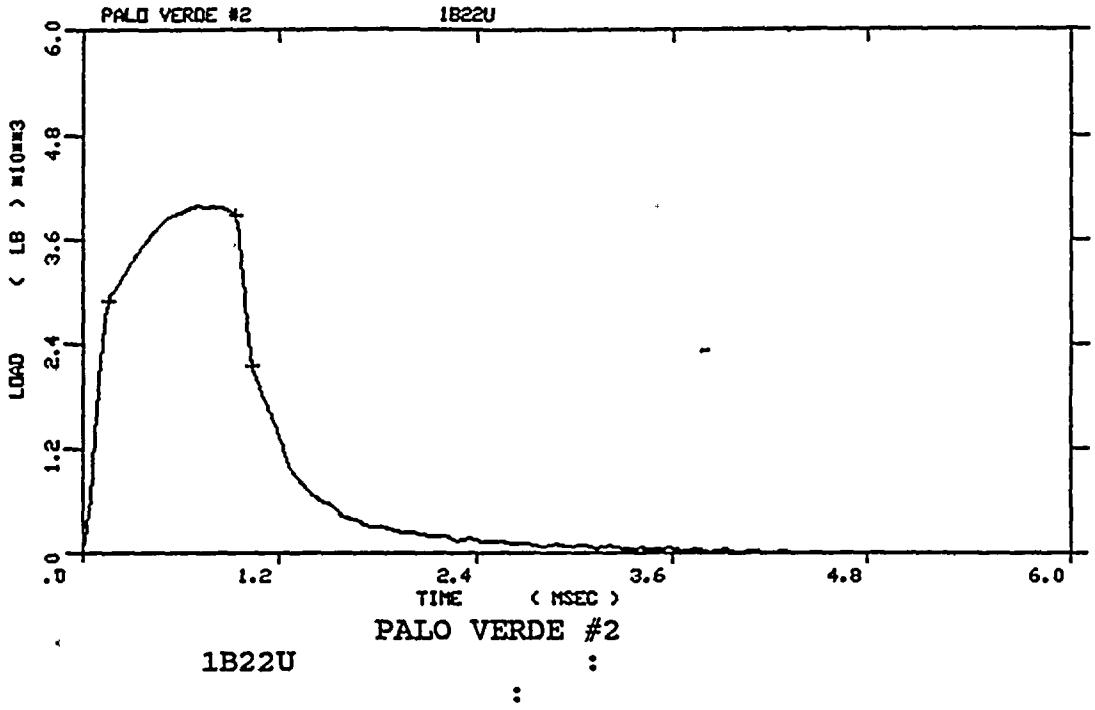

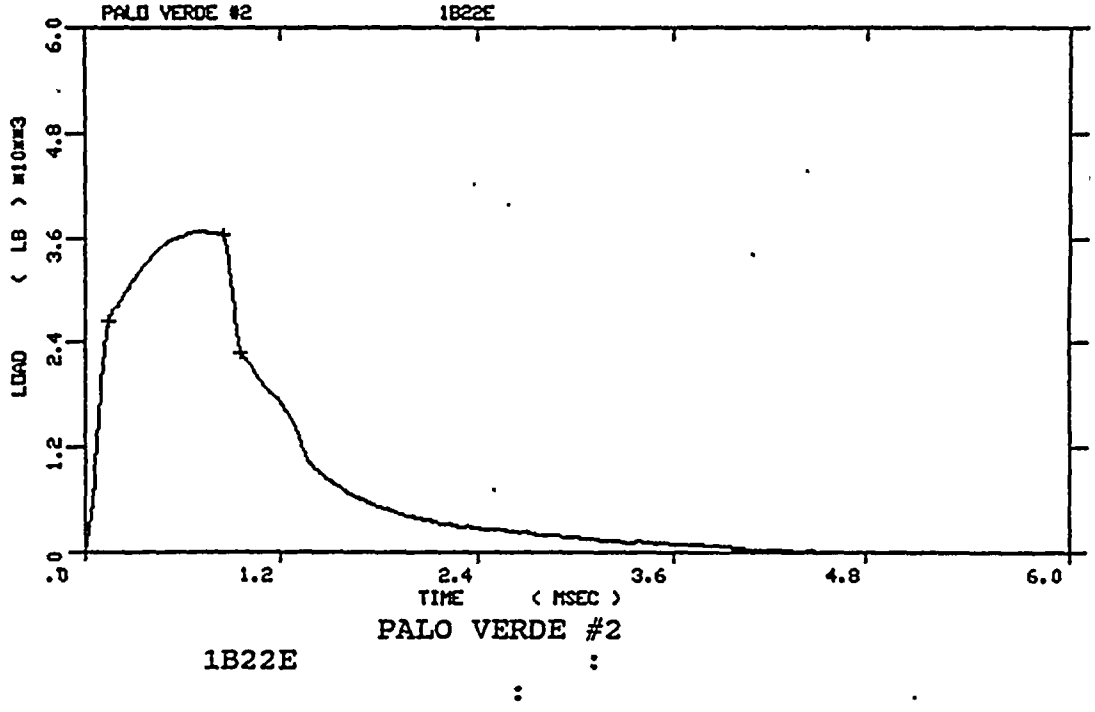

Figure A-11. Load-time records for Specimens 1B22U and 1B22E

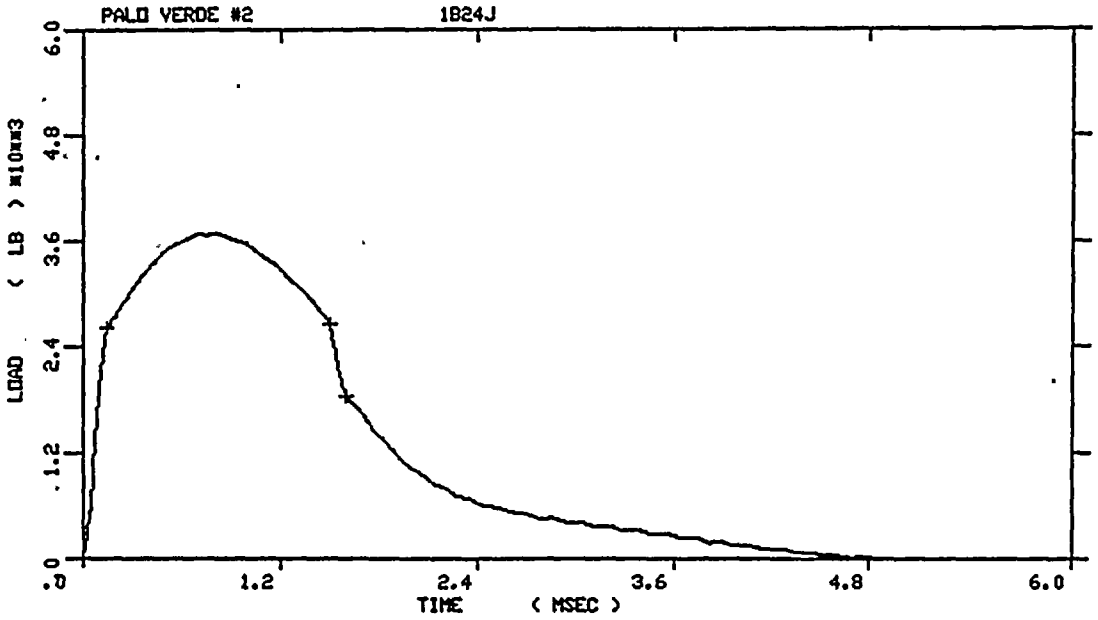

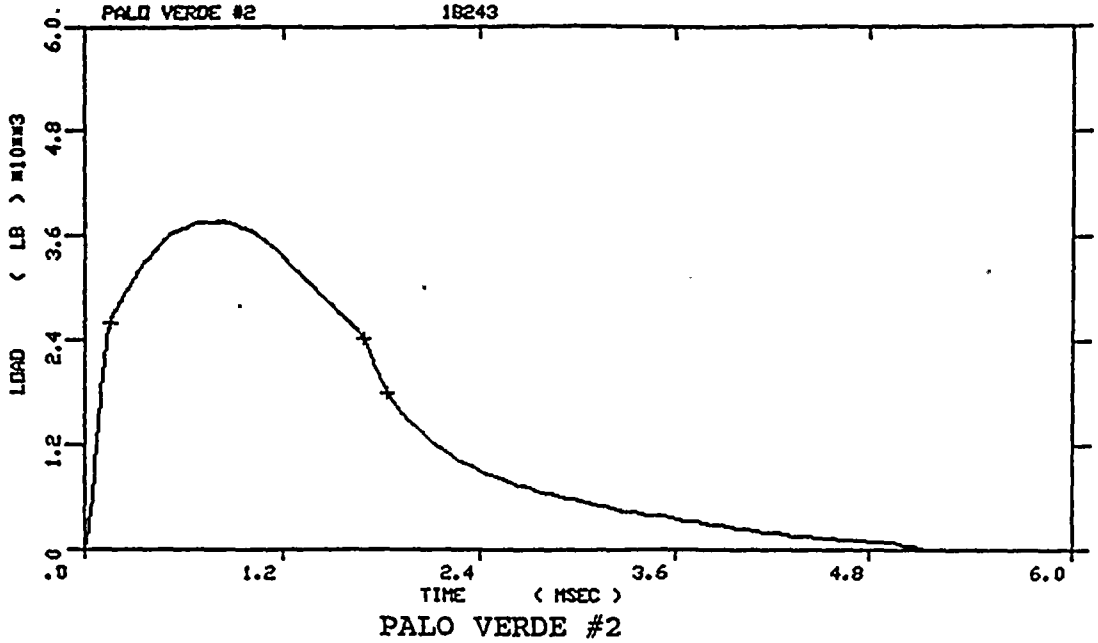

Figure A-12. Load-time records for Specimens 1B24J and 1B243

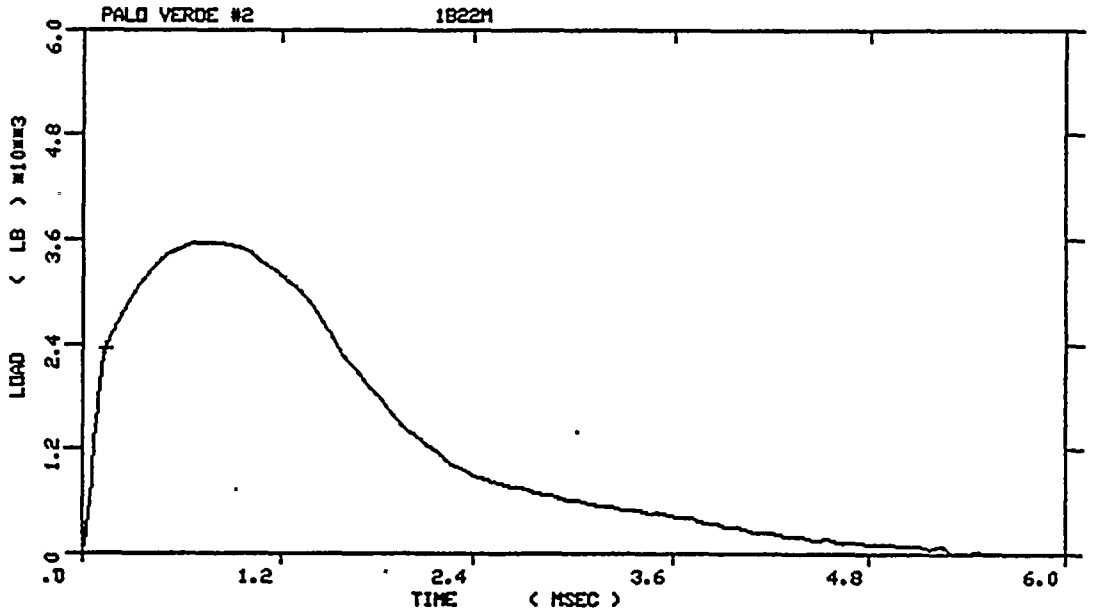

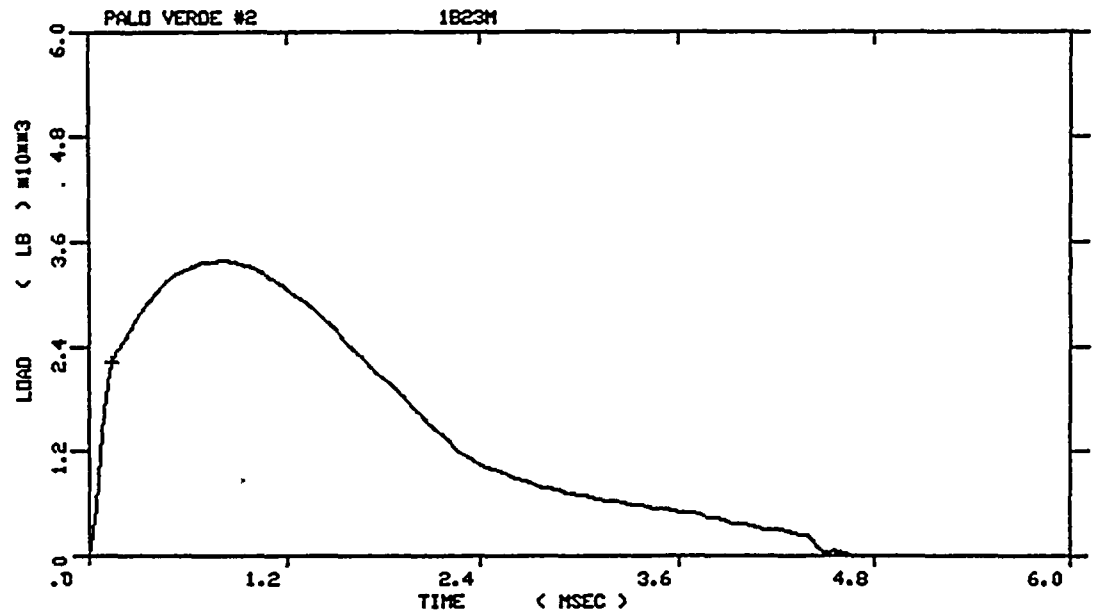

Figure A-13. Load-time records for Specimens 1B22M and 1B23M

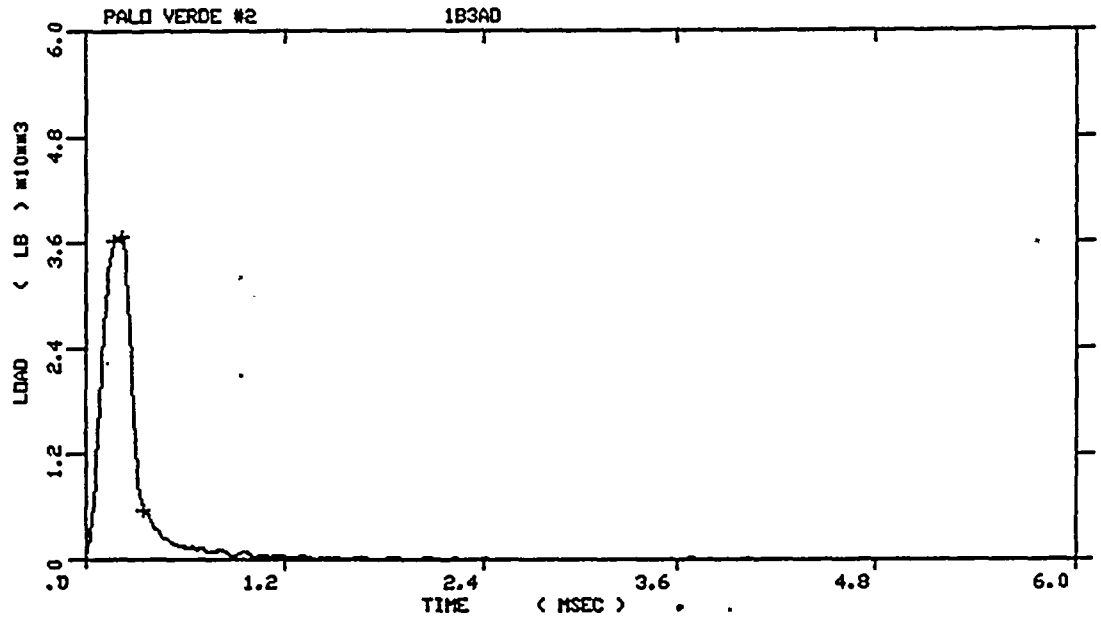

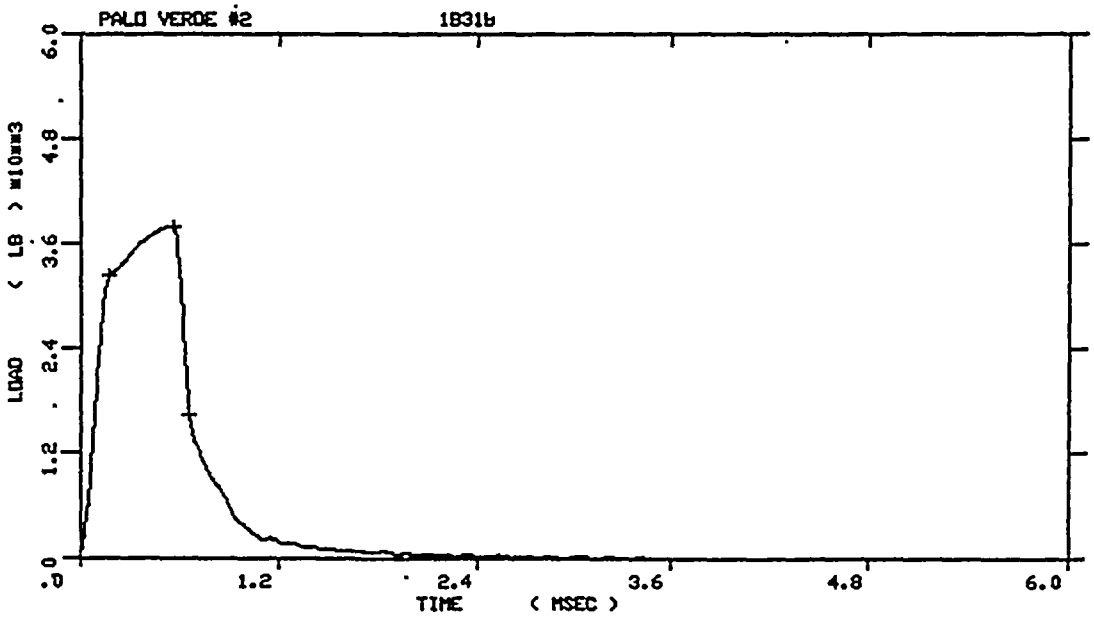

Figure A-14. Load-time records for Specimens 1B3AD and 1B316

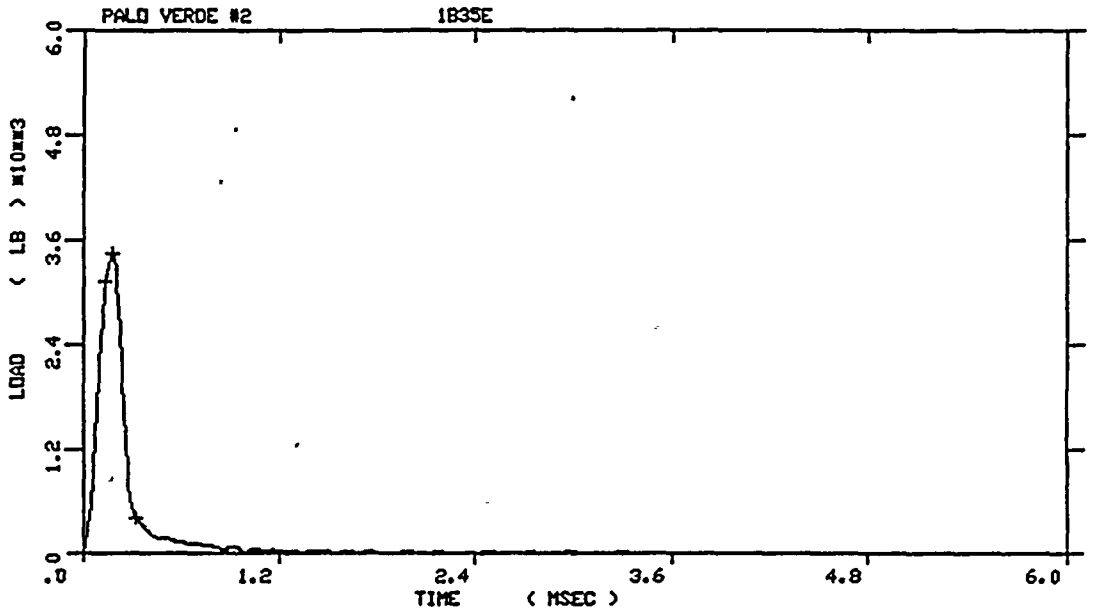

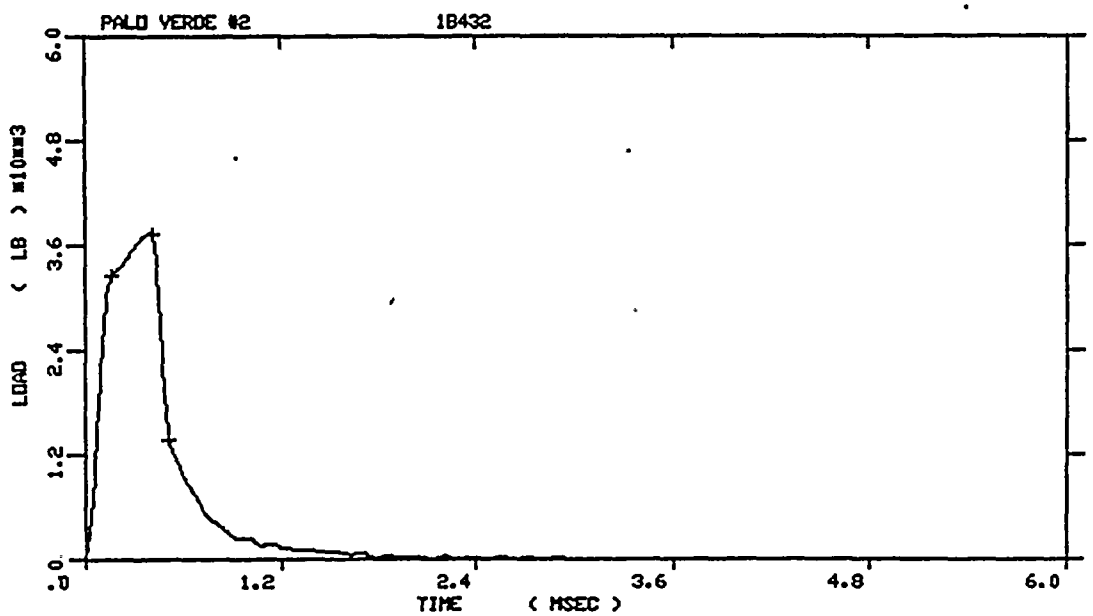

Figure A-15. Load-time records for Specimens 1B35E and 1B342

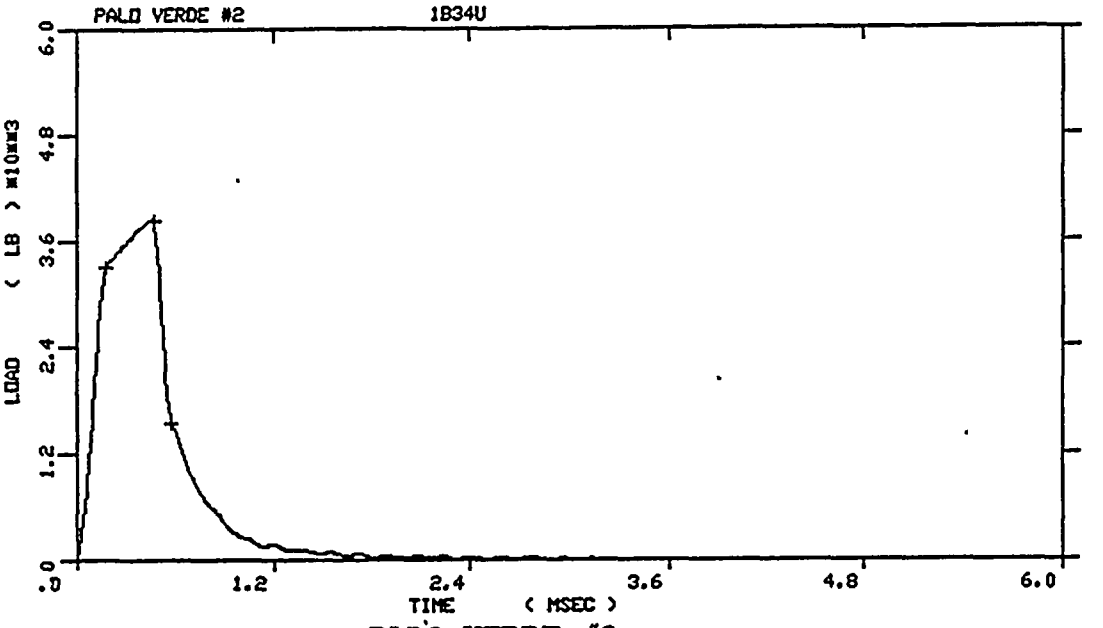

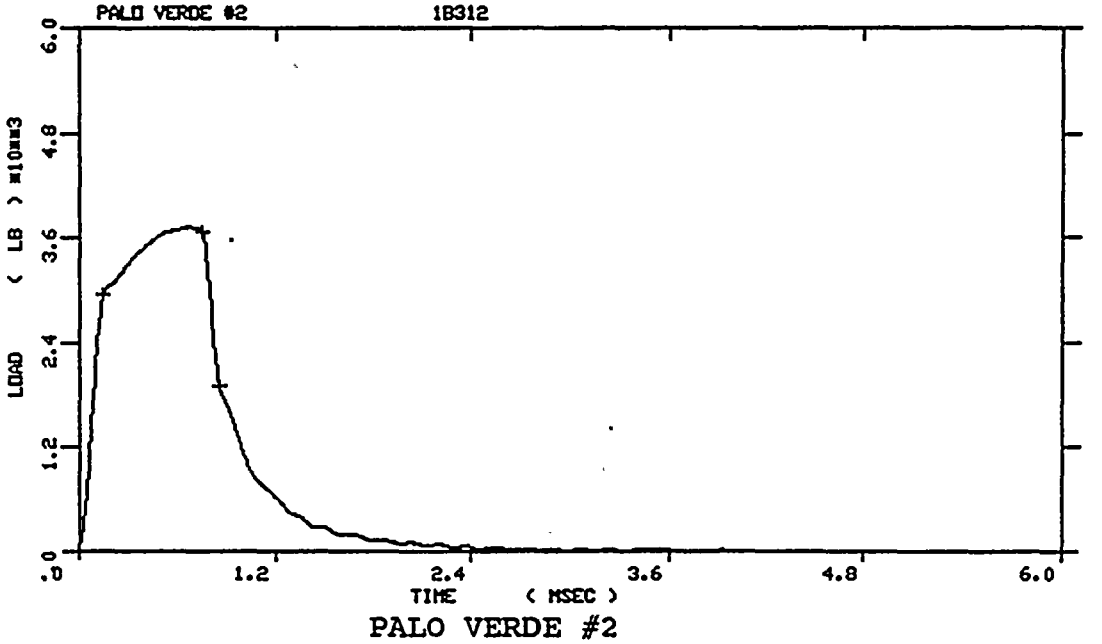

Figure A-16. Load-time records for Specimens 1B34U and 1B312

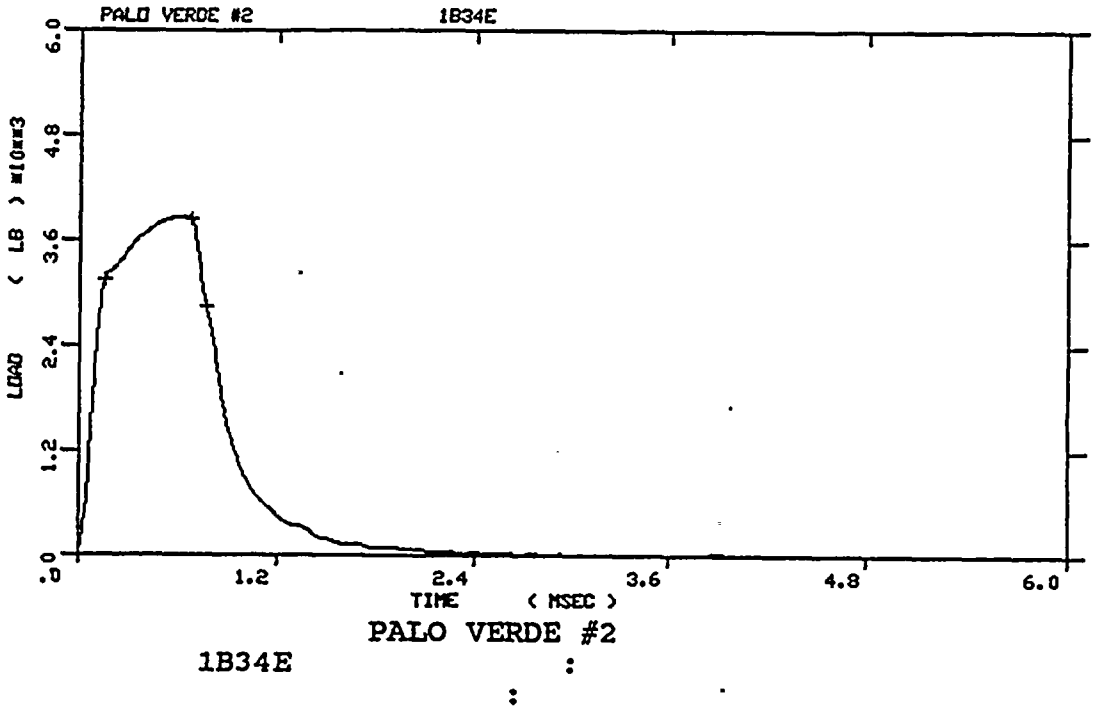

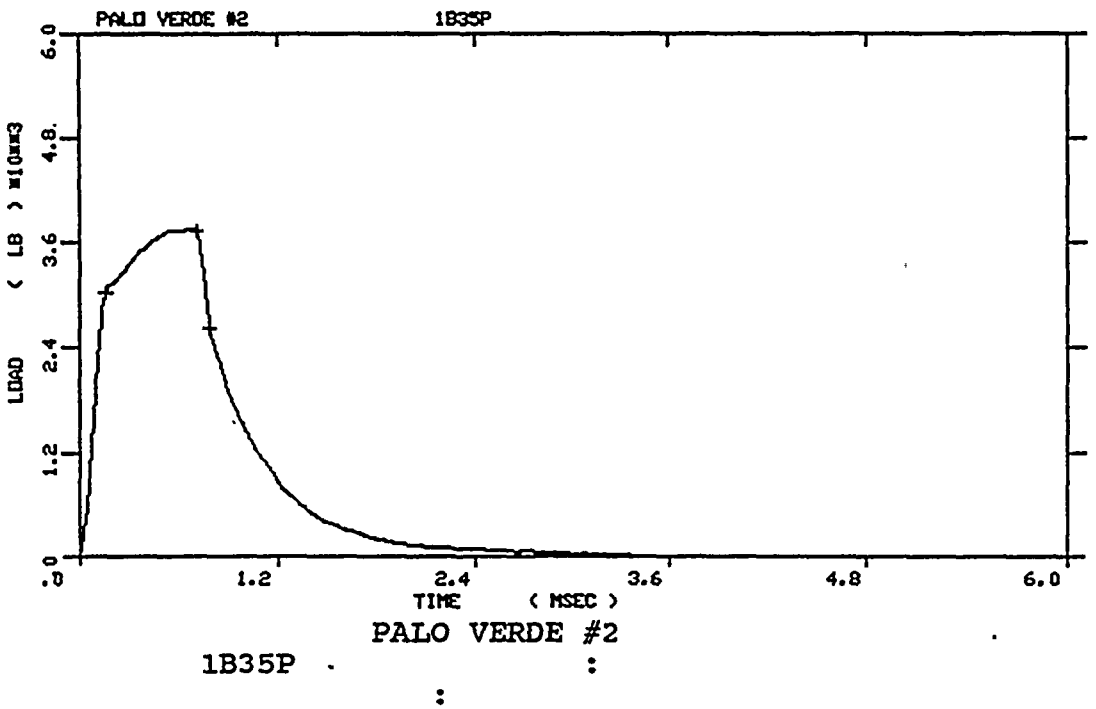

Figure A-17. Load-time records for Specimens 1B34E and 1B35P

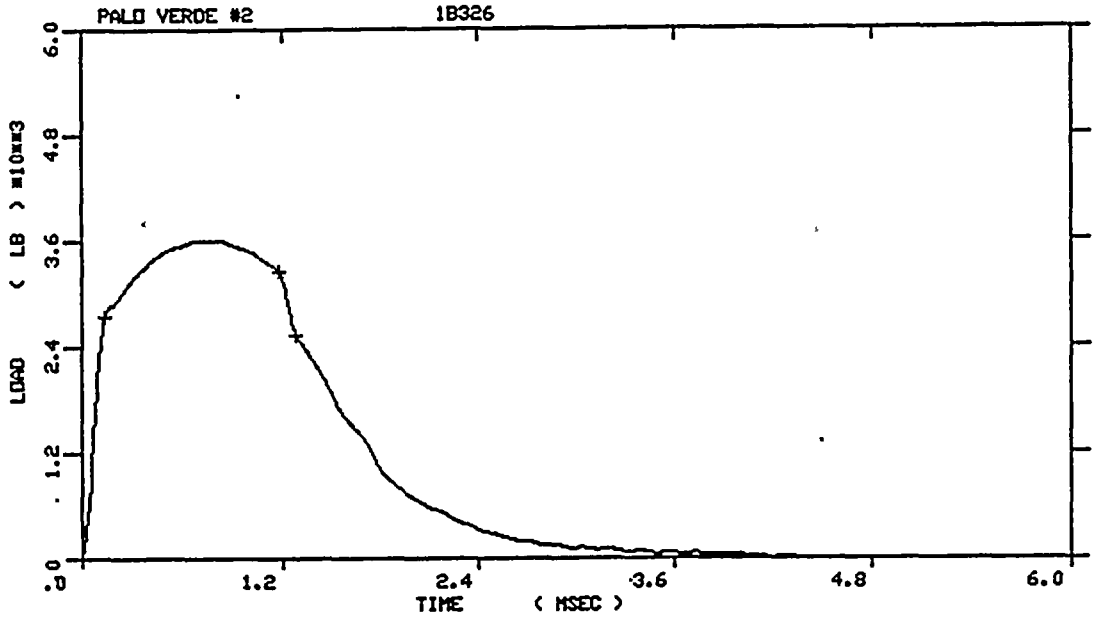

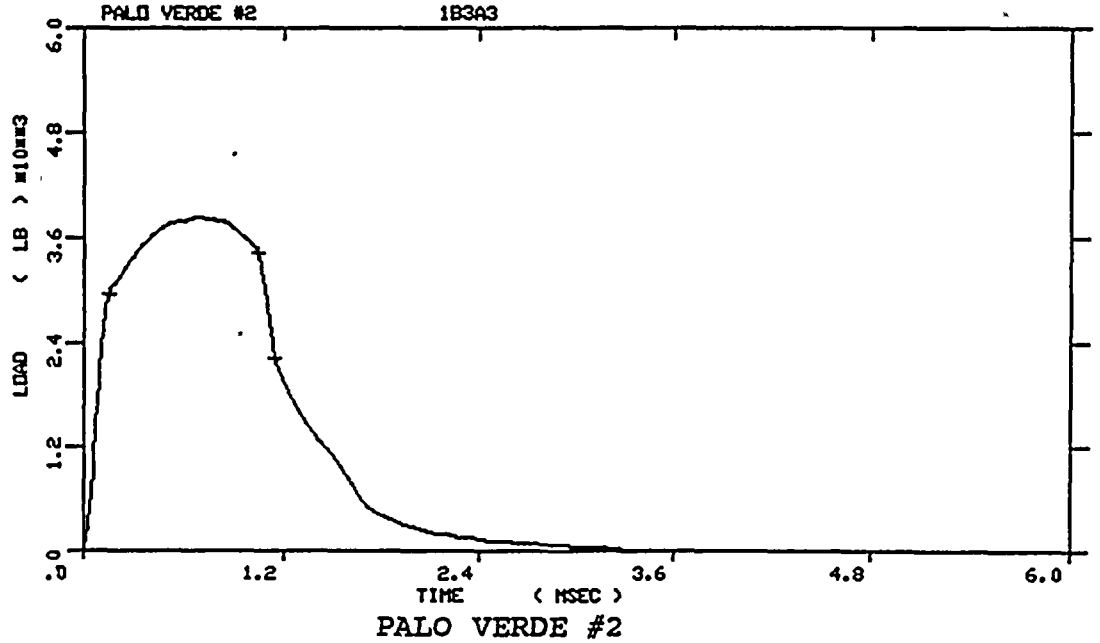

Figure A-18. Load-time records for Specimens 1B326 and 1B3A3

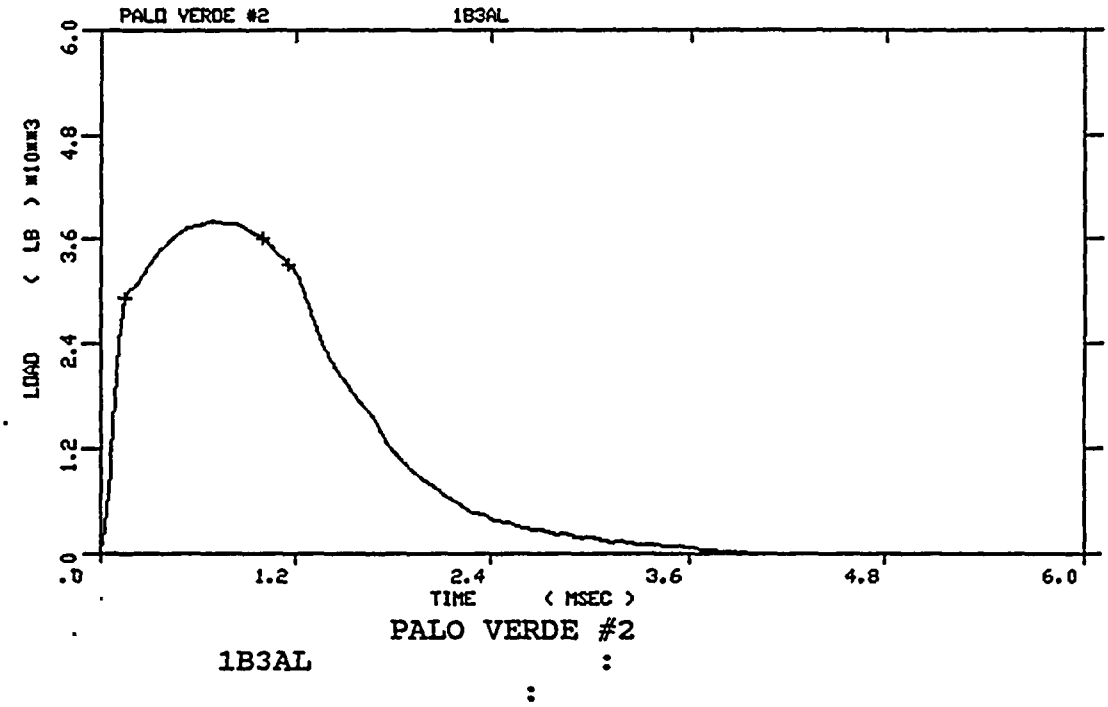

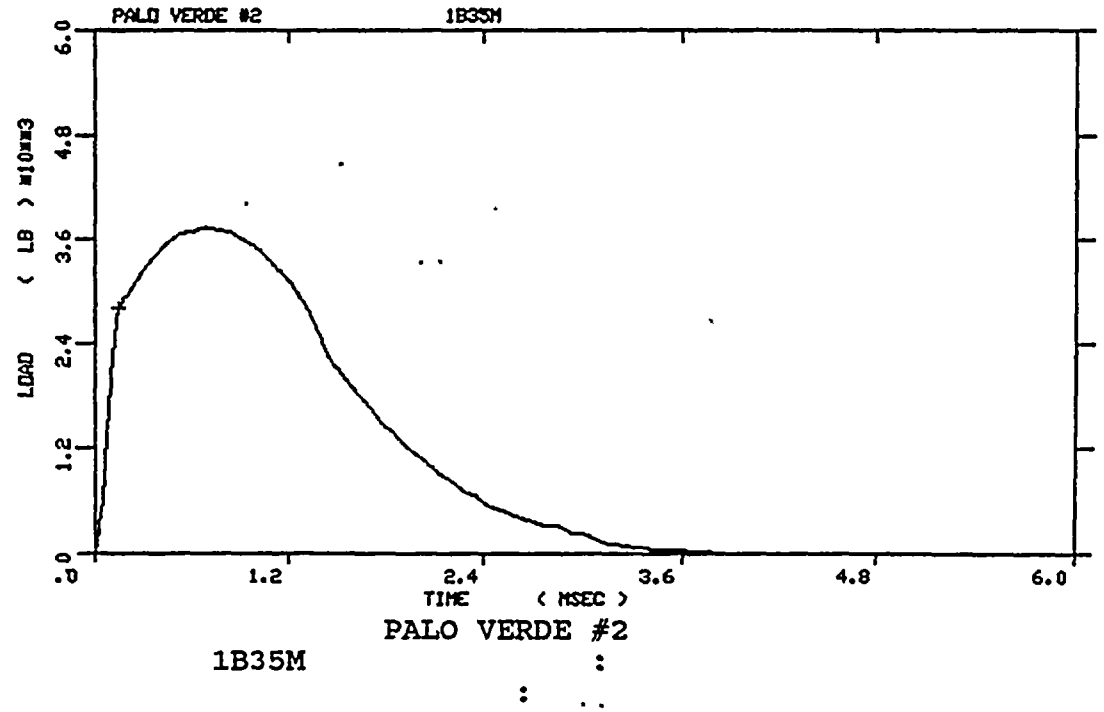

Figure A-19. Load-time records for Specimens 1B3AL and 1B35M

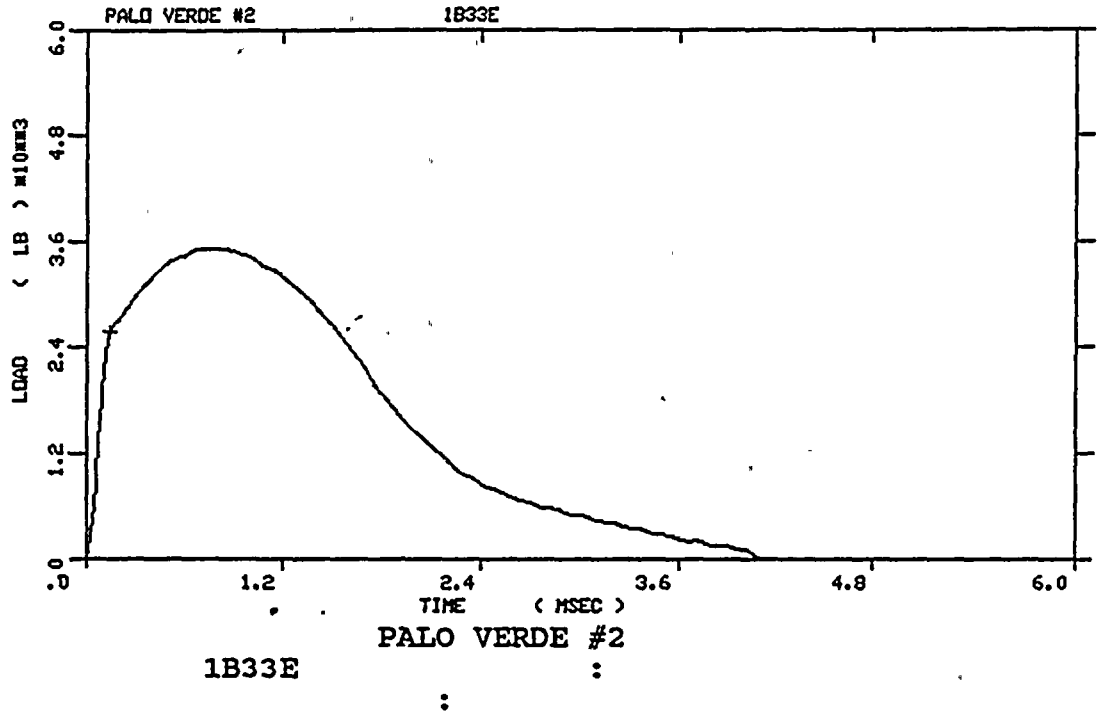

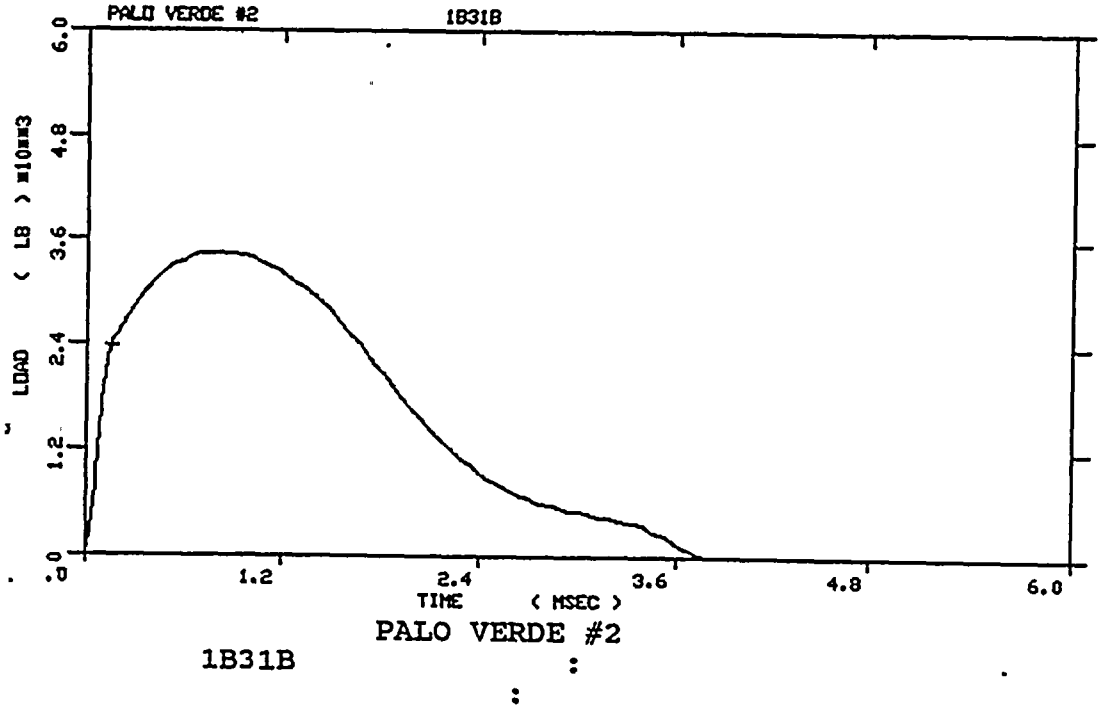

Figure A-20. Load-time records for Specimens 1B33E and 1B31B

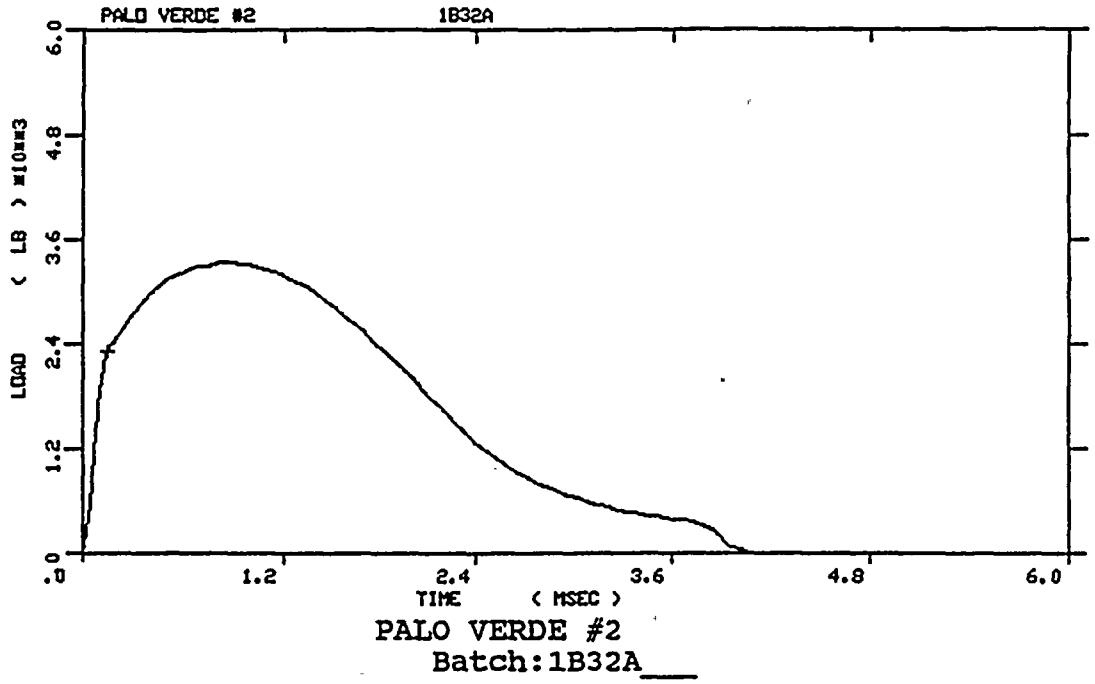

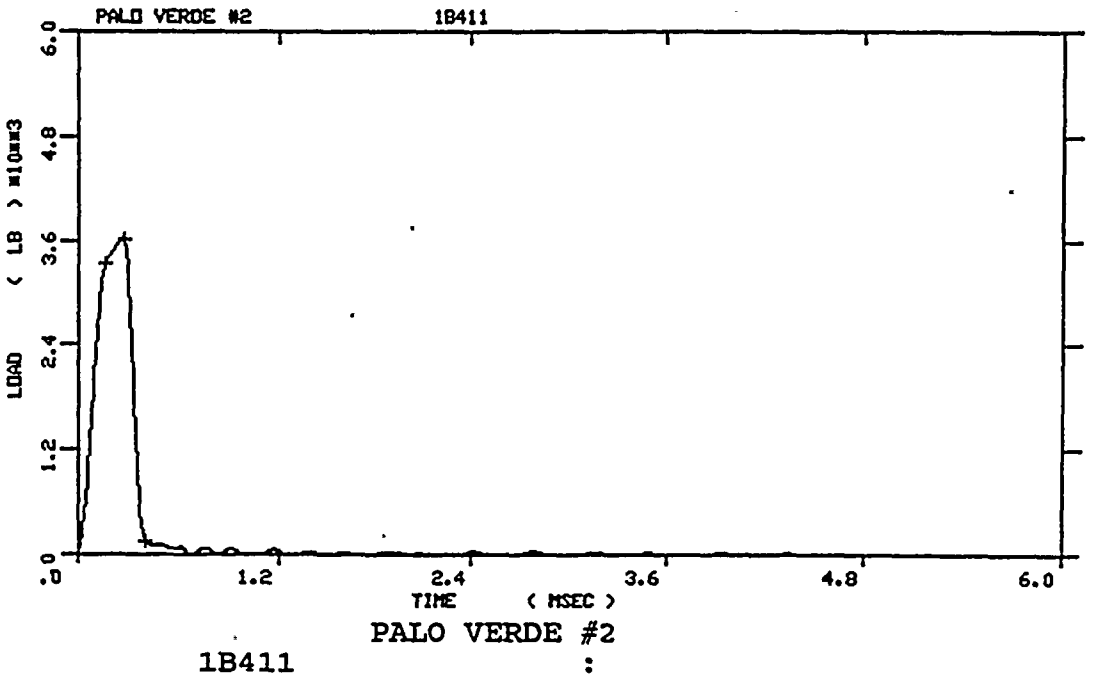

Figure A-21. Load-time records for Specimens 1B32A and 1B411

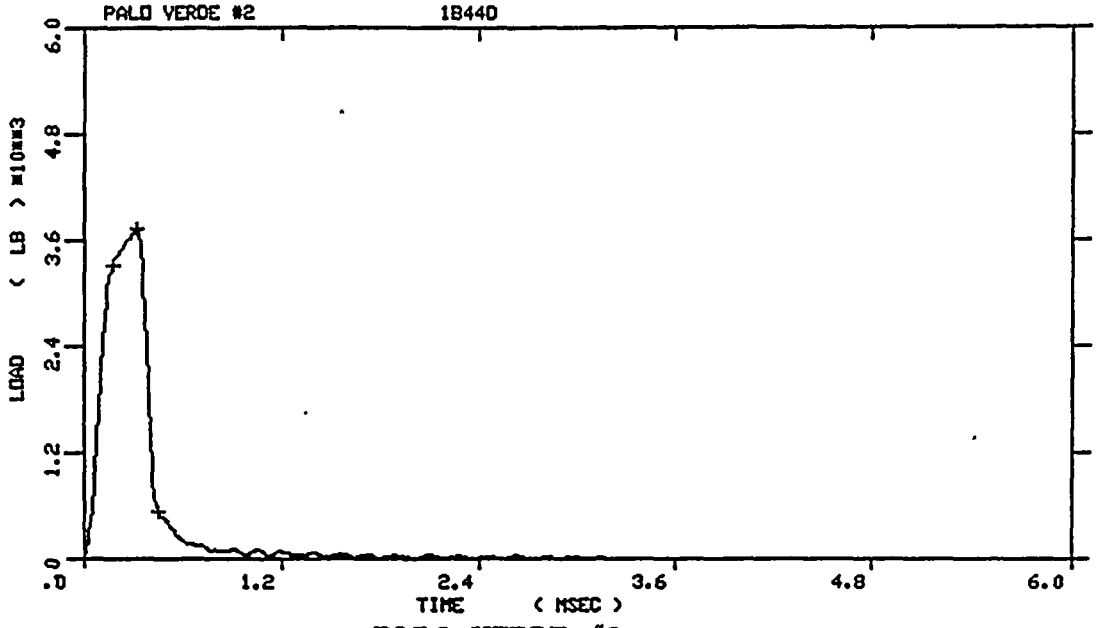

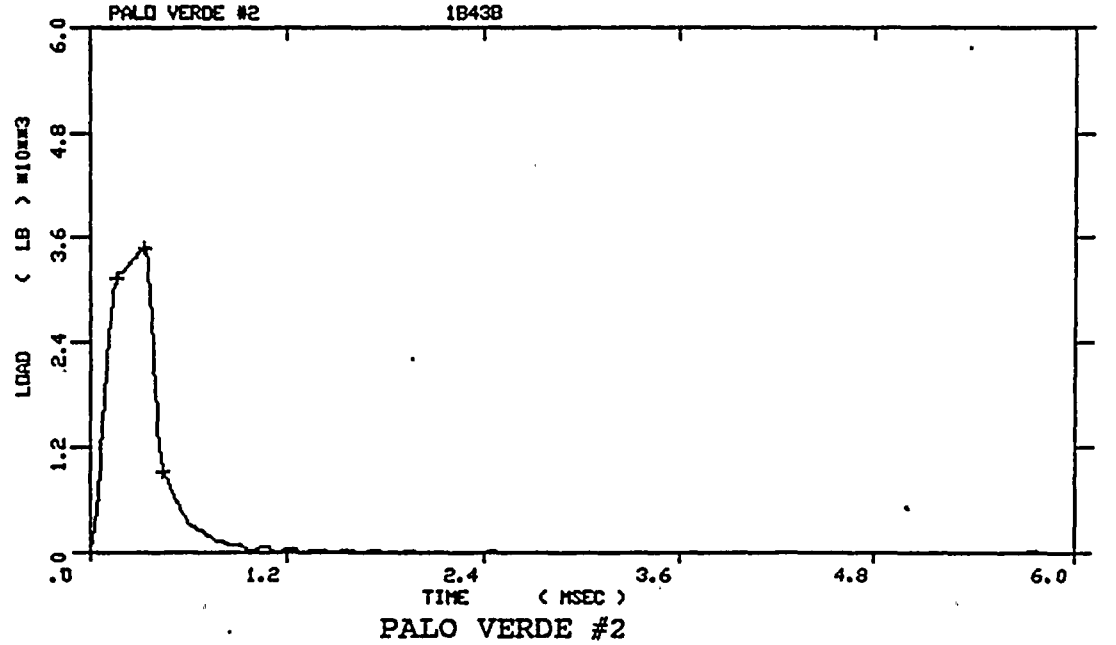

Figure A-22. Load-time records for Specimens 1B44D and 1B43B

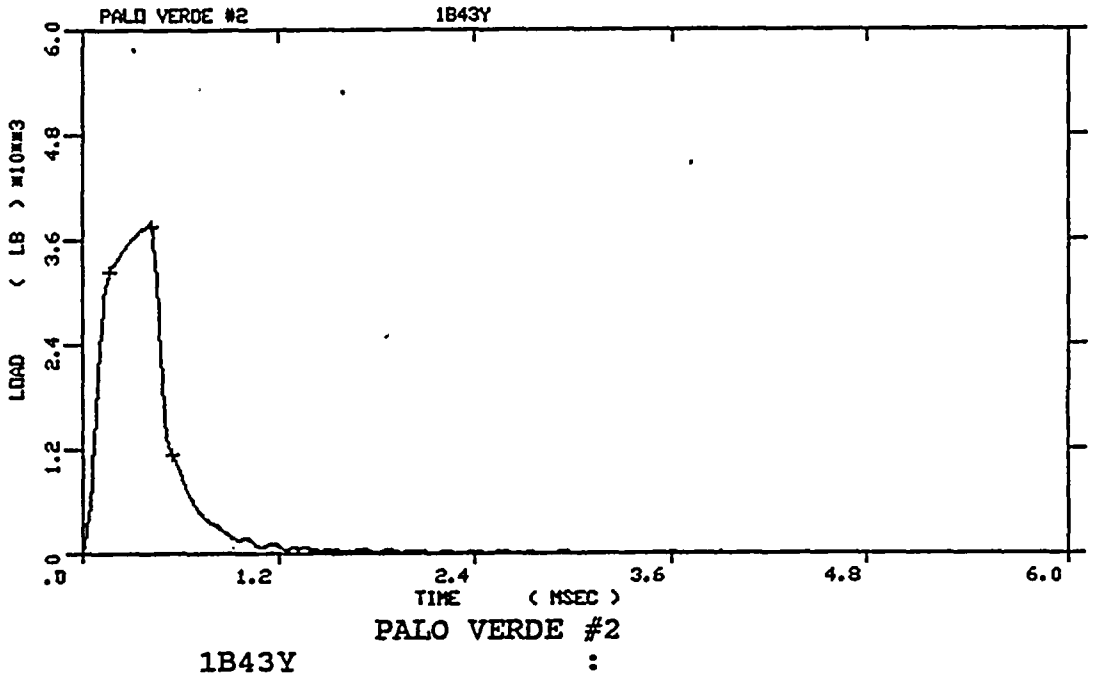

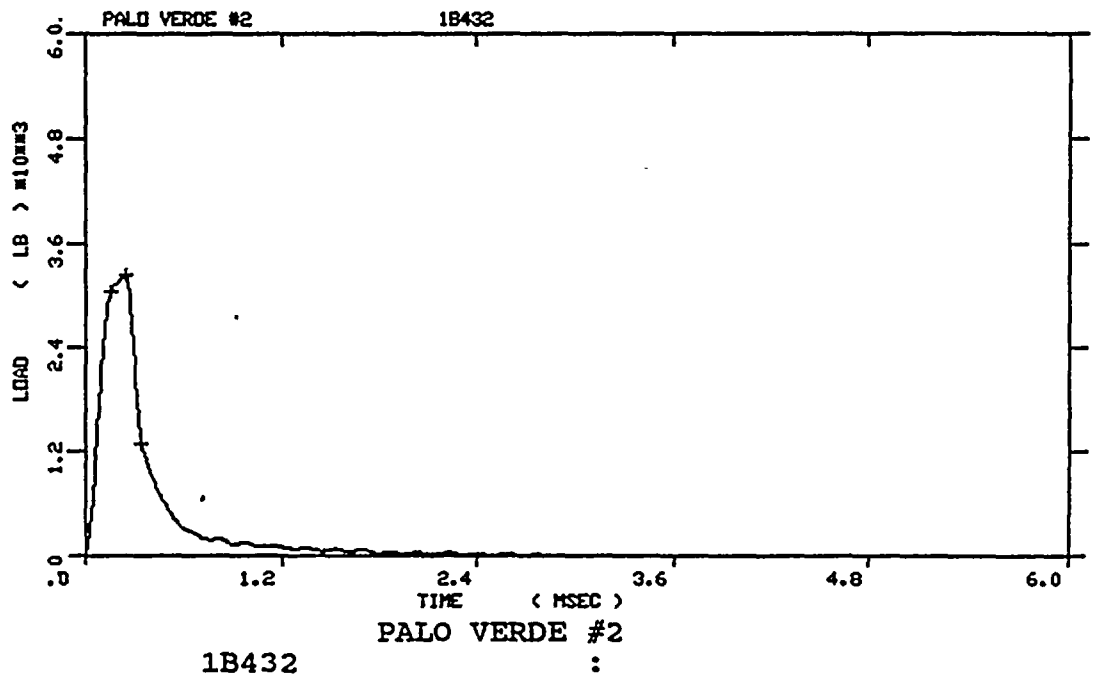

Figure A-23. Load-time records for Specimens 1B43Y and 1B432

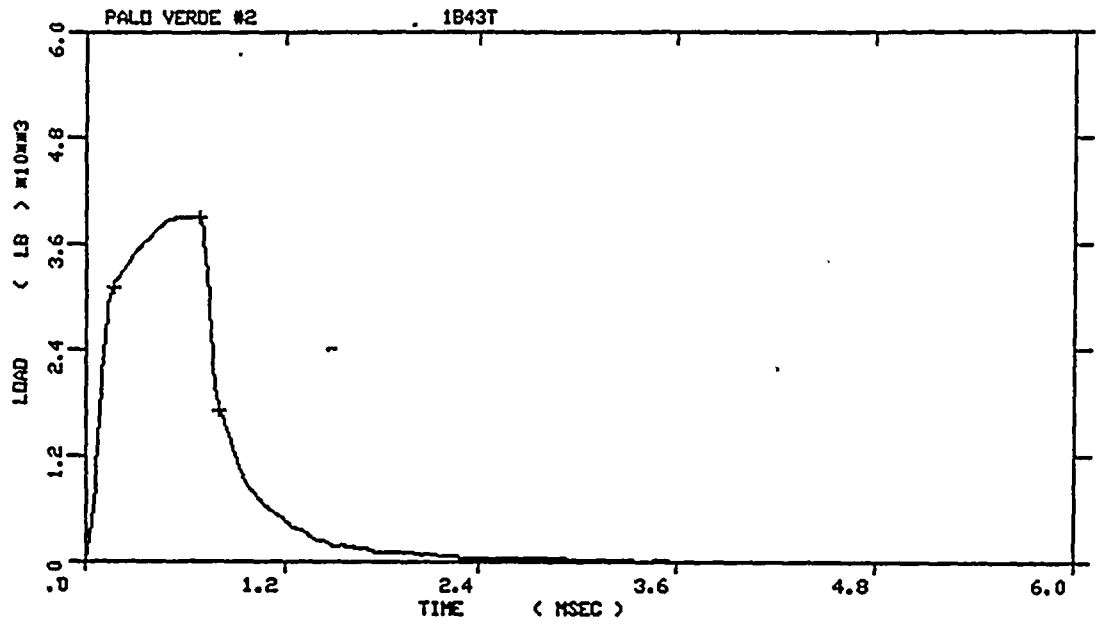

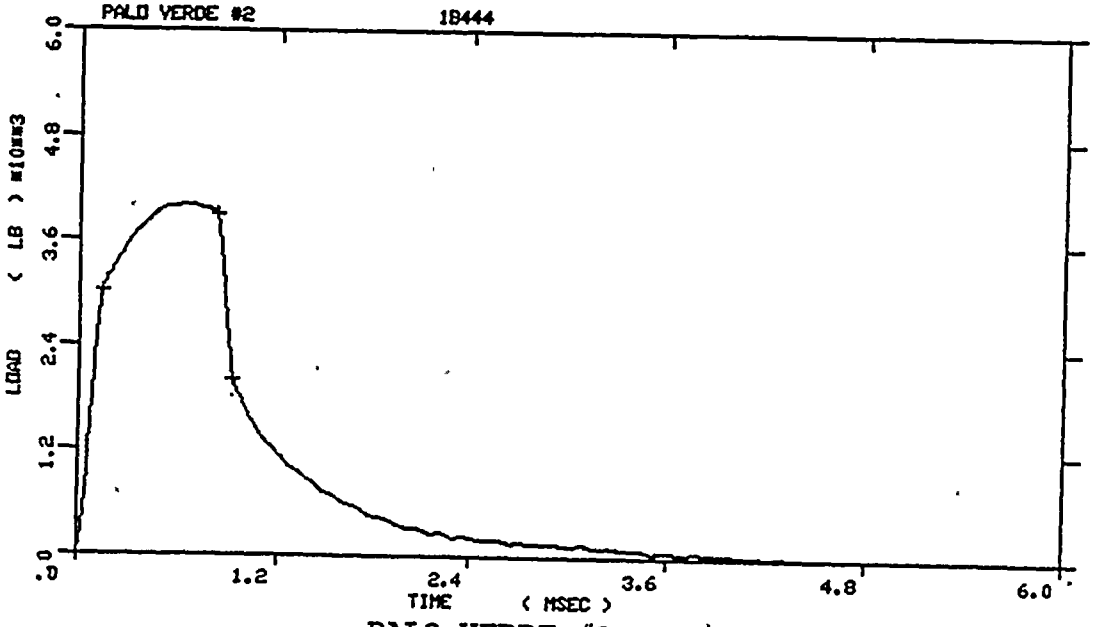

Figure A-24. Load-time records for Specimens 1B43T and 1B444

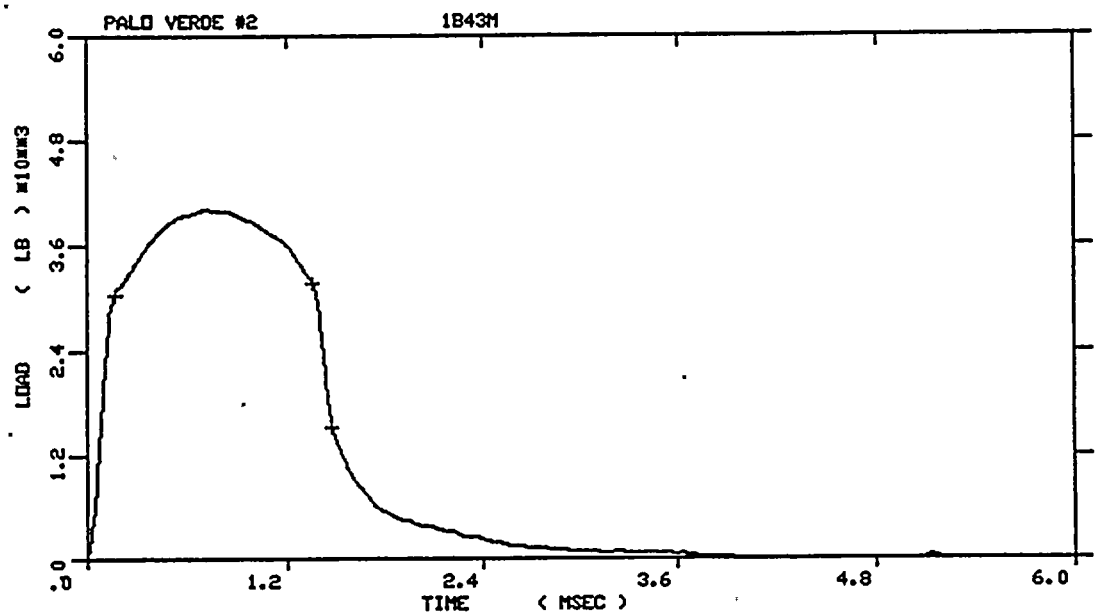

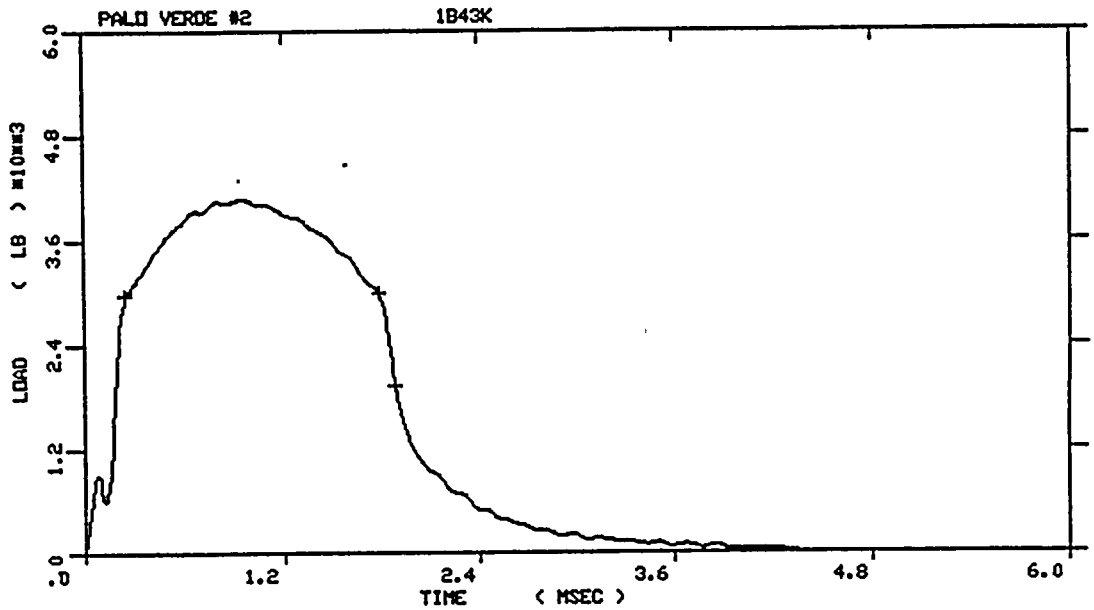

Figure A-25. Load-time records for Specimens 1B43M and 1B43K

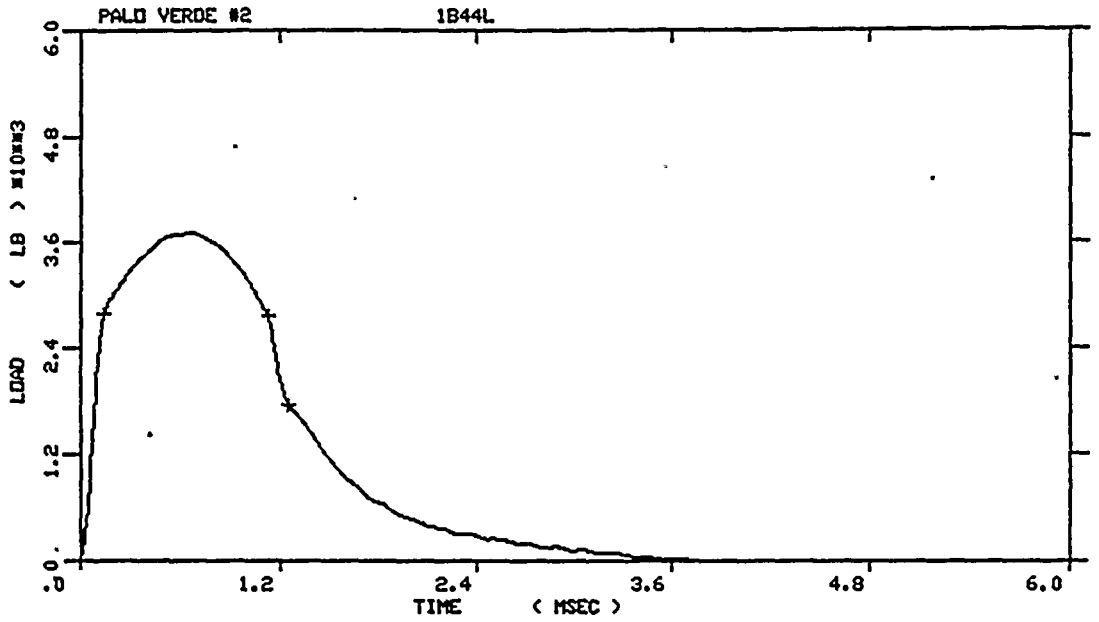

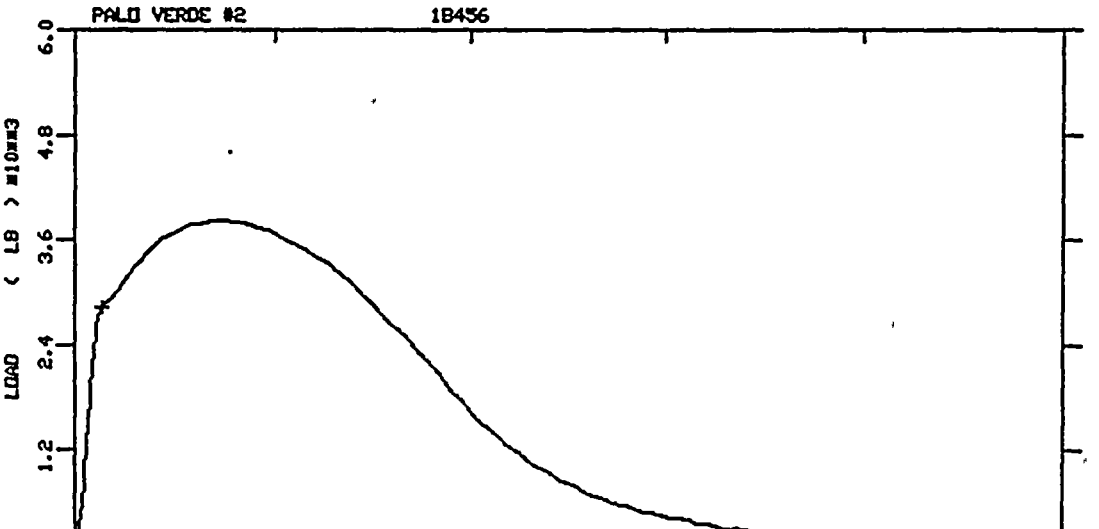

Figure A-26. Load-time records for Specimens 1B44L and 1B456

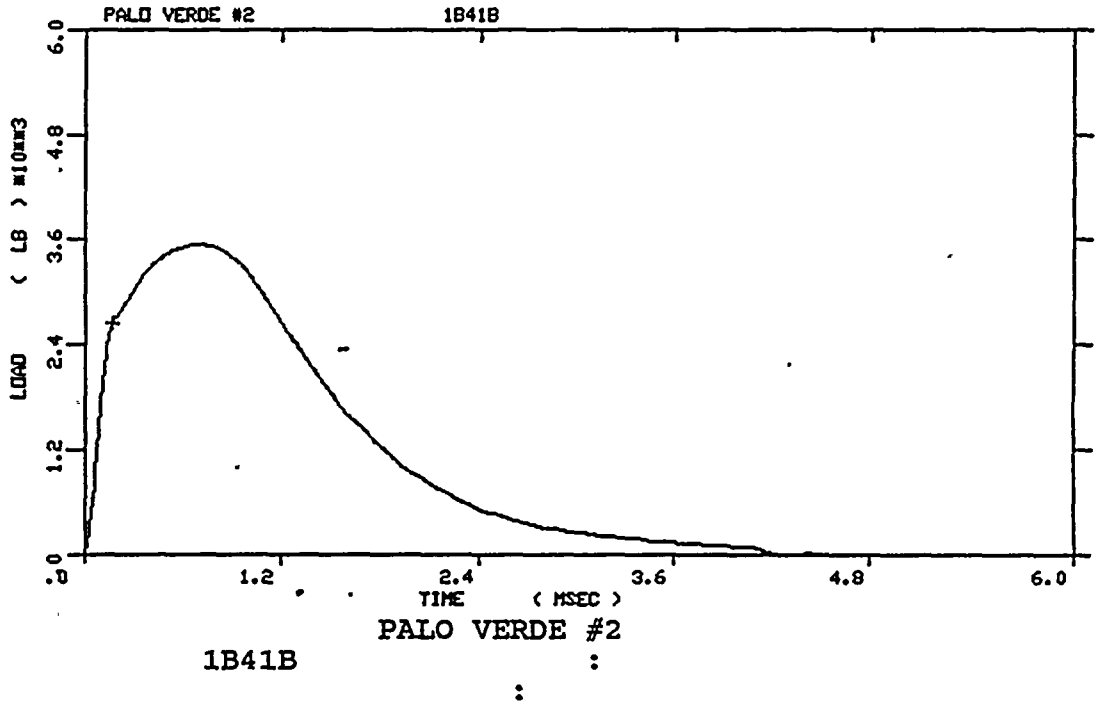

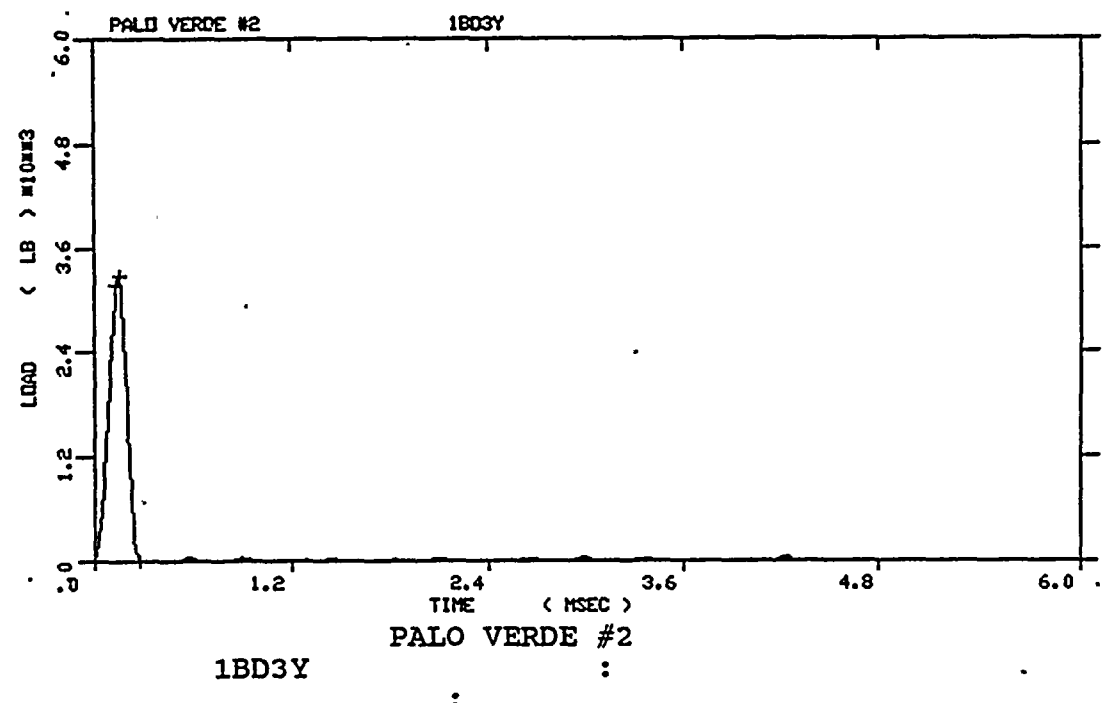

Figure A-27. Load-time records for Specimens 1B41B and 1BD3Y

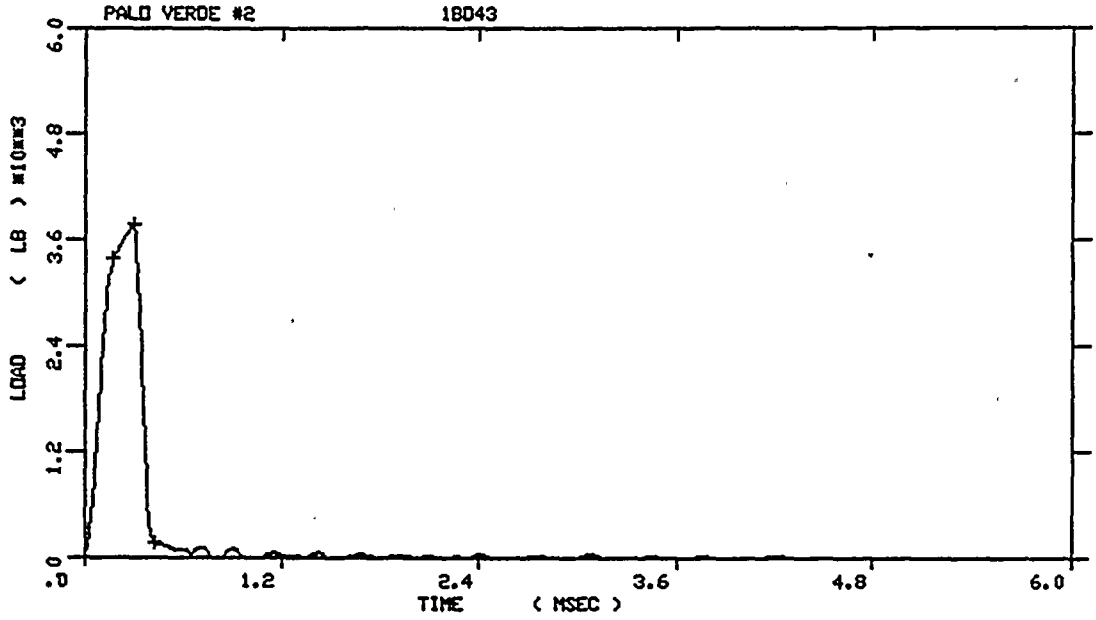

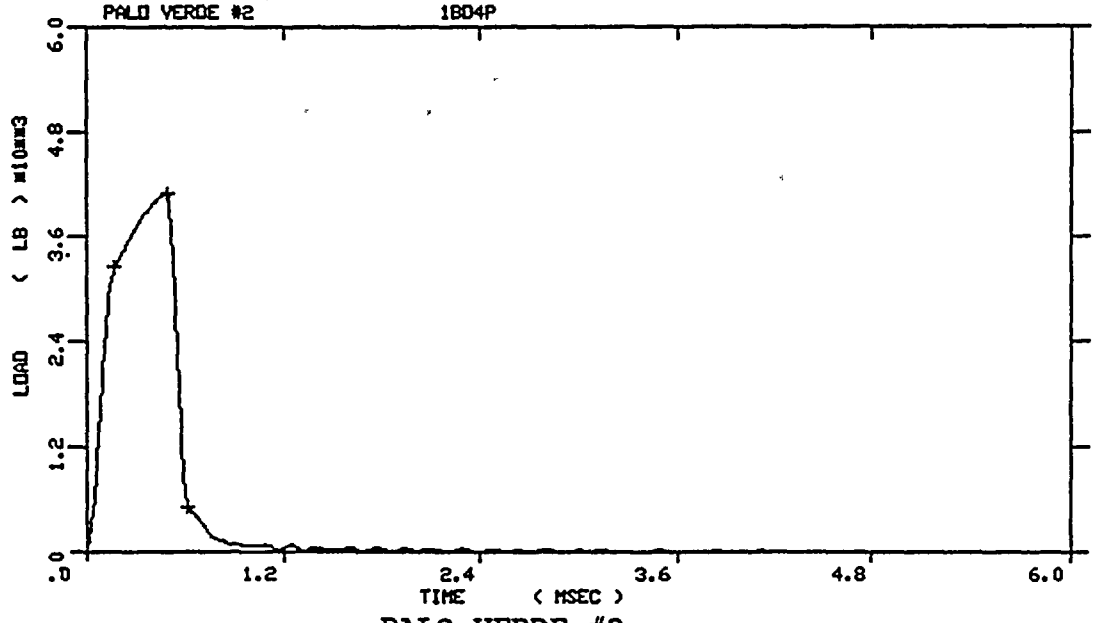

Figure A-28. Load-time records for Specimens 1BD43 and 1BD4P

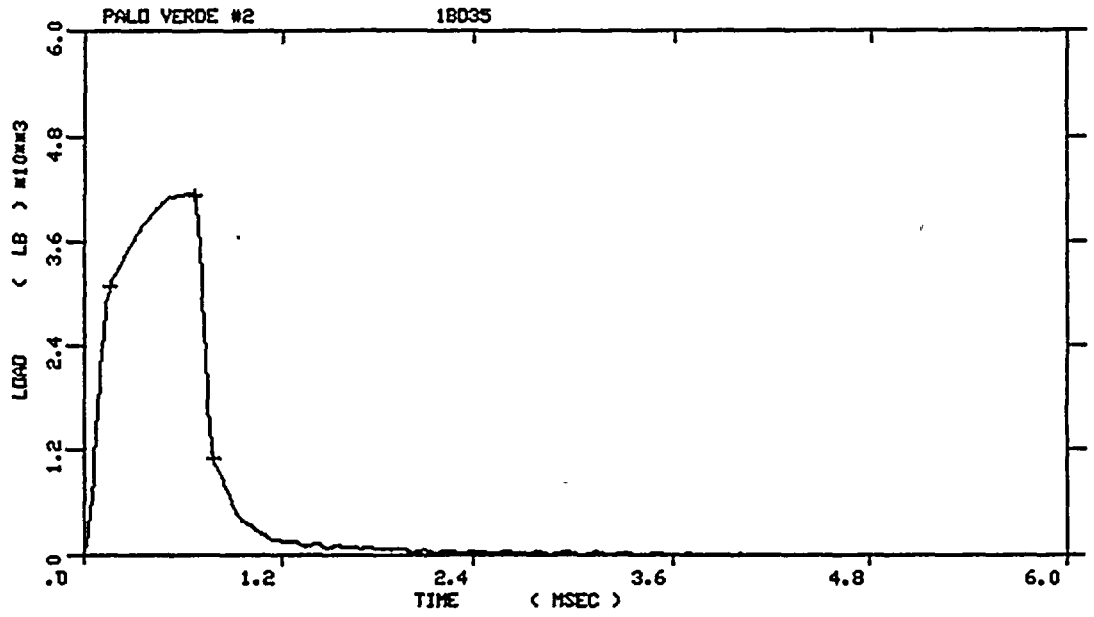

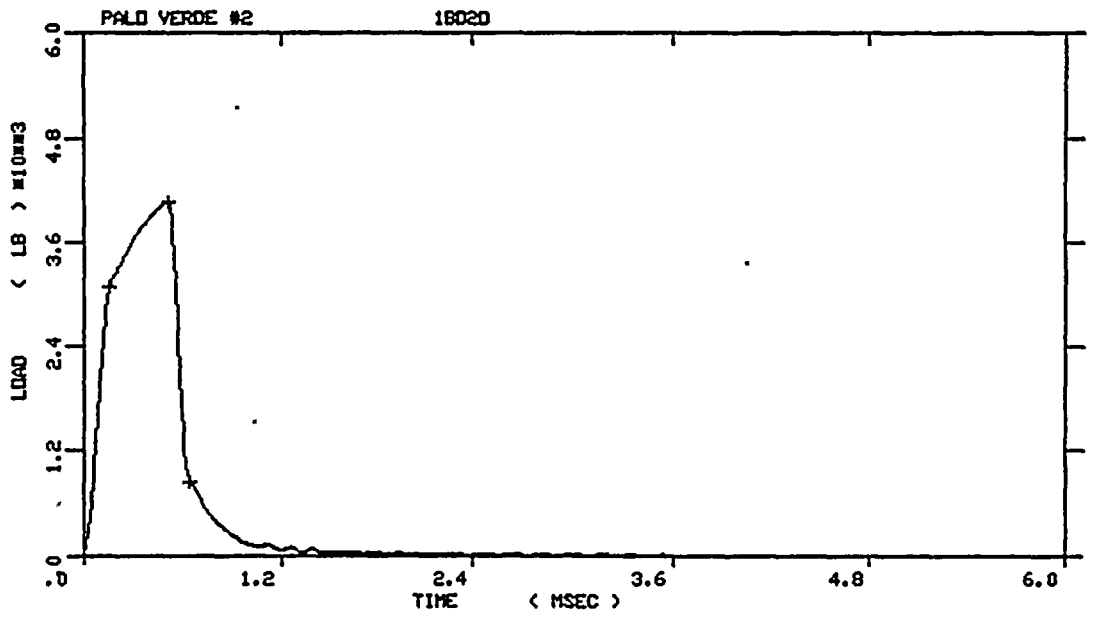

Figure A-29. Load-time records for Specimens 1BD35 and 1BD2D

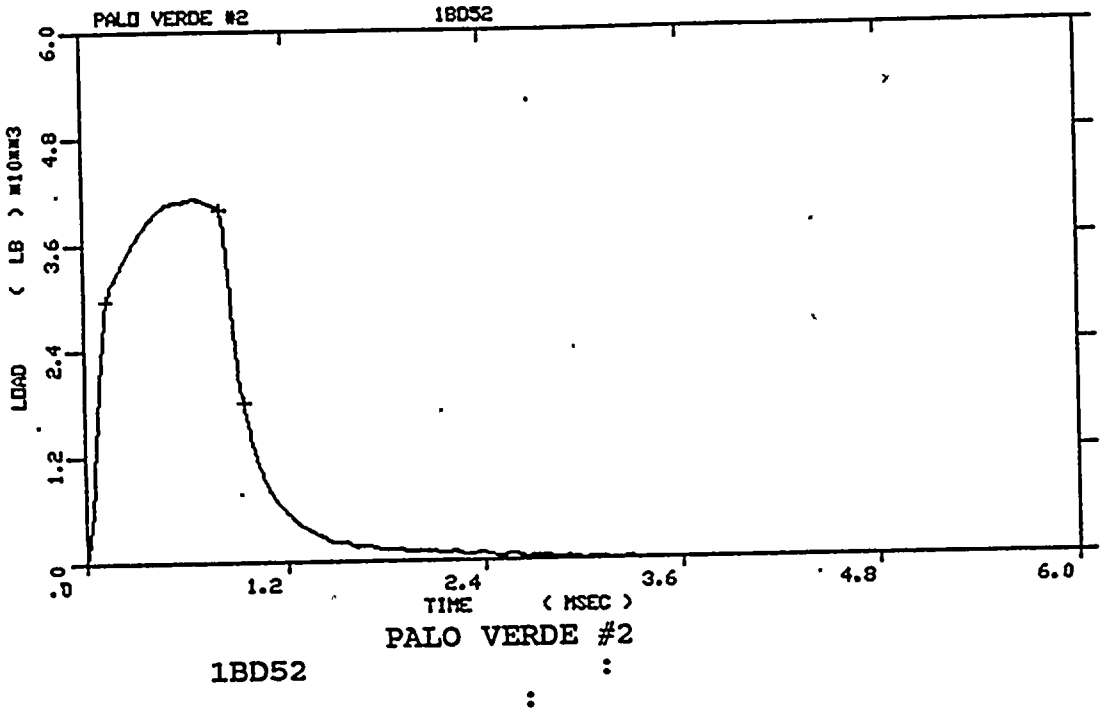

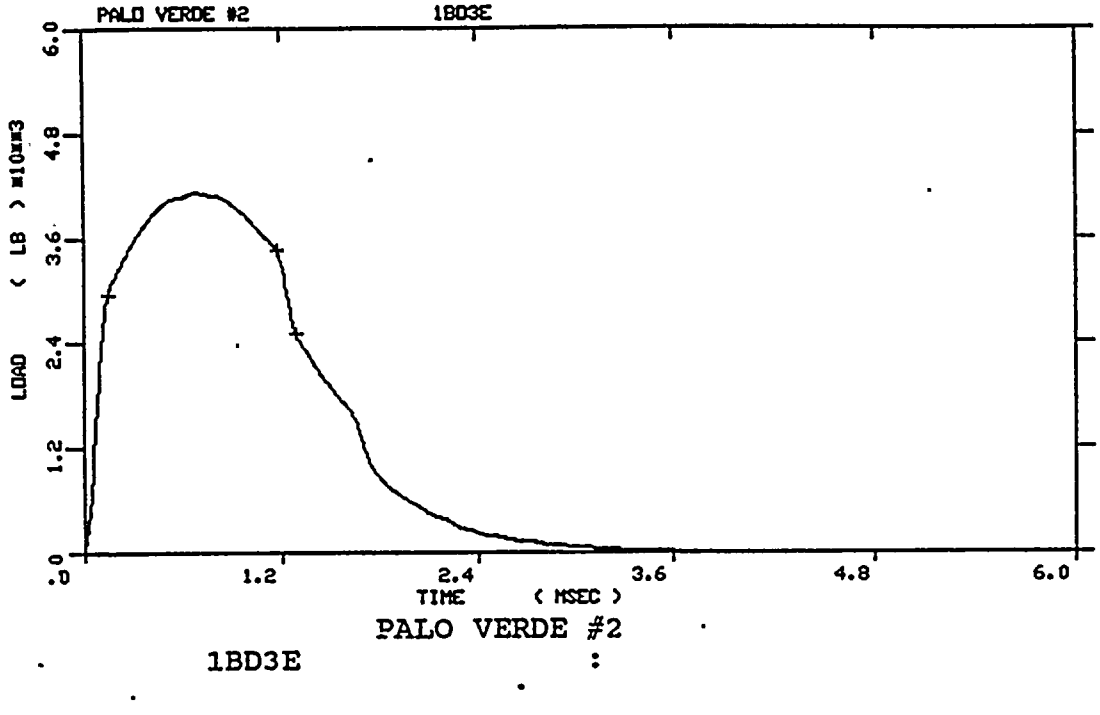

Figure A-30. Load-time records for Specimens 1BD52 and 1BD3E

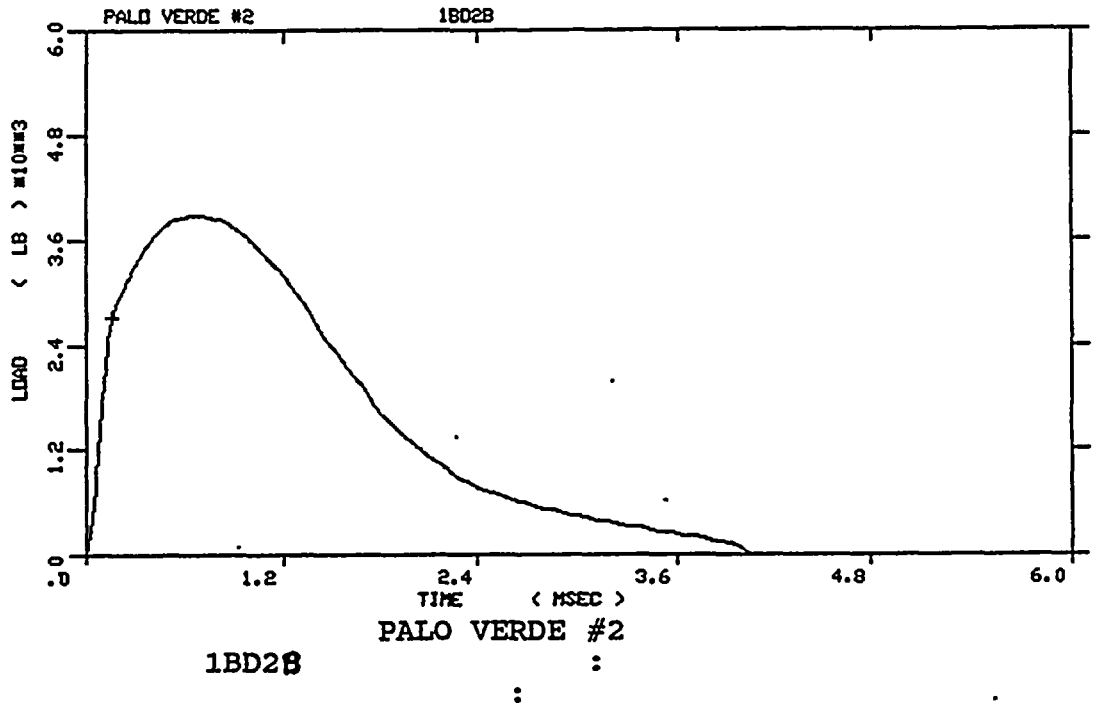

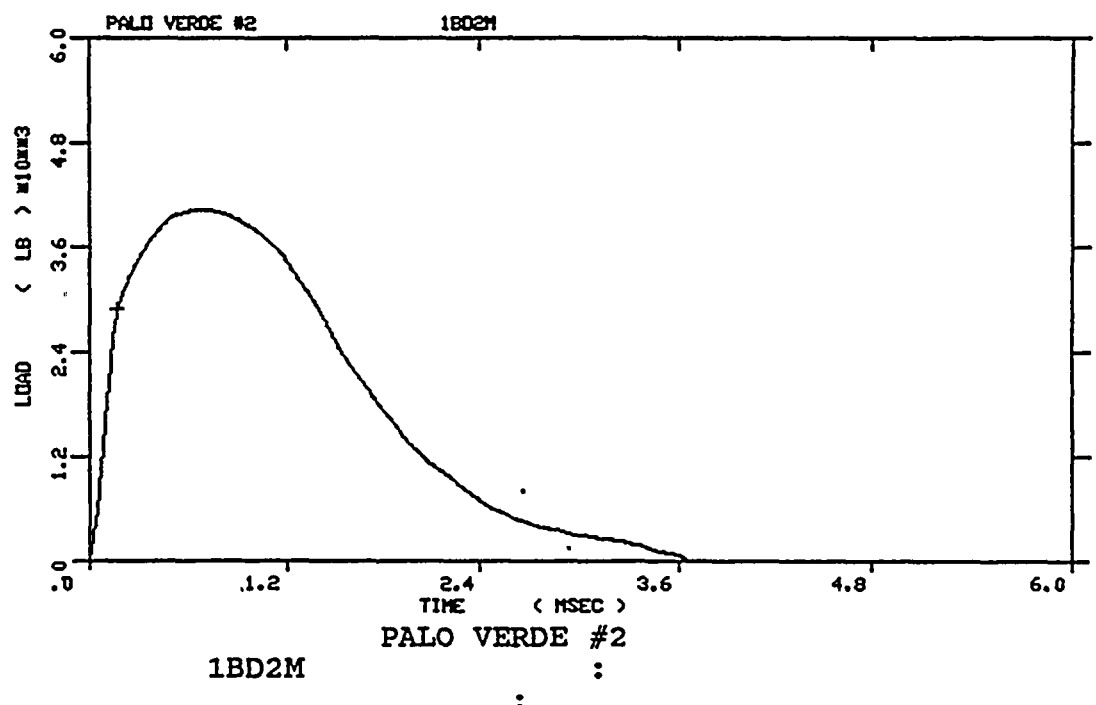

Figure A-31. Load-time records for Specimens 1BD2M and 1BD2B

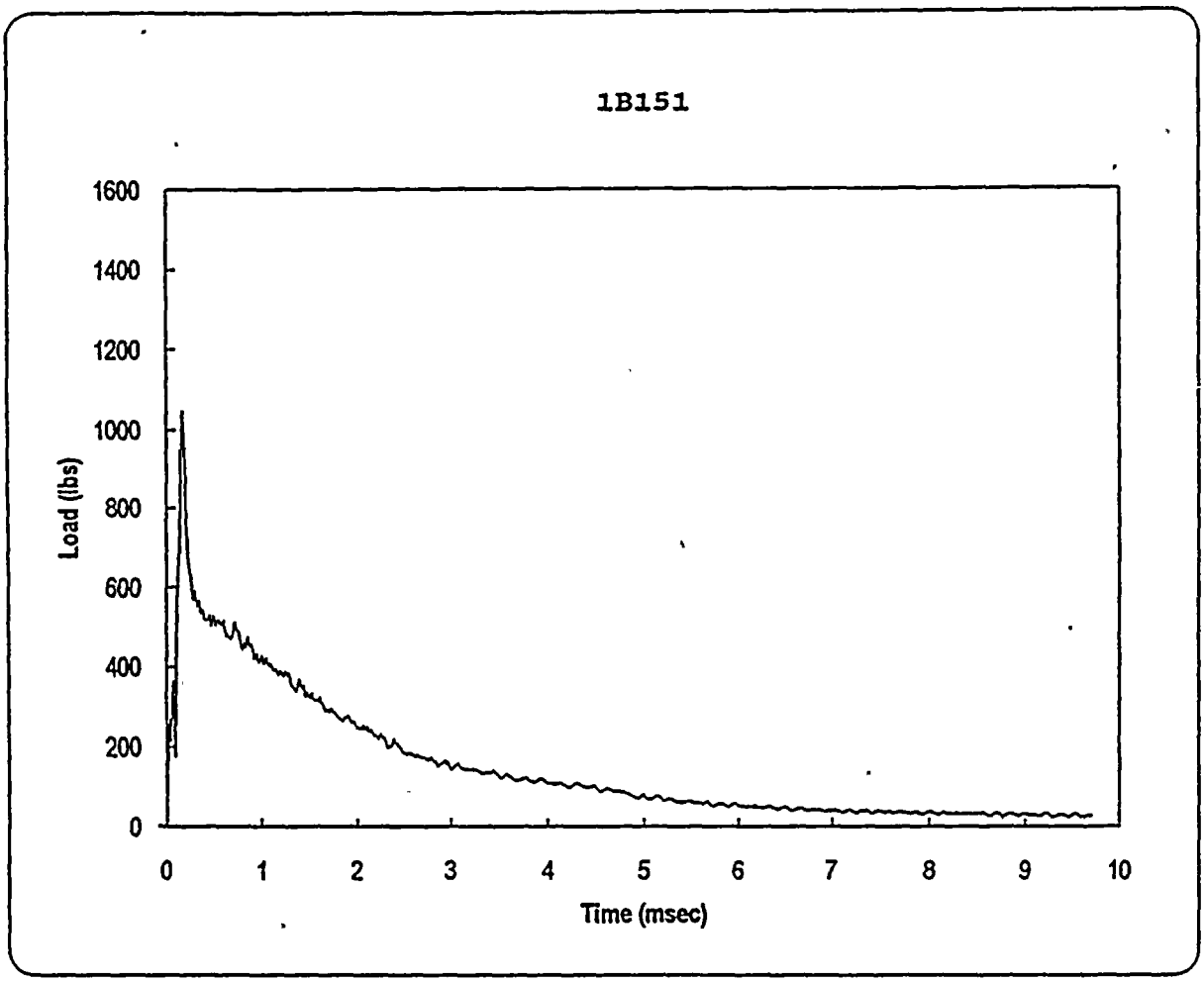

Specimen	1B151
Temperature	0 F
Available Energy	256 in-lbs
Initial Velocity	57.4 in/sec

Time to Yield	0.165 mSec *
Yield Load	1040 lbs *
Time to Maximum	0.170 mSec
Maximum Load	1047 lbs
Energy at Max. Load	3.7 in-lbs

Crack Length	0.176 in
a/W	0.447
Specimen Compliance	45.6
Machine Compliance	63.7

KID	38.2 ksi-in^1/2
Yield Stress	72.2 ksi *

* No General Yielding

Figure A-32. Load-time record and data for precracked specimen 1B151

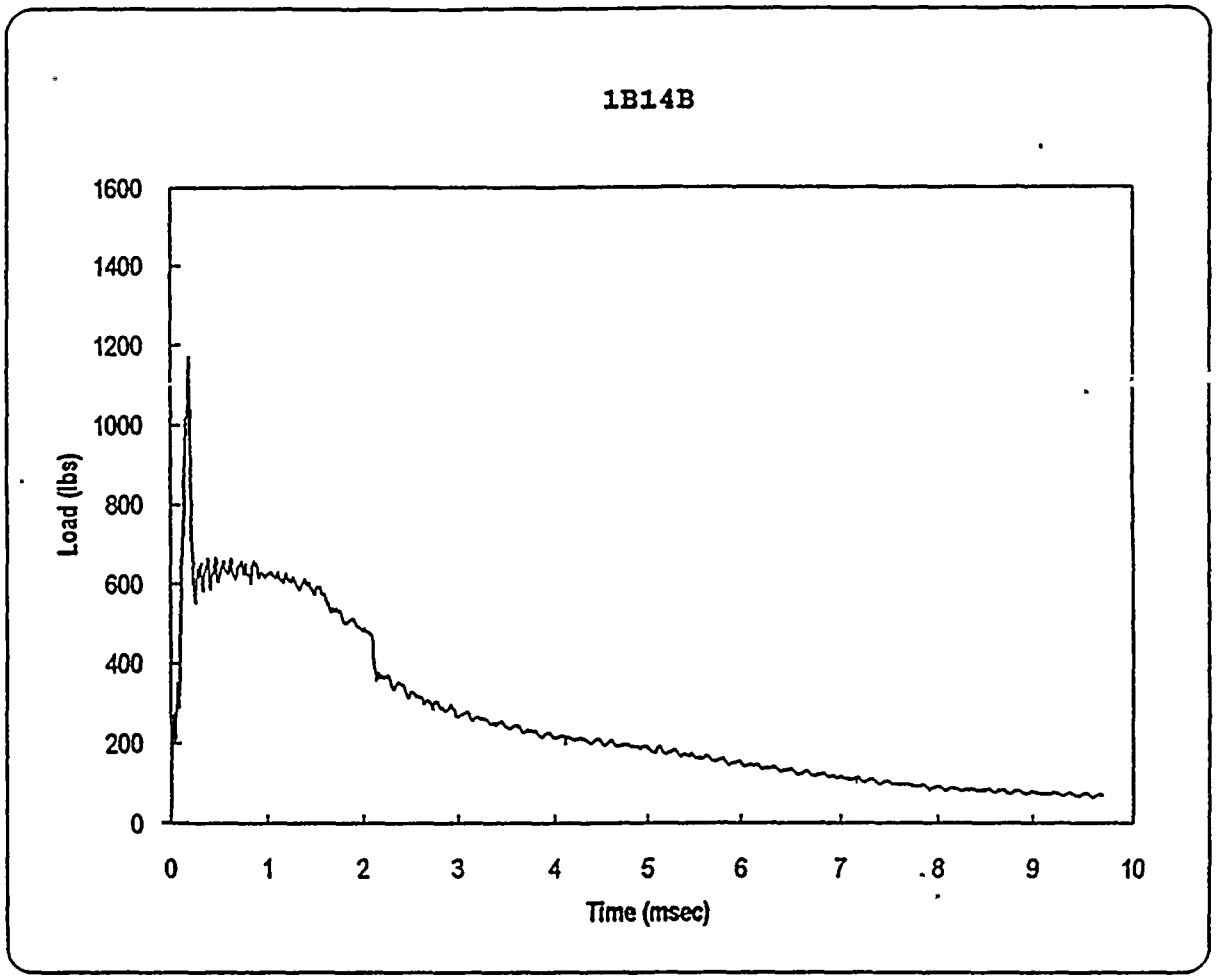

Specimen	1B14B
Temperature	25 F
Available Energy	256 in-lbs
Initial Velocity	57.5 in/sec

Time to Yield	0.180 mSec *
Yield Load	1165 lbs *
Time to Maximum	0.180 mSec
Maximum Load	1172 lbs
Energy at Max. Load	5.1 in-lbs

Crack Length	0.180 in
a/W	0.457
Specimen Compliance	47.3
Machine Compliance	57.1

KID	44.0 ksi-in^1/2
Yield Stress	83.9 ksi *

* No General Yielding

Figure A-33. Load-time record and data for precracked specimen 1B14B

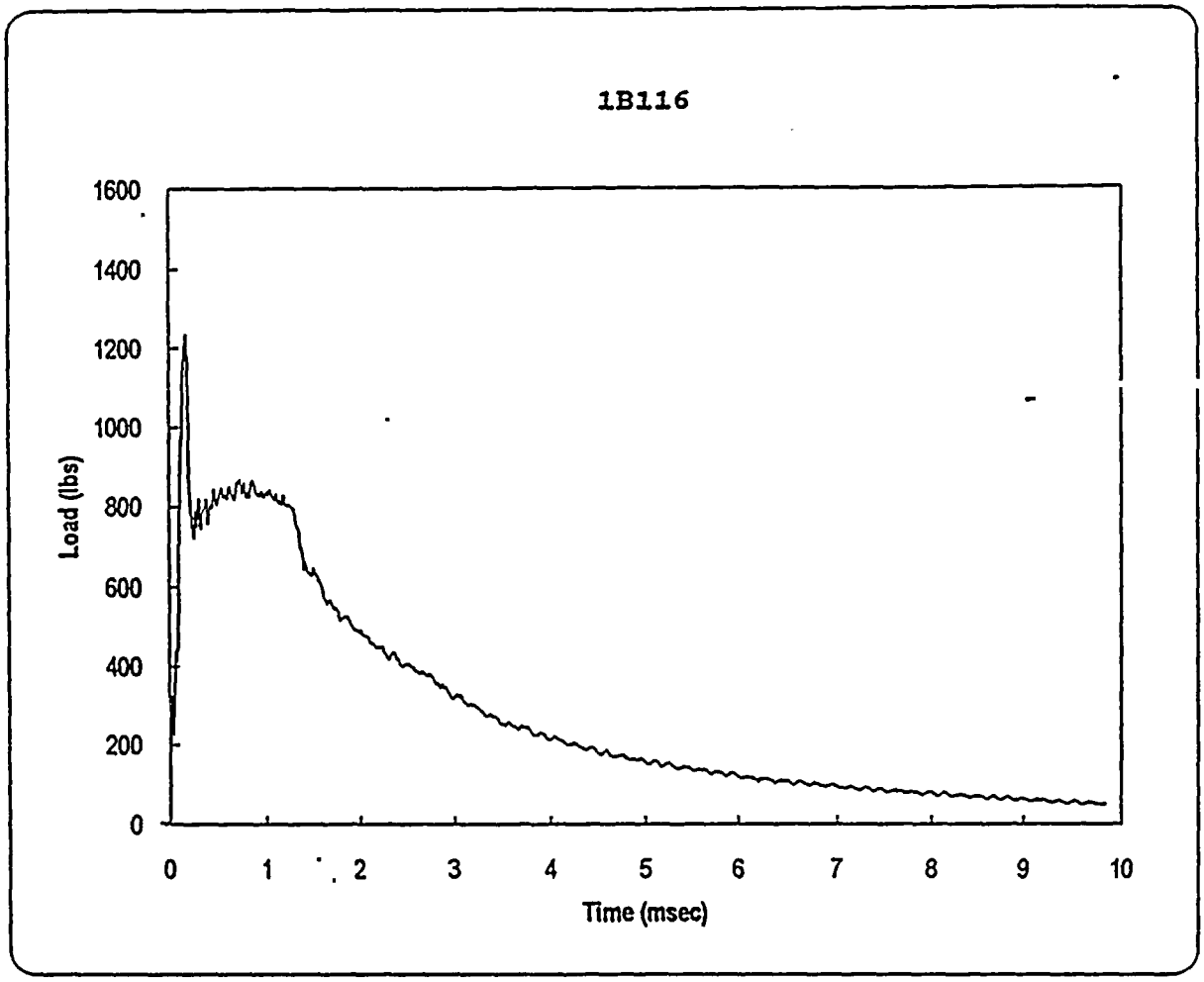

Specimen	1B116
Temperature	50 F
Available Energy	399 in-lbs
Initial Velocity	71.7 in/sec

Time to Yield	0.145 mSec *
Yield Load	1200 lbs *
Time to Maximum	0.170 mSec
Maximum Load	1235 lbs
Energy at Max. Load	7.3 in-lbs

Crack Length	0.176 in
a/W	0.447
Specimen Compliance	45.6
Machine Compliance	53.1

KID	45.0 ksi-in^1/2
Yield Stress	83.3 ksi *

* No General Yielding

Figure A-34. Load-time record and data for precracked specimen 1B116

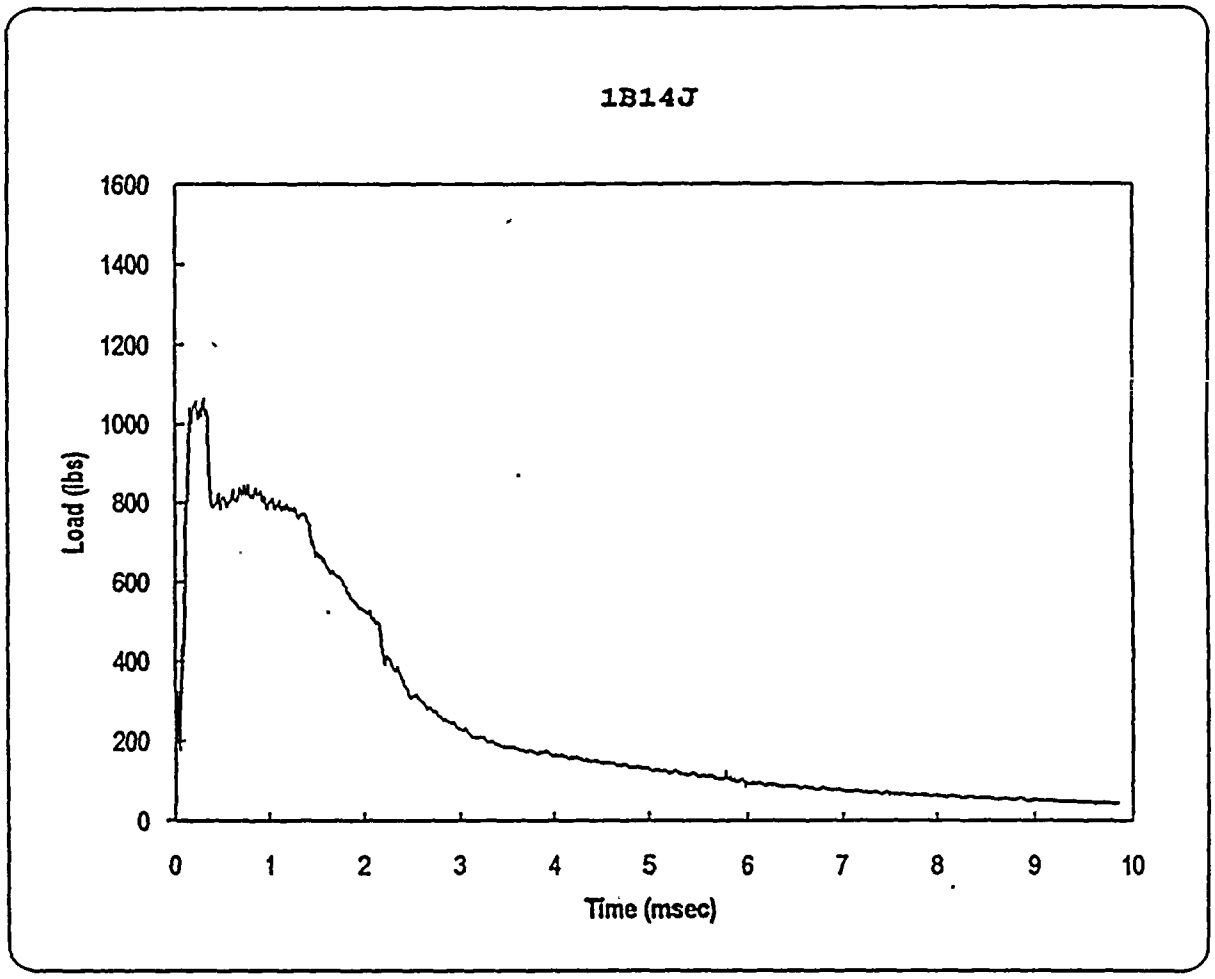

Specimen	1B14J
Temperature	71 F
Available Energy	398 in-lbs
Initial Velocity	71.6 in/sec

Time to Yield	0.157 mSec
Yield Load	1040 lbs
Time to Maximum	0.300 mSec
Maximum Load	1066 lbs
Energy at Max. Load	15.5 in-lbs

Crack Length	0.213 in
a/W	0.541
Specimen Compliance	66.4
Machine Compliance	58.4

KJD	102.9 ksi-in^1/2
Yield Stress	104.8 ksi

Figure A-35. Load-time record and data for precracked specimen 1B14J

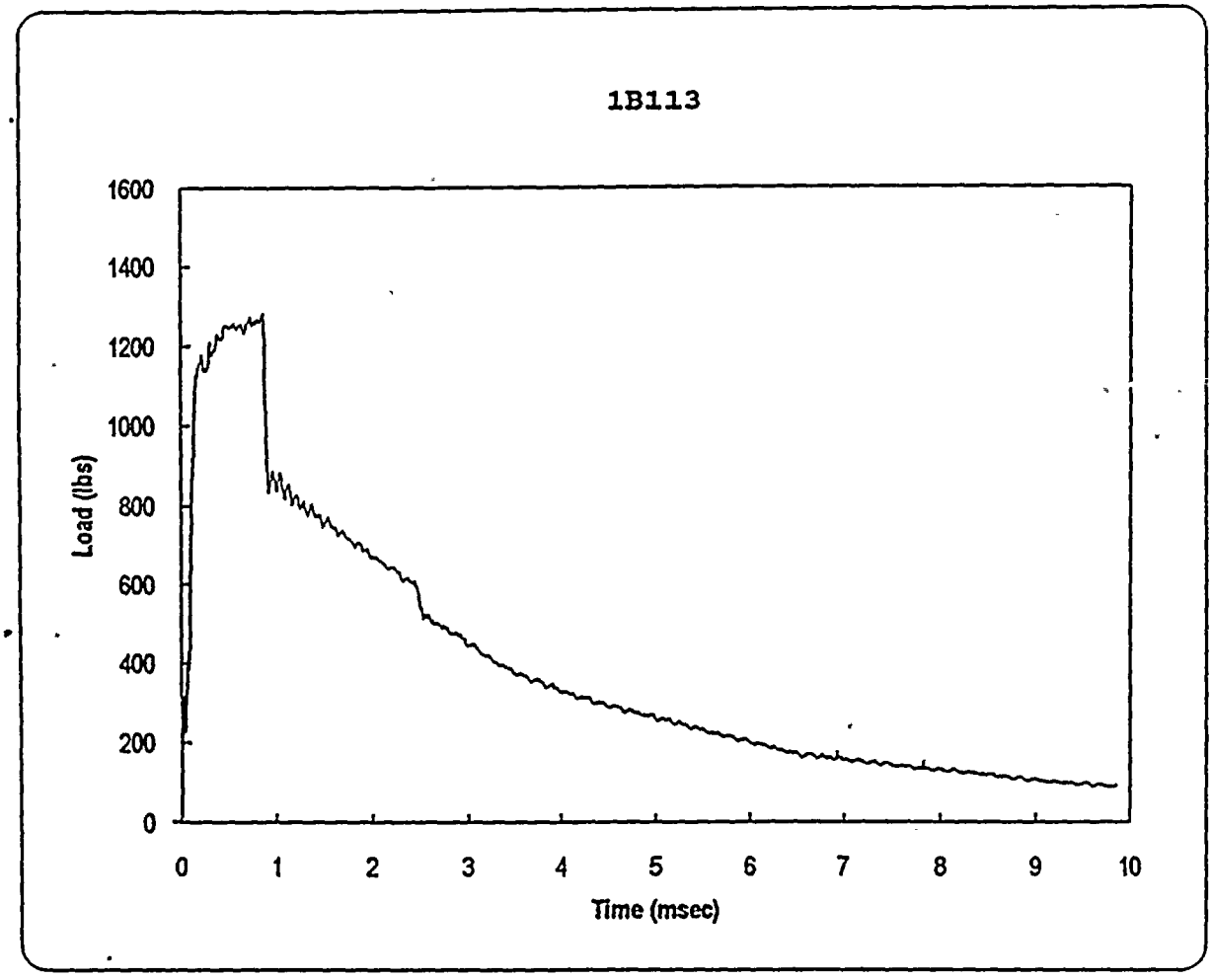

Specimen	1B113
Temperature	76 F
Available Energy	398 in-lbs
Initial Velocity	71.6 in/sec

Time to Yield	0.150 mSec
Yield Load	1120 lbs
Time to Maximum	0.860 mSec
Maximum Load	1285 lbs
Energy at Max. Load	64.4 in-lbs

Crack Length	0.189 in
a/W	0.480
Specimen Compliance	51.6
Machine Compliance	60.7

KJD	210.9 ksi-in^1/2
Yield Stress	87.9 ksi

Figure A-36. Load-time record and data for precracked specimen 1B113

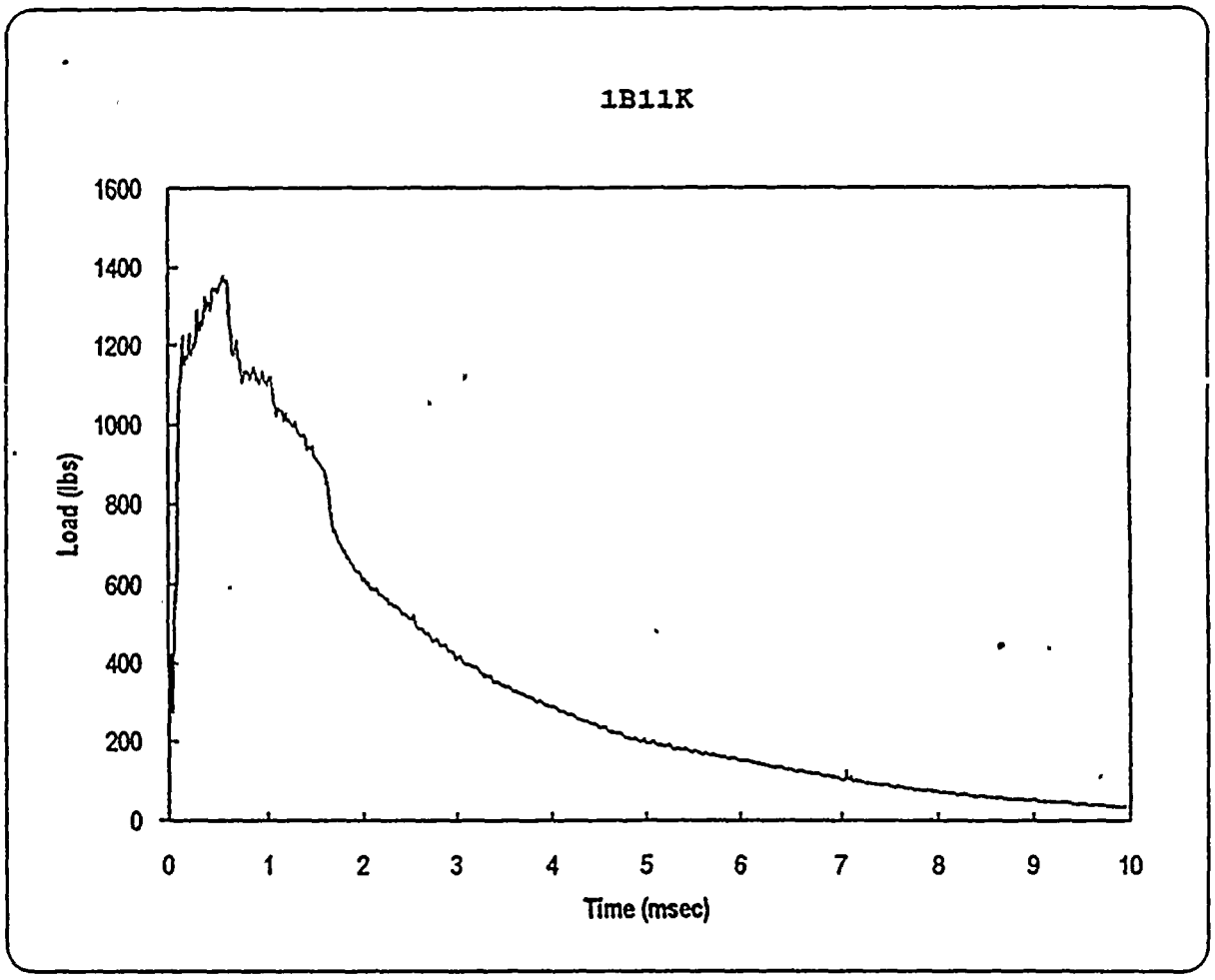

Specimen	1B11K
Temperature	100 F
Available Energy	637 in-lbs
Initial Velocity	90.6 in/sec

Time to Yield	0.135 mSec
Yield Load	1200 lbs
Time to Maximum	0.560 mSec
Maximum Load	1381 lbs
Energy at Max. Load	54.2 in-lbs

Crack Length	0.186 in
a/W	0.472
Specimen Compliance	50.1
Machine Compliance	71.6

KJD	187.4 ksi-in^1/2
Yield Stress	91.5 ksi

Figure A-37. Load-time record and data for precracked specimen 1B11K

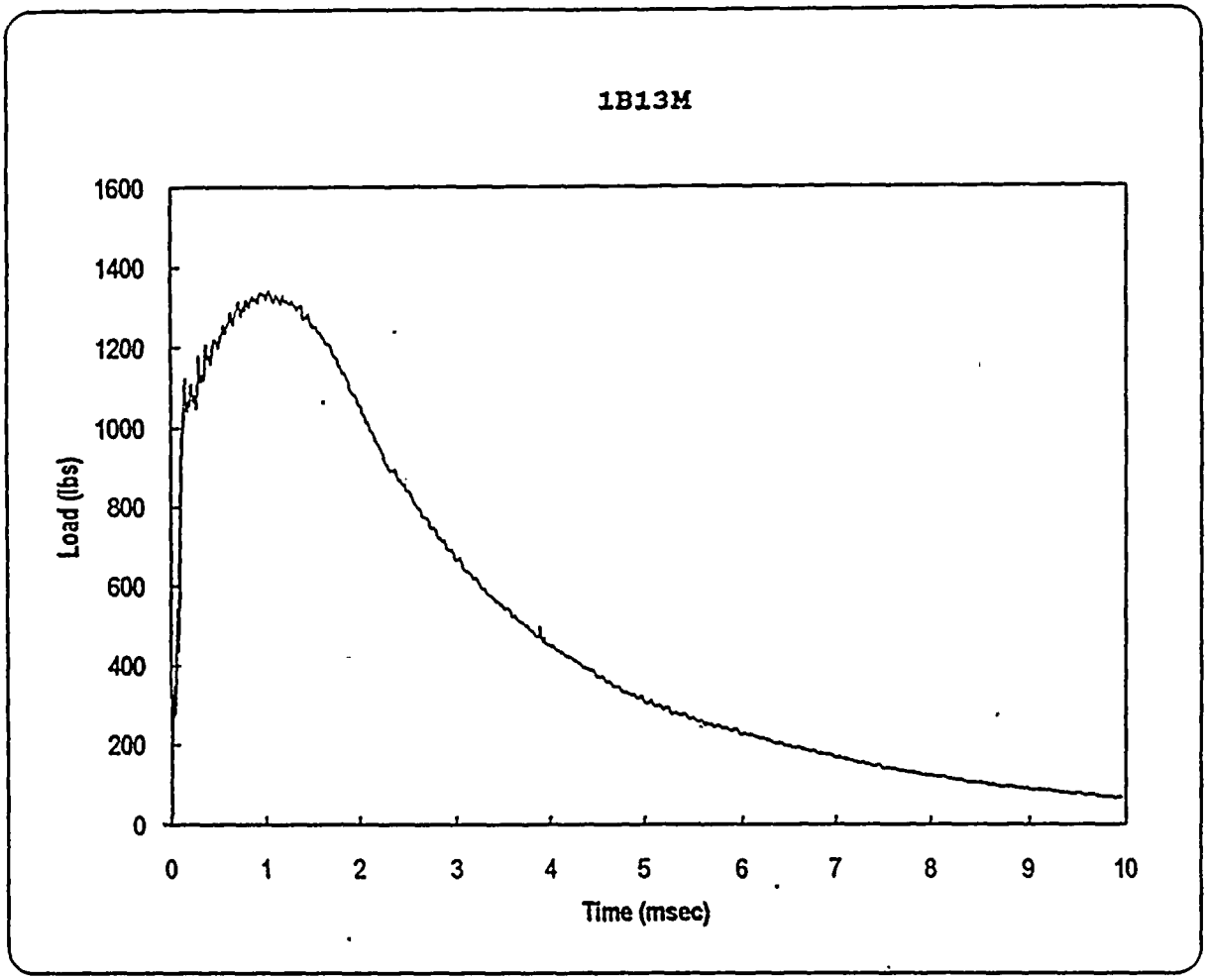

Specimen	1B13M
Temperature	150 F
Available Energy	642 in-lbs
Initial Velocity	90.9 in/sec

Time to Yield	0.140 mSec
Yield Load	1100 lbs
Time to Maximum	1.035 mSec
Maximum Load	1341 lbs
Energy at Max. Load	101.6 in-lbs

Crack Length	0.189 in
a/W	0.480
Specimen Compliance	51.6
Machine Compliance	83.7

KJD	263.6 ksi-in^1/2
Yield Stress	86.4 ksi

Figure A-38. Load-time record and data for precracked specimen 1B13M

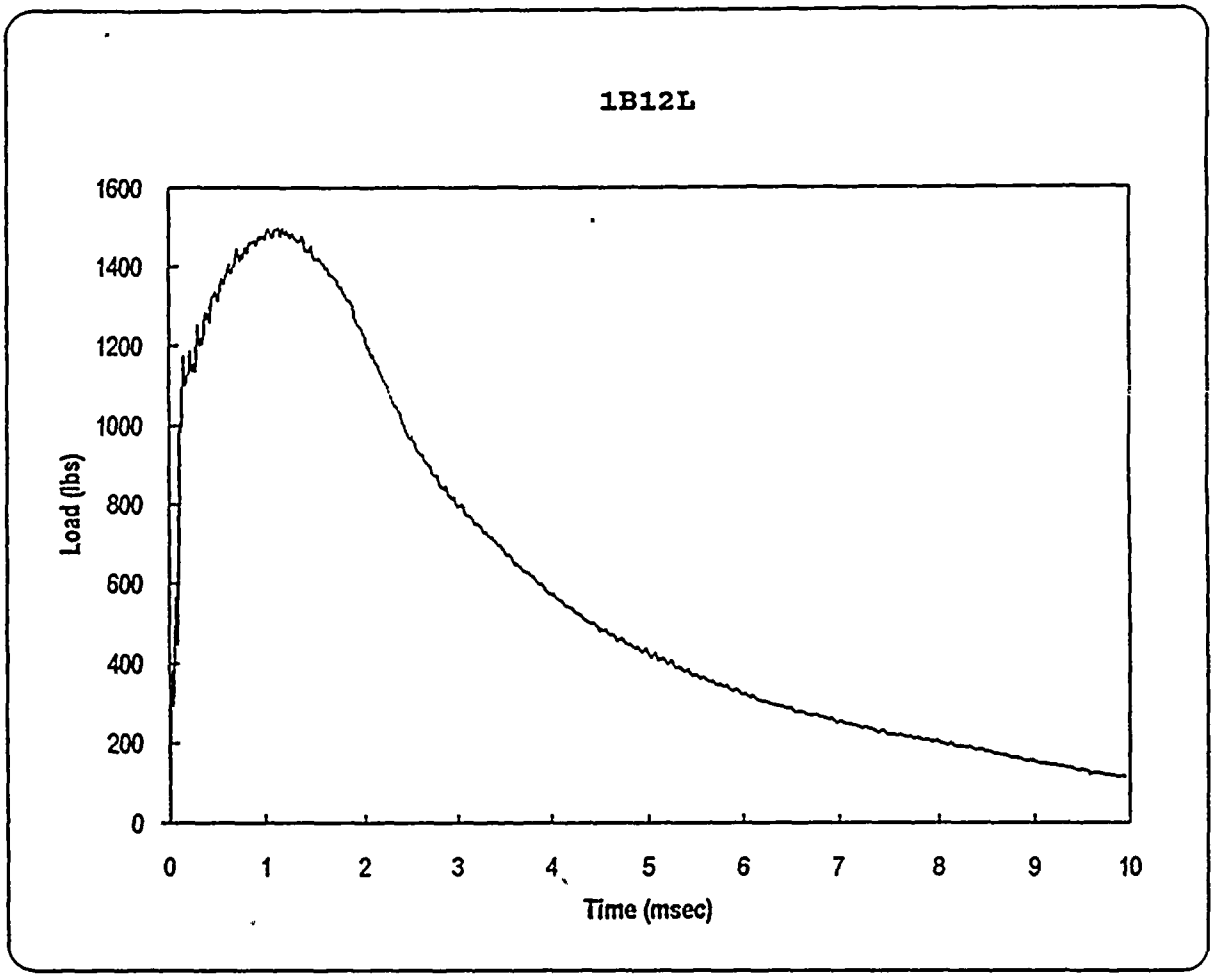

Specimen	1B12L
Temperature	200 F
Available Energy	640 in-lbs
Initial Velocity	90.8 in/sec

Time to Yield	0.145 mSec
Yield Load	1170 lbs
Time to Maximum	1.135 mSec
Maximum Load	1499 lbs
Energy at Max. Load	122.1 in-lbs

Crack Length	0.185 in
a/W	0.470
Specimen Compliance	49.6
Machine Compliance	81.0

KJD	285.0 ksi-in^1/2
Yield Stress	88.4 ksi

Figure A-39. Load-time record and data for precracked specimen 1B12L

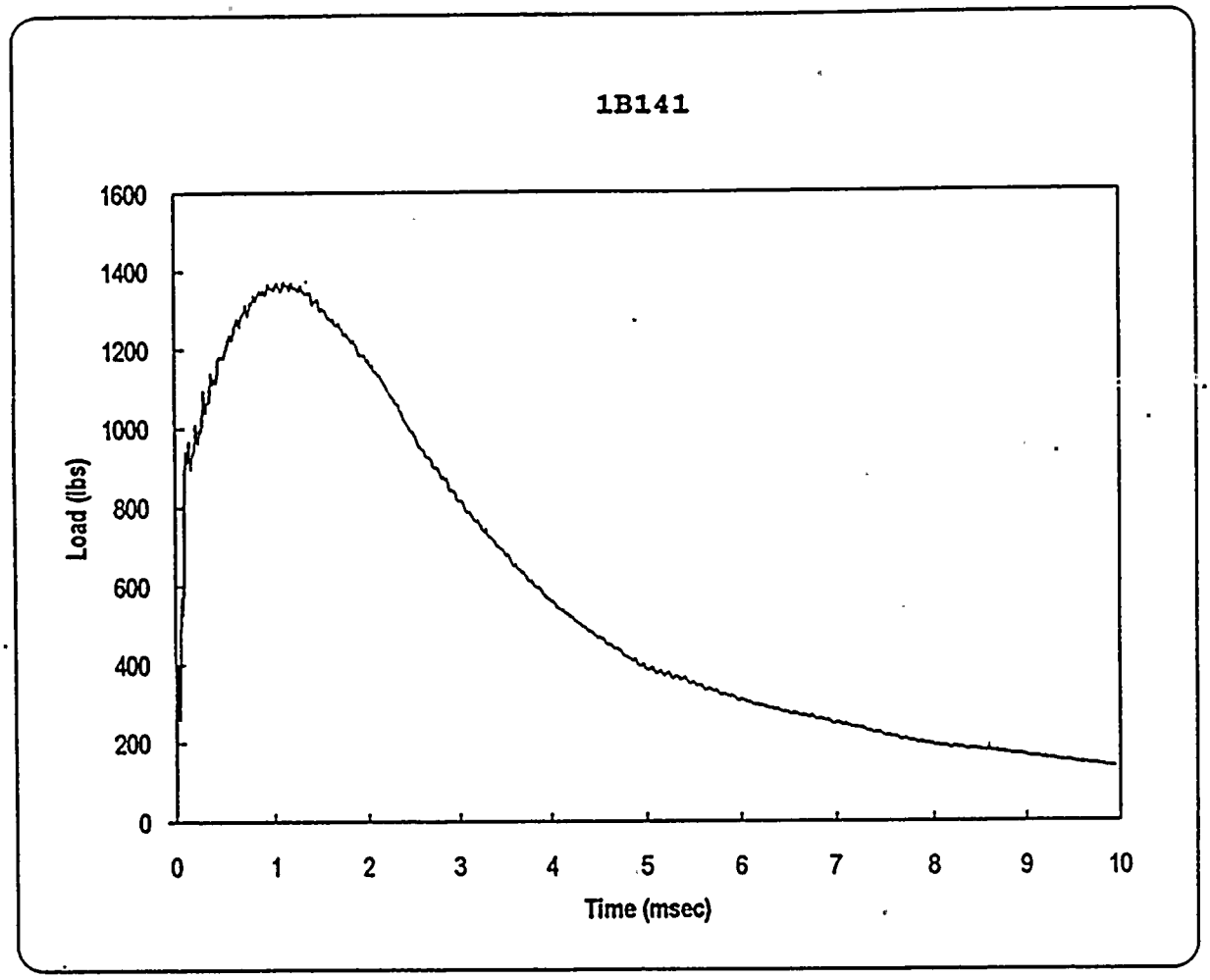

Specimen	1B141
Temperature	250 F
Available Energy	640 in-lbs
Initial Velocity	90.8 in/sec

Time to Yield	0.105 mSec
Yield Load	940 lbs
Time to Maximum	1.105 mSec
Maximum Load	1375 lbs
Energy at Max. Load	108.0 in-lbs

Crack Length	0.181 in
a/W	0.459
Specimen Compliance	47:8
Machine Compliance	70.0

KJD	266.0 ksi-in^1/2
Yield Stress	68.4 ksi

Figure A-40. Load-time record and data for precracked specimen 1B141

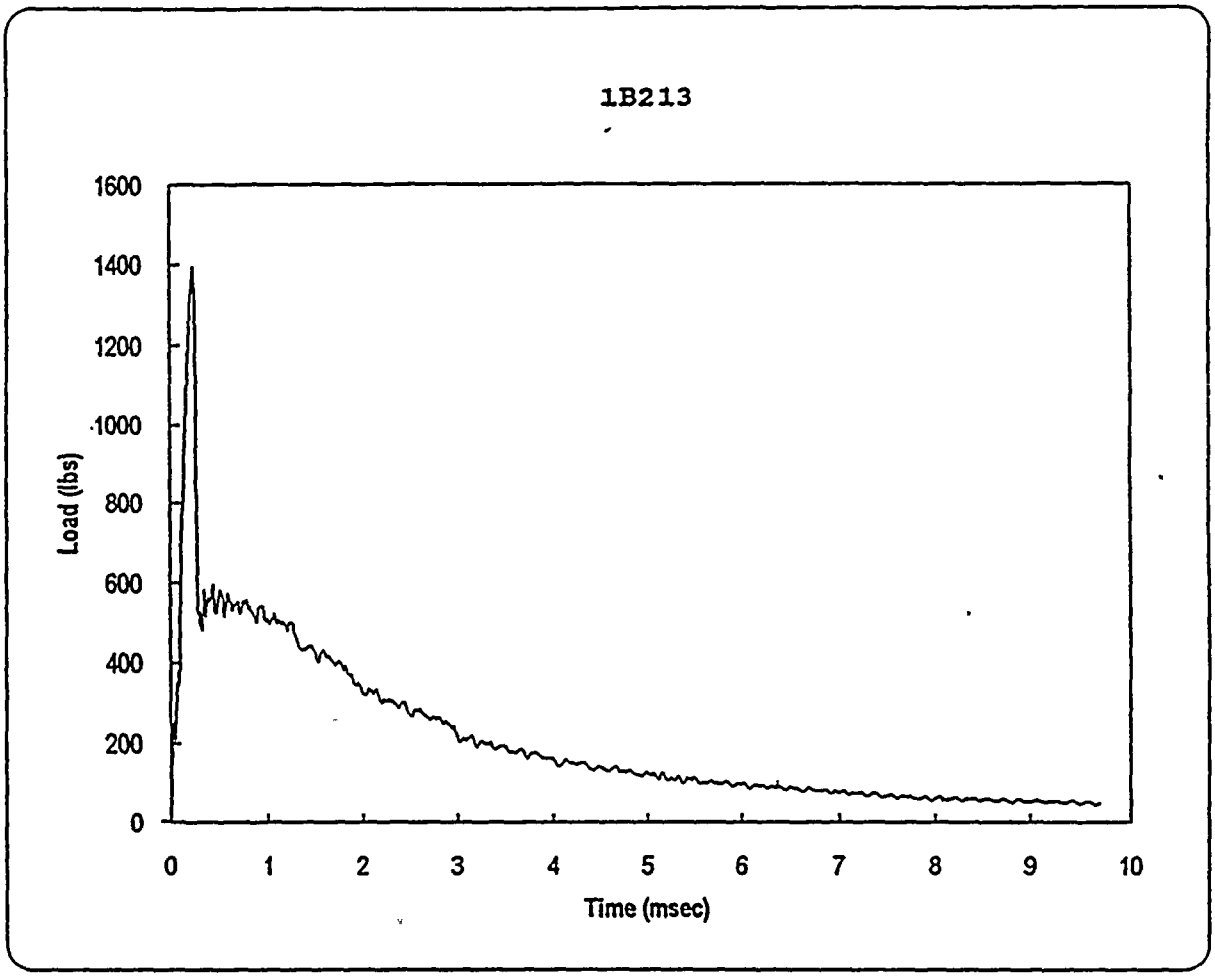

Specimen	1B213
Temperature	25 F
Available Energy	256 in-lbs
Initial Velocity	57.4 in/sec

Time to Yield	0.218 mSec *
Yield Load	1380 lbs *
Time to Maximum	0.225 mSec
Maximum Load	1395 lbs
Energy at Max. Load	8.7 in-lbs

Crack Length	0.175 in
a/W	0.444
Specimen Compliance	45.2
Machine Compliance	61.4

KID	50.4 ksi-in^1/2
Yield Stress	95.0 ksi *

* No General Yielding

Figure A-41. Load-time record and data for precracked specimen 1B213

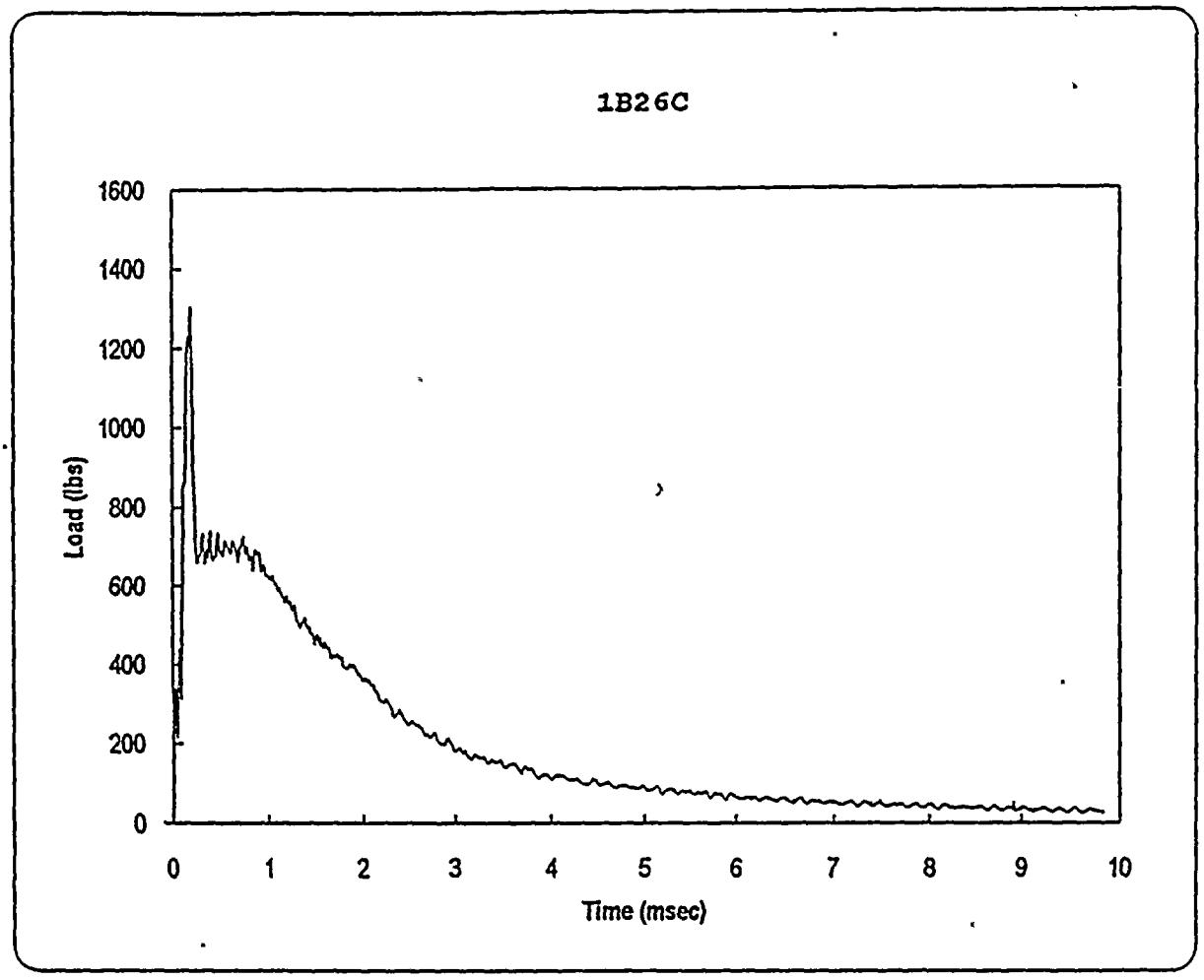

Specimen	1B26C
Temperature	50 F
Available Energy	401 in-lbs
Initial Velocity	71.9 in/sec

Time to Yield	0.155 mSec *
Yield Load	1230 lbs *
Time to Maximum	0.185 mSec
Maximum Load	1306 lbs
Energy at Max. Load	8.1 in-lbs

Crack Length	0.187 in
a/W	0.475
Specimen Compliance	50.6
Machine Compliance	55.2

KID	51.8 ksi-in^1/2
Yield Stress	94.7 ksi *

* No General Yielding

Figure A-42. Load-time record and data for precracked specimen 1B26C

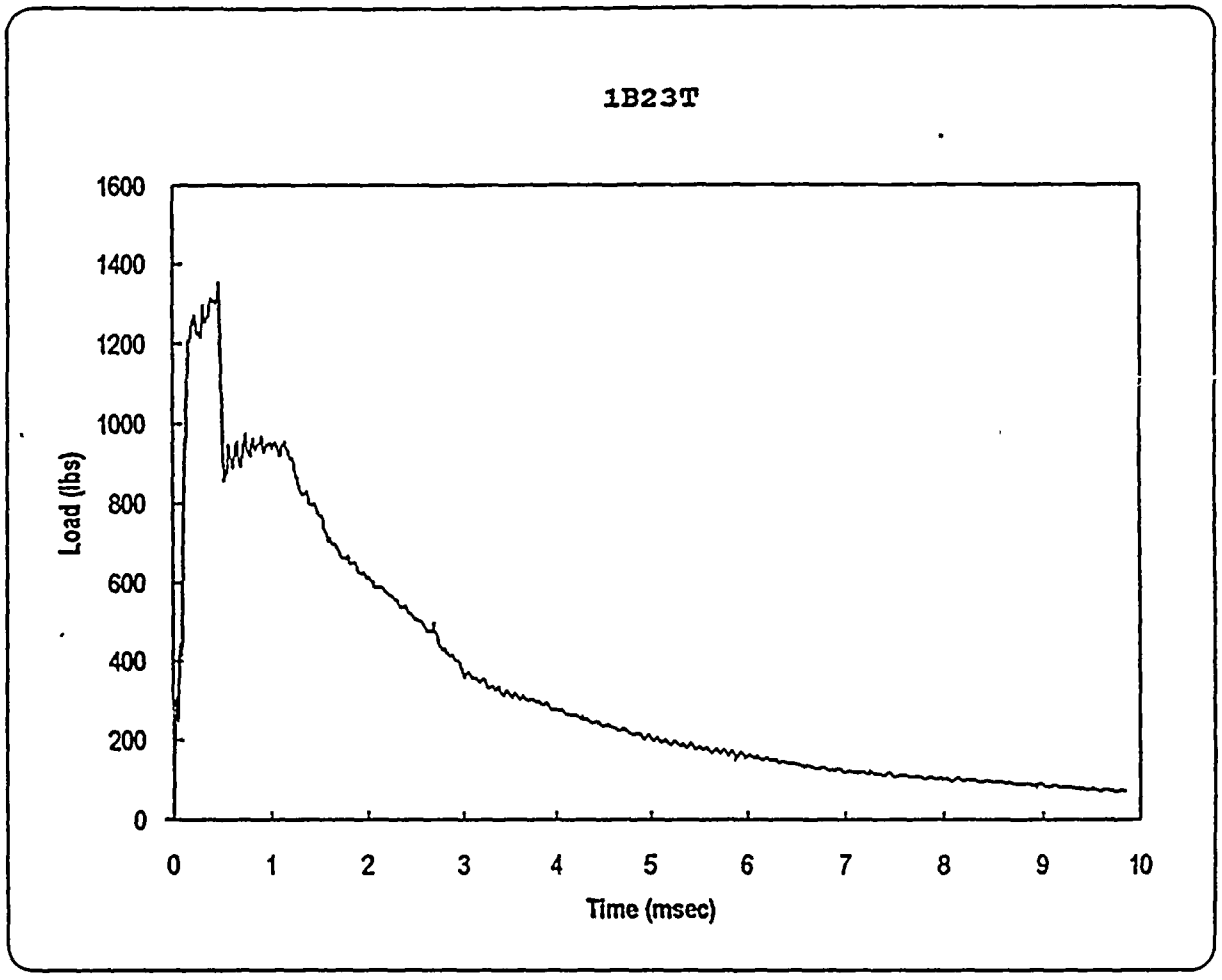

Specimen	1B23T
Temperature	76 F
Available Energy	397 in-lbs
Initial Velocity	71.5 in/sec

Time to Yield	0.155 mSec
Yield Load	1200 lbs
Time to Maximum	0.455 mSec
Maximum Load	1354 lbs
Energy at Max. Load	32.1 in-lbs

Crack Length	0.173 in
a/W	0.439
Specimen Compliance	44.4
Machine Compliance	60.5

KJD	137.1 ksi-in^1/2
Yield Stress	81.1 ksi

Figure A-43. Load-time record and data for precracked specimen 1B23T

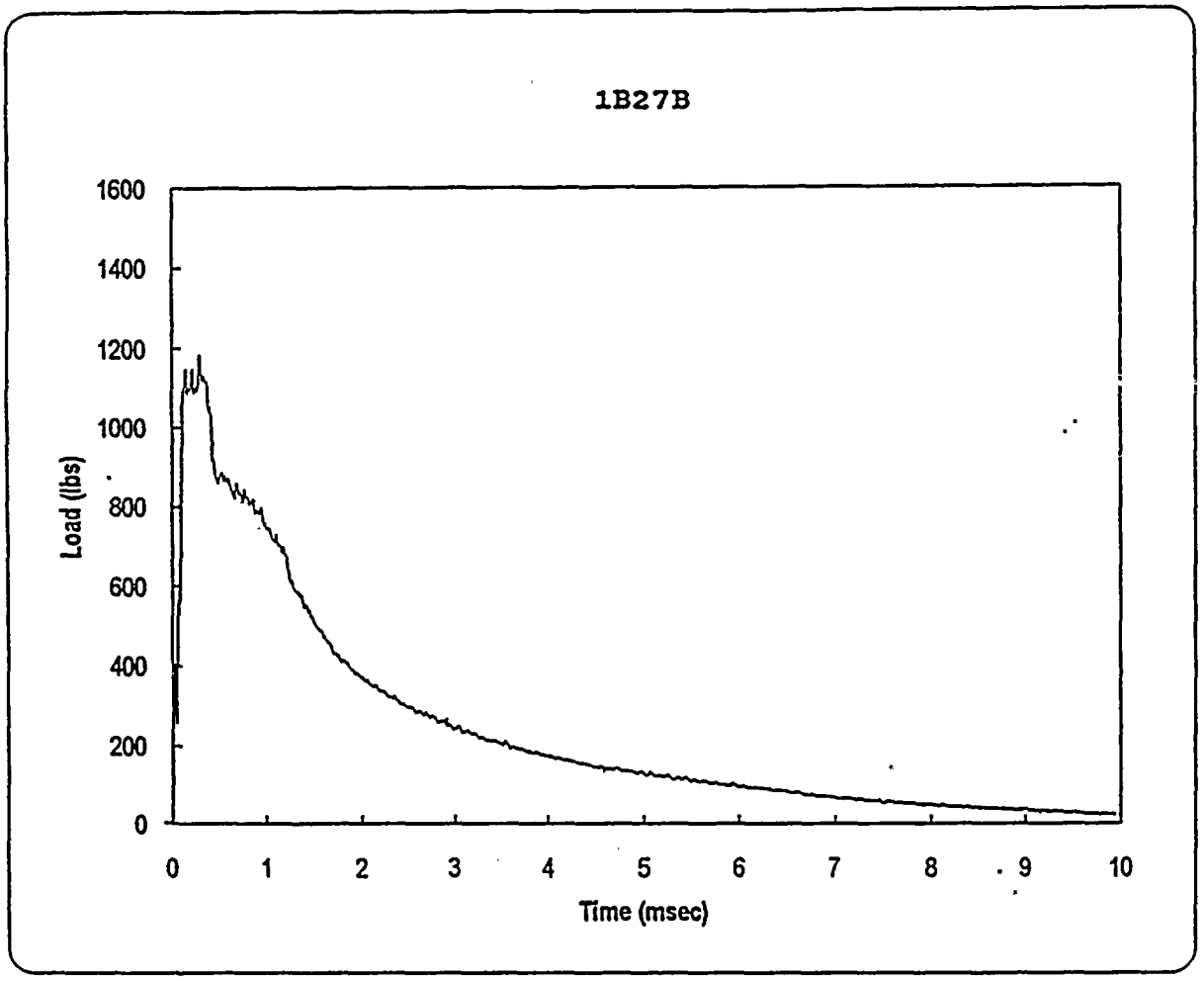

Specimen	1B27B
Temperature	100 F
Available Energy	639 in-lbs
Initial Velocity	90.7 in/sec

Time to Yield	0.110 mSec
Yield Load	1060 lbs
Time to Maximum	0.295 mSec
Maximum Load	1186 lbs
Energy at Max. Load	22.6 in-lbs

Crack Length	0.189 in
a/W	0.480
Specimen Compliance	51.6
Machine Compliance	61.1

KJD	118.1 ksi-in^1/2
Yield Stress	83.2 ksi

Figure A-44. Load-time record and data for precracked specimen 1B27B

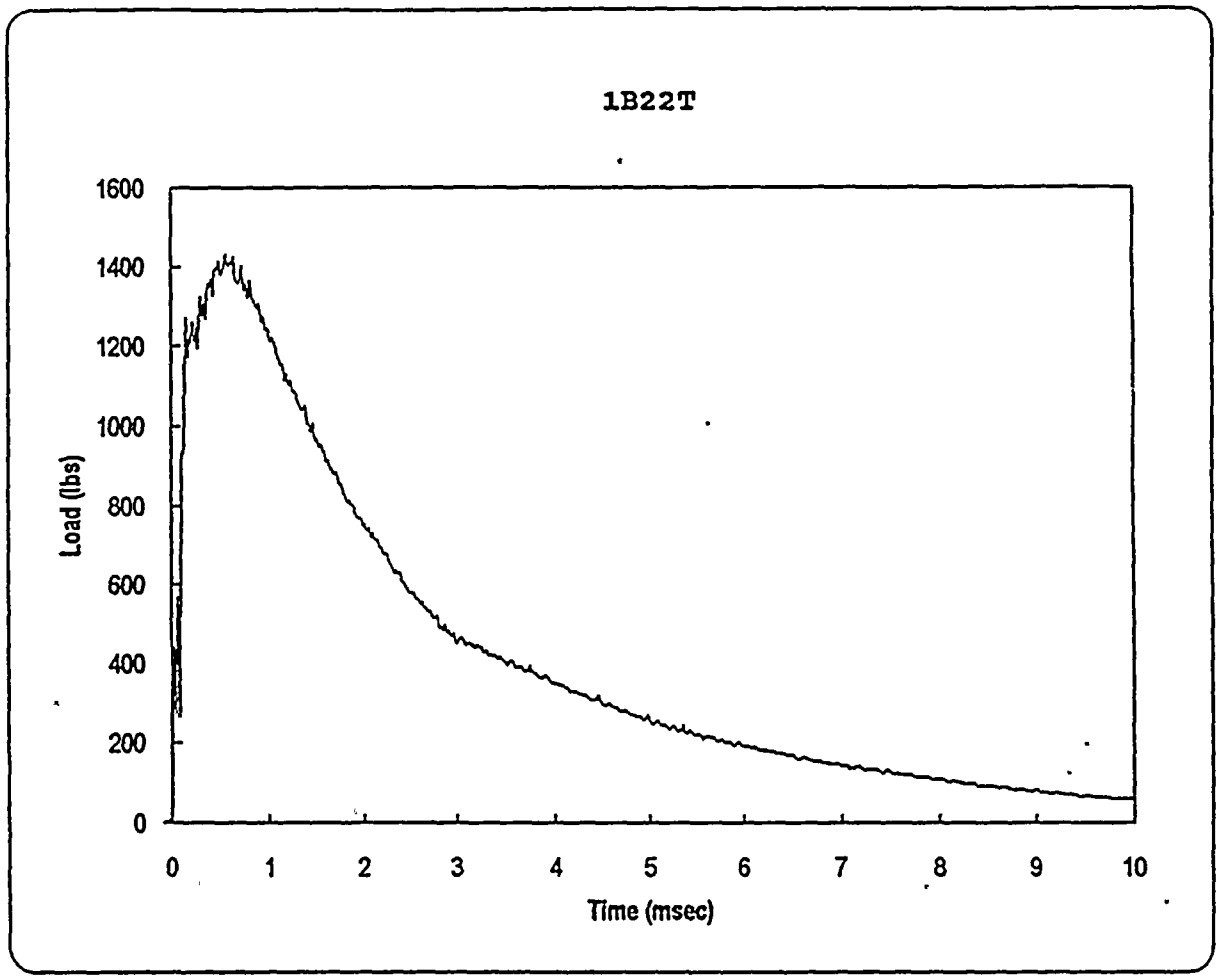

Specimen	1B22T
Temperature	150 F
Available Energy	638 in-lbs
Initial Velocity	90.6 in/sec

Time to Yield	0.150 mSec
Yield Load	1260 lbs
Time to Maximum	0.560 mSec
Maximum Load	1434 lbs
Energy at Max. Load	54.4 in-lbs

Crack Length	0.186 in
a/W	0.472
Specimen Compliance	50.1
Machine Compliance	73.5

KJD	185.7 ksi-in^1/2
Yield Stress	96.1 ksi

Figure A-45. Load-time record and data for precracked specimen 1B22T

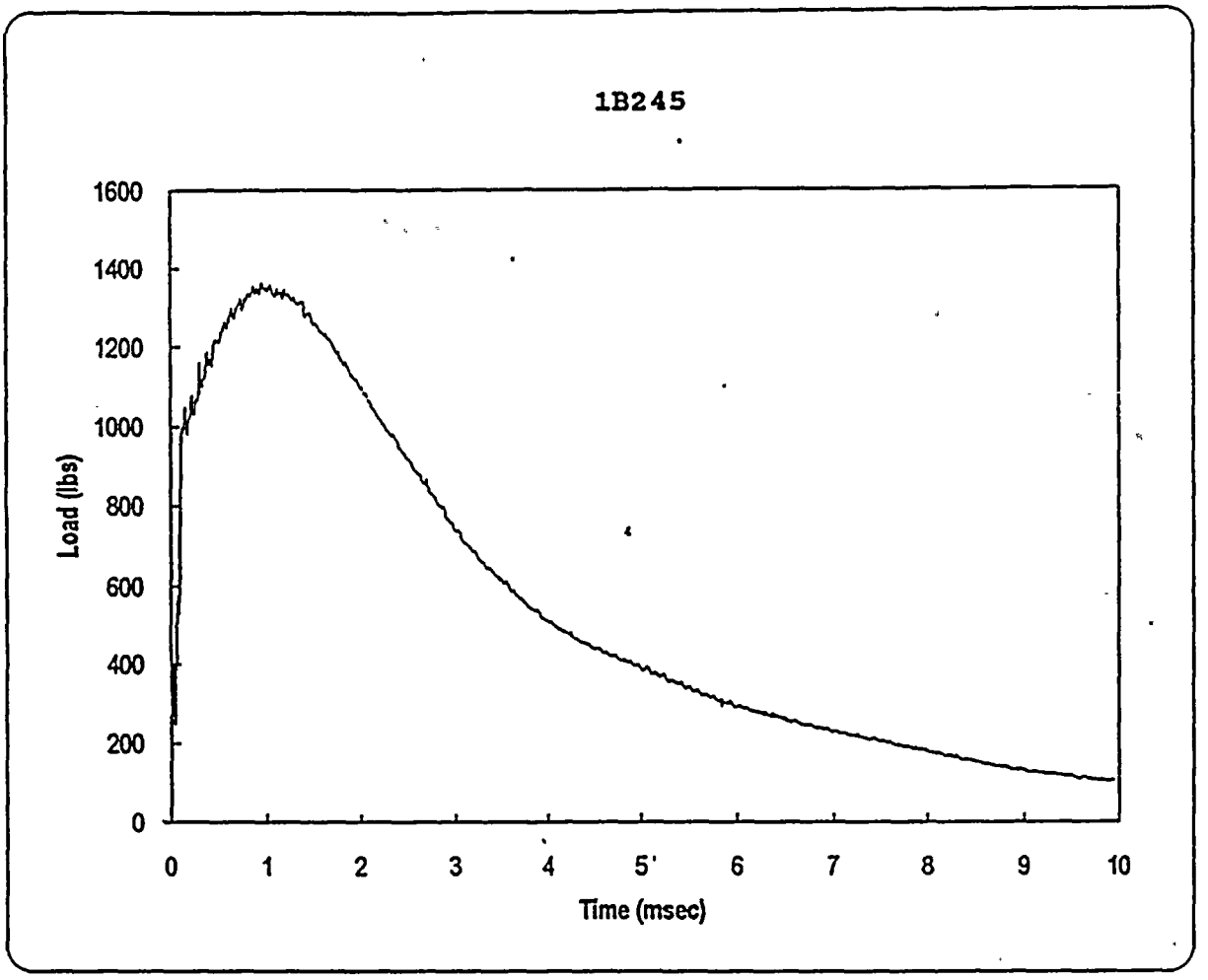

Specimen	1B245
Temperature	200 F
Available Energy	636 in-lbs
Initial Velocity	90.5 in/sec

Time to Yield	0.112 mSec
Yield Load	1080 lbs
Time to Maximum	0.950 mSec
Maximum Load	1365 lbs
Energy at Max. Load	92.1 in-lbs

Crack Length	0.194 in
a/W	0.492
Specimen Compliance	54.2
Machine Compliance	64.1

KJD	254.2 ksi-in^1/2
Yield Stress	89.1 ksi

Figure A-46. Load-time record and data for precracked specimen 1B245

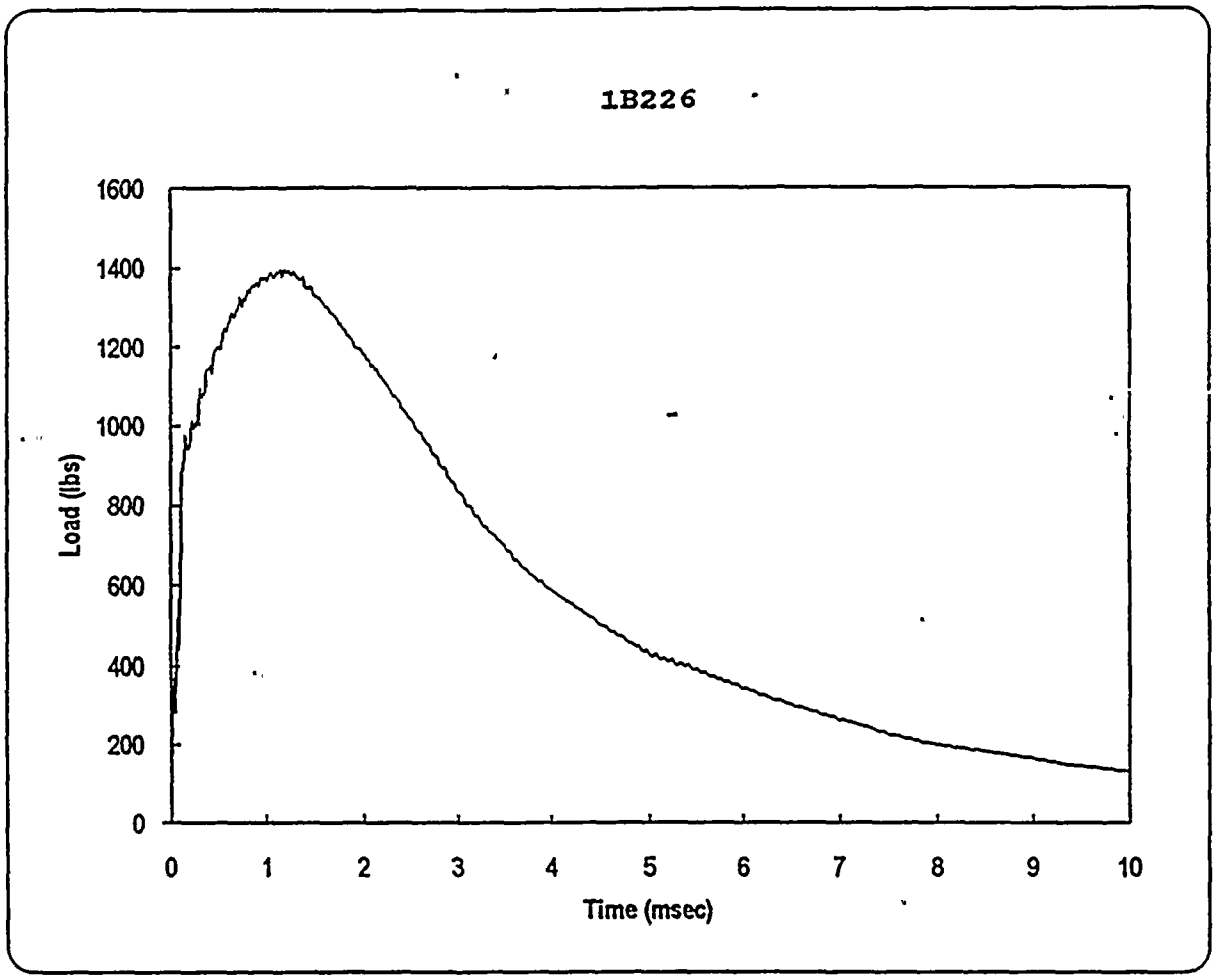

Specimen	1B226
Temperature	250 F
Available Energy	637 in-lbs
Initial Velocity	90.6 in/sec

Time to Yield	0.113 mSec
Yield Load	880 lbs
Time to Maximum	1.145 mSec
Maximum Load	1398 lbs
Energy at Max. Load	112.4 in-lbs

Crack Length	0.184 in
a/W	0.467
Specimen Compliance	49.2
Machine Compliance	86.3

KJD	271.6 ksi-in^1/2
Yield Stress	65.9 ksi

Figure A-47. Load-time record and data for precracked specimen 1B226

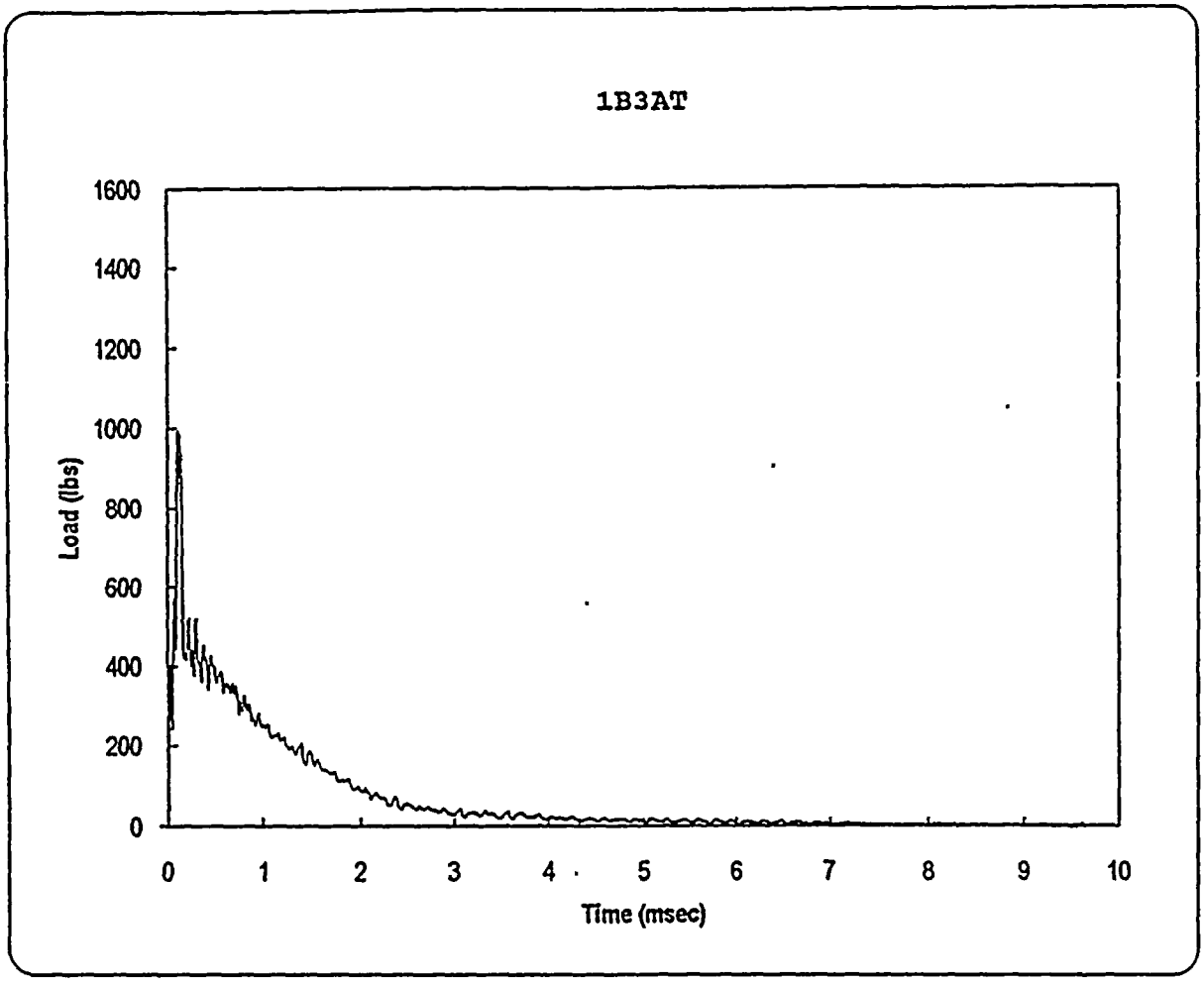

Specimen	1B3AT
Temperature	-50 F
Available Energy	642 in-lbs
Initial Velocity	90.9 in/sec

Time to Yield	0.111 mSec *
Yield Load	990 lbs *
Time to Maximum	0.115 mSec
Maximum Load	995 lbs
Energy at Max. Load	4.2 in-lbs

Crack Length	0.191 in
a/W	0.485
Specimen Compliance	52.6
Machine Compliance	68.8

KID	40.7 ksi-in^1/2
Yield Stress	79.3 ksi *

* No General Yielding

Figure A-48. Load-time record and data for precracked specimen 1B3AT

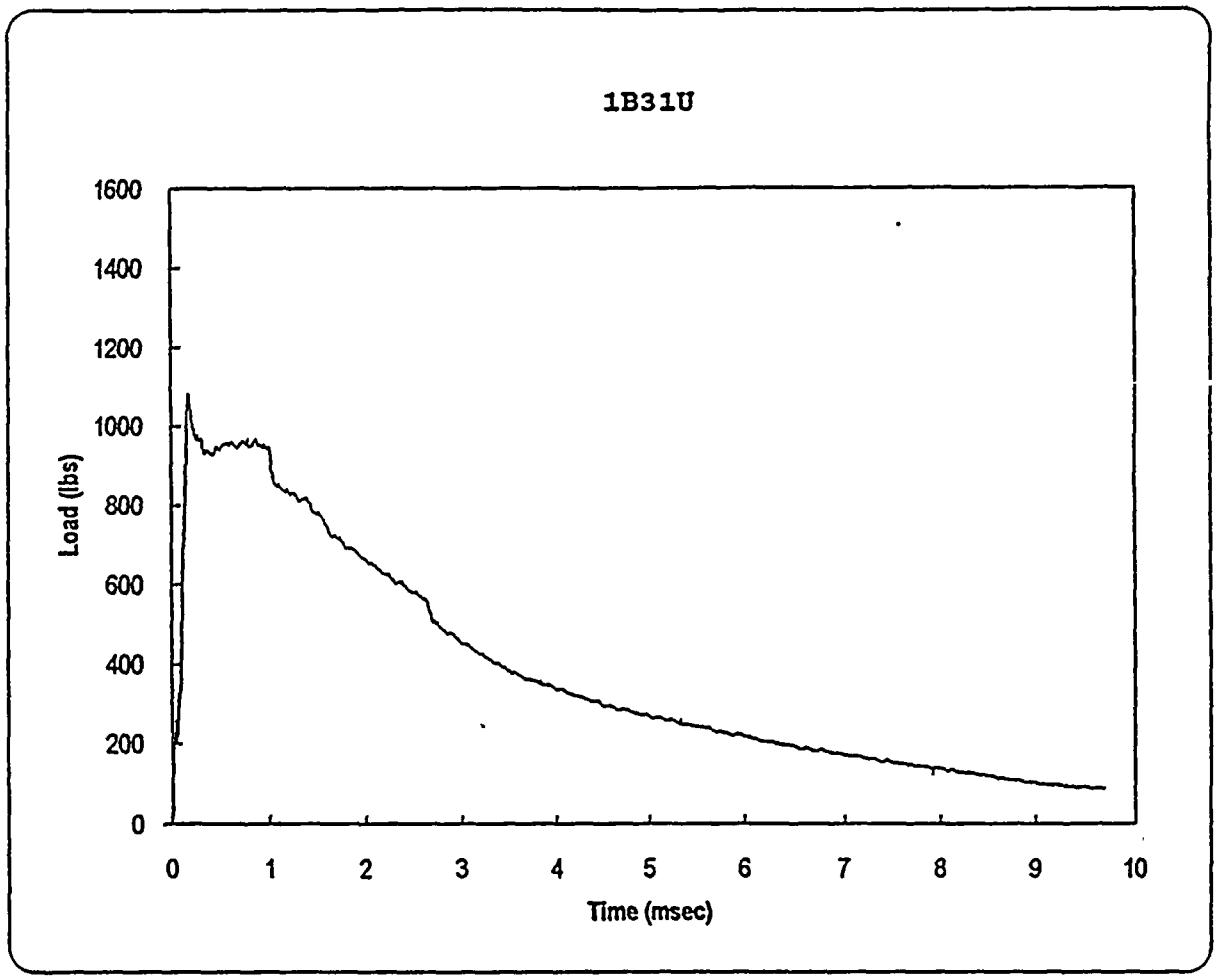

Specimen	1B31U
Temperature	-25 F
Available Energy	257 in-lbs
Initial Velocity	57.5 in/sec

Time to Yield	0.157 mSec *
Yield Load	1030 lbs *
Time to Maximum	0.175 mSec
Maximum Load	1085 lbs
Energy at Max. Load	4.7 in-lbs

Crack Length	0.182 in
a/W	0.462
Specimen Compliance	48.2
Machine Compliance	56.2

KID	41.4 ksi-in^1/2
Yield Stress	75.6 ksi *

* No General Yielding

Figure A-49. Load-time record and data for precracked specimen 1B31U

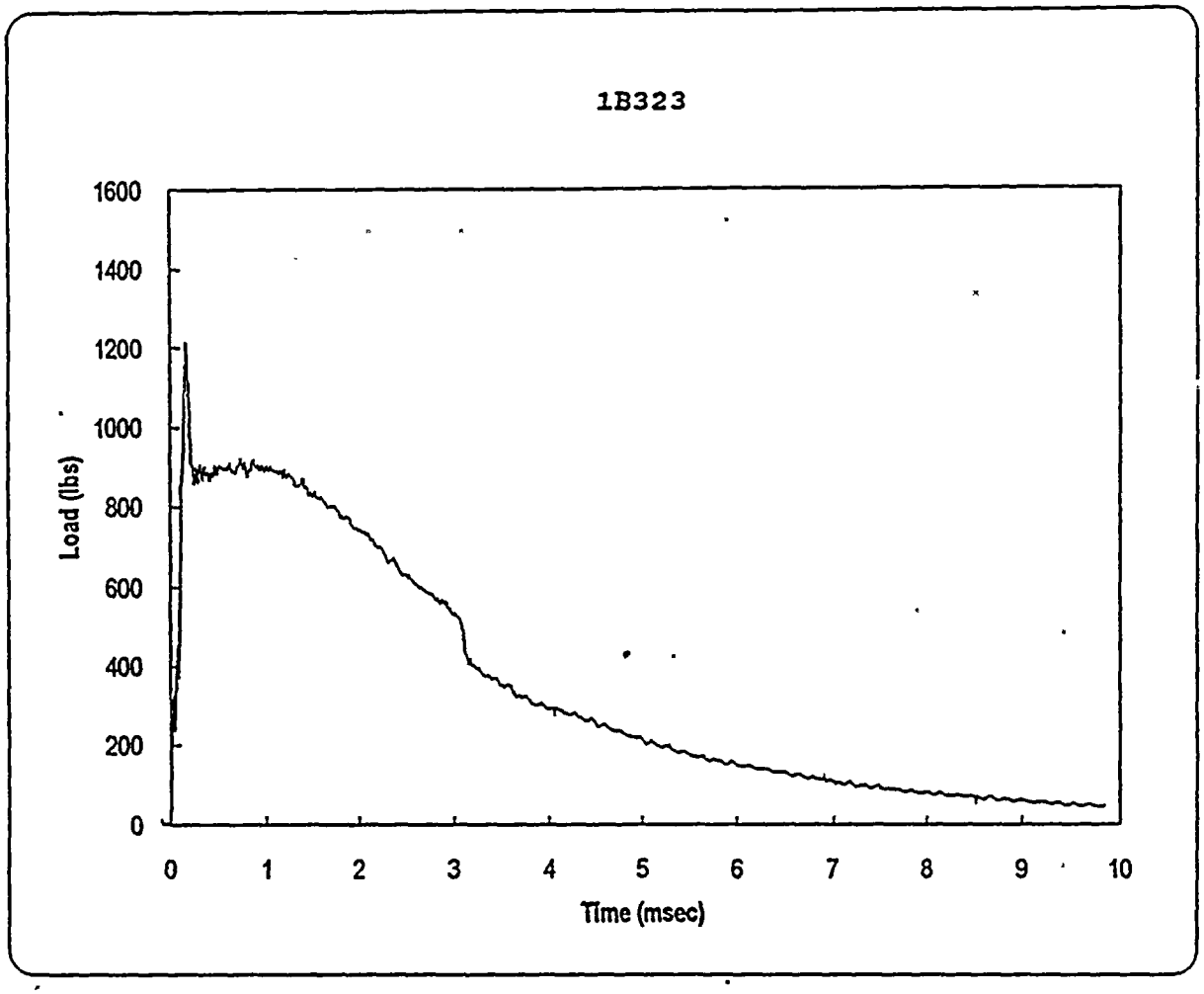

Specimen	1B323
Temperature	0 F
Available Energy	397 in-lbs
Initial Velocity	71.5 in/sec

Time to Yield	0.154 mSec *
Yield Load	1210 lbs *
Time to Maximum	0.155 mSec
Maximum Load	1215 lbs
Energy at Max. Load	5.5 in-lbs

Crack Length	0.186 in
a/W	0.472
Specimen Compliance	50.1
Machine Compliance	56.6

.. KID	47.8 ksi-in^1/2
Yield Stress	92.3 ksi *

* No General Yielding

Figure A-50. Load-time record and data for precracked specimen 1B323

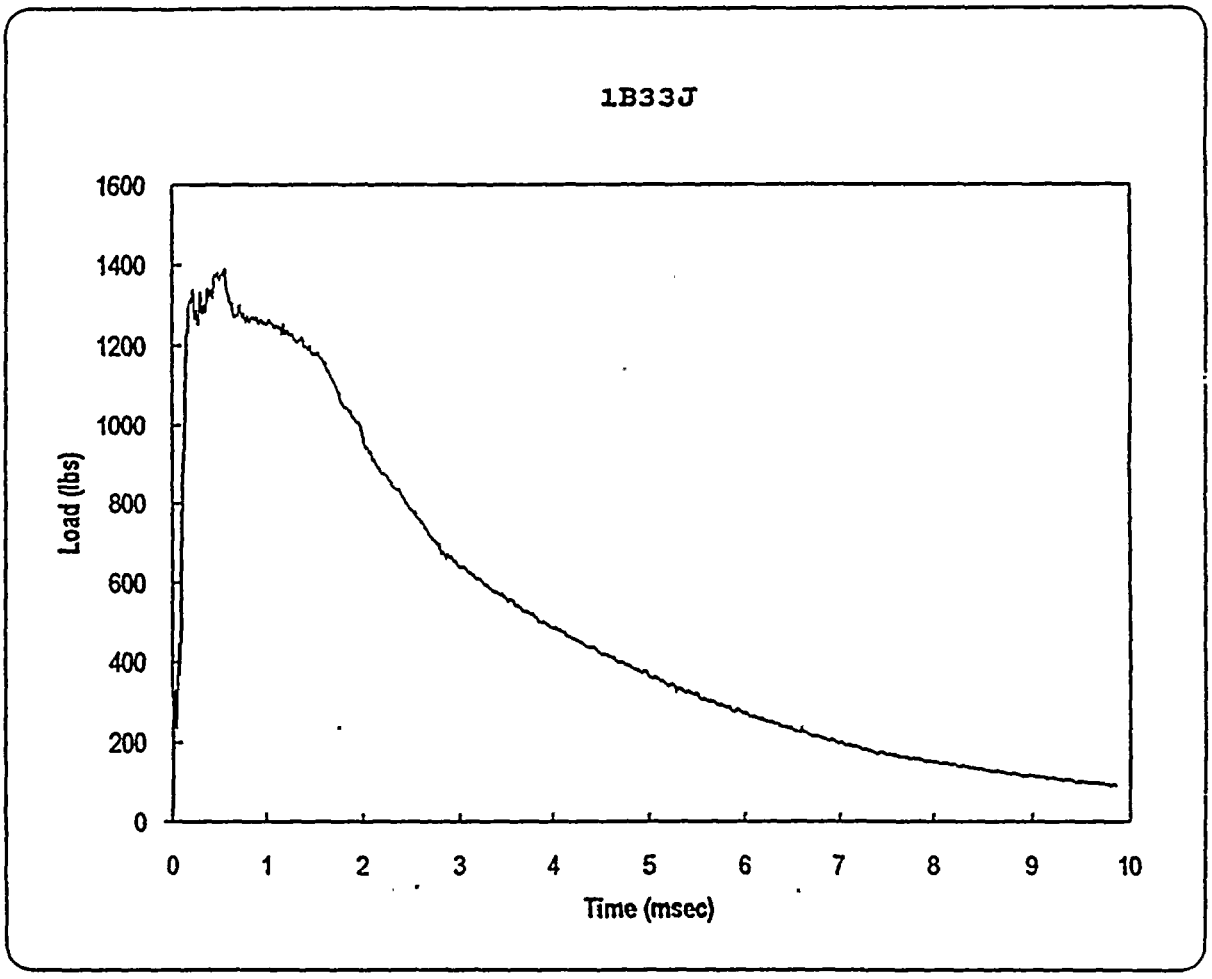

Specimen	1B33J
Temperature	50 F
Available Energy	397 in-lbs
Initial Velocity	71.5 in/sec

Time to Yield	0.150 mSec
Yield Load	1240 lbs
Time to Maximum	0.550 mSec
Maximum Load	1390 lbs
Energy at Max. Load	42.0 in-lbs

Crack Length	0.180 in
a/W	0.457
Specimen Compliance	47.3
Machine Compliance	54.0

KJD	163.5 ksi-in^1/2
Yield Stress	89.4 ksi

Figure A-51. Load-time record and data for precracked specimen 1B33J

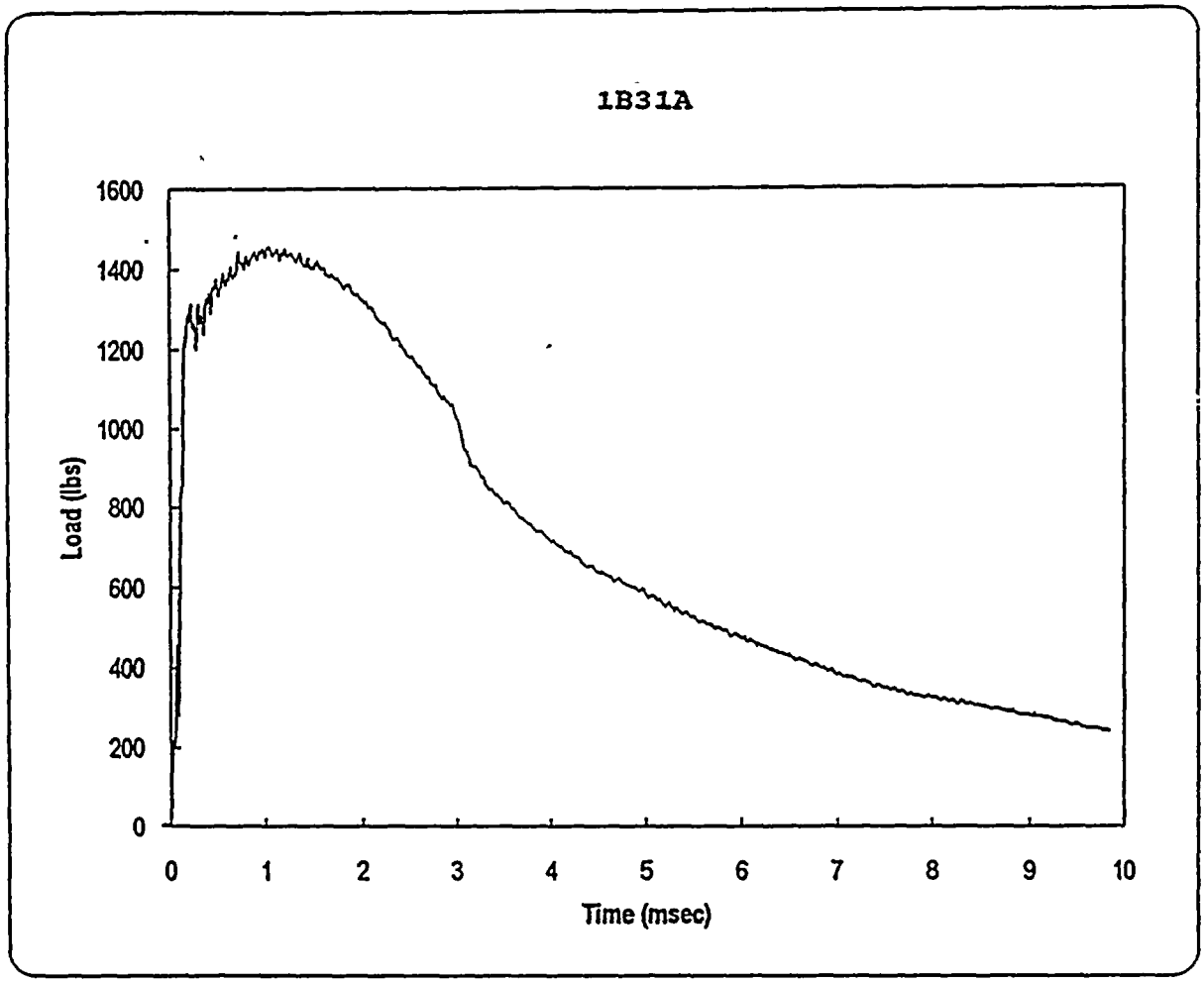

Specimen	1B31A
Temperature	71 F
Available Energy	400 in-lbs
Initial Velocity	71.8 in/sec

Time to Yield	0.150 mSec
Yield Load	1240 lbs
Time to Maximum	1.035 mSec
Maximum Load	1456 lbs
Energy at Max. Load	86.2 in-lbs

Crack Length	0.174 in
a/W	0.442
Specimen Compliance	44.8
Machine Compliance	56.6

KJD	236.4 ksi-in^1/2
Yield Stress	84.5 ksi

Figure A-52. Load-time record and data for precracked specimen 1B31A

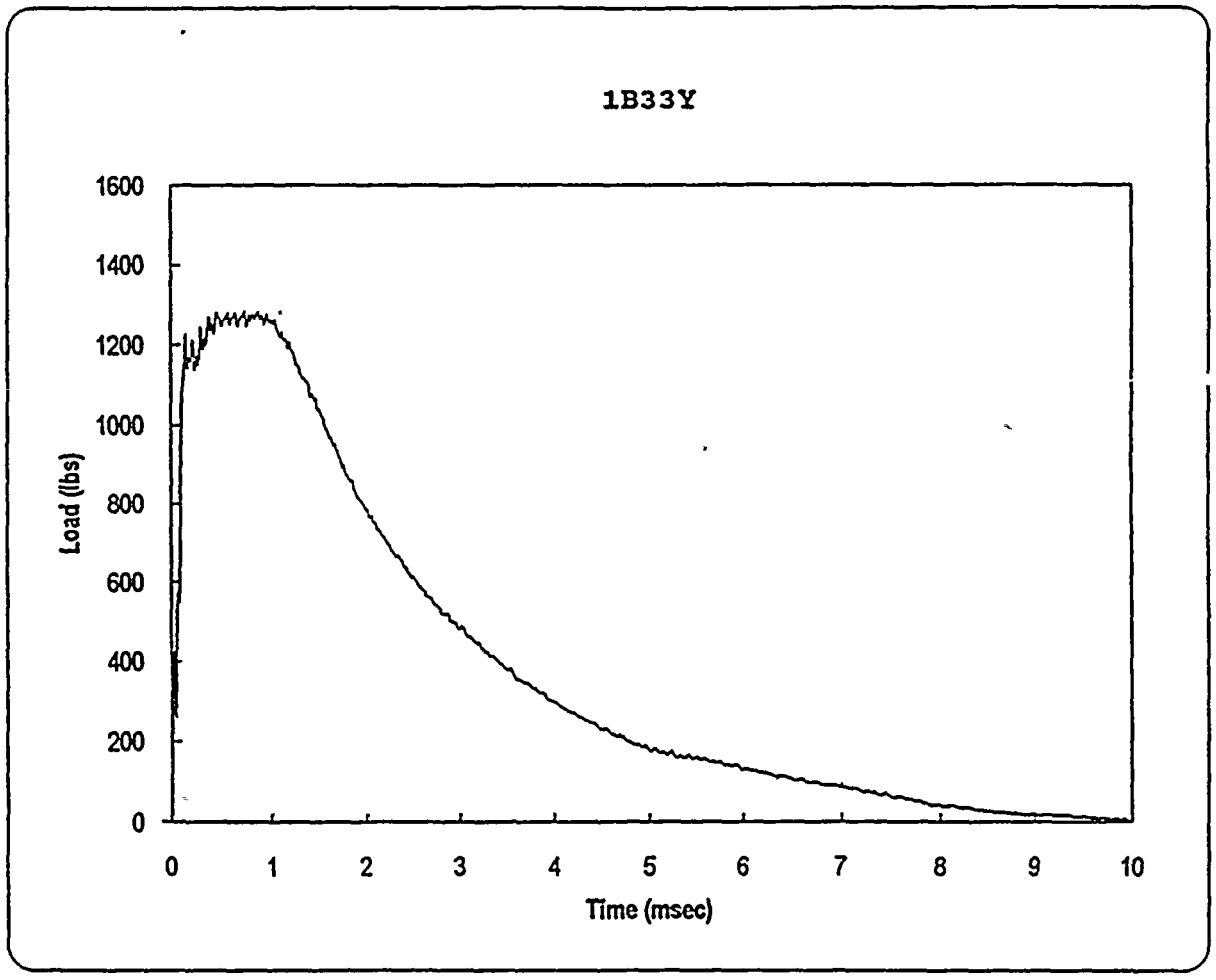

Specimen	1B33Y
Temperature	100 F
Available Energy	636 in-lbs
Initial Velocity	90.5 in/sec

Time to Yield	0.140 mSec
Yield Load	1200 lbs
Time to Maximum	0.720 mSec
Maximum Load	1286 lbs
Energy at Max. Load	70.0 in-lbs

Crack Length	0.184 in
a/W	0.467
Specimen Compliance	49.2
Machine Compliance	76.0

KJD	215.5 ksi-in^1/2
Yield Stress	89.8 ksi

Figure A-53. Load-time record and data for precracked specimen 1B33Y

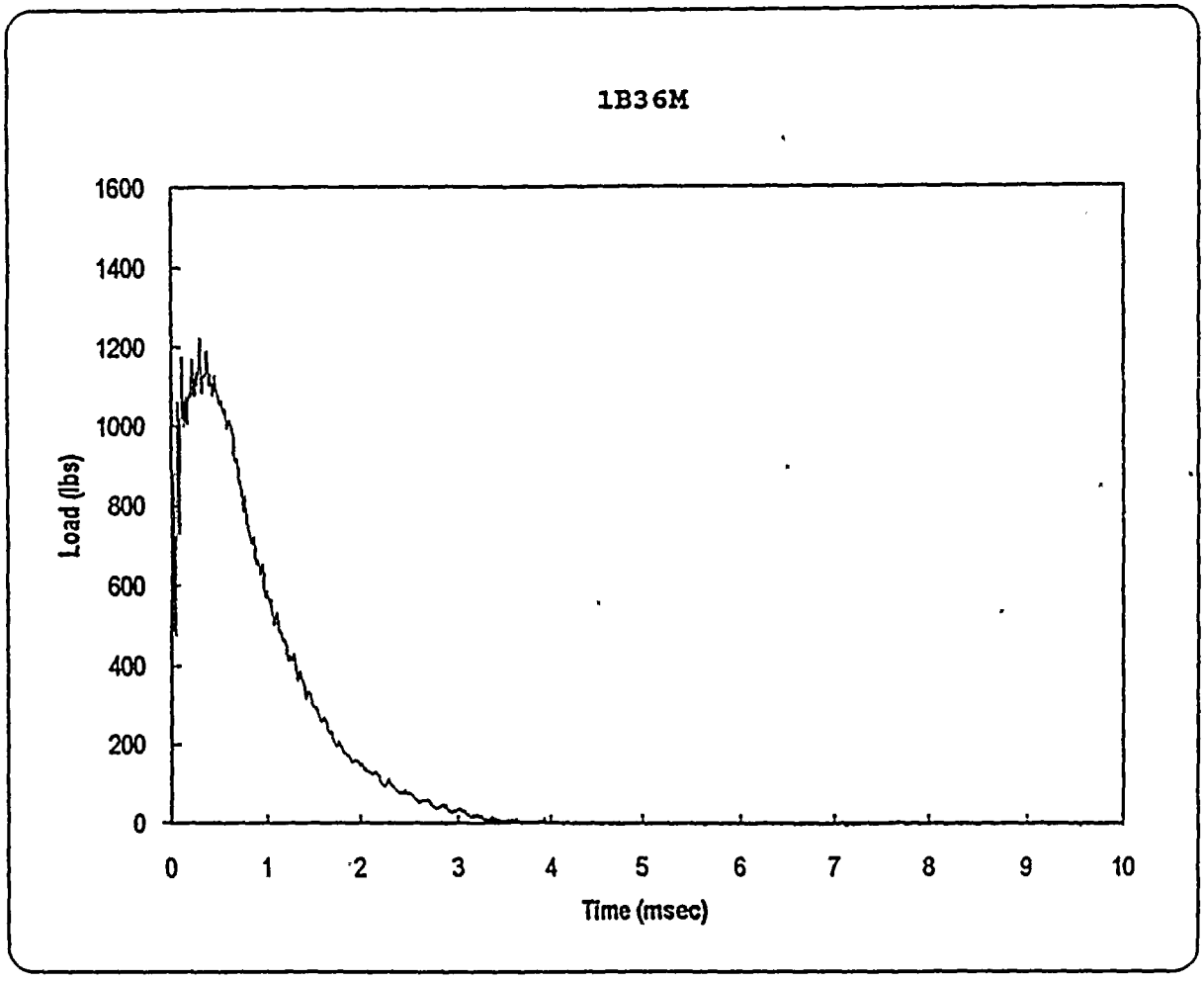

Specimen	1B36M
Temperature	125 F
Available Energy	3201 in-lbs
Initial Velocity	203.0 in/sec

Time to Yield	0.060 mSec
Yield Load	950 lbs
Time to Maximum	0.300 mSec
Maximum Load	1223 lbs
Energy at Max. Load	56.4 in-lbs

Crack Length	0.189 in
a/W	0.480
Specimen Compliance	51.6
Machine Compliance	98.5

KJD	191.7 ksi-in^1/2
Yield Stress	74.6 ksi

Figure A-54. Load-time record and data for precracked specimen 1B36M

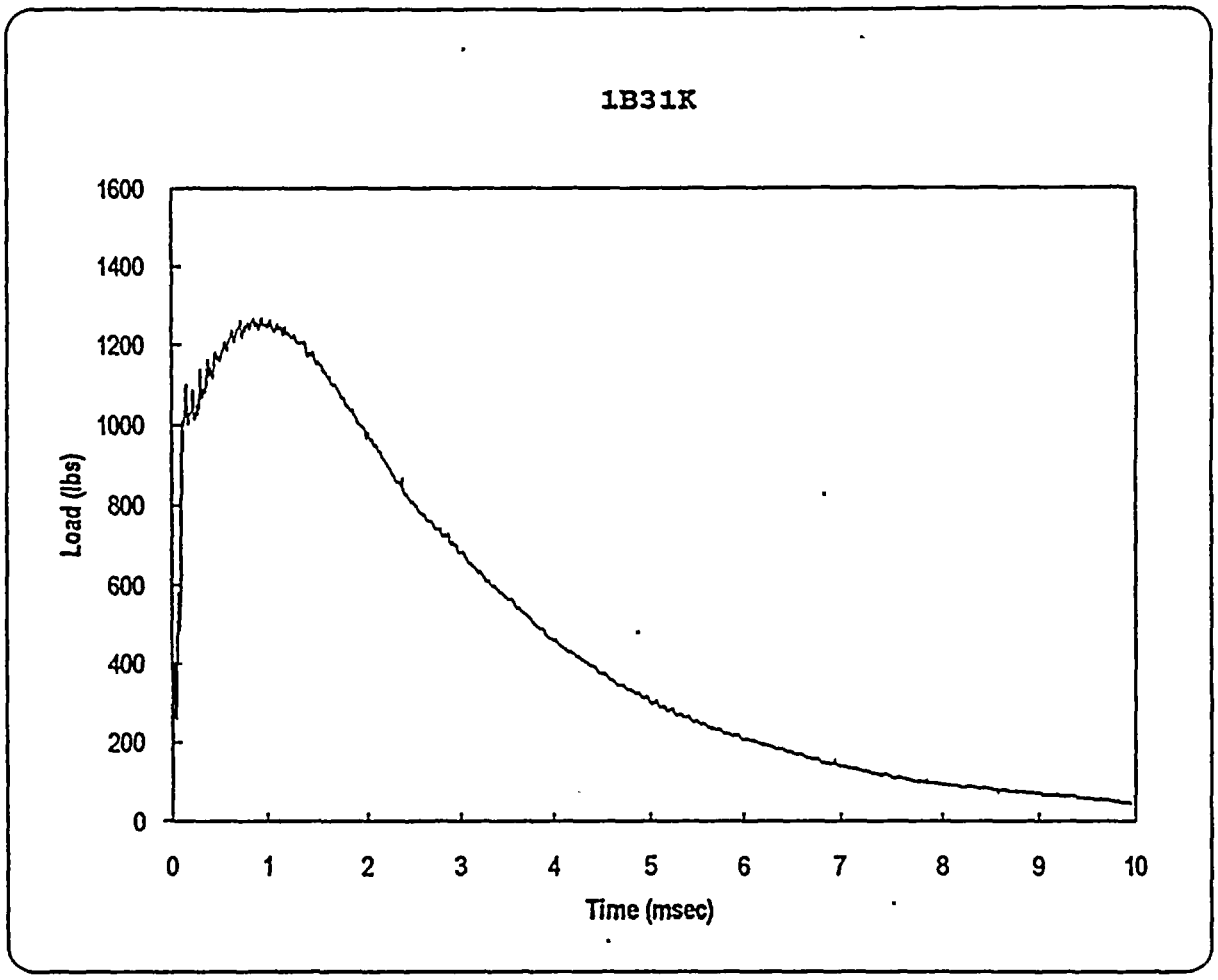

Specimen	1B31K
Temperature	150 F
Available Energy	642 in-lbs
Initial Velocity	90.9 in/sec

Time to Yield	0.110 mSec
Yield Load	1000 lbs
Time to Maximum	0.860 mSec
Maximum Load	1267 lbs
Energy at Max. Load	80.0 in-lbs

Crack Length	0.187 in
a/W	0.475
Specimen Compliance	50.6
Machine Compliance	64.3

KJD	233.8 ksi-in^1/2
Yield Stress	77.0 ksi

Figure A-55. Load-time record and data for precracked specimen 1B31K

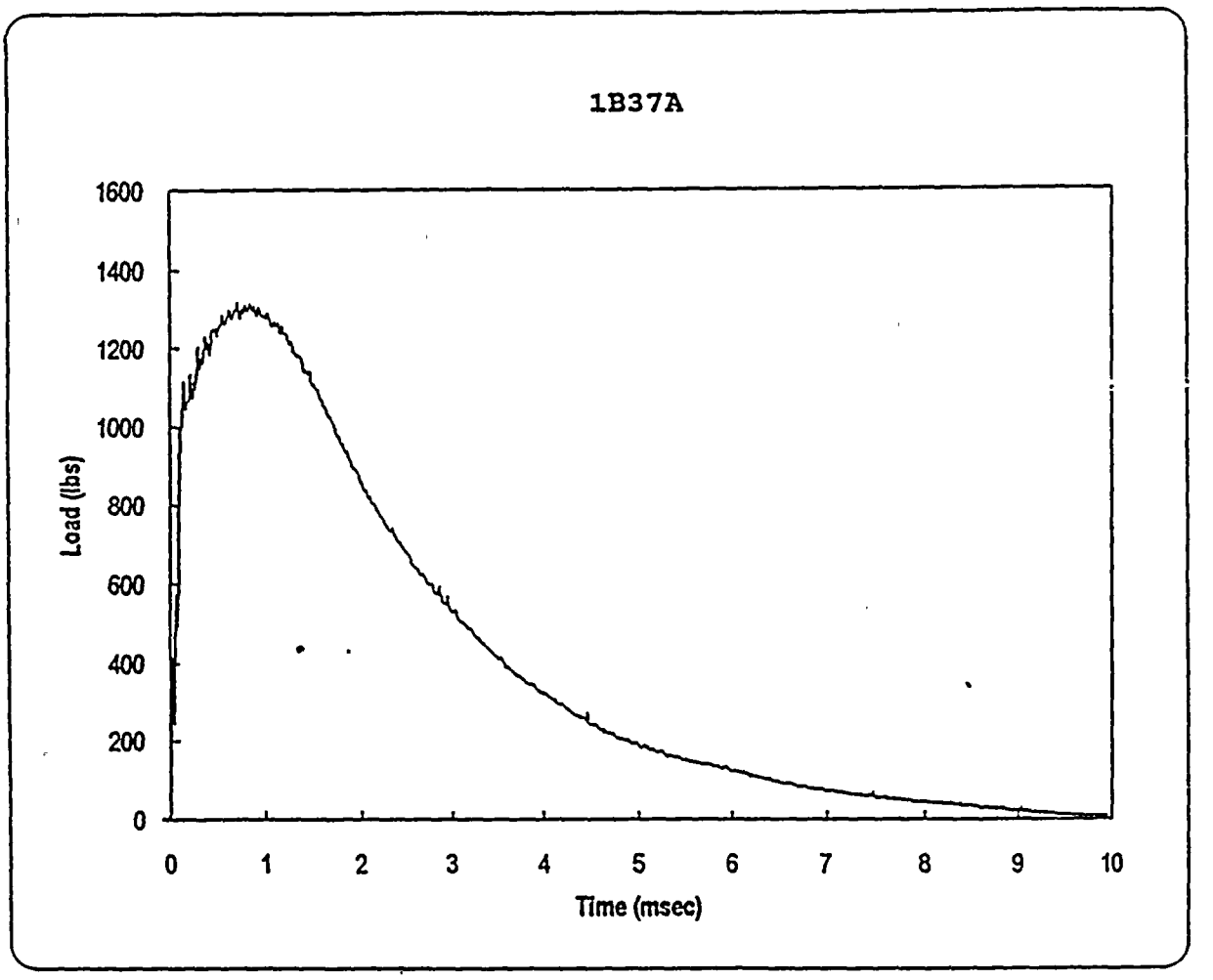

Specimen	1B37A
Temperature	200 F
Available Energy	637 in-lbs
Initial Velocity	90.6 in/sec

Time to Yield	0.110 mSec
Yield Load	1000 lbs
Time to Maximum	0.715 mSec
Maximum Load	1319 lbs
Energy at Max. Load	67.6 in-lbs

Crack Length	0.186 in
a/W	0.472
Specimen Compliance	50.1
Machine Compliance	63.4

KJD	211.8 ksi-in^1/2
Yield Stress	76.3 ksi

Figure A-56. Load-time record and data for precracked specimen 1B37A